

João Pedro Simões Cândido Martins

BEHAVIOUR OF CYLINDRICALLY CURVED STEEL PANELS UNDER IN-PLANE STRESSES

Tese de Doutoramento em Construção Metálica e Mista orientada pelo Professor Doutor Luís Alberto Proença Simões da Silva e pelo Professor Doutor António José Luís dos Reis apresentada ao Departamento de Engenharia Civil da Faculdade de Ciências e Tecnologia da Universidade de Coimbra

Setembro, 2014



UNIVERSIDADE DE COIMBRA

João Pedro Simões Cândido Martins

BEHAVIOUR OF CYLINDRICALLY CURVED STEEL PANELS UNDER IN-PLANE STRESSES

Tese de Doutoramento em Construção Metálica e Mista orientada pelo Professor Doutor Luís Alberto Proença Simões da Silva e pelo Professor Doutor António José Luís dos Reis apresentada ao Departamento de Engenharia Civil da Faculdade de Ciências e Tecnologia da Universidade de Coimbra

Setembro, 2014



UNIVERSIDADE DE COIMBRA



Preface

The work presented herein was performed at the Civil Engineering Department of the Faculty of Sciences and Technology of the University of Coimbra and it is within the framework of the activities of the research unit ISISE (Institute for Sustainability and Innovation in Structural Engineering). It was conducted under the supervision of Professor Luís Alberto Proença Simões da Silva and Professor António José Luís dos Reis.

The research leading to this dissertation had the financial support from the Portuguese Minister for Science and Higher Education through the Portuguese Foundation for Science and Technology under the individual Ph.D. grant (SFRH/BD/70424/2010).

This work is to best of my knowledge original, except where references to other works are made.

João Pedro Martins, Coimbra, 2014

Acknowledgements

I would like to thank Professor Luís Simões da Silva for providing outstanding working conditions during the research period. I would like to thank him also for his support, advice and trust during the last four years. I am grateful to Professor António Reis for his support, availability and valuable ideas. I am also thankful for the hospitality of Professor Darko Beg and his colleagues, who became my friends, during my stay at the University of Ljubljana.

Finally, I wish to express my gratitude to my colleagues and friends with whom this work has been thoroughly discussed.

Resumo

O objectivo do presente trabalho é a análise da estabilidade de painéis cilíndricos metálicos sujeitos a tensões de compressão no seu plano médio e o desenvolvimento de regras de dimensionamento que colmatem as limitações que as normas europeias actualmente apresentam.

Para o caso mais simples, o da compressão uniaxial uniforme, os principais estudos foram reanalisados tendo-se concluindo que, no que respeita a tensão crítica elástica de painéis cilíndricos metálicos, as expressões disponíveis apresentam erros consideráveis. Recorrendo ao método dos elementos finitos e, paralelamente, a uma formulação analítica baseada em métodos energéticos, foram desenvolvidas novas expressões que melhoram significativamente os valores obtidos para tensão crítica e que permitem, também, calcular a mesma para painéis sujeitos a carregamentos de compressão não uniforme. Em relação à tensão última, o método agora proposto apresenta também melhorias significativas, mas é o primeiro a incluir a possibilidade de calcular a tensão última de painéis cilíndricos metálicos sujeitos a flexão pura no seu plano médio e a permitir uma aplicação directa a secções.

Finalmente deve referir-se que, apesar de não se propor nenhum método para a obtenção da tensão última, o comportamento último de painéis cilíndricos sujeitos a compressão uniforme biaxial é caracterizado recorrendo a métodos exclusivamente numéricos.

Palavras-chave: Estabilidade, painéis cilíndricos, estruturas metálicas.

Abstract

The objective of this work is to analyse the stability behaviour of cylindrically curved steel panels under generalised in-plane compressive stresses and to develop design rules which overcome some limitations of current European Standards.

For the simplest case of pure compressive axial stresses, the most relevant works have been revisited and analysed. In what concerns the elastic critical stress of cylindrically curved panels, it was concluded that the expressions which are currently available return non-negligible errors. Relying on the finite element method and, at the same time, on an analytical formulation based on energy methods, new expressions presenting significant improvements and allowing obtaining the elastic critical stress also for panels under non-uniform in-plane loading are presented. Concerning the ultimate resistance, the proposed method also shows improvements, but its main contribution is that it allows obtaining the ultimate resistance also for panels under pure in-plane bending and a direct application to cross-sections.

Finally, it is worth mentioning that, albeit it is not proposed any new method to compute the ultimate load of cylindrically curved panels under biaxial loading, the behaviour of curved panels under this type of loading is analysed relying exclusively on numerical methods.

Keywords: Stability, cylindrically curved panels, steel structures.

Contents

Notation	vii
List of Figures	xv
List of tables	xxxi
1. Introduction	
1.1. Motivation and statement of the problem	1
1.2. The use of curved steel in structural applications.....	3
1.3. Objectives and scope.....	10
1.4. Thesis outline	12
2. Analysis of general thin elastic shells	
2.1. Chapter overview	15
2.2. Brief review on shell theories	16
2.3. Constitutive relations for thin elastic shells.....	23
2.4. Stress resultants for thin elastic shells.....	24
2.5. Shallow shells.....	27
2.6. Energy principles	34
2.7. Methods of analysis of thin shells	36
2.8. Summary	39

3. Stability analysis of plates and cylindrically curved panels

3.1. Chapter overview	41
3.2. Geometry of a cylindrically curved panel.....	42
3.3. Buckling and postbuckling behaviour of flat plates under uniaxial compressive stresses.....	43
3.4. Buckling and postbuckling behaviour of flat plates under biaxial compressive stresses.....	49
3.5. Buckling and postbuckling behaviour of thin cylindrically curved panels under uniaxial compressive stresses.....	54
3.6. Buckling and postbuckling behaviour of thin cylindrically curved panels under circumferential compressive stresses	61
3.7. Buckling and postbuckling behaviour of thin cylindrically curved panels under biaxial compressive stresses	63
3.8. Elastic critical stress <i>vs.</i> ultimate stress and the effect of imperfections.....	64
3.9. Ultimate strength of flat plates under uniaxial in-plane stresses.....	67
3.10. Ultimate strength of plates under biaxial stresses	70
3.11. Ultimate strength of cylindrically curved panels under uniaxial in-plane stresses	72
3.12. Ultimate strength of cylindrically curved panels under circumferential compressive stresses	77
3.13. Ultimate strength of cylindrically curved panels under biaxial compressive stresses.....	80
3.14. Design guidelines and standards.....	80
3.15. Summary	87

4. Numerical models of cylindrically curved panels under compressive stresses	
4.1. Chapter overview	89
4.2. Data for finite element analysis	90
4.3. Types of analyses	96
4.4. Validation of numerical models	100
4.5. Summary	112
5. Characterisation of the behaviour of cylindrically curved panels	115
5.1. Chapter overview	115
5.2. Parametric study on the elastic buckling behaviour of cylindrically curved panels under uniaxial compressive stresses	116
5.3. Parametric study on the ultimate strength of short cylindrically curved panels under uniaxial compressive stresses	130
5.4. Parametric study on the ultimate strength of short cylindrically curved panels under biaxial compressive stresses	144
5.5. Summary	153
6. Imperfection sensitivity of cylindrically curved panels under uniaxial compression	
6.1. Chapter overview	155
6.2. Parametric study	156
6.3. Results and discussion	160
6.4. Summary	189
7. Energy based analytical model of cylindrically curved panels	
7.1. Chapter overview	193
7.2. Energy formulation	194

7.3. Elastic critical stress.....	197
7.4. Summary.....	216
8. Design proposals for cylindrically curved steel panels	
8.1. Chapter overview.....	217
8.2. Numerical evaluation of the elastic critical stress of cylindrically curved panels under uniaxial compressive stresses.....	218
8.3. Extended evaluation of the elastic critical stress of cylindrically curved panels under uniaxial compressive stresses: analytical closed-form solution.....	224
8.4. Detailed comparison between numerical results of the elastic buckling factor and proposed set of formulae for pure compression.....	227
8.5. Ultimate strength of cylindrically curved panels under uniaxial compressive stresses by the effective width method.....	229
8.6. Ultimate strength of cylindrically curved panels under generalised axial stresses.....	247
8.7. Detailed comparison between numerical results and proposed set of formulae for pure compression.....	253
8.8. Application of proposed methodology to the design of cross-sections using the effective width method.....	258
8.9. Summary.....	267
9. Summary and future research	
9.1. Conclusions.....	269
9.2. Future research.....	272
9.3. Original contributions.....	273
9.4. Publications.....	274

Bibliography	279
A.Examples of Mathematica code developed for the analytical study	295

Notation

Roman uppercase letters

A	plate's / panel's cross-section area
A, B, C, D	numerical parameters
A_{eff}	plate's / panel's effective cross-section area
A_L, B_L	Lamé's geometric coefficients
C	shell's membrane rigidity
C_l	correction factor for long curved panels
C_{ult}	correction factor for long cylindrically curved panels
D	shell's flexural rigidity
E	Young's modulus
F	stress function
M_{Rd}	resistant bending moment
M_x, M_y, M_{xy}	internal moments in a shell element
$M_{y,Ed}, M_{z,Ed}$	design bending moment around y -axis and z -axis
N	number of finite elements in the loaded edge of the plate / panel
N_{Ed}	design axial force
N_{Rd}	resistant axial force

N_x, N_y, N_{xy}	internal membrane forces in a shell element
Q_x, Q_y	internal shear forces in a shell element
q_x, q_y, q_z	distributed forces per unit area acting in x , y and z -direction
R	radius of curvature of the panel and shell element
R_{min}	minimum value of the radius of curvature
R_p	residual vector in the Galerkin's method
R_x, R_y	radius of curvature of the shell element at x - and y -direction
R'_x, R'_y	radius of curvature of the shell element at x - and y -direction after deformation
U	strain energy
U_b	bending strain energy
U_m	membrane strain energy
U_n	dimple imperfection amplitude parameter depending on the fabrication tolerance quality class
V	total potential energy
V_2	quadratic term of the total potential energy
W	work done by the applied loads
W_y	cross-section's elastic section modulus around y
$W_{y,eff}, W_{z,eff}$	cross-section's effective elastic section modulus around y and z -direction
Z	curvature parameter
Z_b	Batdorf curvature parameter
Z_t	curvature parameter in the transverse direction

Roman lowercase letters

a	plate's / panel's length
$a_{i,j}$	degrees-of-freedom in the energy formulation
b	plate's / panel's with
b_{eff}	plate's / panel's effective width
$e_{y,N}, e_{z,N}$	neutral axis variation according to y - and z -axis
k_{σ}	elastic critical stress coefficient
$k_{\sigma, long}$	elastic buckling coefficient for long curved panels
$k_{\sigma, min}$	minimum value of the elastic critical stress coefficient
$k_{\sigma, plate}$	plate's elastic critical stress coefficient
$k_{\sigma, Domb\&Leigh}$	elastic critical stress coefficient from Domb & Leigh's proposal
$k_{\sigma, num}$	numerically obtained value for the elastic critical stress coefficient
l_g	relevant gauge length according to clause 8.4.4(2) in EN1993-1-6:2007
l_{LW}	length of the largest longitudinal half-wave
l_{TW}	length of the largest transverse half-wave
m	number of longitudinal half-waves
n	number of transverse half-waves
p_x, p_y, p_z	external forces
q	amplitude of the degree-of-freedom
q_0	initial amplitude of the degree-of-freedom
q_i	undetermined parameters (degrees-of-freedom) in Rayleigh-Ritz and Galerkin's methods
t	plate's / panel's thickness
u	axial displacements (x -direction)

v	transverse displacements (y -direction)
w	out-of-plane displacements (z -direction)

Greek uppercase letters

A_z, B_z	numerical parameters
B_i	factor compensating for the lower bound nature of ρ_i
$\Delta w_{0,eq,EN1993-1-5}$	proposed amplitude by EN1993-1-5:2006 for equivalent geometric imperfections
$\Delta w_{0,eq,EN1993-1-6}$	proposed amplitude by EN1993-1-6:2007 for equivalent geometric imperfections
$\Delta w_{0,eq,EN1993-1-5}^{\text{mod}}$	modified amplitude based on EN1993-1-5:2006 for equivalent geometric imperfections
$\Delta w_{0,eq,EN1993-1-6}^{\text{mod}}$	modified amplitude based on EN1993-1-6:2007 for equivalent geometric imperfections

Greek lowercase letters

α	panel's aspect ratio
$\alpha_{cr,num}$	critical multiplier directly read from numerical results
α_{BC}	numerically calibrated parameter depending on the boundary conditions
α_z	elastic imperfection reduction factor (Tran <i>et al.</i> , 2012)
α_z, c_z, S_z	parameters calibrated with numerical results that reflect the effect of curvature in the shape of the proposed ρ - λ curves

β	numerical parameter representing the influence of curvature on the value of the imperfection factor (Tran <i>et al.</i> , 2012); plastic range factor (Tran, 2012)
γ	stress ratio between two orthogonal directions
γ_M	material coefficient
γ_{M0}	safety coefficient
γ_{xy}	distortion between x - and y -direction
$\gamma_{xy,0}$	membrane distortion between x - and y -direction without the change in curvature
γ_{xz}	distortion between x - and z -direction
γ_{yz}	distortion between y - and z -direction
$\varepsilon_1, \varepsilon_2$	strains defining the plastic plateau before the strain hardening of the material's physical law
ε_x	total strain at x -direction
$\varepsilon_{x,0}$	membrane strain at x -direction without the change in curvature
ε_y	total strain at y -direction
$\varepsilon_{y,0}$	membrane strain at y -direction without the change in curvature
ε_z	total strain at z -direction
η	interaction exponent
η_1	normalised utilisation factor
θ	panel's sectorial angle
θ_{bl}	biaxial load case
$\lambda_{z,0}$	length of the initial plateau where no reduction of the panel's resistance occurs
λ	reduced slenderness parameter

λ'	normalised slenderness parameter (Park <i>et al.</i> , 2009); slenderness limiting the elasto plastic domain of the response of cylindrically curved panels (Tran, 2012)
$\lambda_{0,p}$	length of the initial plateau for flat panels
λ_s	reduced shell slenderness parameter from DNV-RP-C202
ν	Poisson's coefficient
ρ	reduction factor applied to the width of the panel
$\rho_{0,z}$	last branch of Eq. (8.20) setting $\lambda=\lambda_{0,p}$
ρ_i	influence of initial imperfections on the characteristic buckling strength of the curved panel according to DNV-RP-C202
ρ_{long}	reduction factor applied to the width of the panel for long curved panels
ρ_{Num}	numerically obtained reduction factor applied to the width of the panel
ρ_x, ρ_z, χ^w	resistance reduction factors from the reduced stress method
σ, σ_x	membrane stress at x -direction
σ_1, σ_2	maximum and minimum longitudinal stress acting on a plate's / panel's loaded edge
σ_{av}	average value of the membrane stress distribution at x -direction
σ_{cr}^c	elastic critical stress considering the curvature
σ_{cr}	elastic critical stress
σ_E	Euler's elastic critical stress
σ_{Ed}	design axial stress
$\sigma_{k,Rd}$	characteristic buckling strength according to DNV-RP-C202 and the ABS Guide for Buckling and Ultimate Strength Assessment for Offshore Structures

σ_{lim}	limiting value for longitudinal stresses from the reduced stress method
σ_{cr}^p	elastic critical stress without considering the curvature
$\sigma_{x,Ed}, \sigma_{z,Ed}$	design stresses at x - and z -direction
σ_y	membrane stress at y -direction
σ_z	membrane stress at z -direction
τ_{xy}	tangential stress at x -direction in a face perpendicular to y -direction
τ_{xz}	tangential stress at x -direction in a face perpendicular to z -direction
τ_{yx}	tangential stress at y -direction in a face perpendicular to x -direction
τ_{yz}	tangential stress at y -direction in a face perpendicular to z -direction
τ_{zx}	tangential stress at z -direction in a face perpendicular to x -direction
τ_{zy}	tangential stress at z -direction in a face perpendicular to y -direction
ϕ_0, ϕ_1, ϕ_2	numerical parameters
χ	resistance reduction factor
χ_{num}	numerically obtained resistance reduction factor
χ_x	Change in curvature in x -direction
χ_{xy}	Twist in curvature in x - and y -direction
χ_y	Change in curvature in y -direction
ψ	loading type / stress gradient
ψ_i	approximate functions in Rayleigh-Ritz method

Abbreviations

ABS	American Bureau of Shipping
BC	boundary conditions
CEN	European Committee for Standardisation
CoV	coefficient of variation
DNV	Det Norske Veritas
ECCS	European Convention for Constructional Steelwork
FCT	Portuguese Foundation for Science and Technology
FEM	Finite Element Method
GMNIA	geometrically and materially nonlinear analysis with imperfections included
GNA	geometrically nonlinear analysis without imperfections included
GNIA	geometrically nonlinear analysis with imperfections included
ISISE	Institute for Sustainability and Innovation in Structural Engineering
LBA	linear buckling analysis
LW	longitudinal half-wave
MAE	maximum absolute error
MLF	maximum load factor
TW	transverse half-wave

List of Figures

- Figure 1.1: Diagrid Shell by Vladimir Shukhov during construction, Russia (unknown author, 1897)3
- Figure 1.2: *a)* New St. Station in Victorian Times, before redevelopment in the 1960's, Birmingham, England (unknown author, 1885) and *b)* New St. Station by FOA, as viewed from Stephenson St., Birmingham, England (Foreign Office Architects, 2009)4
- Figure 1.3: British Museum Great Court roof by Foster and Partners, London, England (Dunn, 2005)4
- Figure 1.4: Cloud Gate by Anish Kapoor, Chicago, United States of America (Ertürk, 2014).....5
- Figure 1.5: *a)* New Sheppey Bridge, England (unknown author, 2007) and *b)* Zubizuri Bridge in Bilbao, Spain (Lopez, 2007)6
- Figure 1.6: *a)* Bridge over Rio Ave, Portugal and *b)* Bridge over IC19 in Lisbon, Portugal (courtesy of Professor António Reis).....6
- Figure 1.7: *a)* Bellows Falls Arch Bridge, New Hampshire, United States of America (unknown author, 1905) and *b)* Pedro e Inês footbridge, Coimbra, Portugal (Correia, 2009).....7
- Figure 1.8: *a)* Renault Bridge, France (Tran *et al.*, 2012) and *b)* Pedestrian Bridge in Chaves, Portugal (Ribeiro, 2008)8

Figure 1.9:	Stonecutters Bridge cross-section in Hong Kong, China (Vejrurn, 2008).....	8
Figure 1.10:	<i>a)</i> Bending of steel sheet (Newport News Shipbuilding) and <i>b)</i> Welded steel plate forming part of a ship's hull (Newport News Shipbuilding).....	9
Figure 1.11:	SPAR platform under construction (unknown author, 2010) ...	10
Figure 1.12:	Numerical analysis of a cylindrical stiffened composite curved panel with two stiffeners for the Airbus 380 (Pardo & Fernandez, 2010).....	11
Figure 1.13:	Space shuttle external tank components (Nemeth, 1998).....	11
Figure 2.1:	Postbuckling behaviour: <i>a)</i> plated structure and <i>b)</i> shell structure.....	17
Figure 2.2:	Historical perspective and interrelation of different shell theories.....	19
Figure 2.3:	Geometry of a thin shell element.....	25
Figure 2.4:	Thin shell element: <i>a)</i> membrane forces; <i>b)</i> shear forces and bending moment.....	25
Figure 2.5:	Schematic view of: <i>a)</i> plane O_{yz} and <i>b)</i> plane O_{xz} (adapted from Silva Gomes, 2007).....	26
Figure 2.6:	Geometric definition of the relationships in Eq. (2.35).....	29
Figure 3.1:	Geometry of <i>a)</i> plate and <i>b)</i> cylindrically curved panel.....	42
Figure 3.2:	Plot of Eq. (3.5), $n=1$	45
Figure 3.3:	Stress redistribution: <i>a)</i> lateral borders remain straight and <i>b)</i> lateral borders free to deformed (adapted from Simões da Silva & Gervásio, 2007).....	47
Figure 3.4:	Effect of geometric imperfections on the postbuckling behaviour of a plate under uniform compression.....	48

Figure 3.5:	Plot of Eq. (3.9), $n=1$ and $\gamma=-1$	49
Figure 3.6:	Plot of Eq. (3.9), $n=1$ and $\gamma=-0.5$	50
Figure 3.7:	Plot of Eq. (3.9), $n=1$ and $\gamma=0.25$	50
Figure 3.8:	Plot of Eq. (3.9), $n=1$ and $\gamma=1$	51
Figure 3.9:	Plot of Eq. (3.11) and (3.12), $n=1$	52
Figure 3.10:	<i>a)</i> Plate, <i>b)</i> curved panel and <i>c)</i> cylinder behaviour subjected to longitudinal compressive stresses (1 st buckling mode).....	55
Figure 3.11:	Comparison of formulae from Redshaw, Timoshenko, Stowell and Domb & Leigh.....	58
Figure 3.12:	Global and local buckling pattern of curved panels (Möcker & Reimerdes, 2006).....	59
Figure 3.13:	Effect of geometric imperfections on the postbuckling behaviour of a curved panel (plot of Eq. (3.19) for several values of q_0/t).....	60
Figure 3.14:	Scheme of a curved plate under circumferential compressive stresses.....	61
Figure 3.15:	Elastic buckling coefficient for cylindrically curved panels under circumferential compressive stresses (Jetteur & Maquoi, 1984).....	62
Figure 3.16:	Scheme of a curved plate under biaxial compressive stresses...	64
Figure 3.17:	Effective width of a plate under compressive stresses.....	68
Figure 3.18:	Effective width reduction factor according to von Kármán, Winter, Gerard, Faulkner and Johansson.....	69
Figure 3.19:	Effective width reduction factor for curved panels under circumferential stresses according to Jetteur & Maquoi (1984).	79
Figure 3.20:	Basic notions of the reduced stress method.....	82
Figure 4.1:	Material behaviour from Rotter & Schmidt (2008).....	91

Figure 4.2:	Loading and boundary conditions for cylindrically curved panels under uniaxial and biaxial stresses.....	92
Figure 4.3:	Example of a non-converged analysis ($Z=30$ and $\alpha=2.2$; imperfection pattern based on buckling mode 3 with maximum amplitude equal to 2 mm).....	98
Figure 4.4:	Example of a non-converged analysis ($Z=30$ and $\alpha=5.0$; imperfection pattern based on buckling mode 3 with maximum amplitude equal to 10 mm).....	98
Figure 4.5:	Example of a non-converged analysis ($Z=60$ and $\alpha=3.0$; imperfection pattern based on buckling mode 6 with maximum amplitude equal to 7 mm).....	99
Figure 4.6:	Example of a non-converged analysis ($Z=60$ and $\alpha=5.0$; imperfection pattern based on buckling mode 5 with maximum amplitude equal to 10 mm).....	99
Figure 4.7:	Comparison between numerical simulations and values from EN1993-1-5:2006, $\psi=1$	102
Figure 4.8:	Comparison between numerical simulations and values from EN1993-1-5:2006, $\psi=-1$	102
Figure 4.9:	Comparison of numerical simulations and curves proposed by Tran <i>et al.</i> (2012) for $Z=10$ and $\psi=1$	105
Figure 4.10:	Comparison of numerical simulations and curves proposed by Tran <i>et al.</i> (2012) for $Z=25$ and $\psi=1$	105
Figure 4.11:	Comparison of numerical simulations and curves proposed by Tran <i>et al.</i> (2012) for $Z=50$ and $\psi=1$	106
Figure 4.12:	Comparison of numerical simulations and curves proposed by Tran <i>et al.</i> (2012) for $Z=100$ and $\psi=1$	106
Figure 4.13:	Comparison of own numerical simulations and numerical results from Braun (2010).....	107

Figure 5.1:	k_σ (1 st buckling mode) vs. Z curves for panels with $\alpha \leq 1$ and $\psi = 1$ and boundary conditions type 2.....	118
Figure 5.2:	3D plot of k_σ (1 st buckling mode) vs. (Z, α) for $\psi = 1$ and $\psi = -1$	120
Figure 5.3:	2D plot Z vs. α inducing $k_{\sigma, min}$ for different loading cases.....	121
Figure 5.4:	Plot of k_σ (1 st buckling mode) vs. α for $Z = 0$ and $\psi = 1$ for boundary conditions type 1, 2 and 3	121
Figure 5.5:	Plot of k_σ (1 st buckling mode) vs. α for $Z = 20$ and $\psi = 1$ for boundary conditions type 1, 2 and 3	122
Figure 5.6:	Plot of k_σ (1 st buckling mode) vs. α for $Z = 50$ and $\psi = 1$ for boundary conditions type 1, 2 and 3	122
Figure 5.7:	Plot of k_σ (1 st buckling mode) vs. α for $Z = 100$ and $\psi = 1$	123
Figure 5.8:	$(k_{\sigma, min}$ for long panels - $k_{\sigma, min}$ for short panels) vs. Z for panels with $\alpha > 1$ and boundary conditions type 2	124
Figure 5.9:	$k_{\sigma, min}$ for different values of ψ and curvatures and for short cylindrically curved panels with boundary conditions type 2.....	125
Figure 5.10:	Buckling pattern for cylindrically curved panels with boundary conditions type 2 and with $\alpha = 1$ and $\psi = 1$	126
Figure 5.11:	Comparison between Eq. (3.4) and the numerical displacement field at $y = b/2$ for cylindrically curved panels with boundary conditions type 2 and with $\alpha = 1$ and $\psi = 1$	126
Figure 5.12:	Buckling pattern for cylindrically curved panels with boundary conditions type 2 and with α minimising k_σ and $\psi = 1$	127
Figure 5.13:	Comparison between Eq. (3.4) and the numerical displacement field at $y = b/2$ for cylindrically curved panels with boundary conditions type 2 and with α minimising k_σ and $\psi = 1$	127

Figure 5.14:	Buckling pattern for cylindrically curved panels with $Z=100$, with boundary conditions type 2 and with $\alpha=1$ and different loading conditions.....	128
Figure 5.15:	Buckling pattern for cylindrically curved panels with boundary conditions type 2 and with $\alpha=3$ and different curvature.....	129
Figure 5.16:	Comparison of numerical results assuming boundary conditions type 1, 2 and 3 and the Winter curve (pure compression).....	134
Figure 5.17:	Comparison of numerical results assuming boundary conditions type 1, 2 and 3 and the Tran's <i>et al.</i> (2010) proposal for $Z=50$ (pure compression).....	135
Figure 5.18:	Influence of loading type for $\lambda=0.5$	135
Figure 5.19:	Influence of loading type for $\lambda=1$	136
Figure 5.20:	Influence of loading type for $\lambda=1.5$	136
Figure 5.21:	Influence of loading type for $\lambda=2$	137
Figure 5.22:	Influence of loading type for $\lambda=2.5$	137
Figure 5.23:	Influence of loading type for $\lambda=3$	138
Figure 5.24:	Numerical results for the resistance reduction factor for $\psi=1$	139
Figure 5.25:	Numerical results for the resistance reduction factor for $\psi=-1$	140
Figure 5.26:	Relation between curvature and the resistance reduction factor for $\psi=1$	140
Figure 5.27:	Relation between curvature and the resistance reduction factor for $\psi=-1$	141

Figure 5.28:	Validation of the limit for the curvature parameter in EN1993-1-5:2006, $\psi=1$	143
Figure 5.29:	Validation of the limit for the curvature parameter in EN1993-1-5:2006, $\psi=-1$	143
Figure 5.30:	Definition of θ_{bl}	145
Figure 5.31:	Ultimate load factor for cylindrically curved panels under biaxial loading (geometric imperfections applied inwards and $\theta_{bl}=\pi/4$).....	146
Figure 5.32:	Ultimate load factor for cylindrically curved panels under biaxial loading (geometric imperfections applied outwards and $\theta_{bl}=\pi/4$).....	146
Figure 5.33:	Out-of-plane displacement of a cylindrically curved panel with geometric imperfections applied inwards ($Z=10$ and $b/t=100$).....	147
Figure 5.34:	Out-of-plane displacement of a cylindrically curved panel with geometric imperfections applied outwards ($Z=10$ and $b/t=100$).....	148
Figure 5.35:	Ultimate load factor for cylindrically curved panels under biaxial loading (geometric imperfections applied outwards <i>vs.</i> geometric imperfections applied outwards; $\theta_{bl}=\pi/4$ and $b/t=65$).....	149
Figure 5.36:	Ultimate load factor for cylindrically curved panels under biaxial loading (geometric imperfections applied outwards <i>vs.</i> geometric imperfections applied outwards; $\theta_{bl}=\pi/4$ and $b/t=45$).....	149
Figure 5.37:	Ultimate load factor for cylindrically curved panels under biaxial loading ($Z=1$).....	150
Figure 5.38:	Ultimate load factor for cylindrically curved panels under biaxial loading ($Z=10$).....	150

Figure 5.39:	Ultimate load factor for cylindrically curved panels under biaxial loading ($Z=50$).....	151
Figure 5.40:	Ultimate load factor for cylindrically curved panels under biaxial loading ($Z=100$).....	151
Figure 5.41:	Ultimate load factor for cylindrically curved panels under biaxial loading ($Z=9$ and $b/t=65$).....	152
Figure 6.1:	Buckling modes for a cylindrically curved panel with $Z=50$ and $\alpha=2$	158
Figure 6.2:	Shape of buckling mode 2 at $b/2$ for a cylindrically curved panel with $Z=50$ and $\alpha=2$	159
Figure 6.3:	Definition of l_{Lw} and l_{Tw}	159
Figure 6.4:	Examples of “unrealistic” imperfection shapes according to previously defined criteria.....	161
Figure 6.5:	Realistic vs. unrealistic shapes for $Z=40$	163
Figure 6.6:	Realistic vs. unrealistic shapes for $Z=100$	163
Figure 6.7:	Load-displacement curves (end-shortening) curves $Z=10$	164
Figure 6.8:	Load-displacement curves (end-shortening) curves $Z=30$	165
Figure 6.9:	Load-displacement curves (end-shortening) curves $Z=50$	166
Figure 6.10:	Load-displacement curves (end-shortening) curves $Z=100$	167
Figure 6.11:	Load-displacement curve (end-shortening) curves $Z=10$ (<i>worst case scenario: $\alpha=3.6$ (6.6LW_1TW)</i>).....	168
Figure 6.12:	Load-displacement curve (end-shortening) curves $Z=30$ (<i>worst case scenario: $\alpha=4.4$ (8.8LW_1TW)</i>).....	169
Figure 6.13:	Load-displacement curve (end-shortening) curves $Z=50$ (<i>worst case scenario: $\alpha=3.8$ (8.8LW_1TW)</i>).....	169
Figure 6.14:	Load-displacement curve (end-shortening) curves $Z=100$ (<i>worst case scenario: $\alpha=2.0$ (2.2LW_1TW)</i>).....	170

- Figure 6.15: Imperfection amplitude *vs.* ultimate load factor for $Z=10$ and $\alpha=1.0$ (imperfection shapes 1.1LW_1TW and 1.1LW_2TW).....172
- Figure 6.16: Imperfection amplitude *vs.* ultimate load factor for $Z=10$ and $\alpha=1.0$ (imperfection shapes 2.2LW_1TW and 2.2LW_2TW).....172
- Figure 6.17: Imperfection amplitude *vs.* ultimate load factor for $Z=10$ and $\alpha=1.0$ (imperfection shapes 3.3LW_1TW and 3.3LW_2TW).....173
- Figure 6.18: Imperfection amplitude *vs.* ultimate load factor for $Z=10$ and $\alpha=1.0$ (imperfection shapes 3.3LW_1TW and 3.3LW_2TW).....173
- Figure 6.19: Imperfection amplitude *vs.* ultimate load factor for $Z=30$ and $\alpha=1.0$ (imperfection shapes 1.3LW_1TW and 1.1LW_2TW).....174
- Figure 6.20: Imperfection amplitude *vs.* ultimate load factor for $Z=30$ and $\alpha=1.0$ (imperfection shapes 2.2LW_1TW and 2.2LW_2TW).....175
- Figure 6.21: Imperfection amplitude *vs.* ultimate load factor for $Z=30$ and $\alpha=1.0$ (imperfection shapes 3.3LW_1TW and 3.3LW_2TW).....175
- Figure 6.22: Imperfection amplitude *vs.* ultimate load factor for $Z=30$ and $\alpha=1.0$ (imperfection shapes 4.4LW_1TW and 4.4LW_2TW).....176
- Figure 6.23: Imperfection amplitude *vs.* ultimate load factor for $Z=30$ and $\alpha=1.0$ (imperfection shapes 5.5LW_1TW).....176
- Figure 6.24: Imperfection amplitude *vs.* ultimate load factor for $Z=50$ and $\alpha=1.0$ (imperfection shapes 1.3LW_1TW and 1.1LW_2TW).....177
- Figure 6.25: Imperfection amplitude *vs.* ultimate load factor for $Z=50$ and $\alpha=1.0$ (imperfection shapes 2.2LW_1TW and 2.2LW_2TW).....178
- Figure 6.26: Imperfection amplitude *vs.* ultimate load factor for $Z=50$ and $\alpha=1.0$ (imperfection shapes 3.3LW_2TW and 3.5LW_2TW).....178
- Figure 6.27: Imperfection amplitude *vs.* ultimate load factor for $Z=50$ and $\alpha=1.0$ (imperfection shapes 4.4LW_1TW and 4.4LW_2TW).....179
- Figure 6.28: Imperfection amplitude *vs.* ultimate load factor for $Z=50$ and $\alpha=1.0$ (imperfection shapes 5.5LW_1TW).....179

Figure 6.29:	Imperfection amplitude <i>vs.</i> ultimate load factor for $Z=100$ and $\alpha=1.0$ (imperfection shapes $1.5LW_1TW$ and $1.3LW_2TW$)180
Figure 6.30:	Imperfection amplitude <i>vs.</i> ultimate load factor for $Z=100$ and $\alpha=1.0$ (imperfection shapes $2.2LW_1TW$ and $2.2LW_2TW$)181
Figure 6.31:	Imperfection amplitude <i>vs.</i> ultimate load factor for $Z=100$ and $\alpha=1.0$ (imperfection shapes $5.5LW_2TW$)181
Figure 6.32:	General trend of the ultimate load factor with the geometric imperfections' amplitude182
Figure 6.33:	General trend of the ultimate load factor with the number of transverse half-waves184
Figure 6.34:	General trend of the ultimate load factor with the number of longitudinal half waves184
Figure 6.35:	Ultimate load factor for a cylindrically curved panel with $Z=30$ and $\alpha=4.8$185
Figure 6.36:	Distribution of the frequency of buckling modes corresponding to minimum values for the ultimate load factor (all aspect ratios)186
Figure 6.37:	Distribution of the frequency of buckling modes corresponding to minimum values for the ultimate load factor (panels with $\alpha \leq 1.0$)187
Figure 6.38:	Distribution of the frequency of buckling modes corresponding to minimum values for the ultimate load factor (panels with $1.2 \leq \alpha \leq 2.4$)187
Figure 6.39:	Distribution of the frequency of buckling modes corresponding to minimum values for the ultimate load factor (panels with $2.6 \leq \alpha \leq 5.0$)188

Figure 6.40:	Minimum values of the ultimate load factor for models with $b/t=100, 150$ and 200 and maximum amplitude of the imperfection shape based on Eq. (6.1).....	189
Figure 7.1:	Degrees-of-freedom considered in the analysis	195
Figure 7.2:	Comparison between numerical results of elastic critical stress and Eq. (7.22) for $Z=0$ and BC3	200
Figure 7.3:	Comparison between numerical results of elastic critical stress and Eq. (7.22) for $Z=5$ and BC3	200
Figure 7.4:	Comparison between numerical results of elastic critical stress and Eq. (7.22) for $Z=10$ and BC3.....	201
Figure 7.5:	Comparison between numerical results of elastic critical stress and Eq. (7.22) for $Z=40$ and BC3.....	201
Figure 7.6:	Comparison between numerical results of elastic critical stress and Eq. (7.22) for $Z=100$ and BC3.....	202
Figure 7.7:	Comparison between numerical results of elastic critical stress and Eq. (7.25) for BC3.....	203
Figure 7.8:	Comparison between numerical results of elastic critical stress and Eq. (7.37) for $Z=0$ and BC2	205
Figure 7.9:	Comparison between numerical results of elastic critical stress and Eq. (7.37) for $Z=5$ and BC2	206
Figure 7.10:	Comparison between numerical results of elastic critical stress and Eq. (7.37) for $Z=10$ and BC2.....	206
Figure 7.11:	Comparison between numerical results of elastic critical stress and Eq. (7.37) for $Z=40$ and BC2.....	207
Figure 7.12:	Comparison between numerical results of elastic critical stress and Eq. (7.37) for $Z=100$ and BC2.....	207

Figure 7.13:	Comparison between numerical results of elastic critical stress and analytical results obtained from minimising Eq. (7.37) with respect to the aspect ratio for BC2.....	208
Figure 7.14:	Comparison between numerical results of elastic critical stress and analytical results from energy formulations with extra degrees-of-freedom for $Z=0$ and BC3.....	209
Figure 7.15:	Comparison between numerical results of elastic critical stress and analytical results from energy formulations with extra degrees-of-freedom for $Z=5$ and BC3.....	209
Figure 7.16:	Comparison between numerical results of elastic critical stress and analytical results from energy formulations with extra degrees-of-freedom for $Z=10$ and BC3.....	210
Figure 7.17:	Comparison between numerical results of elastic critical stress and analytical results from energy formulations with extra degrees-of-freedom for $Z=40$ and BC3.....	210
Figure 7.18:	Comparison between numerical results of elastic critical stress and analytical results from energy formulations with extra degrees-of-freedom for $Z=100$ and BC3.....	211
Figure 7.19:	Comparison between numerical results of elastic critical stress and analytical results from energy formulations with extra degrees-of-freedom for $Z=100$ (short cylindrically curved panels) and BC3.....	211
Figure 7.20:	Comparison between numerical results of elastic critical stress and analytical results from energy formulations with extra degrees-of-freedom for $Z=0$ and BC2.....	213
Figure 7.21:	Comparison between numerical results of elastic critical stress and analytical results from energy formulations with extra degrees-of-freedom for $Z=5$ and BC2.....	213

Figure 7.22:	Comparison between numerical results of elastic critical stress and analytical results from energy formulations with extra degrees-of-freedom for $Z=10$ and BC2.....	214
Figure 7.23:	Comparison between numerical results of elastic critical stress and analytical results from energy formulations with extra degrees-of-freedom for $Z=40$ and BC2.....	214
Figure 7.24:	Comparison between numerical results of elastic critical stress and analytical results from energy formulations with extra degrees-of-freedom for $Z=100$ and BC2.....	215
Figure 7.25:	Comparison between numerical results of elastic critical stress and analytical results from energy formulations with extra degrees-of-freedom for $Z=100$ (short cylindrically curved panels) and BC2.....	215
Figure 8.1:	k_{σ} , proposed Eq. (8.6) curves for $\psi=1$, $\psi=0$, $\psi=-0.7$ and $\psi=-1$	222
Figure 8.2:	Correlation of the proposed formulae (Eq. (8.6)) for short cylindrically curved panels with numerical results (normalised values).....	222
Figure 8.3:	Correlation of the proposed formulae (Eq. (8.7)) for short cylindrically curved panels with numerical results (normalised values).....	226
Figure 8.4:	Correlation of the proposed formulae (Eq. (8.8)) for short cylindrically curved panels with numerical results (normalised values).....	227
Figure 8.5:	Comparison between Stowell's and Domb & Leigh's formula and proposed formulae in Eq. (8.6) and (8.7).....	229
Figure 8.6:	Comparison between χ - λ and ρ - λ approaches for $\psi=-1$	230
Figure 8.7:	Iterative procedure to compute the width reduction factor ρ	231

Figure 8.8:	Generic output of proposed method	232
Figure 8.9:	Tran <i>et al.</i> (2010) expression for the length of the initial plateau, $\lambda_{0,z}$ ($\psi=1$)	234
Figure 8.10:	Calibration of parameters in Eq. (8.18) for the length of the initial plateau, $\lambda_{0,z}$ ($\psi=-1$)	234
Figure 8.11:	Comparison between numerical results and proposed formulae for $Z=10$ and $b/t=100$	238
Figure 8.12:	Comparison between numerical results and proposed formulae for $Z=30$ and $b/t=100$	238
Figure 8.13:	Comparison between numerical results and proposed formulae for $Z=50$ and $b/t=100$	239
Figure 8.14:	Comparison between numerical results and proposed formulae for $Z=100$ and $b/t=100$	239
Figure 8.15:	Correction factor for long cylindrically curved panels, C_{ult}	240
Figure 8.16:	$\rho_{long,num,Eq.(6.1)}/\rho_{long,proposed}$ for $b/t=100$	242
Figure 8.17:	$\rho_{long,num,Eq.(6.1)}/\rho_{long,proposed}$ for $b/t=150$	242
Figure 8.18:	$\rho_{long,num,Eq.(6.1)}/\rho_{long,proposed}$ for $b/t=200$	243
Figure 8.19:	$\rho_{long,num,Eq.(6.2)}/\rho_{long,proposed}$ for $b/t=100$	243
Figure 8.20:	$\rho_{long,num,Eq.(6.2)}/\rho_{long,proposed}$ for $b/t=150$	244
Figure 8.21:	$\rho_{long,num,Eq.(6.2)}/\rho_{long,proposed}$ for $b/t=200$	244
Figure 8.22:	Correlation of the proposed formulae with FEM results for pure compression (normalised values)	246
Figure 8.23:	Correlation of the proposed formulae with FEM results for pure in-plane bending (normalised values)	247
Figure 8.24:	Correlation of Eq. (8.22) with FEM results for $-1 \leq \psi \leq 1$ (normalised values)	249

Figure 8.25:	Correlation of Eq. (8.22) with FEM results for $\psi=0.5$ (normalised values).....	250
Figure 8.26:	Correlation of Eq. (8.22) with FEM results for $\psi=0$ (normalised values).....	251
Figure 8.27:	Correlation of Eq. (8.22) with FEM results for $\psi=-0.5$ (normalised values).....	251
Figure 8.28:	Comparison between curves proposed by Tran <i>et al.</i> (2012), Tran (2012) and proposed formulae for $Z=10$ and $\psi=1$	254
Figure 8.29:	Comparison between curves proposed by Tran <i>et al.</i> (2012), Tran (2012) and proposed formulae for $Z=30$ and $\psi=1$	254
Figure 8.30:	Comparison between curves proposed by Tran <i>et al.</i> (2012), Tran (2012) and proposed formulae for $Z=50$ and $\psi=1$	255
Figure 8.31:	Comparison between curves proposed by Tran <i>et al.</i> (2012), Tran (2012) and proposed formulae for $Z=100$ and $\psi=1$	255
Figure 8.32:	Design flowchart for cross-sections built-up with cylindrically curved panels.....	259
Figure 8.33:	Generic cross-section under analysis	260
Figure 8.34:	Generic effective cross-section for $\psi=1$ and $\psi=-1$	262
Figure 8.35:	Internal effective widths according to EN1993-1-5:2006 (CEN, 2006a)	263
Figure 8.36:	Evolution of the utilisation factor according to Eq. (8.24) with the increase of the curvature of the bottom flange.....	265

List of tables

Table 3.1:	Values of the minimum buckling coefficient, $k_{\sigma,min}$, for different types of boundary conditions (adapted from Bijlaard, 1957)	46
Table 3.2:	Values of the buckling coefficient, k_{σ} , for different types of in-plane loading (adapted from Timoshenko & Gere, 1961).....	46
Table 3.3:	Values of $k_{\sigma,min}$ for plates under biaxial loading	53
Table 3.4:	Definition of ρ_x and ρ_z and interaction values φ , φ_1 and φ_2 in Eq. (3.31) according to several authors.....	70
Table 3.5:	Values of α_z (Tran <i>et al.</i> , 2012)	75
Table 4.1:	Material properties	91
Table 4.2:	Mesh convergence study for LBA	95
Table 4.3:	Mesh convergence study for GMNIA.....	96
Table 4.4:	Validation of flat models for LBA.....	100
Table 4.5:	Validation of cylindrically curved models under uniform compressive stresses for LBA	101
Table 4.6:	Comparison between numerical results and EN1993-1-5:2006, $\psi=1$ (imperfection amplitude equal to $b/200$)	103
Table 4.7:	Comparison between numerical results and EN1993-1-5:2006, $\psi=-1$ (imperfection amplitude equal to $b/200$).....	103

Table 4.8:	1 st justification for the utilisation of the curvature parameter, $\psi=1$	109
Table 4.9:	1 st justification for the utilisation of the curvature parameter, $\psi=0$	110
Table 4.10:	1 st justification for the utilisation of the curvature parameter, $\psi=-1$	110
Table 4.11:	2 nd justification for the utilisation of the curvature parameter, $\psi=1$	111
Table 4.12:	2 nd justification for the utilisation of the curvature parameter, $\psi=0$	111
Table 4.13:	2 nd justification for the utilisation of the curvature parameter, $\psi=-1$	112
Table 5.1:	Parametric study on the elastic buckling behaviour of cylindrically curved panels	117
Table 5.2:	Comparison between boundary conditions type 1, 2 and 3 (values of the elastic critical stress for $\alpha=1$ and $\psi=1$).....	118
Table 5.3:	Differences between short and long panels with boundary conditions type 2	123
Table 5.4:	Parametric study on the ultimate behaviour of cylindrically curved panels.....	131
Table 5.5:	Comparison between boundary conditions type 1, 2 and 3 (values of the ultimate strength for $\psi=1$ and $\lambda=1$)	133
Table 5.6:	Comparison between boundary conditions type 1, 2 and 3 (values of the ultimate strength for $\psi=1$ and $\lambda=2$)	133
Table 5.7:	Comparison between boundary conditions type 1, 2 and 3 (values of the ultimate strength for $\psi=1$ and $\lambda=3$)	133
Table 5.8:	Validation of the limit for the curvature parameter in EN1993-1-5:2006 ($\psi=1$)	142

Table 5.9:	Validation of the limit for the curvature parameter in EN1993-1-5:2006 ($\psi=-1$).....	142
Table 5.10:	Parametric study on the ultimate behaviour of cylindrically curved panels under biaxial loading.....	144
Table 6.1:	Range of the imperfect sensitivity study parametric study.....	157
Table 6.2:	Amplitudes based on Eqs. (6.1) and (6.2) for each buckling shape presented in Figure 6.15 to Figure 6.18 ($Z=10$ and $\alpha=1.0$).....	171
Table 6.3:	Amplitudes based on Eqs. (6.1) and (6.2) for each buckling shape presented in Figure 6.19 to Figure 6.23 ($Z=30$ and $\alpha=1.0$).....	174
Table 6.4:	Amplitudes based on Eqs. (6.1) and (6.2) for each buckling shape presented in Figure 6.24 to Figure 6.28 ($Z=50$ and $\alpha=1.0$).....	177
Table 6.5:	Amplitudes based on Eqs. (6.1) and (6.2) for each buckling shape presented in Figure 6.29 to Figure 6.31 ($Z=100$ and $\alpha=1.0$).....	180
Table 8.1:	Elastic buckling coefficient for short cylindrically curved panels.....	221
Table 8.2:	a_i , b_i , c_i and d_i coefficients.....	221
Table 8.3:	Statistical evaluation concerning the ratios $k_{\sigma, \text{proposed Eq. (8.6)}}/k_{\sigma, \text{num}}$ for short cylindrically curved panels (normalised values).....	223
Table 8.4:	Statistical evaluation concerning the ratios $k_{\sigma, \text{proposed Eq. (8.6)}}/k_{\sigma, \text{num}}$; $k_{\sigma, \text{Stowell}}/k_{\sigma, \text{num}}$ and $k_{\sigma, \text{Domb\&Leigh}}/k_{\sigma, \text{num}}$ for short cylindrically curved panels subjected only to pure compression (normalised values).....	223
Table 8.5:	Statistical evaluation concerning the ratios $k_{\sigma, \text{proposed Eq. (8.7)}}/k_{\sigma, \text{num}}$ for short cylindrically curved panels (normalised values).....	226

Table 8.6:	Statistical evaluation concerning the ratios $k_{\sigma,proposed Eq. (8.8)}/k_{\sigma,num}$ for short cylindrically curved panels (normalised values).....	227
Table 8.7:	Comparison between Stowell's and Domb & Leigh's formula and proposed formulae in Eq. (8.6) and (8.7).....	228
Table 8.8:	Values of numerical parameters α_z , c_z and S_z for pure compression ($\psi=1$).....	235
Table 8.9:	Values of numerical parameters α_z , c_z and S_z for pure in-plane bending ($\psi=-1$).....	235
Table 8.10:	Values of ϕ_1 , ϕ_2 and ϕ_3	236
Table 8.11:	Comparison between the minimum numerical values ($b/t=100$) and the proposed formulae.....	237
Table 8.12:	Correction factor for long cylindrically curved panels, C_{ult}	240
Table 8.13:	Summarised results from Figure 8.16 to Figure 8.21.....	241
Table 8.14:	Statistical evaluation concerning the ratios $\rho_{proposed}/\rho_{Num}$, for pure compression (normalised values).....	246
Table 8.15:	Statistical evaluation concerning the ratios $\rho_{Tran et al. (2012)}/\rho_{Num}$, ρ_{Tran}/ρ_{Num} $\rho_{Tran et al. (2014)}/\rho_{Num}$ for pure compression (normalised values).....	246
Table 8.16:	Statistical evaluation concerning the ratios $\rho_{proposed}/\rho_{Num}$ for pure in-plane bending (normalised values).....	247
Table 8.17:	Statistical evaluation concerning the ratios $\eta_{1,Eq. (8.22)}/\eta_{1,Num}$, $-1 \leq \psi \leq 1$ (normalised values).....	250
Table 8.18:	Statistical evaluation concerning the ratios $\chi_{Eq. (8.22)}/\chi_{Num}$, $-1 \leq \psi \leq 1$ (normalised values).....	252
Table 8.19:	Comparison between the approaches by Tran <i>et al.</i> (2012), Tran (2012) and proposed formulae for $\lambda=1$ and $\psi=1$	256

Table 8.20:	Comparison between the approaches by Tran <i>et al.</i> (2012), Tran (2012) and proposed formulae for $\lambda=2$ and $\psi=1$	256
Table 8.21:	Comparison between the approaches by Tran <i>et al.</i> (2012), Tran (2012) and proposed formulae for $\lambda=3$ and $\psi=1$	257
Table 8.22:	Comparison between the approach by Tran <i>et al.</i> (2014) and proposed formulae	257
Table 8.23:	Cross-section dimensions	261
Table 8.24:	Gross cross-sectional properties	262
Table 8.25:	Cylindrically curved panel reduction factors for $\psi=1$	263
Table 8.26:	Cylindrically curved panel reduction factors for $\psi=-1$	263
Table 8.27:	Effective cross-sectional properties for $\psi=1$	264
Table 8.28:	Effective cross-sectional properties for $\psi=-1$	264
Table 8.29:	Utilisation factor according to Eq. (8.24) for different load cases	265
Table 8.30:	Normalised utilisation factor according to Eq. (8.24) for different load cases	266

1. Introduction

1.1. Motivation and statement of the problem

The substantiation of this dissertation starts with a very simple statement: there are few design rules (in fact, there is no European standard in the framework of the Eurocodes), design recommendations/guidelines or any other background document (at least relevant enough) allowing an accurate design of curved steel panels in the civil & structural engineering field, namely transversally curved steel panels for structural application. This gap gains a bigger dimension and importance when more and more frequently this type of structural solution is employed in the design of important infrastructures like viaducts and bridges. Therefore, it brings to the structural safety and reliability context an important (and also interesting) issue: Behaviour of cylindrically curved panels under in-plane stresses.

In particular, the work presented herein will show that besides the omission of design methodologies for curved panels by structural Eurocodes, other standards fail to accurately describe the elastic critical and ultimate behaviour of cylindrically curved panels under specific loading and boundary conditions whenever they fall outside their scope of application.

Firstly, the structural Eurocodes do not cover the design of cylindrically curved panel segments. In fact, the scope of EN1993-1-5:2006 (CEN, 2006a) is limited to flat shell elements (or plates). The criterion used in EN1993-1-5:2006 to define a plated element as flat corresponds to the limitation of the plate's curvature to a maximum value given by

$$\frac{b^2}{R.t} < 1 \quad (1.1)$$

where b is the plate's width, R is the radius of curvature of the element and t is the plate's thickness. Similar criteria exist in other codes of practice such as BS5400-3 (BSI, 2000) that limits the curvature to

$$\frac{b^2}{R.t} < \frac{1}{2} \quad (1.2)$$

In addition, EN1993-1-6:2007 (CEN, 2007) is not applicable to this type of elements since its scope is limited to shells of revolution.

Secondly, in the oil & gas industry and offshore construction there are some design recommendations to assess the buckling strength of shells and curved panels: DNV-RCP-202 (DNV, 2010*b*) and the ABS Guide for Buckling and Ultimate Strength Assessment for Offshore Structures (ABS, 2004) to name a few. However, these standards are restricted to very specific boundary conditions and the buckling of cylindrically curved panels is seen as a possible local failure mode of a global structural system: the orthogonally stiffened cylinder.

Thirdly, the aeronautical and aerospace industry has been continuously putting serious effort into the scientific research of the mechanical properties and structural response of cylindrically curved panels used for lightweight flight vehicles and their components under several loading arrangements. There are some accepted and commonly used procedures, namely the so-called *NACA design curves*, but, as some researchers have been claiming in their research outcomes, they are outdated (Nemeth, 1998; Domb & Leigh, 2001).

Finally, over the past years several studies have been performed (Domb & Leigh, 2001; Domb & Leigh, 2002; Domb, 2002; Featherston & Ruiz, 1998; Featherston, 2000; Featherston, 2003; Featherston, 2012; Tran, 2012; Tran *et al.*, 2012; Tran *et al.*, 2014), but none of these authors have dealt comprehensively with different aspects of cylindrically curved panels, namely, different loading arrangements other than pure compression (from pure compression to pure in-plane bending and biaxial compression) and imperfection sensitivity (shapes and amplitudes). Concerning a methodology to assess the safety level

of cross-sections built-up with cylindrically curved panels, the research presented in this work is completely new.

1.2. The use of curved steel in structural applications

1.2.1. Structural curved steel panels in building applications

The use of curved steel is not a novelty, but its use has grown in recent years. The first use of curved structural steel was limited to bar elements that were mainly employed in roof structures as grid-shells (Figure 1.1 and Figure 1.2 *a*).



Figure 1.1: Diagrid Shell by Vladimir Shukhov during construction, Russia (unknown author, 1897)

In recent years, curved shapes are present in almost every bold architectural design, either as reinvented grid-shells, like the roof structure of the British Museum by Foster and Partners (Figure 1.3), or in futuristic uses of curved stainless steel panels, like the urban sculpture *Cloud Gate* by Anish Kapoor (Figure 1.4).

The use of curved stainless steel panels is also employed in the reconstruction of old buildings where curved shapes were also part of the original design, like the refurbishment of the Birmingham New Street Station by Foreign Office Architects (Figure 1.2 *b*).



Figure 1.2: *a)* New St. Station in Victorian Times, before redevelopment in the 1960's, Birmingham, England (unknown author, 1885) and *b)* New St. Station by FOA, as viewed from Stephenson St., Birmingham, England (Foreign Office Architects, 2009)



Figure 1.3: British Museum Great Court roof by Foster and Partners, London, England (Dunn, 2005)



Figure 1.4: Cloud Gate by Anish Kapoor, Chicago, United States of America (Ertürk, 2014)

1.2.2. Structural curved steel panels in bridge applications

Due to a variety of reasons, curved steel panels are also a popular choice in the design of structural elements of bridges all around the world.

Typically, horizontally curved bridges are a consequence of constraints in the longitudinal layout in plan (surrounding buildings in an urban context and/or terrain morphology constraints in other areas¹). However, the use of curved panels also offers aesthetic and cost benefits over more traditional structures even when the mentioned restrictions are inexistent or not important (Linzell *et al.*, 2004). As examples of horizontally curved bridges, Figure 1.5 shows the New Sheppey Bridge, England (horizontally curved steel I-girder which is an example of how morphology of terrain interfered with the bridge design) and the Zubizuri Bridge in Bilbao, Spain which is a bridge by the bridge engineer and architect Santiago Calatrava, known by his beautiful bridge designs (aesthetic criteria).

¹ Horizontally curved bridges “are often one of the few viable options at complicated interchanges or river crossings where limited site space or pier locations are available” (Linzell *et al.*, 2004).

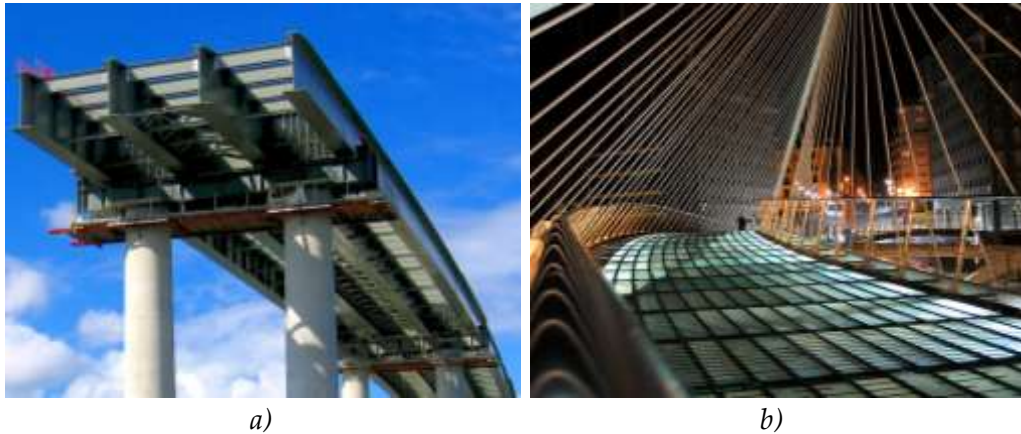


Figure 1.5: *a)* New Sheppey Bridge, England (unknown author, 2007) and *b)* Zubizuri Bridge in Bilbao, Spain (Lopez, 2007)

Another way in which curved panels are being employed as structural elements in steel bridges is in girders curved in elevation, *i.e.* with varying depth – deeper near to the supports and shallower at the middle of the spans. Examples of this use of curved steel are the bridge over Rio Ave in Portugal (Figure 1.6 *a)*), which is an I-girder with the bottom flange curved in elevation and the bridge over motorway IC19 in Portugal (Figure 1.6 *b)*), which is a box-girder bridge with a longitudinally stiffened bottom flange curved in elevation.



Figure 1.6: *a)* Bridge over Rio Ave, Portugal and *b)* Bridge over IC19 in Lisbon, Portugal (courtesy of Professor António Reis)



Figure 1.7: *a)* Bellows Falls Arch Bridge, New Hampshire, United States of America (unknown author, 1905²) and *b)* Pedro e Inês footbridge, Coimbra, Portugal (Correia, 2009)

In opposition to what was common practice in the past, when designing an arch bridge (where the arch was built-up with open iron or steel sections put together forming a truss), nowadays, some arch bridges are designed with curved steel panels which are part of closed sections of the arch.

Figure 1.7 shows examples of old and modern designs of arch bridges, highlighting the evolution between arch trusses to closed sections arches: the Bellows Arch Bridge (old arch bridge designed with open iron sections forming a curved truss which supports the deck) and the Pedro e Inês footbridge, which is a modern bridge design where the arch is made of rectangular steel box (closed) sections.

Finally, curved panels can be employed as transversally curved bottom flanges, as shown in Figure 1.8 and Figure 1.9. The reasons for this solution may be purely the aesthetic criteria as it is the example of the Chaves' Pedestrian Bridge in Portugal (Figure 1.8 *b)*) and/or due to the fact that the curved shape of the bottom flanges provide improved response to wind loads, as is the case of Stonecutters bridge in Hong Kong, China (Figure 1.9). The Renault Bridge

² End of construction date.

in France (Figure 1.8 *a*) is another example of a box-girder with a transversally curved bottom flange.



Figure 1.8: *a*) Renault Bridge, France (Tran *et al.*, 2012) and *b*) Pedestrian Bridge in Chaves, Portugal (Ribeiro, 2008)

Stonecutters Bridge in Hong Kong, China, is a cable-stayed bridge with two main girders with curved bottom flanges. This curved shape of the bottom flanges of both box-girders was deliberately chosen considering the bridge performance with respect to the heavy wind impact and to the bridge overall aerodynamic behaviour (Janjic, 2008).

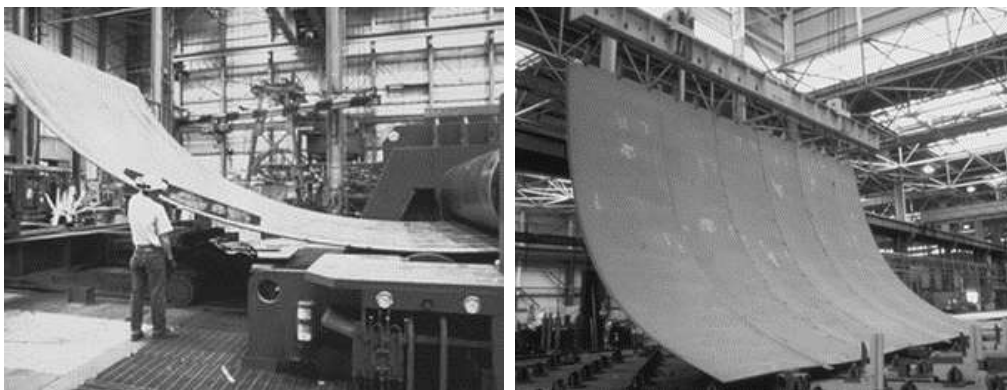


Figure 1.9: Stonecutters Bridge cross-section in Hong Kong, China (Vejrum, 2008)

1.2.3. Structural curved steel panels in offshore and naval applications

In offshore construction and ship building industry, curved steel panels are also a common structural solution. In fact, curved steel elements, namely curved steel panels are a requirement for the overall behaviour of ships and vessels (Figure 1.10) and other offshore structures like SPAR platforms (Figure 1.11).

In recent years, naval architects and engineers have spent a great amount of time discussing the structural performance of curved panels. This is patent in the increasingly number of references dealing with this topic in the *International Ship and Offshore Structures Congress* (Frieze & Sheno, 2006; Jang & Hong, 2009; Fricke & Bronsart, 2012) and in the *International Offshore and Polar Engineering Conference* (Chung *et al.*, 2008; Chung *et al.*, 2009).



a)

b)

Figure 1.10: a) Bending of steel sheet (Newport News Shipbuilding) and b) Welded steel plate forming part of a ship's hull (Newport News Shipbuilding)

1.2.4. Structural curved panels in aeronautical and aerospace applications

The aeronautical industry was, since from the beginning, the main driving force responsible for developments on the stability of curved shells and mainly segments of curved shells, like curved panels. The first papers dealing with

such phenomena were published mainly by mechanical and aerospace engineers and scientists (*e.g.* von Kármán) that were concerned with the buckling of plates and shells for flight vehicles applications. Nowadays, a great amount of effort is still being made to understand the behaviour of thin curved elements, mainly those made by new materials like carbon fibre and other composites. Figure 1.12 shows the results of numerical studies that were carried out to simulate the response of stiffened cylindrically curved panels to be applied in the Airbus 380 (Pardo & Fernandez, 2010).

Curved panels were also used in the famous space shuttle (Figure 1.13) that is now retired from service upon the conclusion of Atlantis' final flight on 21st of July in 2011 (NASA, n.d.).

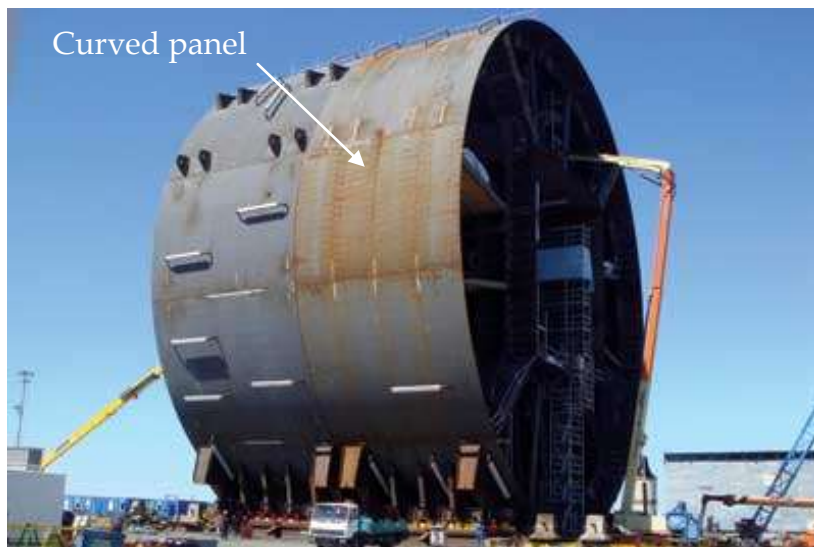


Figure 1.11: SPAR platform under construction (unknown author, 2010)

1.3. Objectives and scope

In this thesis special emphasis is given to cylindrically curved panels under in-plane loading. Specifically, this work aims at obtaining a clear perspective on the behaviour of cylindrically curved panels under general in-plane loading, different boundary conditions and on its structural design in the range of civil engineering applications.

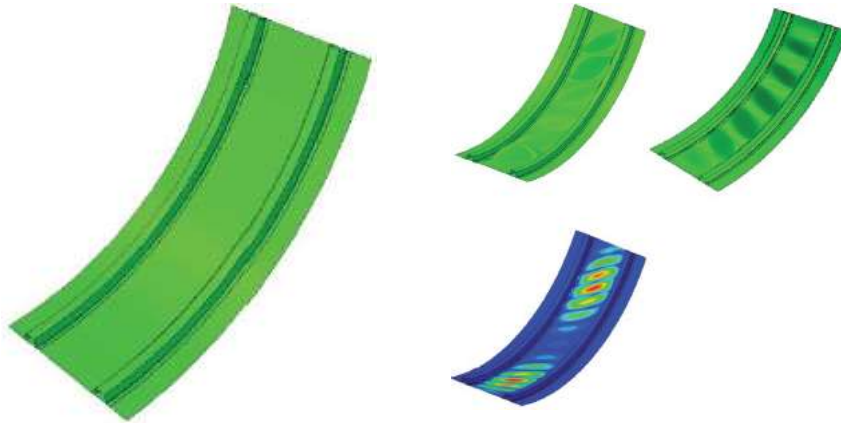


Figure 1.12: Numerical analysis of a cylindrical stiffened composite curved panel with two stiffeners for the Airbus 380 (Pardo & Fernandez, 2010)

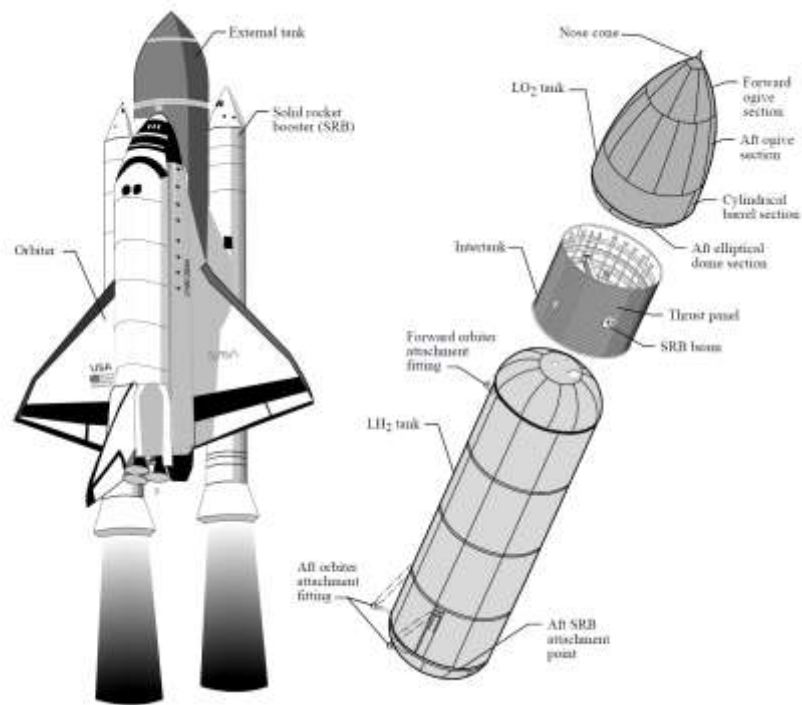


Figure 1.13: Space shuttle external tank components (Nemeth, 1998)

The global priorities of this research are, on one hand, important and valid numerical and analytical results, which can be used by all scientific community, and, on the other, a contribution to fill the present void in design rules at European level. Particularly, the following objectives are highlighted:

- To contribute to the development of the theoretical background in the buckling and postbuckling behaviour of cylindrically curved steel panels in the field of Structural & Civil Engineering;
- To elaborate a reliable numerical model to study the behaviour of cylindrically curved steel panels;
- To characterise the cylindrically curved panel's behaviour under pure compression to pure in-plane bending and biaxial loading;
- To characterise the sensitivity to geometric imperfections of cylindrically curved steel panels;
- Finally, to propose design guidance (effective width based formulae) allowing the designer to verify the resistance of sections built with cylindrically curved steel panels in a consistent and systematic way similarly to the design philosophy of the structural Eurocodes.

1.4. Thesis outline

This thesis is organised into 9 chapters dealing separately with different sub-topics: state-of-the-art revision, numerical and analytical studies, parametric studies, description of new approaches and conclusions.

Chapter 2 introduces the most important analytical concepts about the analysis of general thin elastic shells. It makes a revision of the most important shell theories giving special emphasis to those which are most likely to yield good results for cylindrically curved panels. Additionally, this chapter introduces important energy principles which will be the starting point of the energy formulation in Chapter 7.

Chapter 3 provides a concise overview of the overall stability behaviour (elastic critical behaviour, postbuckling behaviour and ultimate behaviour) of steel plates and cylindrically curved steel panels under several in-plane loading

(ranging from pure axial compression to pure in-plane bending, and from circumferential compression to biaxial loading). Important knowledge and terms about how these structural applications cope with the application of the referred loading are revisited making reference to earlier work whenever it is necessary.

Additionally, a brief description of the methods to assess the safety of plated steel structures and cylindrically curved steel panels proposed by selected standards (EN1993-1-5:2006, DNV-RP-C201 and DNV-RP-C202) is made.

Chapter 4 is dedicated to the description of the numerical analysis based on the finite element method. The numerical models are validated against previous results from related works. This chapter is intended to give all background information required for Chapters 5 and 6.

Chapter 5 is entirely devoted to the three parametric studies on the behaviour of cylindrically curved steel panels: the first on the elastic critical behaviour of panels under compressive stresses, the second on the ultimate strength of panels under pure compression and pure in-plane bending and the last one on the ultimate strength of panels under biaxial compression.

Chapter 6 presents a comprehensive study on the imperfection sensitivity of cylindrically curved panels. In this study conclusions are drawn on how both the pattern (reflecting buckling modes) and amplitudes of geometric imperfections affect the ultimate load of cylindrically curved steel panels.

Chapter 7 is reserved for the analytical study of the structural response of cylindrically curved panels. Here an energy formulation capable of predicting the elastic critical stress and the postbuckling behaviour of curved panels is presented. A new simple expression able to return the elastic critical stress of cylindrically curved panels under particular boundary conditions is obtained.

In Chapter 8, new methods for computing the elastic critical stress and the ultimate load of cylindrically curved panels are proposed. These are complemented by statistical studies where their accuracy is studied.

Later, the revisited works of some authors providing methods to compute the elastic critical stress and the ultimate load of cylindrically curved panels made in Chapter 3 are compared to the methods now developed.

Finally, in Chapter 9 a general summary of the work presented throughout this thesis is given and an outlook indicating some areas which have room for future research work is made.

2. Analysis of general thin elastic shells

2.1. Chapter overview

This chapter focuses on the behaviour and analysis of general thin elastic shells. It also aims at providing a literature review with a special emphasis on shell theories and methods of analysis of thin shells. Additionally, it introduces important energy related concepts that are required for Chapter 7.

Sec. 2.2 to sec. 2.5 introduces a brief review on thin shell theories. Some shells' definitions and basic assumptions are initially presented in sec. 2.2, complemented by an historical review of shell theories (linear, nonlinear and specialised theories). Then, in sec. 2.3 and in sec. 2.4, the constitutive relations and the stress resultants for thin elastic shells are presented. Finally, sec. 2.5 concludes with a concise enlightenment of the theories which are most likely able to predict the behaviour of curved plated elements: shallow shell theory and Donnell-Mushtari-Vlasov shell theory.

Sec. 2.6 and 2.7 describe some approximate methods of analysis of thin shells. Sec. 2.6 initiates with the description of the total potential energy function and with two important energy principles: the principle of stationary total potential energy and the principle of minimum total potential energy. Subsequently, in sec. 2.7, the Rayleigh-Ritz approximated method is described. Finally, the finite element method is also introduced and described.

Finally, sec. 2.8 summarises and highlights the most important concepts and makes clear the relation between them and concepts in subsequent chapters.

2.2. Brief review on shell theories

2.2.1. Shells as a structural solution

Shells as a structural solution are applied in many fields of engineering such as civil, aerospace, aeronautical, offshore and naval engineering. Additionally, thin shells feature prominently as a practical solution in specific branches of structural engineering such as bridge engineering (Tran *et al.*, 2012). The wide application of shell structures in engineering is justified by the following advantages (Ventsel & Krauthammer, 2001):

- Efficiency in load carrying performance;
- High strength *vs.* weight ratio, *i.e.* shell structures may be, from this point of view, optimal structures;
- High value from an architectural point of view, as shells can be harmoniously integrated in both urban and landscape contexts and areas.

However, shell structures are very slender structures presenting stability issues that must be taken into account when predicting its overall structural behaviour. As opposed to plates (Figure 2.1*a*), for the majority of shell structures the buckling resistance (Figure 2.1*b*) can be significantly lower than the theoretical elastic buckling load since shells are very sensitive to initial imperfections and its postbuckling behaviour is highly unstable.

In short, shell-like structures due to their curvature can support much more efficiently external loads than other structures, resulting in a much stronger and stiffer load resistant mechanism but present stability issues that must be taken into account during their analysis.

2.2.2. Definitions and fundamentals of thin shells

A thin shell is a thin-walled three-dimensional body for which one dimension (thickness, denoted by the letter t) is significantly lower than the other two

dimensions and is characterised by its non-plane initial shape (*i.e.* finite radius of curvature). The geometric space that sets at equal distances from the two surfaces of the shell is called middle surface.

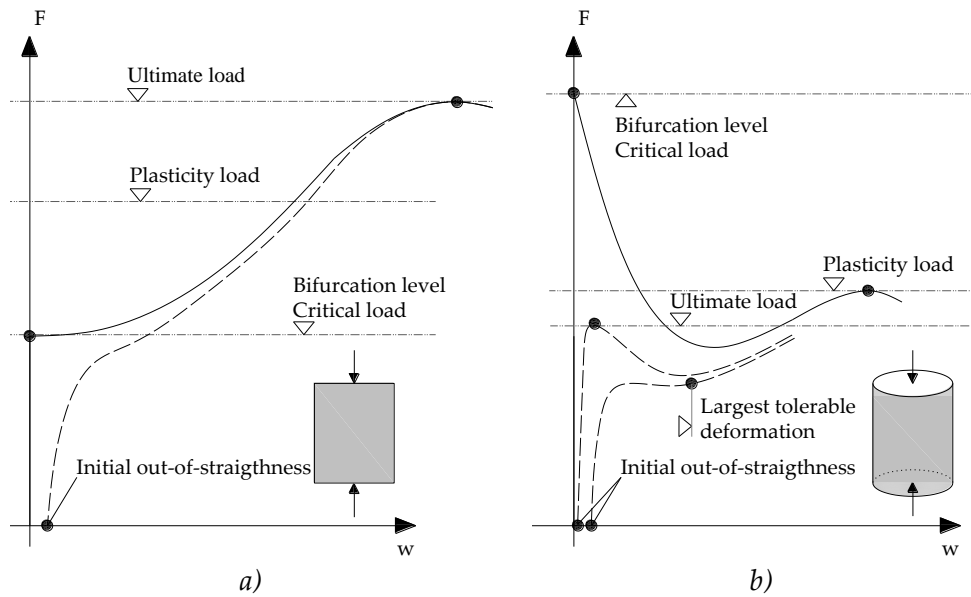


Figure 2.1: Postbuckling behaviour: *a)* plated structure and *b)* shell structure

In other words, shells have all the properties of plates plus curvature. Curvature is one of the most important parameters in shells' behaviour since depending on it a shell is classified as cylindrical, conical, spherical, ellipsoidal, and toroidal and torispherical (Samuelson & Eggwertz, 1992) and these different shapes, together with support conditions and constitutive law of the material, will determine the shell's response to external forces.

Additionally, at each point of the shell's middle surface there are two main directions of curvature mutually perpendicular. A locally reference coordinate system $Oxyz$ is defined so that the plane Oxy is tangent to the middle surface of the shell at the point considered and the z -axis is perpendicular to the middle surface. The Ox and Oy axes are oriented in the principal directions of curvature at the point considered, R_x and R_y being the principal radii of curvature according to x and y , respectively.

From another point of view, a shell may be classified as thin by the t/R ratio (where R denotes the radius of curvature of the middle surface). According to Novozhilov a shell that satisfies the following criteria can be considered as thin, otherwise shells should be considered thick (Novozhilov, 1959)

$$(t/R)_{\max} \leq 0.05 \quad (2.1)$$

Some authors (Samuelson & Eggwertz, 1992) agree that the previous inequality is insufficient and sets very roughly the frontier between thin and thick shells since it depends also upon the nature of the shells boundary conditions, external loads, etc.

2.2.3. Historical review on shell theories

In this sub-section a literature survey on shell theories is carried out. The most important theories are mentioned and categorised as linear, nonlinear and specialised shell theories. The diagram showed in Figure 2.2 summarises some interrelations between different shell theories and results from an extensive literature survey (Leissa, 1973; Brush & Almroth, 1975; Yamaki, 1984; Teng & Hong, 1998; Ventsel & Krauthammer, 2001; Teng & Rotter, 2004; Amabili, 2008; and Nemeth, 2013). It is highlighted that the number of works presenting specialised shell theories is high and, therefore, a decision was made to refer only those theories that might be useful throughout this thesis.

As already discussed in the previous sub-section, shells can be classified either as thin shells or thick shells. A calculation that considers the thickness into the analysis of the state-of-stress is very complex and time-consuming. That is the main reason why most common shell theories do not take into account the thickness, regarding, instead, the shell as a two-dimensional body (looking only to its middle surface) endowed with mechanical properties in the form of elastic resistance both stretching and bending actions within the surface (Calladine, 1983). Thus, the approach on thin shell theories is based on the reduction of the equations of elasticity from three to two dimensions (Calladine, 1983), *i.e.* the

deformations throughout the shell body are completely defined by deformations and changes in curvature of the geometry of the middle surface.

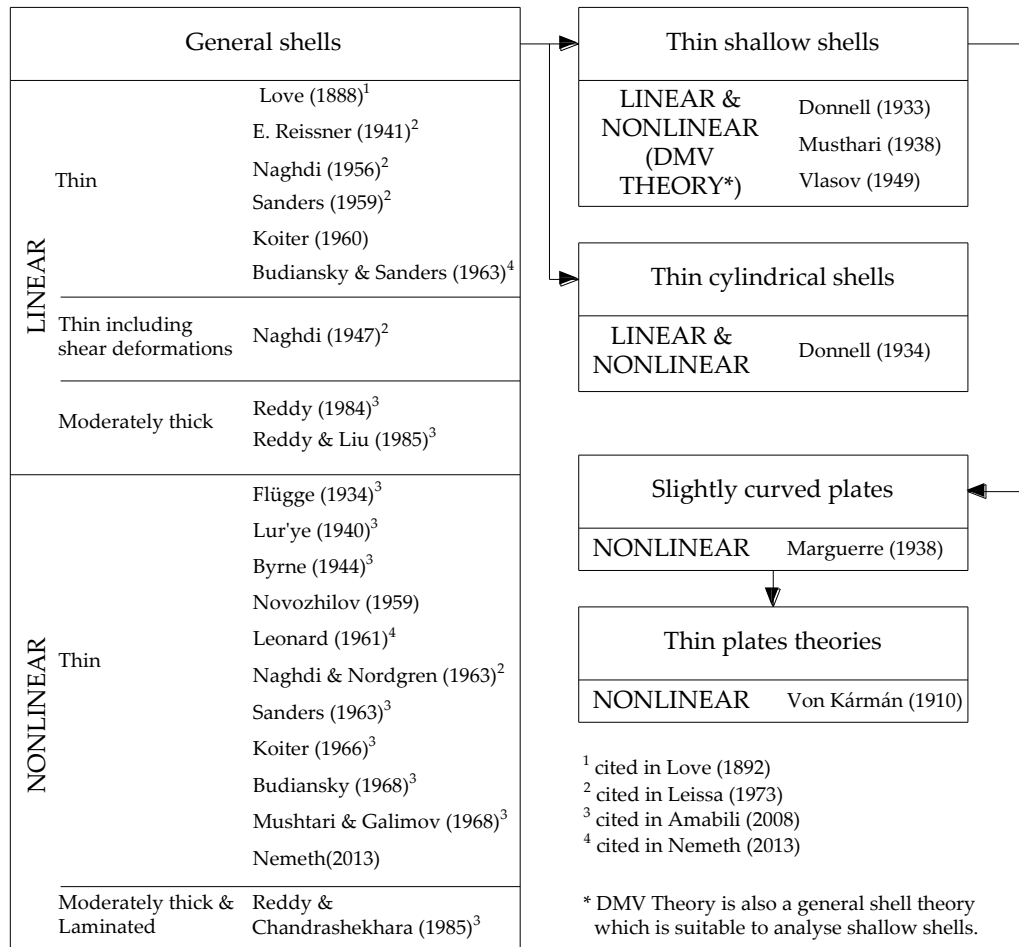


Figure 2.2: Historical perspective and interrelation of different shell theories

In the context of thin shells with constant thickness this simplification of the problem is based on Kirchhoff-Love hypothesis:

- Plane sections normal to the initial middle surface remain plane and normal to the deformed middle surface. This hypothesis implies that strains γ_{xz} and γ_{yz} are negligible;
- The transverse normal stress σ_z and strain ϵ_z are very small when com-

pared with other normal stresses and strains components and may be neglected.

The simplest shell theories are those which consider the shell as thin and are based upon linear elasticity concepts and on the simplifying Kirchhoff-Love hypothesis. Generally speaking, these theories are applicable whenever a shell presents small elastic deformations (*i.e.* equilibrium equations can be derived for the undeformed configuration neglecting displacements). These shell theories are called first-order-approximation³ linear thin shell theories. Among the researchers/authors that have developed linear thin shell theories are: Love in 1888, Reissner in 1941, Naghdi in 1956, Sanders in 1959, Koiter in 1960 and Budiansky and Sanders in 1963 (see Figure 2.2 for references).

In contrast to thin elastic shells, the analysis of thick elastic shells must include the effect of shear deformability. The simplest way of doing so is to continue to assume the shell as thin and only dropping the first Kirchhoff-Love hypothesis replacing it by the following:

- Plane sections normal to the initial middle surface remain plane but not necessarily normal to the deformed middle surface.

The theories derived under these assumptions are called second-order-approximation linear thin shell theories. Examples of this type of shell theories are works from: Naghdi in 1947 and Reissner in 1949 (see Figure 2.2 for references).

In the other hand, when the shell's thickness is of a magnitude that forces a three-dimensional analysis, both Kirchhoff-Love hypothesis are abandoned and the transverse shear deformations and normal stress effects are incorporated. Examples of this typology of shell theories are those proposed by Reddy in 1984 and by Reddy & Liu in 1985 (see Figure 2.2 for references).

³ In this work, the following definition will be used: "The order of a particular approximate theory will be established by the order of the terms in the thickness coordinate that are retained in the strain and constitutive equations" (p. 21, Baker *et al.*, 1972).

In short, unlike nonlinear shell theories, linear shell theories determine a unique position of equilibrium for any shell with given loading/boundary conditions. However, a shell under identical loading/boundary conditions may have several possible positions of equilibrium. In a very broad way, for a theory to be capable of predicting all the several equilibrium positions it has to include the nonlinear terms of the shell behaviour.

The “behaviour of an elastic shell is said to be nonlinear if, under static conditions, the deflection of any point of the shell is not proportional to the magnitude of an applied load” (p. 1, Libai & Simmonds, 2005). Two sources of nonlinearity can be identified: geometric and material. A theory that takes into account finite or large deformations is referred to as a geometrically nonlinear theory of thin shells (*i.e.* strain-displacement relations are nonlinear but the stress-strain relations are linear). Additionally, a shell may be materially nonlinear with respect to the stress–strain relations or present imperfections like lack of homogeneity and residual stresses.

Geometric nonlinearity manifests itself in the governing equations in two ways. Firstly, displacements strain components are related to displacements by means of nonlinear equations. Secondly, a shell element that experiences large variations in its shape with increasing deformation cannot set up equilibrium equations based on a non-deformed configuration as in the linear shell theory.

Large-displacement theory of thin plates originates mainly from von Kármán’s work (Von Kármán (1910), cited in Berger & Fife (1966)). Reissner in 1950 presented a nonlinear shell theory with a narrow field of application: symmetrical loaded shells of revolution. Novozhilov in 1953, Leonard in 1961, Naghdi & Nordgren in 1963, Sanders in 1963, Koiter in 1966, Budiansky in 1968, Mushtari & Galimov in 1968 and Nemeth in 2013, derived more general nonlinear theories (see Figure 2.2 for references).

At the same time general theories of thin shells were developed, several specialised theories (linear and nonlinear) including features of singular types of shells appeared. The reasons determining the scopes for each specialised shell theory are:

- The geometry of the shell;
- The support conditions;
- The deformation ranges of the middle surface;
- The type of loading, which together with the shell geometry and support conditions defines the state of stress of the shell.

Among others, examples of specialised shell theories are the membrane theory and the shallow shell theory.

Shallow shells are frequently referred to as curved plates. Marguerre in 1937 established the governing equations for plates having an initial curvature being, together with Vlasov in 1949, one of the first authors to work on shallow shells theories (see Figure 2.2 for references). Shallow shells can be analysed by a particular shell theory named after their authors: the Donnell-Vlasov-Mushtari theory (also known as DMV theory). It should be noted that DMV theory may also be applied to analyse non-shallow shells (see Figure 2.2 for references).

2.2.4. Types of state of stress of thin shells

When an analysis is carried out on a general linear theory assumption is assumed that bending stresses are of the same order as the membrane stresses. In some cases, due to the geometry, loading conditions and support system, it is possible to introduce simplifications that lead to distinct states of stress:

- When bending stresses are negligible compared to the membrane stresses the type of state of stress is called membrane state of stress. The governing equations of the membrane theory are obtained directly from the equations of the general shell theory by neglecting the effects of bending and twisting moments, as well as the transverse shear forces. One example of pure membrane state of stress is a hollow spherical shell subjected to internal and/or external uniform pressure;
- On the other hand, when the membrane stresses are negligible compared with the bending stresses the type of state of stress is referred to as pure flexural state of stress;

- If membrane and bending stresses are of the same order of magnitude the state of stress is called mixed state of stress. This state of stress often occurs near the edges of the shell.

It should be noted that “definitions of the ‘membrane’ and ‘pure flexural’ states of stress are not quite correct because the membrane state of stress admits an existence of small bending stresses and, in turn, small membrane stresses may occur in a pure flexural state of stress” (p. 346, Ventsel & Krauthammer, 2001).

2.3. Constitutive relations for thin elastic shells

The most general form of Hooke’s law is, for isotropic materials, given in three dimensions. In this case, as the object of this study is thin shells and remembering the previous assumption according to which $\sigma_z = 0$, Hooke’s law is only derived for the specific case of plane stress. Under these conditions, strains are obtained from stresses according to Eqs. (2.2) to (2.5)

$$\varepsilon_x = \frac{1}{E}(\sigma_x - \nu\sigma_y) \quad (2.2)$$

$$\varepsilon_y = \frac{1}{E}(\sigma_y - \nu\sigma_x) \quad (2.3)$$

$$\varepsilon_z = -\frac{\nu}{E}(\sigma_y + \sigma_x) \quad (2.4)$$

$$\gamma_{xy} = \frac{2(1+\nu)}{E}\tau_{xy} \quad (2.5)$$

Neglecting Eq. (2.4) and solving Eqs. (2.2), (2.3) and (2.5) in order to σ_x , σ_y and τ_{xy} , Hooke’s law returns

$$\sigma_x = \frac{E}{1-\nu^2}(\varepsilon_x + \nu\varepsilon_y) \quad (2.6)$$

$$\sigma_y = \frac{E}{1-\nu^2}(\varepsilon_y + \nu\varepsilon_x) \quad (2.7)$$

$$\tau_{xy} = \frac{E}{2(1+\nu)} \gamma_{xy} \quad (2.8)$$

Generally, the strains are divided into *membrane strains* and *bending strains* (or *changes in curvature*)⁴ as follows

$$\varepsilon_x = \varepsilon_{x,0} - z \left(\frac{1}{R_x} - \frac{1}{R'_x} \right) = \varepsilon_{x,0} - z\chi_x \quad (2.9)$$

$$\varepsilon_y = \varepsilon_{y,0} - z \left(\frac{1}{R_y} - \frac{1}{R'_y} \right) = \varepsilon_{y,0} - z\chi_y \quad (2.10)$$

$$\gamma_{xy} = \gamma_{xy,0} - 2z\chi_{xy} \quad (2.11)$$

Introducing Eqs. (2.9) to (2.11) into Eqs. (2.6) to (2.8) yields the stress-strain relations in terms of membrane and bending strains

$$\sigma_x = \frac{E}{1-\nu^2} \left[\varepsilon_{x,0} + \nu\varepsilon_{y,0} - z(\chi_x + \nu\chi_y) \right] \quad (2.12)$$

$$\sigma_y = \frac{E}{1-\nu^2} \left[\varepsilon_{y,0} + \nu\varepsilon_{x,0} - z(\chi_y + \nu\chi_x) \right] \quad (2.13)$$

$$\tau_{xy} = \frac{E}{2(1+\nu)} (\gamma_{xy,0} - 2z\chi_{xy}) \quad (2.14)$$

where $\varepsilon_{x,0}$, $\varepsilon_{y,0}$ and $\gamma_{xy,0}$ are the membrane strain components; and χ_x , χ_y and χ_{xy} are the changes in curvature or bending strains (always related to the middle surface of the shell).

2.4. Stress resultants for thin elastic shells

Figure 2.3 to Figure 2.4 represent a thin shell element for which two principal directions are defined (which are orthogonal one to each other), each point of its middle surface establishing a coordinate plane, Oxy , tangent to the shell's

⁴ A complete description and deduction of these expressions is made by Ugural (1981).

middle surface. This thin shell element is in equilibrium under the applied forces (p_x , p_y and p_z) and the internal stresses (σ_x , σ_y , $\tau_{xy}=\tau_{yx}$ and $\tau_{yz}=\tau_{zy}$).

With reference to Figure 2.4 and Figure 2.5 the internal forces are presented in Eqs. (2.15) to (2.24). Neglecting z/R_x and z/R_y ($t \ll R_x$ and $t \ll R_y$)⁵ leads to the simplified version of these equations.

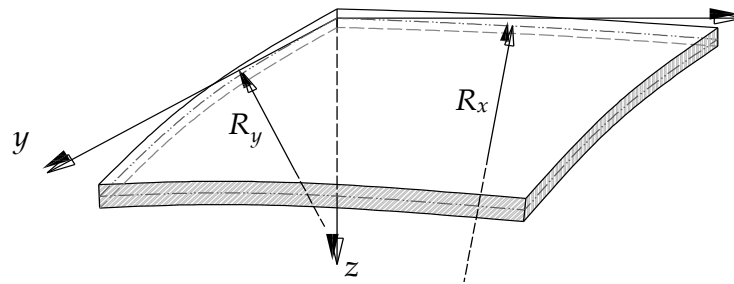


Figure 2.3: Geometry of a thin shell element

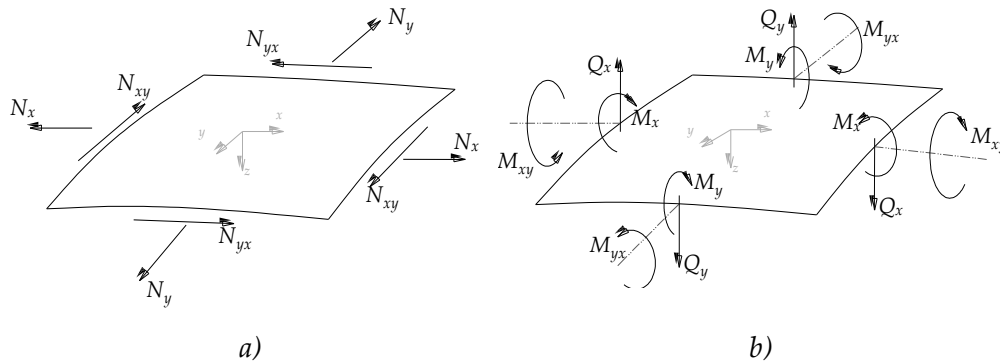


Figure 2.4: Thin shell element: a) membrane forces; b) shear forces and bending moment

⁵ It should be noticed that it is not enough to consider $t \ll R_x$ and $t \ll R_y$ to neglect the z/R_x and z/R_y quantities; it is also necessary to neglect the terms t^3/R_x and t^3/R_y which result from integration of z/R_x and z/R_y through thickness. For some geometry of curved panels present of following chapters, this simplification may be abusive and the stress resultant calculation should be corrected accordingly, i.e. without neglecting the terms t^3/R_x and t^3/R_y .

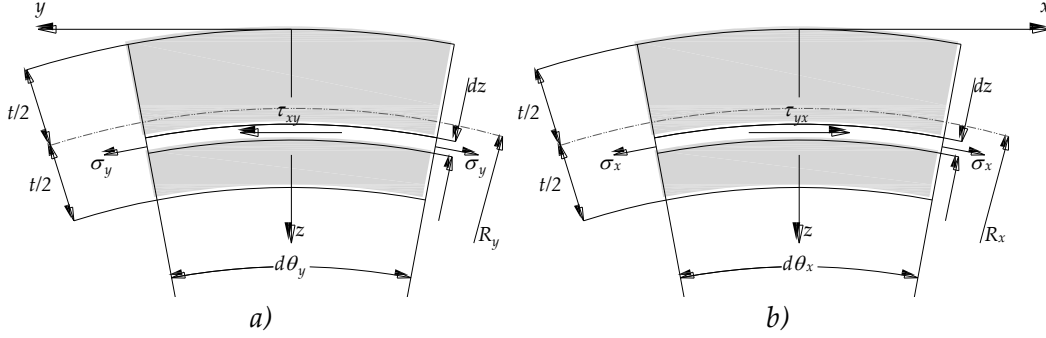


Figure 2.5: Schematic view of: a) plane O_{yz} and b) plane O_{xz}
(adapted from Silva Gomes, 2007)

$$N_x = \int_{-t/2}^{t/2} \frac{\sigma_x (R_y - z) d\theta_y}{R_y} dz = \int_{-t/2}^{t/2} \sigma_x \left(1 - \frac{z}{R_y}\right) dz = \int_{-t/2}^{t/2} \sigma_x dz \quad (2.15)$$

$$N_y = \int_{-t/2}^{t/2} \frac{\sigma_y (R_x - z) d\theta_x}{R_x} dz = \int_{-t/2}^{t/2} \sigma_y \left(1 - \frac{z}{R_x}\right) dz = \int_{-t/2}^{t/2} \sigma_y dz \quad (2.16)$$

$$N_{xy} = \int_{-t/2}^{t/2} \frac{\tau_{xy} (R_y - z) d\theta_y}{R_y} dz = \int_{-t/2}^{t/2} \tau_{xy} \left(1 - \frac{z}{R_y}\right) dz = \int_{-t/2}^{t/2} \tau_{xy} dz \quad (2.17)$$

$$N_{yx} = \int_{-t/2}^{t/2} \frac{\tau_{yx} (R_x - z) d\theta_x}{R_x} dz = \int_{-t/2}^{t/2} \tau_{yx} \left(1 - \frac{z}{R_x}\right) dz = \int_{-t/2}^{t/2} \tau_{yx} dz \quad (2.18)$$

$$Q_x = \int_{-t/2}^{t/2} \frac{\tau_{xz} (R_y - z) d\theta_y}{R_y} dz = \int_{-t/2}^{t/2} \tau_{xz} \left(1 - \frac{z}{R_y}\right) dz = \int_{-t/2}^{t/2} \tau_{xz} dz \quad (2.19)$$

$$Q_y = \int_{-t/2}^{t/2} \frac{\tau_{yz} (R_x - z) d\theta_x}{R_x} dz = \int_{-t/2}^{t/2} \tau_{yz} \left(1 - \frac{z}{R_x}\right) dz = \int_{-t/2}^{t/2} \tau_{yz} dz \quad (2.20)$$

$$M_x = \int_{-t/2}^{t/2} \frac{\sigma_x (R_y - z) d\theta_y}{R_y} z dz = \int_{-t/2}^{t/2} \sigma_x \left(1 - \frac{z}{R_y}\right) z dz = \int_{-t/2}^{t/2} \sigma_x z dz \quad (2.21)$$

$$M_y = \int_{-t/2}^{t/2} \frac{\sigma_y (R_x - z) d\theta_x}{R_x} z dz = \int_{-t/2}^{t/2} \sigma_y \left(1 - \frac{z}{R_x}\right) z dz = \int_{-t/2}^{t/2} \sigma_y z dz \quad (2.22)$$

$$M_{xy} = \int_{-t/2}^{t/2} \frac{\tau_{xy} (R_y - z) d\theta_y}{R_y} z dz = \int_{-t/2}^{t/2} \tau_{xy} \left(1 - \frac{z}{R_y}\right) z dz = \int_{-t/2}^{t/2} \tau_{xy} z dz \quad (2.23)$$

$$M_{yx} = \int_{-t/2}^{t/2} \frac{\tau_{yx}(R_x - z)d\theta_x}{R_x} z dz = \int_{-t/2}^{t/2} \tau_{yx} \left(1 - \frac{z}{R_x}\right) z dz = \int_{-t/2}^{t/2} \tau_{yx} z dz \quad (2.24)$$

From the analysis of this previous set of equations it is concluded that N_{xy} is equal to N_{yx} and M_{xy} is equal to M_{yx} only if z/R_x and z/R_y are neglected.

Next, in order to relate the stress resultants to the shell deformations, σ_x , σ_y and τ_{xy} are expressed in terms of strains. Introducing Hooke's law for a plane stress into Eqs. (2.15) to (2.24), leads to Eqs. (2.25) to (2.30)

$$N_x = C(\varepsilon_{x,0} + \nu\varepsilon_{y,0}) \quad (2.25)$$

$$N_y = C(\varepsilon_{y,0} + \nu\varepsilon_{x,0}) \quad (2.26)$$

$$N_{xy} = N_{yx} = C \frac{1-\nu}{2} \gamma_{xy,0} \quad (2.27)$$

$$M_x = D(\chi_x + \nu\chi_y) \quad (2.28)$$

$$M_y = D(\chi_y + \nu\chi_x) \quad (2.29)$$

$$M_{xy} = M_{yx} = D(1-\nu)\chi_{xy} \quad (2.30)$$

where C and D are the membrane and flexural rigidities, respectively, given by

$$C = \frac{Et}{1-\nu^2} \quad (2.31)$$

$$D = \frac{Et^3}{12(1-\nu^2)} \quad (2.32)$$

2.5. Shallow shells

2.5.1. General

A shallow shell is like a slightly curved plate, *i.e.* a shell whose smallest radius of curvature at each point is large when compared with the largest lengths measured along the middle surface (Leissa, 1973). It is possible to define a shallow shell as a shell that in any point of its middle surface satisfies the following expressions

$$\left(\frac{\partial Z}{\partial x}\right)^2 < 0.05 \quad (2.33)$$

$$\left(\frac{\partial Z}{\partial y}\right)^2 < 0.05 \quad (2.34)$$

where $Z=Z(x,y)$ represents the equation of the middle surface.

According to Koiter a shell is said to be shallow if the relation between the characteristic wavelength of its deformed configuration l , and the smallest radius of curvature of the middle surface R_{min} , is negligible, *i.e.* $l/R_{min} \ll 1$ (Koiter, 1967). Vlasov defined shallow shell as a shell whose rise is limited to 20% of the smallest dimension of the shell in its plane (projection on the coordinate plane Oxy) (Vlasov, 1949). Later in 1959, Novozhilov showed that this definition leads to errors exceeding 5% (Novozhilov, 1959).

The theory that deals with this kind of shells is called shallow shell theory and can be applied from cylindrically curved panels to more general geometries like doubly curved panels. It is presented in sec. 2.5.3 after a more general shell theory: the Donnell-Mushtari-Vlasov nonlinear general thin shell theory in sec. 2.5.2.

2.5.2. Donnell-Mushtari-Vlasov nonlinear general thin shell theory

First, a brief geometric introduction of a general shell is made. Using Figure 2.6 as reference it is possible to define infinitesimal distances ds_x and ds_y . These distances can be given by the following expressions

$$ds_1 = A_L dx ; ds_2 = B_L dy \quad (2.35)$$

where A_L and B_L are the Lamé coefficients for a given coordinate system and are defined by the following expressions (Brush & Almroth, 1975)

$$A_L = \left[\left(\frac{\partial X}{\partial x}\right)^2 + \left(\frac{\partial Y}{\partial x}\right)^2 + \left(\frac{\partial Z}{\partial x}\right)^2 \right]^{1/2} \quad (2.36)$$

$$B_L = \left[\left(\frac{\partial X}{\partial y} \right)^2 + \left(\frac{\partial Y}{\partial y} \right)^2 + \left(\frac{\partial Z}{\partial y} \right)^2 \right]^{1/2} \quad (2.37)$$

where $X=X(x,y)$, $Y=Y(x,y)$ and $Z=Z(x,y)$.

The Donnell-Mushtari-Vlasov theory, or DMV theory, assumes the fundamental hypotheses of the classical theory formulated by Love in 1888 (cited in Love, 1892). Besides these hypotheses, DMV theory also assumes that the shell shows infinitesimal deformations and moderate rotations. These last hypotheses indicate that this theory, as previously mentioned, is suitable to analyse shallow shells.

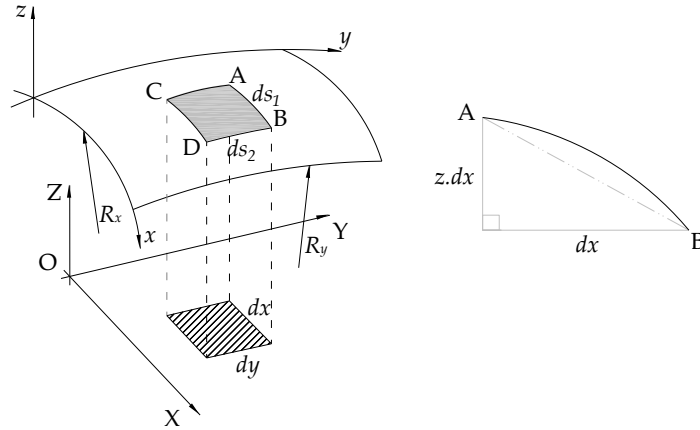


Figure 2.6: Geometric definition of the relationships in Eq. (2.35)

As previously stated, DMV theory takes into account rotations. Thus, the kinematic relationships incorporate them as follows (Brush & Almroth, 1975)

$$\varepsilon_{x,0} = \frac{1}{A_L} \frac{\partial u}{\partial x} + \frac{1}{A_L B_L} \frac{\partial A_L}{\partial y} v + \frac{w}{R_x} + \frac{1}{2} \left(-\frac{1}{A_L} \frac{\partial w}{\partial x} \right)^2 \quad (2.38)$$

$$\varepsilon_{y,0} = \frac{1}{B_L} \frac{\partial v}{\partial y} + \frac{1}{A_L B_L} \frac{\partial B_L}{\partial x} u + \frac{w}{R_y} + \frac{1}{2} \left(-\frac{1}{B_L} \frac{\partial w}{\partial y} \right)^2 \quad (2.39)$$

$$\gamma_{xy,0} = \frac{1}{A_L} \frac{\partial v}{\partial x} + \frac{1}{B_L} \frac{\partial u}{\partial y} - \frac{1}{A_L B_L} \left(\frac{\partial B_L}{\partial x} v + \frac{\partial A_L}{\partial y} u \right) + \left(-\frac{1}{A_L} \frac{\partial w}{\partial x} \right) \left(-\frac{1}{B_L} \frac{\partial w}{\partial y} \right) \quad (2.40)$$

$$\chi_x = -\frac{1}{A_L} \frac{\partial}{\partial x} \left(\frac{1}{A_L} \frac{\partial w}{\partial x} - \frac{u}{R_x} \right) - \frac{1}{A_L B_L} \frac{\partial A}{\partial y} \left(\frac{1}{B_L} \frac{\partial w}{\partial y} - \frac{v}{R_y} \right) \quad (2.41)$$

$$\chi_y = -\frac{1}{B_L} \frac{\partial}{\partial y} \left(\frac{1}{B_L} \frac{\partial w}{\partial y} - \frac{v}{R_y} \right) - \frac{1}{A_L B_L} \frac{\partial B_L}{\partial x} \left(\frac{1}{A_L} \frac{\partial w}{\partial x} - \frac{u}{R_x} \right) \quad (2.42)$$

$$\begin{aligned} \chi_{xy} = & -\frac{1}{A_L B_L} \left(\frac{\partial^2 w}{\partial x \partial y} - \frac{1}{A_L} \frac{\partial A_L}{\partial y} \frac{\partial w}{\partial x} - \frac{1}{B_L} \frac{\partial B_L}{\partial x} \frac{\partial w}{\partial y} \right) + \\ & + \frac{1}{R_x} \left(\frac{1}{B_L} \frac{\partial u}{\partial y} - \frac{1}{A_L B_L} \frac{\partial A_L}{\partial y} u \right) + \\ & + \frac{1}{R_y} \left(\frac{1}{A_L} \frac{\partial v}{\partial x} - \frac{1}{A_L B_L} \frac{\partial B_L}{\partial x} v \right) \end{aligned} \quad (2.43)$$

Introducing Eqs. (2.38) to (2.43) into Eqs. (2.25) to (2.30) leads to

$$\begin{aligned} N_x = & C \left[\frac{1}{A_L} \frac{\partial u}{\partial x} + \frac{1}{A_L B} \frac{\partial A_L}{\partial y} + \frac{w}{R_x} + \frac{1}{2} \left(-\frac{1}{A_L} \frac{\partial w}{\partial x} \right)^2 + \right. \\ & \left. + v \left(\frac{1}{B} \frac{\partial v}{\partial y} + \frac{1}{A_L B} \frac{\partial B}{\partial x} + \frac{w}{R_y} + \frac{1}{2} \left(-\frac{1}{B} \frac{\partial w}{\partial y} \right)^2 \right) \right] \end{aligned} \quad (2.44)$$

$$\begin{aligned} N_y = & C \left[\frac{1}{B} \frac{\partial v}{\partial y} + \frac{1}{A_L B} \frac{\partial B}{\partial x} + \frac{w}{R_y} + \frac{1}{2} \left(-\frac{1}{B} \frac{\partial w}{\partial y} \right)^2 + \right. \\ & \left. + v \left(\frac{1}{A_L} \frac{\partial u}{\partial x} + \frac{1}{A_L B} \frac{\partial A_L}{\partial y} + \frac{w}{R_x} + \frac{1}{2} \left(-\frac{1}{A_L} \frac{\partial w}{\partial x} \right)^2 \right) \right] \end{aligned} \quad (2.45)$$

$$\begin{aligned} N_{xy} = N_{yx} = & C \frac{1-\nu}{2} \left[\frac{1}{A_L} \frac{\partial v}{\partial x} + \frac{1}{B_L} \frac{\partial u}{\partial y} - \frac{1}{A_L B_L} \left(\frac{v \partial B_L}{\partial x} + \frac{v \partial A_L}{\partial y} \right) + \right. \\ & \left. + \left(-\frac{1}{A_L} \frac{\partial w}{\partial x} \right) \left(-\frac{1}{B_L} \frac{\partial w}{\partial y} \right) \right] \end{aligned} \quad (2.46)$$

$$\begin{aligned} M_x = & D \left[-\frac{1}{A_L^2} \frac{\partial^2 w}{\partial x^2} + \frac{1}{A_L^3} \frac{\partial A_L}{\partial x} \frac{\partial w}{\partial x} - \frac{1}{A_L B_L^2} \frac{\partial A_L}{\partial y} \frac{\partial w}{\partial y} + \right. \\ & \left. + v \left(-\frac{1}{B_L^2} \frac{\partial^2 w}{\partial y^2} + \frac{1}{B_L^3} \frac{\partial B_L}{\partial y} \frac{\partial w}{\partial y} - \frac{1}{A_L^2 B_L} \frac{\partial B_L}{\partial x} \frac{\partial w}{\partial x} \right) \right] \end{aligned} \quad (2.47)$$

$$M_x = D \left[-\frac{1}{B_L^2} \frac{\partial^2 w}{\partial y^2} + \frac{1}{B_L^3} \frac{\partial B_L}{\partial y} \frac{\partial w}{\partial y} - \frac{1}{A_L^2 B_L} \frac{\partial B_L}{\partial x} \frac{\partial w}{\partial x} + \right. \\ \left. + \nu \left(-\frac{1}{A_L^2} \frac{\partial^2 w}{\partial x^2} + \frac{1}{A_L^3} \frac{\partial A_L}{\partial x} \frac{\partial w}{\partial x} - \frac{1}{A_L B_L^2} \frac{\partial A_L}{\partial y} \frac{\partial w}{\partial y} \right) \right] \quad (2.48)$$

$$M_{xy} = M_{yx} = D(1-\nu) \left(-\frac{1}{A_L B_L} \frac{\partial^2 w}{\partial x \partial y} + \frac{1}{A_L^2 B_L} \frac{\partial A_L}{\partial y} \frac{\partial w}{\partial x} - \frac{1}{A_L B_L^2} \frac{\partial B_L}{\partial x} \frac{\partial w}{\partial y} \right) \quad (2.49)$$

Eqs.(2.50) to (2.52) represent the equilibrium equations in x , y and z -direction

$$\frac{\partial}{\partial x} (B_L N_x) + \frac{\partial}{\partial y} (A_L N_{xy}) - \frac{\partial B_L}{\partial x} N_y + \frac{\partial A_L}{\partial x} N_{xy} = -A_L B_L p_x \quad (2.50)$$

$$\frac{\partial}{\partial y} (A_L N_y) + \frac{\partial}{\partial x} (B_L N_{xy}) - \frac{\partial A_L}{\partial y} N_x + \frac{\partial B_L}{\partial x} N_{xy} = -A_L B_L p_y \quad (2.51)$$

$$\frac{\partial}{\partial x} \left[\frac{1}{A_L} \frac{\partial}{\partial x} (B_L M_x) \right] - \frac{\partial}{\partial y} \left(\frac{1}{B_L} \frac{\partial A_L}{\partial y} M_x \right) + \frac{\partial}{\partial y} \left[\frac{1}{B_L} \frac{\partial}{\partial y} (A_L M_y) \right] - \frac{\partial}{\partial x} \left(\frac{1}{A_L} \frac{\partial B_L}{\partial x} M_y \right) + \\ + 2 \left[\frac{\partial^2 M_{xy}}{\partial x \partial y} + \frac{\partial}{\partial x} \left(\frac{1}{A_L} \frac{\partial A_L}{\partial y} M_{xy} \right) + \frac{\partial}{\partial y} \left(\frac{1}{B_L} \frac{\partial B_L}{\partial x} M_{xy} \right) \right] - A_L B_L \left(\frac{N_x}{R_x} + \frac{N_y}{R_y} \right) - \\ - \left[\frac{\partial}{\partial x} \left(B_L N_x \left(-\frac{1}{A_L} \frac{\partial w}{\partial x} \right) + B_L N_{xy} \left(-\frac{1}{B_L} \frac{\partial w}{\partial y} \right) \right) + \right. \\ \left. + \frac{\partial}{\partial y} \left(A_L N_y \left(-\frac{1}{B_L} \frac{\partial w}{\partial y} \right) + A_L N_{xy} \left(-\frac{1}{A_L} \frac{\partial w}{\partial x} \right) \right) \right] = -A_L B_L p_z \quad (2.52)$$

It should be noted that Eq. (2.52) (equilibrium according to z -direction, *i.e.* according to the direction that is normal to the middle surface of the shell) includes the (i) shear forces (expressed in terms of M_x , M_y and M_{xy}), and (ii) the membrane components according to z -direction (deformed configuration – geometrically nonlinear theory) (Reis & Camotim, 2012).

Finally, introducing Eqs. (2.44) to (2.49) into Eqs. (2.50) to (2.52) leads to the nonlinear differential equations for the DMV theory expressed in terms of displacement w .

Alternatively, the nonlinear equilibrium equations may be obtained from the

total potential energy expression for general shells “by routine application of the principle of stationary potential energy” (p. 197, Brush & Almroth, 1975) (sec. 2.6.2).

Finally, it can be seen that the Lamé coefficients can be specified to obtain kinematic relationships for specific geometries, for example, for rectangular flat plate the Lamé coefficients are $A_L=1$ and $B_L=1$ and $R_x=\infty$ and $R_y=\infty$, and for circular thin cylindrical shell are $A_L=1$ and $B_L=R_y$ and $R_x=\infty$.

2.5.3. Nonlinear shallow shell theory

Shallow shells are frequently required to be analysed by a geometrically nonlinear theory because shallow shells are less stiff than other shells, which means that for the same applied transverse load, the displacements and mainly the rotations are larger than in other shells having the same planar dimensions.

From the element [ABCD] and its projection in the Oxy plane represented in Figure 2.6 is clear that the following simplifications can be made

$$ds_1 = \left[1 + \left(\frac{\partial Z}{\partial x} \right)^2 \right]^{1/2} dx \quad (2.53)$$

$$ds_2 = \left[1 + \left(\frac{\partial Z}{\partial y} \right)^2 \right]^{1/2} dy \quad (2.54)$$

Furthermore, the nonlinear terms can be neglected leading to the following further simplifications

$$ds_1 = dx \quad (2.55)$$

$$ds_2 = dy \quad (2.56)$$

i.e. $A_L=1$ and $B_L=1$. Therefore, it is correct, when analysing shallow shells, to consider as orthogonal the curvilinear system of coordinates. In conclusion, the intrinsic geometry of a shallow shell is identical to the geometry of a plane of its projection. This actually represents the first basic assumption of the theory of shallow shells (Ventsel & Krauthammer, 2001). The second assumption of shal-

low shells theory is that the effect of transverse shear forces in in-plane equilibrium equations is negligible and the influence of the deflections, w , predominates over the influences of the in-plane displacements u and v in the bending response of the shell. Replacing the Lamé coefficients by 1 in DMV equations leads to the nonlinear equations of shallow shells. The kinematic equations are

$$\varepsilon_{x,0} = \frac{\partial u}{\partial x} + \frac{w}{R_x} + \frac{1}{2} \left(-\frac{\partial w}{\partial x} \right)^2 \quad (2.57)$$

$$\varepsilon_{y,0} = \frac{\partial v}{\partial y} + \frac{w}{R_y} + \frac{1}{2} \left(-\frac{\partial w}{\partial y} \right)^2 \quad (2.58)$$

$$\gamma_{xy,0} = \frac{\partial v}{\partial x} + \frac{\partial u}{\partial y} + \frac{\partial w}{\partial x} \frac{\partial w}{\partial y} \quad (2.59)$$

$$\chi_x = -\frac{\partial^2 w}{\partial x^2} \quad (2.60)$$

$$\chi_y = -\frac{\partial^2 w}{\partial y^2} \quad (2.61)$$

$$\chi_{xy} = -\frac{\partial^2 w}{\partial x \partial y} \quad (2.62)$$

The force-displacement relationships are given as follows

$$N_x = C \left[\frac{\partial u}{\partial x} + \frac{w}{R_x} + \frac{1}{2} \left(-\frac{\partial w}{\partial x} \right)^2 + \nu \left(\frac{\partial v}{\partial y} + \frac{w}{R_y} + \frac{1}{2} \left(-\frac{\partial w}{\partial y} \right)^2 \right) \right] \quad (2.63)$$

$$N_y = C \left[\frac{\partial v}{\partial y} + \frac{w}{R_y} + \frac{1}{2} \left(-\frac{\partial w}{\partial y} \right)^2 + \nu \left(\frac{\partial u}{\partial x} + \frac{w}{R_x} + \frac{1}{2} \left(-\frac{\partial w}{\partial x} \right)^2 \right) \right] \quad (2.64)$$

$$N_{xy} = N_{yx} = C \frac{1-\nu}{2} \left[\frac{\partial v}{\partial x} + \frac{\partial u}{\partial y} + \frac{\partial^2 w}{\partial x \partial y} \right] \quad (2.65)$$

$$M_x = -D \left[\frac{\partial^2 w}{\partial x^2} + \nu \frac{\partial^2 w}{\partial y^2} \right] \quad (2.66)$$

$$M_y = -D \left[\frac{\partial^2 w}{\partial y^2} + \nu \frac{\partial^2 w}{\partial x^2} \right] \quad (2.67)$$

$$M_{xy} = M_{yx} = -D(1-\nu) \frac{\partial^2 w}{\partial x \partial y} \quad (2.68)$$

And, finally, the equilibrium equations

$$\frac{\partial N_x}{\partial x} + \frac{\partial N_{xy}}{\partial y} = -p_x \quad (2.69)$$

$$\frac{\partial N_y}{\partial y} + \frac{\partial N_{xy}}{\partial x} = -p_y \quad (2.70)$$

$$\begin{aligned} \frac{\partial^2 M_x}{\partial x^2} - 2 \frac{\partial^2 M_{xy}}{\partial x \partial y} + \frac{\partial^2 M_y}{\partial y^2} + \left(\frac{\partial^2 w}{\partial x^2} - \frac{1}{R_x} \right) N_x + \\ + 2 \frac{\partial^2 w}{\partial x \partial y} N_{xy} + \left(\frac{\partial^2 w}{\partial y^2} - \frac{1}{R_y} \right) N_y = -p_z \end{aligned} \quad (2.71)$$

Alternatively, Eq. (2.71) can be written only with respect to the terms related to the membranes forces and the displacement field w

$$D \nabla^4 w + \left(\frac{\partial^2 w}{\partial x^2} + \frac{1}{R_x} \right) N_x + 2 \frac{\partial^2 w}{\partial x \partial y} N_{xy} + \left(\frac{\partial^2 w}{\partial y^2} + \frac{1}{R_y} \right) N_y = -p_z \quad (2.72)$$

The corresponding linear governing equations are obtained neglecting the nonlinear terms in Eqs. (2.57) to (2.59).

2.6. Energy principles

2.6.1. General

In the next sub-sections the total potential energy of thin general shells is introduced. Additionally, the principles of stationary total potential energy and of minimum total potential energy are stated. A complete demonstration or proof of these principles is not given in this section since it can be found with great amount of detail in the works of several authors (e.g. Reddy, 2002).

2.6.2. Total potential energy of thin elastic shells

For a general shell element, the total potential energy V of an elastic body, Eq. (2.74), is obtained by adding the strain energy, U given by Eq. (2.73), and

the work done by the load W . The strain energy of a general thin elastic shell may be divided into two components: membrane strain energy U_m , given by Eq. (2.75) and pure bending strain energy U_b , given by Eq. (2.76) (Koiter, 1960).

$$U = U_m + U_b \quad (2.73)$$

$$V = U - W \quad (2.74)$$

$$U_m = \frac{C}{2} \iint \left(\varepsilon_{x,0}^2 + \varepsilon_{y,0}^2 + 2\nu\varepsilon_{x,0}\varepsilon_{y,0} + \frac{1-\nu}{2}\gamma_{xy,0}^2 \right) AB \, dx dy \quad (2.75)$$

$$U_b = \frac{D}{2} \iint \left(\chi_x^2 + \chi_y^2 + 2\nu\chi_x\chi_y + 2(1-\nu)\chi_{xy}^2 \right) AB \, dx dy \quad (2.76)$$

The work done by external loads is given by (Brush & Almroth, 1975)

$$W = \int_0^a \int_0^b (p_x u + p_y v + p_z w) AB \, dx dy \quad (2.77)$$

where a is the shell's element length, b is the shell's element width and p_x , p_y and p_z are the distributed forces per unit area acting in x , y and normal directions, respectively. Eqs. (2.75) and (2.76) are easily derived from Eq. (2.78), which represents the most general expression for the strain energy of an elastic body, and recurring to Hooke's law as presented in sec. 2.3.

$$U = \frac{1}{2} \int_V \left(\sigma_x \varepsilon_x + \sigma_y \varepsilon_y + \sigma_z \varepsilon_z + \tau_{xy} \gamma_{xy} + \tau_{yz} \gamma_{yz} + \tau_{xz} \gamma_{xz} \right) dV \quad (2.78)$$

2.6.3. The principle of stationary total potential energy

The principle of stationary energy states that when the equilibrium configuration of an elastic body is perturbed by the introduction of an infinitesimal displacement field, the total potential energy remains constant. Mathematically, this principle is translated by the following equation

$$\delta V = \frac{\partial V}{\partial q_i} = 0 \quad (2.79)$$

where q_i represents the introduced infinitesimal displacements.

2.6.4. The principle of minimum total potential energy

The principle of minimum potential energy states “an equilibrium configuration is stable whenever the total potential energy of the system displays a minimum” (p. 34, translated from Portuguese, Reis & Camotim, 2012). Mathematically, this principle is illustrated by the following conditions (the first variation of the total potential energy is null and the second is positive)

$$\delta V = 0 \wedge \delta^2 V > 0 \quad (2.80)$$

where symbol δ is the variational operator used in calculus of variations.

Another way to enunciate this principle is “of all displacements fields which satisfy the prescribed constraint conditions, the correct state is that which makes the total potential energy of the structure a minimum” (p. 74, Tauchert, 1974).

2.7. Methods of analysis of thin shells

2.7.1. General

As already seen in the previous section, there are relevant problems in the field of engineering which may be well described in terms of partial differential equations. With some exceptions, an analytical solution is not possible to obtain or it is very complex. This fact is explained by two reasons: there is no analytical solution for the differential equations describing the problem and/or because the quantity of differential equations to solve is too large.

Problems that have exact solutions have very simple geometry and very simple loading and boundary conditions, like:

- Axially loaded simply supported cylindrical shells of revolution;
- Simply supported rectangular plates under uniform compression;
- Simply supported circular plates.

For more complex problems it is necessary to use approximate methods. Generally speaking, approximate methods return an exact solution for discretised geometries (in opposition to the continuum) of the problem.

In problems involving conservative systems⁶, several approximate methods (whose theoretical fundamentals lies on the calculus of variations) have been applied to determine numerical values of natural frequencies and buckling stresses. Among those methods, the ones worth mentioning are the Rayleigh-Ritz (sec. 2.7.2) and Galerkin methods⁷. The solutions obtained by the Rayleigh-Ritz and Galerkin methods are an approximation of the true solution of the differential equations describing the problem. This is due to the fact that the solutions are in the form of a finite linear combination of undetermined parameters and appropriate functions that need to satisfy the boundary conditions. Additionally, it should be highlighted that the main differences between the two methods are: while the Rayleigh-Ritz method acts on the total potential energy of the function (meaning that it is only applicable to conservative problems), the Galerkin method acts on the equilibrium differential equations (Reis & Camotim, 2012); and while the Rayleigh-Ritz method requires only the essential boundary conditions, the Galerkin method requires both essential and natural boundary conditions.

Another classical method to obtain approximate solutions consists in approximating exact derivatives by finite differences computed in respect to a grillage point system. This method is known as finite difference method. Although it is suitable to return an approximate solution of a complex problem this method needs to solve a considerable amount of linear differential equations that were only possible to be solved with the aid of computers.

Finally, in sec. 2.7.3 the finite element method (FEM) is mentioned. This computational method is the most commonly used numerical method nowadays. In fact, in the past couple of decades it progressively became a valuable tool for structural engineers, ceasing to be used exclusively by researchers. In a

⁶ From physics is known that “A conservative system is a system in which work done by a force is: (i) independent of path; (ii) equal to the difference between the final and initial values of an energy function; (iii) completely reversible” (Young *et al.*, 2010).

⁷ The Rayleigh-Ritz and the Galerkin methods are probably the most prominent methods and are referred to as the “classical variational methods” (Reddy, 2002).

simplistic way, the FEM is a computational technique which goal is to provide approximate solutions of boundary value problems. In conservative problems the finite element method is similar to the Rayleigh-Ritz method. The difference lies in the way the system is discretised. In FEM, the system is modelled with finite elements establishing a mesh with an approximate shape of the initial problem and in Rayleigh-Ritz method the system is discretised by defining a finite number of degrees-of-freedom that are able to reproduce the mechanical response to external loading.

2.7.2. Rayleigh-Ritz method

The Rayleigh-Ritz method was developed by Ritz to solve equilibrium and eigenvalue conservative problems (*i.e.* problems with potential energy) using the same approach used by Rayleigh to analyse free vibrations (Brush & Almroth, 1975).

In the Rayleigh-Ritz method the structure's displacement field is approximated by functions containing a finite number of independent parameters or in other words "the continuous structure is approximated by a system having a finite number of degrees-of-freedom" (p. 89, Tauchert, 1974). These functions have to satisfy only the kinematic boundary conditions of the problem, disregarding the static boundary conditions. Summarising, in the Rayleigh-Ritz method, a dependent unknown⁸ u is approximated by a finite linear combination u_n

$$u \approx u_n = \sum_{i=1}^n q_i \psi_i \quad (2.81)$$

where q_i are undetermined parameters (degrees-of-freedom) and ψ_i are the approximation functions that have to be previously chosen and, as already mentioned, have to satisfy the kinematic boundary conditions. The undetermined parameters q_i are obtained by applying the principle of stationary total potential energy (see sec. 2.6.3).

⁸ In the field of structural analysis the unknown is usually the displacement field.

Finally, it should be noted that when the continuous structure is idealised into a system with a finite number degrees-of-freedom, additional constraints are being added to the structure. These imaginary constraints become more and more significant when reducing the degrees-of-freedom making the discretised structure stiffer than it really is. This means that a procedure using the Rayleigh-Ritz method returns smaller values for the displacements and, in the case of eigenvalue analysis (linear stability analysis) higher values of critical loads.

2.7.3. Finite element method (FEM)

Before the emergence of the FEM, all analysis carried out to solve structures were done by means of direct solving the partial differential equations underlying the behaviour of the structure. As aforementioned, this approach was only possible in very rare cases with simple geometries and loading conditions.

Thus, the main idea of the finite element method is to systematically find very simple approximation functions, ψ_i , for each finite element and then requiring them to cope with continuity equations (*i.e.* the displacement field must be continuous and differentiable in all domain of the problem), equilibrium equations and constitutive laws.

Theoretically, the solution obtained by application of the FEM tends to the exact one if the dimension of the finite element tends to zero (*i.e.* the number of finite elements replacing the real structure tends to infinity) or if the degree of interpolation of the finite element tends to infinity (*i.e.* the degree of the approximation functions of the finite element tends to infinity).

In Chapter 4 (numerical studies) this method will be used and its main assumptions within cylindrically curved steel panel applications will be thoroughly described.

2.8. Summary

In conclusion, this chapter started with a revision of the historical evolution of shell theories and also with the most important definitions (where the defini-

tion of shallow shells, together with the explanation of the nonlinear shallow shell theory, stand out). It was also concluded that shallow shell theory, namely DMV theory is the most suitable theory to study cylindrically curved panels.

Finally, it is highlighted the fact that this chapter defines and introduces the most important concepts that are crucial for the progress into the subsequent chapters:

- Firstly, the topics covered in sec. 2.5 together with those in sec. 2.6, are crucial for the progress of Chapter 7: Energy based analytical model. In fact, the expressions presented in Chapter 7, are derived from total potential energy formulations where the strain-displacement relations are given by the nonlinear shell theory presented in sec. 2.5.3 and are inserted into Eq. (2.78);
- Secondly, sec. 2.7.3 initiates a very important task in this work: the numerical study, which is presented in Chapter 4: Numerical models of curved panels under compressive stresses. Apart from expressions in Chapter 7, the remaining proposed formulae are calibrated using numerical results.

3. Stability analysis of plates and cylindrically curved panels

3.1. Chapter overview

This chapter presents and discusses the stability behaviour of simply supported cylindrically curved panels. Additionally, since plates are seen as a particular case of cylindrically curved panels, a concise introduction to the stability of plates is also made.

Therefore, after an introductory description of a cylindrically curved panel's geometry in sec. 3.2, the buckling and postbuckling behaviour of plates under uniaxial compressive stresses is tackled in sec. 3.3 and under biaxial loading in sec. 3.4. Thus, the most important features of the elastic critical behaviour and postbuckling behaviour of simply supported plates are reviewed and covered in these sections.

In sec. 3.5 to sec. 3.7 the same framework is used to characterise the behaviour of simply supported cylindrically curved panels (uniaxial compressive stresses, circumferential compressive stresses and biaxial compressive stresses, respectively).

In sec. 3.9 to sec. 3.13 a revision of the ultimate behaviour is made for plates and cylindrically curved panels. Once again, more emphasis is given to the ultimate behaviour of cylindrically curved panels. In sec. 3.9, the classical formulae based on the effective concept are revisited. Sec. 3.10 revises the ultimate resistance of plates under biaxial loading, and sec. 3.11 undertakes a

deeper literature review on the ultimate resistance of cylindrically curved panels under uniaxial compressive stresses including the consideration of boundary conditions other than simply supported and loading conditions other than uniform compressive stresses. Sec. 3.12 and sec. 3.13 review the ultimate resistance of cylindrically curved panels under circumferential compressive stresses and under biaxial loading, respectively. Current design methods for the assessment of the resistance of plated structures and curved panels are described in sec. 3.14. In particular, the design methods from EN1993-1-5:2006, DNV-RP-C201 and DNV-RP-C202 are briefly presented.

Finally, in sec. 3.15 a summary of the entire chapter is made establishing relevant aspects to take into account in subsequent chapters.

3.2. Geometry of a cylindrically curved panel

Taking as reference Figure 3.1, the notation for the geometry of a plate and of a cylindrically curved panel is given as follows:

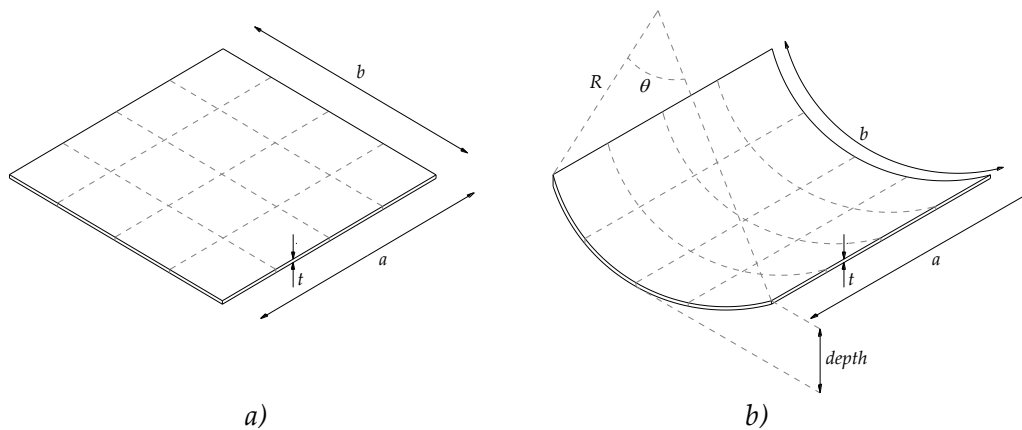


Figure 3.1: Geometry of a) plate and b) cylindrically curved panel

- a is the length of the plate/panel;
- b is the width of the plate/panel;
- t is the thickness of the plate/panel;
- R is the radius of curvature of the panel;
- θ is the sectorial angle of the panel.

Classically, the curvature of a cylindrically curved panel is denoted by Z , called the curvature parameter, defined by the following expression

$$Z = \frac{b^2}{R.t} \quad (3.1)$$

The adoption of the letter Z for the curvature parameter is due to Batdorf (Batdorf, 1947a; Batdorf, 1947b; Batdorf, 1947c) who defined a similar parameter, but taking into account the Poisson's coefficient ν

$$Z_b = \frac{b^2}{R.t} \sqrt{1-\nu^2} \quad (3.2)$$

Besides the curvature parameter for curved panels, Eq. (3.2), Batdorf defined another one for cylinders (which is similar to the former but replacing b^2 by a^2). Another important aspect related to the geometry of a cylindrically curved panel is the coordinate system. In order to follow the classical notation, whenever a shell element is referred (local coordinate system) the following notation applies: x and y are the directions defining the plane tangent to a reference point of the shell's element and z -direction is the respective perpendicular direction (definition used through Chapter 2 and 7, see Figure 7.1); otherwise (with exception of sec. 8.8), whenever a curved panel is being referred (global coordinate system) x is the longitudinal direction, y is the strong axis direction (out-of-plane direction) and z is the weak axis direction (definition used through the remaining chapters, see Figure 4.2).

3.3. Buckling and postbuckling behaviour of flat plates under uniaxial compressive stresses

3.3.1. Linear elastic buckling behaviour

Although linear buckling theory is not enough to accurately predict the complete behaviour of a structure⁹, it still plays an important role in its design

⁹ "The theoretical or elastic critical local buckling load is not on its own a satisfactory basis for design. Ultimate strength of plates may be less than the critical buckling load due to yielding or may be in excess of the critical buckling load due to beneficial post-buckling reserve" (p. 128, Ziemian, 2010).

process. In fact, almost all standards deliver formulae and diagrams that allow calculating the elastic critical stress for common cases. The elastic critical stress value is fundamental in plated structures design as it is necessary when calculating the slenderness parameter. For a simply supported rectangular plate subjected to uniform compression, the elastic critical stress can be mathematically defined since the linear buckling theory does not take into account geometric and material nonlinearities. However, in the presence of complex support conditions and/or loading arrangements it is usually necessary to use approximate numerical or semi-analytical methods such as the Rayleigh-Ritz (sec. 2.7.2 and Chapter 7) or the Galerkin methods. For even more complex problems advanced software tools are available that use the finite element method (sec. 2.7.3 and Chapter 4) or the finite strip method to calculate accurately the elastic critical stress value. A derivation of the elastic critical stress of plates and curved panel based on energy principles applying the Rayleigh-Ritz method is performed in Chapter 7.

The first one to deduce Eq. (3.3) – elastic buckling stress of a long simply supported rectangular plate subjected to uniform compression, with an assumed buckling shape given by Eq. (3.4) – was Bryan in 1891 (Ziemian, 2010).

$$\sigma_{cr} = k_{\sigma} \frac{\pi^2 E}{12(1-\nu^2)} \left(\frac{t}{b}\right)^2 \quad (3.3)$$

$$w = q \sin\left(\frac{m\pi x}{a}\right) \sin\left(\frac{n\pi y}{b}\right) \quad (3.4)$$

The elastic critical stress value depends on the value of the buckling coefficient k_{σ} that is calculated from Eq. (3.5). This equation takes the value 4 (minimum value) for a simply supported plate under uniform compression with one transversal half-wave ($n=1$) (Figure 3.2)

$$k_{\sigma} = \left(\frac{m}{\alpha} + \frac{n^2}{m}\alpha\right)^2 \quad (3.5)$$

where α is the plate's aspect ratio, defined as the quotient between the plate's length, a , and the plate's width, b , m is the number of longitudinal half-waves

and n the number of transversal half-waves of the buckled shape. For short plates (*i.e.* aspect ratio less than 1) Eq. (3.5) does not have a minimum value (Figure 3.2). Therefore, the buckling coefficient must be directly obtained by the same equation (instead of being, in a simplified manner, equal to 4).

For other support conditions and/or for non-uniform loading, different values for the minimum buckling coefficient are obtained (Timoshenko & Gere, 1961; Bijlaard, 1957). Table 3.1 and Table 3.2 show some values for diverse in-plane loading and boundary conditions.

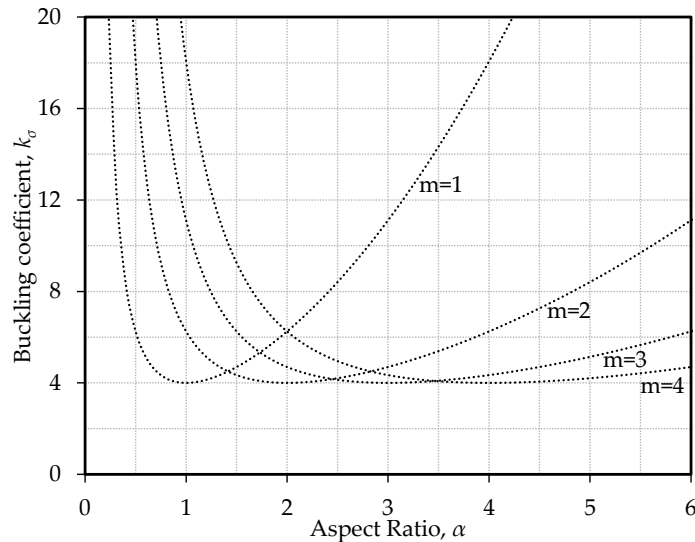


Figure 3.2: Plot of Eq. (3.5), $n=1$

When plates are stiffened the complexity of the analysis increases since the plate may show multiple buckling modes: global buckling of the plate, local buckling of the stiffened plate along longitudinal stiffeners, local buckling of the unstiffened plate along longitudinal stiffeners and local buckling of the stiffeners. Besides thickness, aspect ratio and material, the buckling stress of a simply supported stiffened plate depends on the number of stiffeners and their second moment of area. Several classical methods have been developed to compute the elastic critical stress of a stiffened plate (Seide & Stein, 1949; Bleich, 1952; Klöppel & Sheer, 1960; Timoshenko & Gere, 1961; Klöppel & Möller, 1968). These

authors presented tables and diagrams for very limited configurations, *e.g.* diagrams presented by Klöppel are applicable only for “weak” stiffeners (Galéa & Martin, 2010). In addition to these methods, there are, nowadays, advanced tools capable of predicting the elastic critical stress of a stiffened plate accurately: FEM, CFSM and EBPlate (CTICM, 2007) are examples of such tools.

Table 3.1: Values of the minimum buckling coefficient, $k_{\sigma, min}$, for different types of boundary conditions (adapted from Bijlaard, 1957)

<i>Loading, ψ</i>	<i>Unloaded edges simply supported</i>	<i>Unloaded edges fixed</i>	<i>Top edge free</i>		<i>Bottom edge free</i>	
			<i>Bottom edge simply supported</i>	<i>Bottom edge fixed</i>	<i>Top edge simply supported</i>	<i>Top edge fixed</i>
-1	23.9	39.6	0.85	2.15	-	-
-2/3	15.7	-	-	-	-	-
-1/3	11.0	-	-	-	-	-
0	7.8	13.6	0.57	1.61	1.70	5.93
1/3	5.8	-	-	-	-	-
1	4.0	6.97	0.42	1.33	0.42	1.33

Table 3.2: Values of the buckling coefficient, k_{σ} , for different types of in-plane loading (adapted from Timoshenko & Gere, 1961)

<i>Type of loading, ψ</i>	<i>Aspect ratio, α</i>								
	<i>0.40</i>	<i>0.50</i>	<i>0.60</i>	<i>0.67</i>	<i>0.75</i>	<i>0.80</i>	<i>0.90</i>	<i>1.00</i>	<i>1.50</i>
-1	29.1	25.6	24.1	23.9	24.1	24.4	25.6	25.6	24.1
-1/3	18.7	-	12.9	-	11.5	11.2	-	11.0	11.5
0	15.1	-	9.7	-	8.4	8.1	-	7.8	8.4
1/3	10.8	-	7.1	-	6.1	6.0	-	5.8	6.1

3.3.2. Postbuckling behaviour

The change between equilibrium states of a perfect plate occurs by stable symmetric bifurcation. This type of bifurcation is responsible by the stable postbuckling behaviour of a plate (see Figure 2.1). In fact, at the same time buckling occurs, a loss of stiffness and a redistribution of stresses characterised by the transformation of membrane potential energy into bending energy also occurs (Figure 3.3). Furthermore, when it comes to determining the postbuckling behaviour of a structural system, it is necessary to consider nonlinear terms in the equilibrium equations (established as the basis of the deformed configuration) and also a moderate- or large-deflection plate theory.

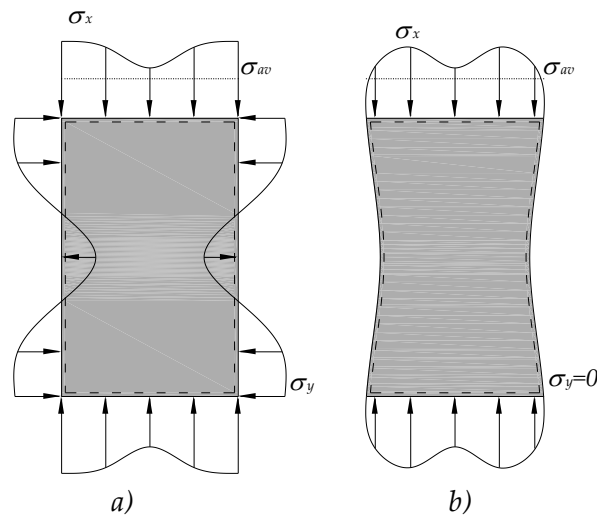


Figure 3.3: Stress redistribution: a) lateral borders remain straight and b) lateral borders free to deformed (adapted from Simões da Silva & Gervásio, 2007)

The postbuckling equilibrium path for a simply supported square plate without imperfections with all edges constrained (remaining straight after buckling, Figure 3.3a) can be deduced by von Kármán's equations or obtaining the equilibrium equations from the total potential energy function. The resulting equilibrium path is (Reis & Camotim, 2012)

$$\frac{\sigma}{\sigma_{cr}} = 1 + \frac{8}{3}(1-\nu^2)\left(\frac{q}{t}\right)^2 \quad (3.6)$$

where q is the maximum out-of-plane displacement of the plate. The deduction of Eq. (3.6) is not made in this section. For deeper information readers should consult classical references on the subject (*e.g.* Chajes, 1974).

However, a real structure is not imperfection free, therefore imperfections must be taken into account (it is brought to the attention of the reader that a deeper insight on imperfections is made in sec. 3.7). Figure 3.4 shows how geometric imperfections can affect the postbuckling behaviour of a simply supported plate under uniform compression. Again, the postbuckling equilibrium path for a plate with imperfections (assuming an imperfection shape or initial displacement field given by Eq. (3.8)) can be derived from the same large-deflection equations. The resulting equilibrium path is given by the following expression (Reis & Camotim, 2012)

$$\frac{\sigma}{\sigma_{cr}} = \left[1 + \frac{8}{3} (1 - \nu^2) \frac{(q^2 + 3qq_0 + 2q_0^2)}{t^2} \right] \frac{q}{q + q_0} \quad (3.7)$$

$$w_0 = q_0 \sin\left(\frac{\pi x}{a}\right) \sin\left(\frac{\pi y}{b}\right) \quad (3.8)$$

where q_0 is the maximum amplitude of the initial geometric imperfection.

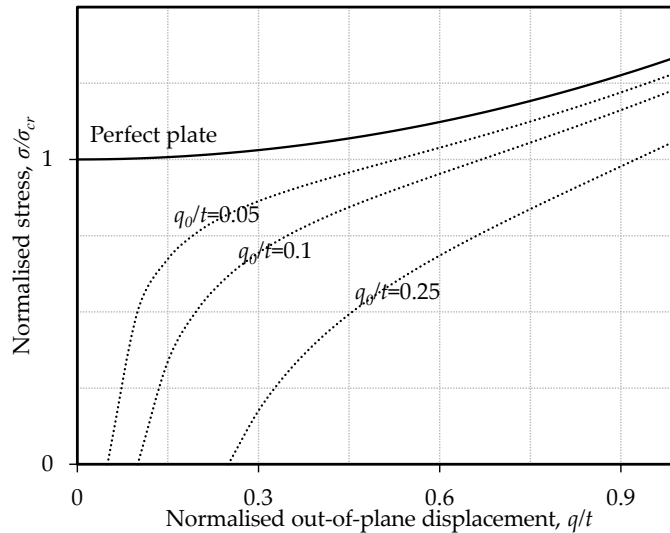


Figure 3.4: Effect of geometric imperfections on the postbuckling behaviour of a plate under uniform compression

3.4. Buckling and postbuckling behaviour of flat plates under biaxial compressive stresses

3.4.1. Linear elastic buckling behaviour

The elastic buckling stress of a rectangular isotropic plate under biaxial compression can be calculated using Eq. (3.3) setting the buckling coefficient equal to (Brush & Almroth, 1975; Reddy, 2007)¹⁰

$$k_{\sigma} = \frac{\left(\frac{m^2}{\alpha^2} + n^2\right)^2}{\frac{m^2}{\alpha^2} + n^2 \gamma} \quad (3.9)$$

where γ is the ratio between the stresses in the two orthogonal directions ($=-\sigma_y/\sigma_x$). Figure 3.5 to Figure 3.8 plot Eq. (3.9) for several values of γ .

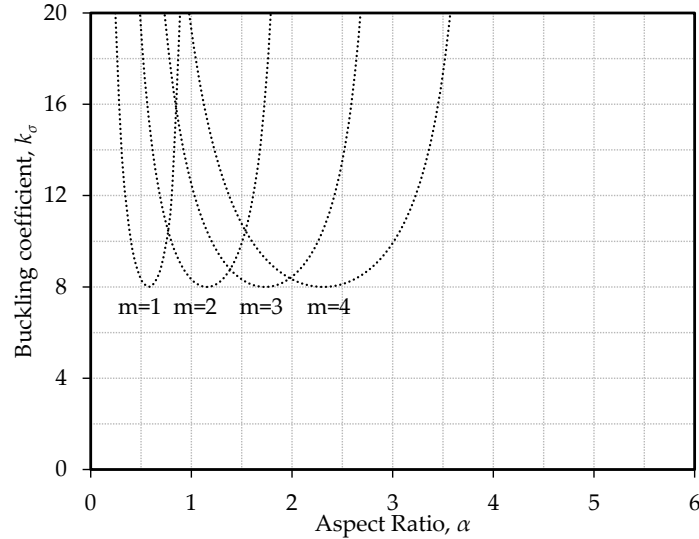


Figure 3.5: Plot of Eq. (3.9), $n=1$ and $\gamma=-1$

¹⁰ The derivation is given in the mentioned references.

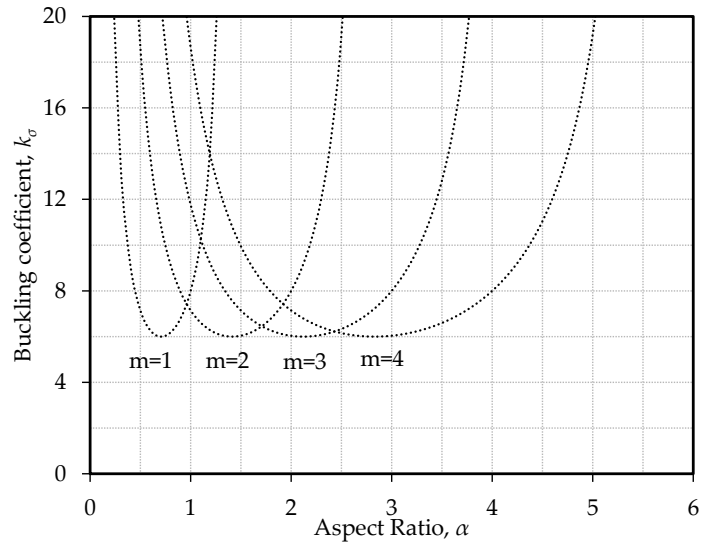


Figure 3.6: Plot of Eq. (3.9), $n=1$ and $\gamma=-0.5$

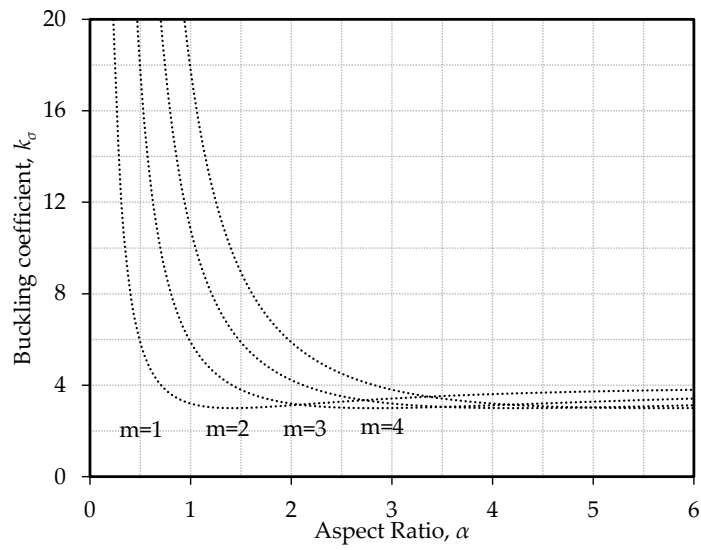


Figure 3.7: Plot of Eq. (3.9), $n=1$ and $\gamma=0.25$

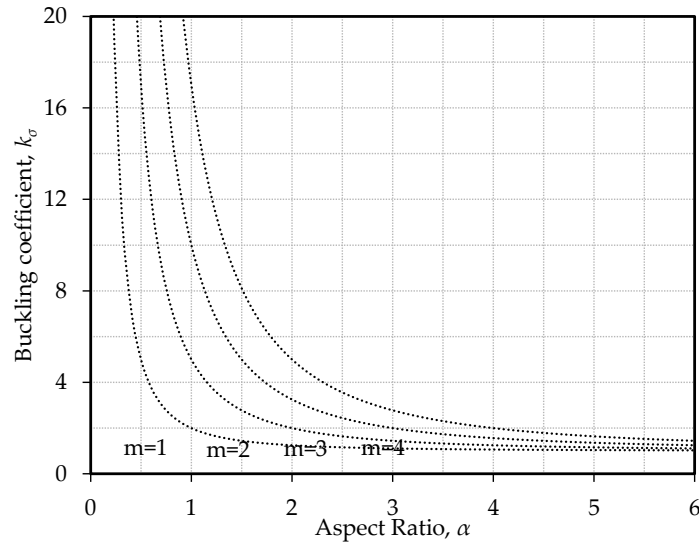


Figure 3.8: Plot of Eq. (3.9), $n=1$ and $\gamma=1$

As one would expect, for negative values of γ (*i.e.* tensile stresses at y -direction) the elastic buckling coefficient is higher than for plates under uniaxial compressive stresses (*i.e.* $\gamma=0$) and for positive values of γ (*i.e.* compressive stresses on the y -direction) the elastic buckling coefficient is lower than for plates under uniaxial compressive stresses. These statements are easily proven by setting to zero the first derivative of k_σ function to α and studying the behaviour of the function $k_\sigma(\alpha)$ when α is in the vicinity of infinity. The first process yields the values of aspect ratio for which k_σ takes a minimum value (Eq. (3.10) only shows positive real solutions)

$$\frac{\partial k_\sigma}{\partial \alpha} = 0 \Leftrightarrow \alpha = \frac{m}{\sqrt{n^2 - 2n^2\gamma}} \quad (3.10)$$

Analysing Eq. (3.10) it is concluded that it only represents a real number for $\gamma < 0.5$ (this conclusion results from imposing $n^2 - 2n^2\gamma > 0$). Replacing α by the expression obtained in Eq. (3.10) into Eq. (3.9) yields an expression of the minimum values of the elastic buckling coefficient

$$k_{\sigma, \min} = \frac{(2n^2 - 2n^2\gamma)^2}{n^2 - n^2\gamma} \quad \text{for } \gamma < 0.5 \quad (3.11)$$

For values $\gamma \geq 0.5$ the minimum value of the elastic buckling coefficient occurs only for in the vicinity of infinity

$$k_{\sigma, \min} = \lim_{\alpha \rightarrow +\infty} \frac{\left(\frac{m^2}{\alpha^2} + n^2\right)^2}{\frac{m^2}{\alpha^2} + n^2\gamma} = \frac{n^2}{\gamma} \quad \text{for } \gamma \geq 0.5 \quad (3.12)$$

Figure 3.9 plots the two expressions which return the minimum values of the elastic critical stress coefficient of plates under biaxial loading. As it was initially stated, it is now easy to accept that for $\gamma < 0$ (compression-compression), k_{σ} for plates under biaxial loading is higher than for plates under uniaxial compressive stresses and for $\gamma > 0$ (tension-compression), k_{σ} is lower than for plates under uniaxial compressive stresses. Table 3.3 summarises the expressions for computing the elastic buckling coefficient of plates under biaxial loading, giving also some examples of k_{σ} for several values of γ .

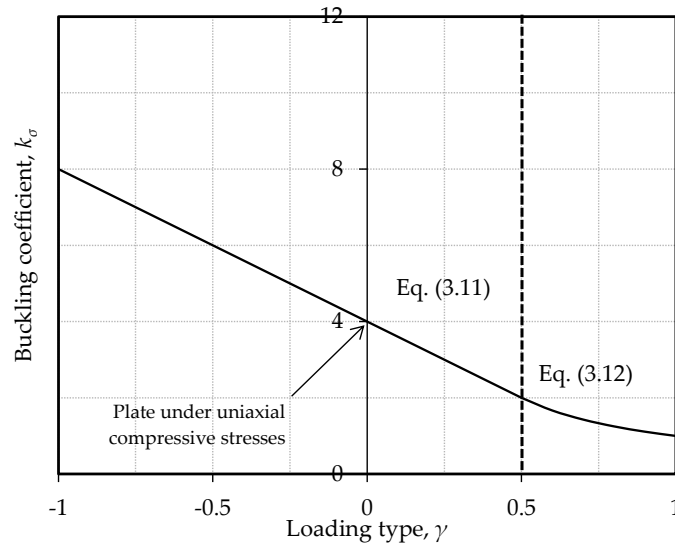


Figure 3.9: Plot of Eq. (3.11) and (3.12), $n=1$

Table 3.3: Values of $k_{\sigma,min}$ for plates under biaxial loading

<i>Type of loading, γ</i>	<i>Minimum values of k_{σ} ($n=1$)</i>	<i>Expression of $k_{\sigma,min}$</i>
-1	8	
-1/2	6	$\frac{(2n^2 - 2n^2\gamma)^2}{n^2 - n^2\gamma}$
0	4	
1/4	3	
1/2	2	$\frac{n^2}{\gamma}$
1	1	γ

3.4.2. Postbuckling behaviour

As already discussed, when a plate is under uniaxial loading it has a postbuckling reserve strength due to its ability of developing tensile membrane stresses (in an orthogonal direction to the load application) that have an overall stabilising effect, allowing the plate to reach higher loads than the theoretical bifurcation load. If compressive membrane stresses are added in the orthogonal direction to the main loading ($\gamma < 0$), *i.e.* in the direction of the stabilising stresses, the stabilisation effect is lost and the postbuckling strength reserve decreases. On the other hand, if extra tensile membrane stresses are added in the orthogonal direction ($\gamma > 0$) to the main loading, the stabilising effect is enhanced and the postbuckling strength reserve increases.

Although the sign of the orthogonal stresses is a crucial aspect for the postbuckling behaviour, there are other aspects that are almost as important, namely the plate's aspect ratio and the boundary conditions (Braun, 2010).

According to Braun, the aspect ratio is a fundamental parameter since it dictates the type of behaviour of the plate: plate-like or column-like behaviour (the latter cannot benefit from the development of stabilising tensile stresses). Additionally, for non-squared panels, *i.e.* for plates where column-like behaviour is relevant, the shape of the imperfections becomes important. Boundary conditions also play an important role in the postbuckling behaviour since the

stresses redistribution to the edges strongly depends on how the edges are fixed (see also 0). In this regard, Braun studied the influence of in-plane edge restraints and of rotational edge restraints. In both cases it was found that the more constrained the boundary condition the higher the postbuckling strength reserve will be (Braun, 2010).

3.5. Buckling and postbuckling behaviour of thin cylindrically curved panels under uniaxial compressive stresses

3.5.1. Linear elastic buckling behaviour

The buckling of cylindrically curved panels is a subject that has been studied for many years. However, this topic was not as popular as flat plates, which can explain some inconsistencies when predicting curved panel's critical stress using classical semi-analytical formulae. The misconceptions about curved panel's critical behaviour are well illustrated by Gerard's definition of its behaviour: "A curved plate loaded in axial compression buckles in the same manner as cylinder when the plate curvature is large, and when the plate curvature is small it buckles essentially as flat plate. Between these two limits, there is a transition from one type of behaviour to the other" (p. 54, Gerard & Becker, 1957). This characterisation of the buckling behaviour of cylindrically curved panels is not entirely correct as it is patent in a former work by Stowell in 1943 (Stowell, 1943) and recently demonstrated numerically by Tran *et al.* (2012). Whereas Gerard defends that cylindrically curved panels buckle similarly to a cylinder when the panel's curvature is large, Tran showed numerically that the critical stress of cylindrically curved panels tends to half the value of the cylinder's critical stress (in this work R , a , t and the boundary conditions are constant; b varies from 0 to $2\pi R$). This occurs due to the fact that even though the curved panel is a full cylinder of revolution, the longitudinal edges are independent from each other (*i.e.* the curved panel is a cylinder of revolution with a longitudinal cut-out). In what concerns the opposite limit, when the radius of curvature tends to infinity, the panel buckles as a flat plate. Figure 3.10 highlights the differences between plates, curved panels and cylinders. It

is clear that the buckling pattern of a curved panel has little in common with the buckling pattern of a cylinder. This is due to the fact that curved panels do not develop tensile circumferential membrane stresses in the same way as cylinders do, resulting in distinct buckling modes from those observed in cylinders (Martins *et al.*, 2013). Additionally, the existing formulae predicting the elastic critical stress of cylindrically curved panels (which are limited to uniform compressive stresses) present considerable errors (Martins *et al.*, 2013).

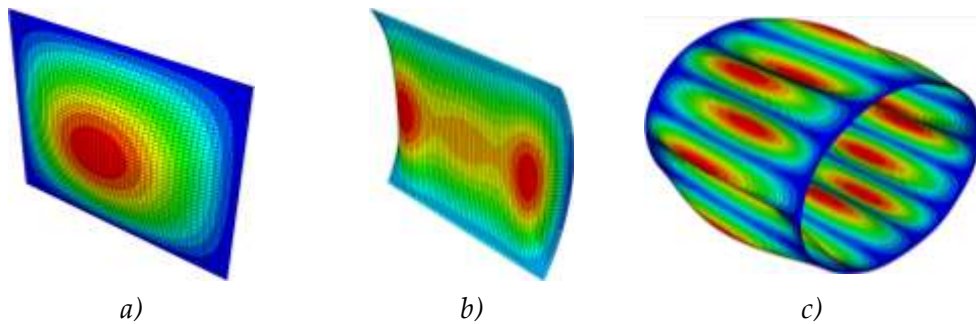


Figure 3.10: *a)* Plate, *b)* curved panel and *c)* cylinder behaviour subjected to longitudinal compressive stresses (1st buckling mode)

Redshaw carried out work mainly based on the use of energy methods such as the Rayleigh–Ritz method to determine theoretical buckling loads for curved panels under compression, Eq. (3.13), pure shear and combinations of both types of loading (Redshaw, 1934). Eq. (3.13) reduces to the flat plate buckling stress as one limit and to the classical cylinder buckling stress as the other limit (as already mentioned this trend for the behaviour of a curved panel is erroneous).

$$\sigma_{cr} = \frac{\pi^2 E}{6(1-\nu^2)} \left(\frac{t}{b}\right)^2 \left(1 + \sqrt{1 + \frac{12(1-\nu^2)}{\pi^4} Z^2}\right) \quad (3.13)$$

In 1936, Timoshenko based on approximated expressions for the plate's out-of-plane displacement, proposed a different expression, Eq. (3.14) (Timoshenko & Gere, 1961)

$$\sigma_{cr} = \begin{cases} \frac{\pi^2 E}{12(1-\nu^2)} \left(\frac{t}{b}\right)^2 \left(4 + \frac{3(1-\nu^2)}{\pi^4} Z^2\right) & \text{if } Z \leq \frac{4\pi^2}{\sqrt{12(1-\nu^2)}} \\ \frac{\pi^2 E}{12(1-\nu^2)} \left(\frac{t}{b}\right)^2 \left(\frac{4\sqrt{3(1-\nu^2)}}{\pi^2} Z\right) & \text{if } Z > \frac{4\pi^2}{\sqrt{12(1-\nu^2)}} \end{cases} \quad (3.14)$$

Later in 1943 Stowell proposed a modification of Redshaw's formula for cases in which the curvature of the plate is larger, Eq. (3.15) (Stowell, 1943)

$$\sigma_{cr} = k_{\sigma,plate} \frac{\pi^2 E}{24(1-\nu^2)} \left(\frac{t}{b}\right)^2 \left(1 + \sqrt{1 + \frac{48(1-\nu^2)}{\pi^4} \left(\frac{Z}{k_{\sigma,plate}}\right)^2}\right) \quad (3.15)$$

Furthermore, in this report, Stowell claims "The tests that have been made indicate, however, that the effect of curvature cannot always be relied upon to follow consistently the gradual increase in critical stress with increase in curvature" (p. 9, Stowell, 1943). In fact, the problem of non-negligible errors between experimental data and proposed formulae was corroborated by other authors who carried out experimental programs on curved panels, *e.g.* Cox & Clenshaw (1941); Crate & Levin (1943); Welter (1946); Schuette (1948).

In 1947, Batdorf proposed design curves devised to fit theoretical curves to experimental data using an equivalent Donnell's equation and proposed a solution by Fourier series that was afterwards calibrated with test data (Batdorf, 1947a; Batdorf, 1947b; Batdorf, 1947c). These design curves, which were based on the erroneous assumption that critical stress was equivalent to ultimate stress, still could not fully explain the discrepancies between theoretical and experimental results. These inconsistencies would be solved with the appearance of the concept of imperfection sensitivity and with the awareness that elastic critical stress was in fact different from ultimate stress (sec. 3.9 and sec. 3.11).

In 1963, using the Galerkin method and assuming a buckling shape described by Eq. (3.4), Volmir (1963) proposed the following expression to compute the elastic buckling stress of a simply supported curved square panel with all edges constrained (*i.e.* edge's deformation is constant along its length)

$$\sigma_{cr} = \frac{\pi^2 E}{12(1-\nu^2)} \left(\frac{t}{b}\right)^2 \left(4 + \frac{3(1-\nu^2)}{\pi^4} Z^2\right) \quad (3.16)$$

This is exactly the same formula as the first branch of Eq. (3.14). However, his most important contribution was the derivation of a formula to characterise the postbuckling behaviour (sec. 3.5.2).

In 2001 Domb and Leigh (Domb & Leigh, 2001), using FEM numerical analysis, refined Batdorf's curves and obtained more accurate values for the buckling coefficient of cylindrically curved panels under uniform compressive stresses.

$$k_\sigma = \begin{cases} 10^{\sum_{i=0}^3 c_i [\log(Z(1-\nu^2))]^i} & \text{if } 1 \leq Z(1-\nu^2) \leq 23.15 \\ c [Z(1-\nu^2)]^d & \text{if } 23.15 \leq Z(1-\nu^2) \leq 200 \end{cases} \quad (3.17)$$

where $c_0=0.6021$, $c_1=0.005377$, $c_2=0.192495$, $c_3=0.002670$, $c=0.4323$ and $d=0.9748$.

For very large values of Z , Figure 3.11 shows that formulae from Redshaw and Timoshenko tend to the elastic critical stress of cylinders of revolution; formulae from Stowell and Domb & Leigh tend to half of the elastic critical stress of cylinders of revolution (Tran *et al.* (2012) also reached this conclusion as already mentioned).

Magnucki & Mackiewicz in 2006 and Wilde *et al.* in 2007 studied the problem of an axially compressed cylindrical panel with three edges simply supported and one edge free (Magnucki & Mackiewicz, 2006; Wilde *et al.*, 2007). The range of validity of these studies is limited to values between $\pi/2$ and π of the sectorial angle θ . For smaller values of the sectorial angle, $\pi/6 \leq \theta \leq \pi/2$, Chu & Krishnamoorthy performed a similar study in 1967 (cited in Magnucki & Mackiewicz, 2006). In the first paper the authors solved the Donnell's equations for linear buckling of shells that were reduced to a generalised eigenvalue problem with the use of the Galerkin method. Wilde *et al.* (2007) developed an analytical model to predict the elastic buckling stress and performed a numerical study where a finite element model was modelled and the results compared to those obtained by Magnucki & Mackiewicz one year earlier. The comparison of the

solutions obtained with the analytical and numerical procedures showed that the differences between these results were small.

Eipakchi & Shariati in 2011 presented a study concerning the buckling stresses of cylindrically curved panels subjected to axial stress with the two opposite sides simply supported and the two other edges free or simply supported. The authors proposed an analytical method based on perturbation methods to find the buckling axial stress of a cylindrically curved panel (Eipakchi & Shariati, 2011).

Types of loading other than pure compression were studied by Featherston & Ruiz (1998), Featherston (2000), Domb & Leigh (2002), Domb (2002) and Amani (2011). However, none of these authors either studied or proposed formulae to compute the elastic critical stress of cylindrically curved panels under combinations of pure compression and pure in-plane bending.

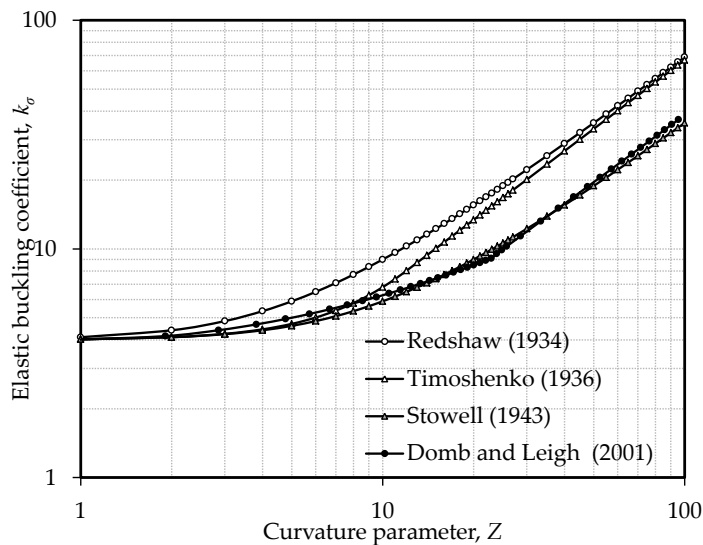


Figure 3.11: Comparison of formulae from Redshaw, Timoshenko, Stowell and Domb & Leigh

Similarly to flat stiffened plates, stiffened cylindrically curved panels may present four different buckling modes: global buckling of the cylindrically curved panel, local buckling of the stiffened cylindrically curved panel along longitu-

dinal stiffeners, local buckling of the unstiffened cylindrically curved panel along longitudinal stiffeners and local buckling of the stiffeners (Figure 3.12).

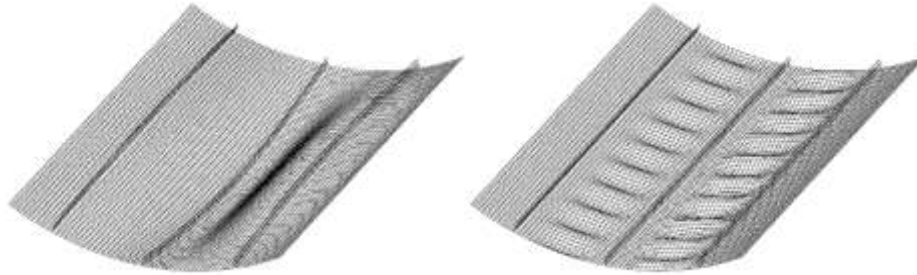


Figure 3.12: Global and local buckling pattern of curved panels
(Möcker & Reimerdes, 2006)

3.5.2. Postbuckling behaviour

“In contrast to columns, which have a neutral postbuckling path, and plates, which exhibit a stable post-buckling behaviour, shells (in which curved panels are included) usually have a very unstable postbuckling behaviour that strongly influences their buckling characteristics” (p. 625, Singer *et al.*, 2002). In fact, the change in equilibrium between equilibrium states of a perfect curved panel also occurs by bifurcation and it is denominated by asymmetric bifurcation. This type of bifurcation may lead to a stable or to an unstable postbuckling path. In practical terms, the postbuckling path will be determined by the imperfection direction.

Figure 3.13 shows the stable and unstable postbuckling paths for a cylindrically curved panel. The initial postbuckling behaviour of long narrow cylindrically curved panels was studied and discussed by Koiter (1956), Gerard & Becker (1957), Volmir (1963), Pope (1965), Tamate & Sekine (1969). Koiter considered the radial displacements suppressed along the longitudinal edges, *i.e.* simply supported unloaded edges. He demonstrated that as a consequence of increasing curvature the elastic buckling stress would have also to increase. On the other hand, Koiter also showed that increasing curvature led to highly unstable responses. On the field of advanced postbuckling response, Koiter stated: “it would appear to be not too bold a conjecture that the behaviour of a narrow

curved panel in the advanced postbuckling stage approaches the behaviour of a flat panel of equal width" (p. 76, Koiter, 1956). The postbuckling equilibrium path for a simply supported square panel without imperfections with all edges constrained (remain straight after buckling) can be deduced using the Galerkin method as in Volmir's work (Volmir, 1963; Chajes, 1974; Reis & Camotim, 2012)

$$\frac{\sigma}{\sigma_{cr}} = 1 + \frac{8}{3}(1-\nu^2) \left(1 + \frac{2}{\pi^4} Z^2\right) \left(\frac{q}{t}\right)^2 - \frac{10(1-\nu^2)}{\pi^4} Z \left(\frac{q}{t}\right) \quad (3.18)$$

Similarly to what has been done for plates, the postbuckling equilibrium path for the same curved panel with imperfections is given by

$$\frac{\sigma}{\sigma_{cr}} = \left[1 + \frac{8}{3}(1-\nu^2) \frac{(q^2 + 3qq_0 + 2q_0^2)}{t^2} \left(1 + \frac{2}{\pi^4} Z^2\right) - \frac{10(1-\nu^2)}{\pi^4} Z \left(\frac{q}{t} + q_0\right) \right] \frac{q}{q + q_0} \quad (3.19)$$

In Figure 3.13 it is shown how geometric imperfections can affect the postbuckling behaviour of a curved panel – $q_0/t > 0$ means that the imperfection is applied inwards and $q_0/t < 0$ means that the imperfection is applied outwards (see also 3.7).

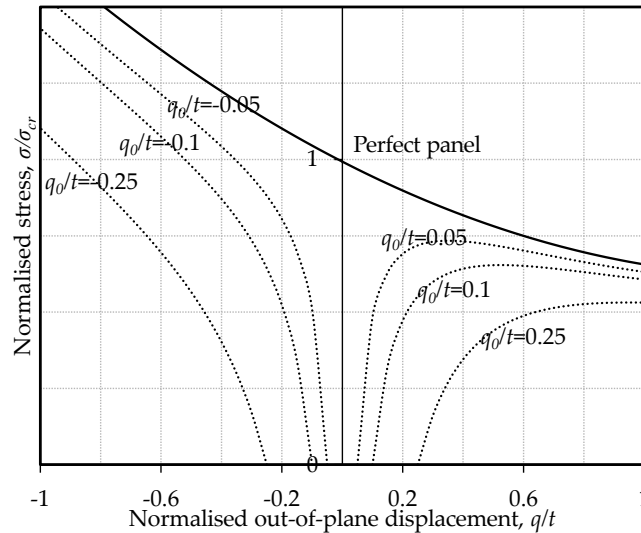


Figure 3.13: Effect of geometric imperfections on the postbuckling behaviour of a curved panel (plot of Eq. (3.19) for several values of q_0/t)

3.6. Buckling and postbuckling behaviour of thin cylindrically curved panels under circumferential compressive stresses

3.6.1. Linear elastic buckling behaviour

In steel construction, it is common to find unstiffened curved panels under compressive circumferential stresses (Figure 3.14). Due to the presence of curvature, the linear behaviour of the curved panel is immediately altered. This means that even for stockier panels (low values of slenderness) the width is reduced according to a reduction factor (see 3.12) which has an upper limit given by the following expression (Jetteur & Maquoi, 1984) (making $Z_t \rightarrow 0$, i.e. $R \rightarrow \infty$, it is easy to conclude that for flat plates $\rho_t = 1$)

$$\rho_t = 1 - \frac{8}{\pi^2 \left(1 + \frac{\pi^6}{96(1-\nu^2) Z_t^2} \right)} \quad (3.20)$$

where Z_t is the curvature parameter in the circumferential direction, given by Eq. (3.21) and the elastic critical stress of a cylindrically curved panel under circumferential compressive stresses is given by Eq. (3.22) (Jetteur & Maquoi, 1984).

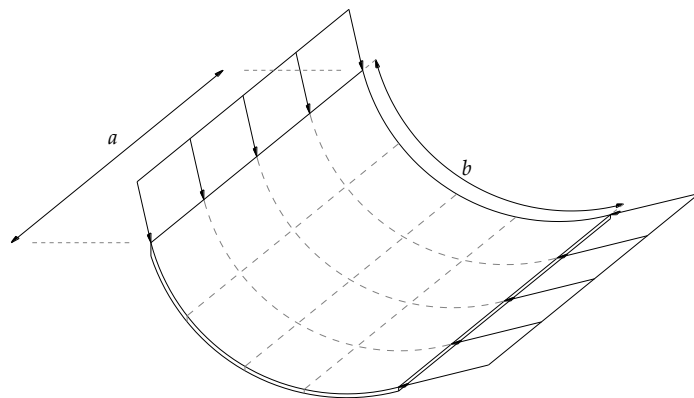


Figure 3.14: Scheme of a curved plate under circumferential compressive stresses

$$Z_t = \frac{a^2}{Rt} \quad (3.21)$$

$$\sigma_{cr} = \frac{3\rho_t}{4\rho_t - 1} \left(\frac{m}{\alpha} + \frac{\alpha}{m} \right)^2 \frac{\pi^2 E}{12(1-\nu^2)} \left(\frac{t}{b} \right)^2 \quad (3.22)$$

Again, for $Z_t=0$, Eq. (3.22) yields the same expression as does Eq. (3.3) for $k_\sigma=4$, *i.e.* the same expression for a flat plate under uniform compression is obtained. It is highlighted the fact that Eq. (3.22) returns always higher values than the elastic critical stress of a flat plate. The elastic buckling coefficient of cylindrically curved panels under circumferential compressive stresses is plotted in Figure 3.15.

It is worth stressing out the fact that for values of Z_t greater than 11, Eq. (3.22) returns a negative value. This means that this expression only is able to compute the value of the elastic critical stress for panels with low curvature. In fact, Jetteur & Maquoi (1984) refer the absence of numerical simulations for values of Z_t greater than 3.5 indicating that the authors did not investigate the behaviour for medium to high values of curvature.

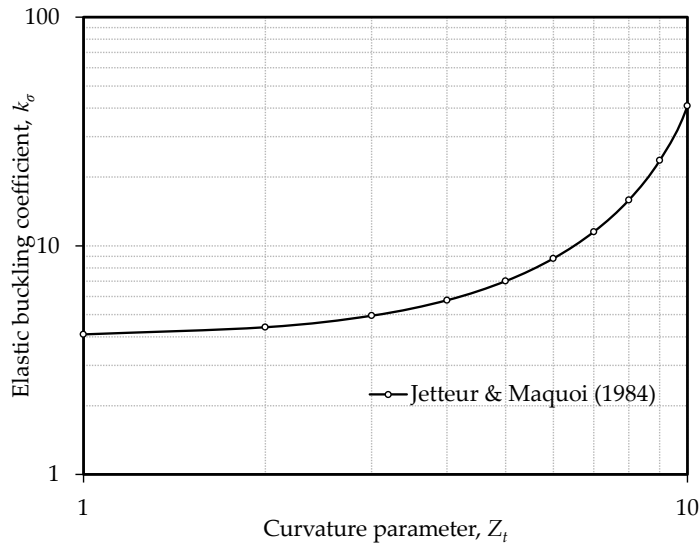


Figure 3.15: Elastic buckling coefficient for cylindrically curved panels under circumferential compressive stresses (Jetteur & Maquoi, 1984)

3.6.2. Postbuckling behaviour

The literature on the postbuckling of thin cylindrically curved panels under circumferential compressive stresses is very scarce. The only relevant documents are those by Jacques (1983) (cited in Jetteur & Maquoi (1984)) and Jetteur & Maquoi (1984). In the work of Jetteur & Maquoi, the postbuckling behaviour of the cylindrically curved panel under circumferential compressive stresses is completely defined by a set of equations that result from a variational analysis. Eq. (3.24) describing the out-of-plane deformation in the postbuckling regime is

$$\left[\frac{1}{\sigma_e} \left(\sigma_0 - \frac{8}{3\pi} \sigma_{red,1} - \frac{3}{4} \sigma_{red,2} \right) + \left(\frac{m}{\alpha} + \frac{\alpha}{m} \right)^2 \right] q = 0 \quad (3.23)$$

where q is the maximum value of the out-of-plane displacement (only the non-linear component), σ_0 represents a constant compression stress in the circumferential direction and $\sigma_{red,1}$ translates the loss of stiffness of the curved panel in the nonlinear (postbuckling) regime while $\sigma_{red,2}$ translates the stress redistribution known to happen to flat plates in the after buckling occurs.

3.7. Buckling and postbuckling behaviour of thin cylindrically curved panels under biaxial compressive stresses

3.7.1. Linear elastic buckling behaviour

Among the few authors that have studied the linear elastic buckling behaviour of biaxially loaded panels (Figure 3.16), the work of Hilburger *et al.* (2001) is here highlighted. The authors have reached several important conclusions in what concerns the linear elastic buckling behaviour of curved panels under biaxial loading, being one of the most important the fact that only panels under compression along the curved edges ($N_y/N_x = 0$) exhibits a bifurcation point; the remaining cases where $N_y/N_x \neq 0$ the curved panels exhibit a limit point. This is due to the fact that the loading in the transverse direction is responsible for pre-buckling out-of-plane deformations that act as geometric imperfections forcing the structural systems to adopt equilibrium configurations different

from the initial one for load values lower than the bifurcation point for a panel under uniaxial compression (N_x only). The same conclusion was later reached by Girish & Ramachandra (2008).

3.7.2. Postbuckling behaviour

In what concerns the postbuckling behaviour of cylindrical curved panels, the research outcomes from the two previously referred authors are similar: both Hilburger *et al.* (2001) and Girish & Ramachandra (2008) have concluded that the higher the value N_x/N_y the lower the limit point occurs; there is a specific value of N_x/N_y , which will clearly depend on the geometry of the curved panel, that defines the transition from an unstable postbuckling path to a stable postbuckling path.

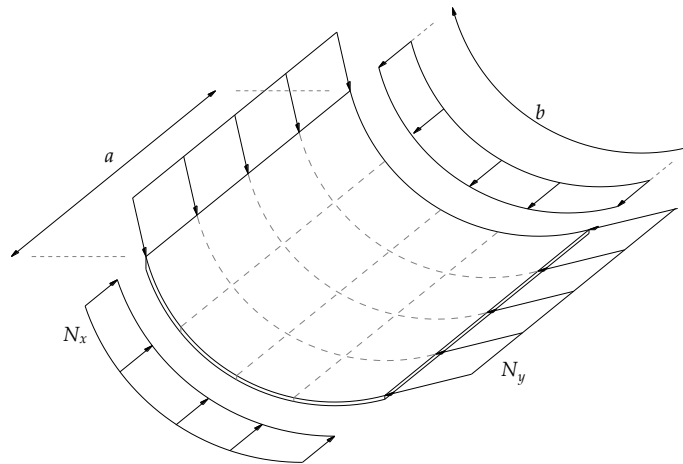


Figure 3.16: Scheme of a curved plate under biaxial compressive stresses

3.8. Elastic critical stress *vs.* ultimate stress and the effect of imperfections

The first attempts to compute ultimate strength of plates and shells assumed a perfect geometry of the structure and were based on the idea that the ultimate strength was the same as the elastic critical load. As experimental results revealed, theoretical results based upon these assumptions could not provide a

reliable model to compute the ultimate strength. These inconsistencies were only overcome with the awareness that imperfections are unavoidable (having a non-negligible effect on the ultimate strength) and that the elastic critical stress is radically different from the ultimate stress.

The most important works on this change on fundamental knowledge of shell stability are those from von Kármán *et al.* (1932) who for the first time use the effective width method to compute the ultimate strength of plates, von Kármán & Tsien (1941) and Donnell & Wan (1945) who calculated the load deformation curve for perfect and imperfect cylinders under pure compressive stresses, and the works of Koiter (1945) and, later, Budiansky & Hutchinson (1964), proving that initial imperfections were the main reason for the poor correlation for thin shells that buckle in the elastic domain. However, these studies have a serious limitation: they all assumed a constant imperfection shape during the application of load and/or displacement (Rotter & Schmidt, 2008).

Nowadays, the way to consider that imperfections are a variable parameter during the analysis of any kind of structure relies on advanced numerical applications using the finite element method. The finite element method allows performing fully nonlinear analysis (geometrically and materially nonlinear analysis with imperfections) and requires imperfections to be modelled explicitly as part of the model's geometry. The following types of imperfections may be considered:

- Geometric imperfections: imperfections applied to the initial shape of the structure. According to Schmidt (2000), Rotter (2004) and Braun (2010), these geometric imperfections may be: realistic shapes, the "worst" shape, stimulating imperfections, fabrication-oriented shapes, eigenmode affine and collapse affine shapes;
- Material imperfections: mainly residual stresses due to welding and/or forming processes and lack of material homogeneity;
- Loading systems imperfections: imperfections related to geometric imperfections but occurring at load application level (*i.e.* eccentricities at the point of application of the load).

The most common way to introduce imperfections into the analysis is to model only equivalent geometric imperfections¹¹. Since the appearance of hardware capable of efficiently solving problems using the finite element method, imperfection related studies have been extensively carried out. In the field of cylinders of revolution the following works are highlighted: Schenk & Schüeller (2003), that performed an extensive numerical study on random imperfection shapes; the works on the sensitivity to imperfections related to fabrication process that have been carried out by Pircher (Pircher, M., & Bridge, R. (2001) and Pircher (2004)); and the works of Teng & Song (2001) and Song *et al.* (2004), that have performed extensive numerical simulations comparing different geometric patterns of imperfections based on eigenmode affine shapes, nonlinear buckling modes shapes, postbuckling deformed shapes and weld depressions. On the specific field of cylindrically curved panels the recent works by Featherston (Featherston, 2003 and Featherston, 2012) are emphasised. In the first paper the imperfection sensitivity of curved panels is explored under the combined effect of axial and shear stresses. Two shapes for the imperfection shapes were considered which were combined with a range of amplitudes (from $0.1t$ to $3.0t$). It was concluded that the sensitivity to imperfections increases for curved panels with lower radius of curvature (*i.e.* curved panels with higher curvature parameter), and decreases when the aspect ratio is decreased. In the second paper, further numerical analysis using an adaptive mesh and with a geometric imperfection shape obtained from optical measurement of five specimens. Additionally, the specimens were experimentally tested in a compression rig and the numerical results were validated using the experiments resulting data. It was concluded that besides the geometric imperfection's amplitude, the geometric imperfection's shape is of high importance when determining the ultimate strength of curved panels. Moreover, a comprehensive parametric study on imperfection sensitivity of cylindrically curved panels is performed in Chapter 6.

¹¹ In what concerns the pattern and amplitude of equivalent geometric imperfections, ECCS manual on shell structures stability (Rotter & Schmidt, 2008) gives an extensive and accurate historical review of the most important works.

3.9. Ultimate strength of flat plates under uniaxial in-plane stresses

3.9.1. General

In the case of flat plates the postbuckling path is stable (Figure 2.1a)) and therefore, provided that the yield stress is higher than the critical stress (*i.e.* plates with medium to high slenderness), the postbuckling reserve can be exploited.

Several methods have been proposed to compute the ultimate strength of a plate under compressive stresses (effective width method, reduced stress method and yield line theory, to name a few). In the next sub-sections the effective width method is described in sec. 3.9.2 and the methods proposed by European standards (EN1993-1-5:2006) are presented further in this chapter in sec. 3.14.1.

3.9.2. Effective width method

In 1932, von Kármán *et al.* (1932) proposed a simplified method to obtain an approximation for the ultimate load carried by the buckled flat plate. According to his method the ultimate resistance is totally supported by two strips of equal width (effective width), located along the unloaded edges (longitudinal edges). The effective width concept is illustrated in Figure 3.17 and by Eqs. (3.24) and (3.25) and it may be regarded as the width of the plate which is under a uniform stress distribution, equal to the effective stress distribution in the total width of the plate.

In other words, this method establishes that the plate's width is divided into effective (at the longitudinal edges of the plate) and non-effective parts (at the central buckled part of the plate) as shown in Figure 3.17. Immediately before collapse the stress distribution in the plate's effective part is equal to f_y .

$$\rho = \frac{b_{eff}}{b} = \frac{1}{\lambda} \quad (3.24)$$

$$N_{Rd} = \int_0^b \sigma dx = b_{eff} t f_y = \rho b t f_y \quad (3.25)$$

where ρ is the reduction factor, b_{eff} is the effective width of the plate, b is the

actual width of the plate and λ is the reduced slenderness parameter of the plate given by

$$\lambda = \sqrt{\frac{f_y}{\sigma_{cr}}} \quad (3.26)$$

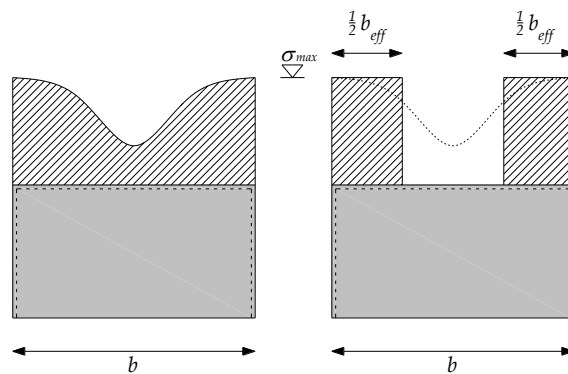


Figure 3.17: Effective width of a plate under compressive stresses

Without any room for doubt, the introduction of the concept of effective by von Kármán was a breakthrough in computing the ultimate strength of plates under compression. However, when compared to experimental results, this method only predicts accurately the ultimate strength for plates with very high values of slenderness (in this domain of slenderness the effects of initial imperfections are negligible and plates buckle in the elastic domain). This means that the von Kármán's formula is not appropriate for plates with medium values of slenderness where the effect of initial imperfections plays an important role in the ultimate strength. The realisation of this fact led other researchers to investigate deeper and propose formulae to predict the ultimate strength plates.

Among those researchers it is worth mentioning the works of Winter (1947), Eq. (3.27), Gerard (1957), Eq. (3.28), Faulkner (1965) (cited in Simões da Silva & Gervásio, 2007), Eq. (3.29), Usami (1993) and Johansson (1999) (cited in Simões da Silva & Gervásio, 2007), Eq. (3.30). Figure 3.18, compares these formulae.

Classically, Winter's formula is the most generally accepted one. It was adapted to stress gradient loading (Dubas & Gehri, 1986) and is still in use to estimate

the ultimate strength of internal plate elements in EN1993-1-5:2006 (CEN, 2006a), Eq. (3.49), and also in DNV-RP-201 (DNV, 2010a).

$$\begin{cases} \rho = 1 & \text{if } \lambda < 0.673 \\ \rho = \frac{1}{\lambda} \left(1 - \frac{0.22}{\lambda} \right) & \text{if } \lambda \geq 0.673 \end{cases} \quad (3.27)$$

$$\begin{cases} \rho = 1 & \text{if } \lambda < 0.792 \\ \rho = \frac{0.82}{\lambda^{0.85}} & \text{if } \lambda \geq 0.792 \end{cases} \quad (3.28)$$

$$\begin{cases} \rho = 1 & \text{if } \lambda < 0.55 \\ \rho = \frac{1.05}{\lambda} \left(1 - \frac{0.26}{\lambda} \right) & \text{if } \lambda \geq 0.55 \end{cases} \quad (3.29)$$

$$\begin{cases} \rho = 1 & \text{if } \lambda < 0.75 \\ \rho = \frac{1}{\lambda} \left(1 - \frac{0.1875}{\lambda} \right) & \text{if } \lambda \geq 0.75 \end{cases} \quad (3.30)$$

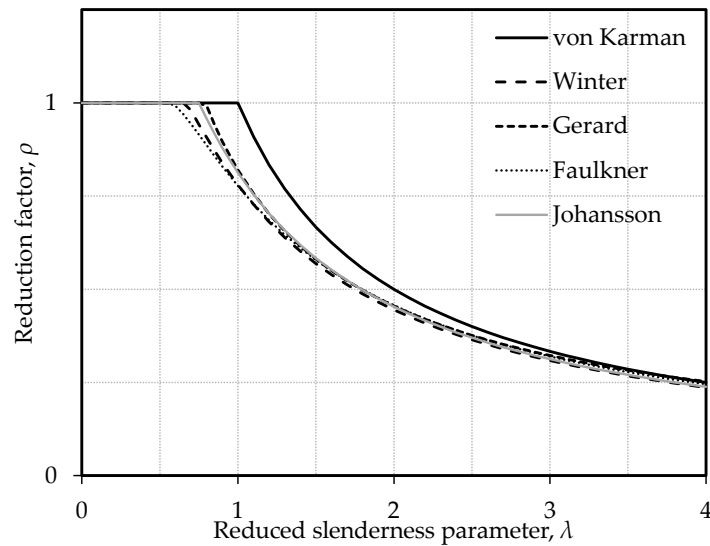


Figure 3.18: Effective width reduction factor according to von Kármán, Winter, Gerard, Faulkner and Johansson

In spite of the general acceptance of this design formula some authors stress out the fact that Winter's formula gives higher results than experiments for more slender welded plates (Clarín, 2007) and, sustained by numerical results, Veljkovic & Johansson (2009) claim that Winter formula does not incorporate accurately enough the possibility of material imperfections, namely residual stresses.

3.10. Ultimate strength of plates under biaxial stresses

3.10.1. General

In what concerns the evaluation of the ultimate strength of plates under biaxial loading, there are several studies along the past years that addressed this topic: Becker *et al.* (1970), Faulkner *et al.* (1973), Becker & Colao (1977), and Stonor *et al.* (1983) (who conducted experimental studies); and Valsgard (1980), Dier & Dowling (1980) and Cui *et al.* (2002) (who conducted numerical studies). All these authors proposed interaction formulae that can be generally expressed by Eq. (3.31).

$$\left(\frac{\sigma_{x,Ed}}{\rho_x f_y} \right)^{e_1} + V \left(\frac{\sigma_{x,Ed}}{\rho_x f_y} \right) \left(\frac{\sigma_{z,Ed}}{\rho_z f_y} \right) + \left(\frac{\sigma_{z,Ed}}{\rho_z f_y} \right)^{e_2} = 1 \quad (3.31)$$

Table 3.4: Definition of ρ_x and ρ_z and interaction values V , e_1 and e_2 in Eq. (3.31) according to several authors

Reference	ρ_x according to	ρ_z according to	V	e_1	e_2
Faulkner <i>et al.</i> (1973)	Faulkner (1965)	Own calc.	0	1	2
Valsgard (1980)	Faulkner (1965)	Valsgard (1979)	-0.25	1	2
Dier & Dowling (1980)	Own calc.	Own calc.	0.45	2	2
Stonor <i>et al.</i> (1983)	-	-	0	1.5	1.5
Cui <i>et al.</i> (2002)	Own calc.	Valsgard (1979)	0.1135	2	2

The difference between proposed interaction formulae relies on the definition of the reductions factors ρ_x and ρ_z (that can be evaluated according different authors, *e.g.* Winter's and Faulkner's formulae) and on the values of V , e_1 and e_2 (see Table 3.4).

Guedes Soares & Gordo (1996) reassessed some of the existing results and design methods for plates subjected to biaxial compression and concluded that the already adopted method in standards at that time¹² was valid, Eq. (3.32).

$$\left(\frac{\sigma_{x,Ed}}{\rho_x f_y}\right)^2 + \left(\frac{\sigma_{z,Ed}}{\rho_z f_y}\right)^2 = 1 \quad (3.32)$$

where ρ_x is the longitudinal reduction in biaxial compression (given by Faulkner's formula, Eq. (3.29)) and ρ_z is the transverse reduction in biaxial compression (given by Valsgard formula, see Guedes Soares & Gordo (1996)). However, the authors recommended that the formula should only be used for plates with relative high values for the plate's slenderness ($\lambda > 1.3$) while for stockier plates the von Mises criteria is adopted.

3.10.2. Braun (2010)

Recently, Braun (2010) exhaustively reviewed and evaluated earlier work in this field (including those already mentioned) concluding that: (i) a comparison of interaction curves proposed by all authors is difficult since they intensely rely upon the definition for the reference strength (*i.e.* the method used to assess the resistance to uniaxial compressive loading in both directions, *e.g.* Winter's and Faulkner's formulae); (ii) the reference strengths that are currently being used in standards and being applied in design are more favourable when compared to the ones which were used in the past. Additionally, the author questions the usability of the results from earlier work, carrying out own simulations which were the basis for his proposed interaction equation,

¹² Presently, the method proposed in DNV-RP-C201 (described in sec. 3.14.2) is different from the former DNV Offshore Standard (DNV, 1977) which was valid in 1996.

Eq. (3.33). The key parameters in Braun's parametric study were the slenderness (which was accounted for by changing the b/t ratio of the plates from 30 to 100), the plate's aspect ratio ($\alpha=1$ and $\alpha=3$), the imperfection shape (1 half-wave *vs.* 3 half-waves eigenmode shapes) and the in-plane and rotational edge boundary conditions (simply supported *vs.* clamped edges where all edges are constrained or all edges unconstrained).

$$\left(\frac{\sigma_{x,Ed}}{\rho_x f_y / \gamma_{M1}}\right)^2 + \left(\frac{\sigma_{z,Ed}}{\rho_z f_y / \gamma_{M1}}\right)^2 - V \left(\frac{\sigma_{x,Ed}}{\rho_x f_y / \gamma_{M1}}\right) \left(\frac{\sigma_{z,Ed}}{\rho_z f_y / \gamma_{M1}}\right) \leq 1 \quad (3.33)$$

where V is an interaction factor given by $\rho_x \cdot \rho_z$, when $\sigma_{x,Ed}$ and $\sigma_{z,Ed}$ are both in compression, or equal to 1, when at least $\sigma_{x,Ed}$ or $\sigma_{z,Ed}$ are in tension. In this formulation, Braun indicates that both the longitudinal reduction factor and the transverse reduction factor are to be calculated according to section 4.5.4(1) of EN1993-1-5:2006 (CEN, 2006).

The main conclusions of this work were that the aspect ratio together with the imperfection shape are of the utmost importance since they determine the lower bound resistance for non-square plates (in this case for plates with $\alpha=3$); and that the boundary conditions also determine the ultimate resistance of plates under biaxial loading, being the lower bound of that resistance given for the case where all edges are simply supported and unconstrained.

3.11. Ultimate strength of cylindrically curved panels under uniaxial in-plane stresses

3.11.1. General

As for plates, the ultimate strength of unstiffened cylindrically curved panels is governed by numerous parameters such as the postbuckling behaviour, boundary conditions, constitutive law of the material, geometric imperfections and material imperfections. Additionally, it depends on the curvature, expressed as the curvature parameter Z .

In the field of shell structures, Schmidt (2000) reviewed the most important contributions. Particularly relevant are the already referred works of von Kármán & Tsien (1941) and Donnell & Wan (1945) who calculated the load deformation curve for perfect and imperfect cylinders under pure compressive stresses, and the works of Koiter (1945), and Budiansky & Hutchinson (1964). Among the authors that have studied specifically the ultimate strength of cylindrically curved panels are Gerard & Becker (1957), Gerard (1959), Featherston & Ruiz (1998), Featherston (2000), Yumura *et al.* (2005) (cited in Yao *et al.*, 2006), Magnucki & Mackiewicz (2006) Wilde *et al.* (2007) and Park *et al.* (2009).

Featherston and Ruiz in 1998 and Featherston in 2000 carried out a series of tests to determine the accuracy of the theoretical elastic buckling loads and ultimate loads. Finite element analyses were compared to experimental results to evaluate this method as an alternative to determine collapse loads and postbuckling behaviour (Featherston & Ruiz, 1998; Featherston, 2000).

Later in 2003, Featherston presented a study where imperfection sensitivity of curved panels under combined compression and shear was addressed. The main conclusions of this study were that the imperfection sensitivity decreased with the increase of curvature and that in the majority of cases introduction of imperfections with the shape of the second eigenmode led to the maximum reduction in the ultimate strength¹³.

In 2005, Yumura *et al.* (2005) (cited in Yao *et al.*, 2006) investigated buckling/plastic collapse behaviour of compressed cylindrically curved plates. The authors performed an elastic eigenvalue analysis, an elastic large deflection analysis to investigate the characteristics of postbuckling behaviour and a series of elastic plastic large deflection analysis to clarify the buckling/plastic collapse behaviour (in Yao *et al.*, 2006).

Recently, Park in 2009 performed some studies to predict the buckling strength and ultimate strength of a simply supported cylindrically curved

¹³ Tran (2012) also reached the conclusion that the first buckling mode did not return the minimum collapse load for cylindrically curved panels (see sec. 3.11.2).

plate. The buckling strength and ultimate strength formulae are empirically derived based on a finite element method analysis (Park *et al.*, 2009).

$$\frac{\bar{\sigma}}{\sigma_{cr}} = \begin{cases} 1 & \text{if } \lambda' < 1 \\ \frac{2}{\lambda'} - \frac{1}{\lambda'^2} & \text{if } \lambda' \geq 1 \end{cases} \quad \lambda' = \lambda \sqrt{\frac{\sigma_{cr}^p}{\sigma_{cr}^c}} \quad \text{and} \quad \lambda = \frac{b}{t} \sqrt{\frac{f_y}{E}} \quad (3.34)$$

where λ' is the normalised slenderness parameter taking into account the effect of curvature by considering the value of the elastic critical stress, σ_{cr}^p is the elastic critical stress of the panel without curvature and σ_{cr}^c is elastic critical stress of the curved panel.

3.11.2. Tran (2012) and Tran *et al.* (2012)

Tran (2012) proposed two alternative methods to compute the ultimate strength of simply supported cylindrically curved panels subject to uniform axial compression. These approaches return a reduction factor that is applied to the plastic resistance of the panel ($f_y.b.t$) giving its ultimate strength.

The first one is based on a modification of the Ayrton-Perry approach (Tran *et al.*, 2012)

$$\chi = \frac{2\beta}{\beta + \lambda + \sqrt{(\beta + \lambda)^2 - 4\beta(\lambda - \alpha_z(\lambda - \lambda_{z,0}))}} \quad (3.35)$$

$$\beta = \frac{1 + 0.97^Z}{2} \quad (3.36)$$

$$\lambda_{z,0} = 0.2 + 0.473(0.95^Z) \quad (3.37)$$

where α_z is the elastic imperfection reduction factor (Table 3.5), $\lambda_{z,0}$ is the length of the initial plateau where no reduction of the panel's resistance occurs and β a numerical parameter and it represents the influence of curvature on the value of the imperfection factor.

Tran (2012) also proposed a second approach based on the Ayrton-Perry approach but, as it is very similar to the one described above, it will not be considered here.

Table 3.5: Values of α_z (Tran *et al.*, 2012)

Z	0	10	20	30	≥40
α_z	0.28	0.38	0.33	0.21	0.13

The second approach is based on EN1993-1-6:2007 (CEN, 2007) (Tran, 2012) and proposes the following set of formulae

$$\chi = \begin{cases} 1 & \text{if } \lambda \leq \lambda_{z,0} \\ 1 - \beta \left(\frac{\lambda - \lambda_{z,0}}{\lambda' - \lambda_{z,0}} \right) & \text{if } \lambda_{z,0} \leq \lambda \leq \lambda' \\ \frac{\alpha_z}{\lambda^2} & \text{if } \lambda' \leq \lambda \end{cases} \quad (3.38)$$

$$\lambda_{z,0} = 0.2 + 0.473e^{-\frac{Z}{20}} \quad (3.39)$$

$$\lambda' = 0.673 + 0.54e^{-\frac{4}{Z}} \quad (3.40)$$

$$\beta = 0.54e^{-\frac{2.7}{Z}} \quad (3.41)$$

$$\alpha_z = A_z \lambda + B_z \quad (3.42)$$

$$A_z = \frac{1 + e^{-Z/33}}{2} \quad (3.43)$$

$$B_z = (1 - \beta)\lambda'^2 - A_z \lambda' \quad (3.44)$$

where $\lambda_{z,0}$ is the squash limit relative slenderness (or the initial plateau length), α_z is the elastic imperfection reduction factor¹⁴, β is the plastic range factor, η is an interaction exponent and λ' ¹⁵ is the slenderness limiting the elasto-plastic domain of the response of cylindrically curved panels.

¹⁴ α_z is used (as in the first approach) instead of α (as in the original proposal) in order to avoid possible confusion with aspect ratio.

¹⁵ λ' is used instead of λ_p (as is used in the original proposal) in order to avoid possible confusion with plate slenderness.

These studies were conducted assuming simply supported square panels with varying curvature ($0 \leq Z \leq 100$) where the loaded edges are constrained, *i.e.* the displacement along the edges is constant. The shape for geometric imperfections (equivalent geometric imperfections) is based on the first buckling mode with amplitude $\max(a/200; b/200)$. It is claimed that imperfections defined in this manner (similarly to the definition proposed in EN1993-1-5:2006) lead to safe results. Following the first study, Tran (2012) explored the imperfection sensitivity of cylindrically curved panels further: he concluded that initial shapes based upon the first buckling mode were not leading to minimum values of the ultimate strength. Nevertheless, in that study, it is pointed out that the maximum difference on the ultimate load when different buckling modes are chosen is only 3%. This led the author claiming that “The use of the first buckling mode as a shape for imperfection remains acceptable (...)” (translated from French, p. 95, Tran, 2012). However, as it will be exposed in Chapter 6, this is not true for all geometries of cylindrically curved panels. In the aforementioned chapter, an extensive parametric study on geometric imperfection sensitivity of cylindrically curved panels is performed. One of the conclusions is that, for certain combinations of curvature and aspect ratio, the ultimate load value varies not negligibly with amplitude and shape (which is based upon buckling modes). Within the parametric study limits, Tran’s method (χ - λ approach) is reliable but it depends on the calculation of the critical load by Stowell’s formula (Eq. (3.15)) thus not allowing the elastic critical stress to be obtained numerically.

Finally, it is only valid for square cylindrically curved panels under pure compressive loading leaving out different aspect ratios and loading conditions.

3.11.3. Tran *et al.* (2014) proposal

Recently, Tran *et al.* (2014) based on the Design of Experiment Methodology and on a quasi-Monte Carlo method for sampling definition proposed a reliable formula for computing the ultimate load factor for both stiffened and unstiffened cylindrically curved panels under pure compressive loads.

For the case of unstiffened panels, Eq. (3.45) gives the ultimate load factor depending on the aspect ratio, α , on the curvature parameter, Z , and on the thickness to width ratio, t/b .

$$\chi = (-0.09 + 0.326\alpha - 0.148\alpha^2) + (40.6 + 0.314Z)\left(\frac{t}{b}\right) - (444 + 8.40Z)\left(\frac{t}{b}\right)^2 \quad (3.45)$$

The big advantage of this formula when compared to the formulae proposed by Tran (2012) and Tran *et al.* (2012) is that it allows computing the ultimate load factor for cylindrically curved panels with different values of aspect ratio.

Nevertheless, it is highlighted that, as in Tran (2012) and Tran *et al.* (2012), this formula is calibrated with numerical results that only incorporate imperfections based on the first buckling mode and with amplitude of $b/200$. A discussion on the effect of shapes and amplitudes for the geometric imperfections on the ultimate load of cylindrically curved panels will be performed in Chapter 6.

Additionally, the parametric range of is rather limited. In fact, in Tran *et al.* (2014) proposal t/b ratio varies from 0.01 to 0.04; aspect ratio varies from 0.6 to 1.6 and b/R varies from 0 to 1. For panels with constant thickness equal to 10mm, these limits represent a parametric study with a range from 0.4 to 2.1 for the reduced slenderness parameter and a range from 0 to 26 for the curvature parameter. The justification given by the authors for this parametric range lies on usual geometric configuration of panels in bridge engineering. Although these geometric limits might be accurate, such limited parametric range does not allow the generalisation of formulae for other types of applications.

3.12. Ultimate strength of cylindrically curved panels under circumferential compressive stresses

3.12.1. General

According to Dubas & Gehri (1986), the problems to be taken into account when flanges curved in elevation are present in design are the following:

- The hyperbolic stress distribution over the girder depth for lower values of R/b ;

- Transverse bending of the flange produced by the radial components of the longitudinal stresses $\sigma.dA/R$, and the accompanying non-uniform distribution of these longitudinal stresses;
- Corresponding radial stresses in the webs.

In I-girders curved in elevation, studies of several authors (Massonet & Save, 1963; Vandepitte, 1982; and Vandepitte & Verhegge, 1983; all cited in Dubas & Gehri, 1986) show that, for stocky flanges, the ultimate strength is little affected by the presence of curvature.

However, in box-girders curved in elevation, the compressed flange usually has a significantly higher slenderness. To control the potential instability phenomena that might arise, several design standards and recommendations, based on experimental and computational results, indicate a limit value for the curvature (Dubas & Gehri, 1986). These limits, which were already mentioned in Chapter 1, are imposed to the curvature parameter of the plate, which should, in this case, be regarded in the transverse direction, Eq. (3.21).

Nevertheless, in several bridge designs (*e.g.* bow-string arch bridges), this limitation is impossible to cope with. In fact, in order to verify the values imposed by EN1993-1-5:2006 for the curvature parameter at the same time the radii of curvature are kept in a small range of values, the plates would have to be unfeasibly and uneconomically thick.

3.12.2. Jetteur & Maquoi (1984)

To overcome this gap in standards, Jacques *et al.* (1983) examined the problem of the buckling of unstiffened curved plates using the finite element method and, later, in 1984, Jetteur & Maquoi (1984) developed an approach based on a two-field variational principle and obtained a simplified formulation that models the physical response of cylindrically curved panels under compressive circumferential stresses. Part of the formulation was already presented in sec. 3.6, namely, the expressions for the linear elastic response.

Next, the formulae giving the reduction factors are presented. First, and mak-

ing $m/\alpha=1$, the complete analytical solution is addressed (where ρ_t is given by Eq. (3.20))

$$\rho = \min \left(\frac{1}{3} \left[1 + \frac{2}{\lambda^2} - \frac{1 + \frac{8}{\lambda^2}}{32\rho_t - 5} (1 - \rho_t) \right]; \rho_t \right) \quad (3.46)$$

Adding to this analytical solution, the authors of this study proposed two simplified approaches, the first based on von Kármán's formulae and the second based on Faulkner's formulae, Eq. (3.47)

$$\begin{cases} \rho = \rho_t & \text{if } \lambda < \frac{0.576}{\rho_t} \\ \rho = \frac{1.05}{\lambda} \left(1 - \frac{0.26}{\rho_t \lambda} \right) & \text{if } \lambda \geq \frac{0.576}{\rho_t} \end{cases} \quad (3.47)$$

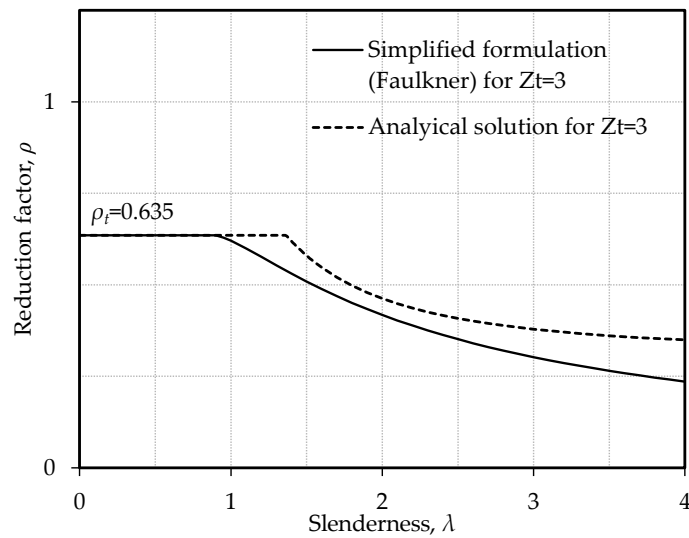


Figure 3.19: Effective width reduction factor for curved panels under circumferential stresses according to Jetteur & Maquoi (1984)

The difference between the two formulations is clear from Figure 3.19 (which plots both Eq. (3.46) and (3.47)). However, it should be pointed out that the

analytical solution does not account for the presence of imperfections, while the simplified formulation, due to its origin (from Faulkner's effective width formula) does.

It is also highlighted the fact that in this formulation the slenderness of the curved plates is evaluated by Eq. (3.26) as it is for flat plates.

3.13. Ultimate strength of cylindrically curved panels under biaxial compressive stresses

In what concerns the evaluation of the ultimate strength of cylindrically curved panels, literature is (to the extent of the author's knowledge) inexistent. All papers deal almost exclusively with the buckling and postbuckling behaviour of cylindrically curved panels (see sec. 3.7) omitting its ultimate structural response. Although some design standards (*e.g.* DNV-RP-C202, see sec. 3.14.3) allows computing the ultimate strength of cylindrically curved panels (within a full revolution orthogonally stiffened shell context) under biaxial loading, supporting background information seems to be missing or inaccessible.

This lack of literature and background information further justifies the need to study cylindrically curved panels under biaxial loading (sec. 5.4).

3.14. Design guidelines and standards

3.14.1. EN1993-1-5:2006 design procedure for plated structures under in-plane stresses

In section 4 of EN1993-1-5:2006 (CEN, 2006a) design rules are provided for built-up cross-sections from welded plates of class 4, based on the effective width method. Alternatively, EN1993-1-5:2006 (CEN, 2006a) provides the reduced stress method in section 10.

The effective width method for evaluating the stability of a plated cross-section under compressive stresses made according to the following expression

$$\eta_1 = \frac{N_{Ed}}{\frac{f_y A_{eff}}{\gamma_{M0}}} + \frac{M_{y,Ed} + N_{Ed} e_{y,N}}{\frac{f_y W_{y,eff}}{\gamma_{M0}}} + \frac{M_{z,Ed} + N_{Ed} e_{z,N}}{\frac{f_y W_{z,eff}}{\gamma_{M0}}} \leq 1 \quad (3.48)$$

where A_{eff} is cross-section's effective area, $W_{y,eff}$ and $W_{z,eff}$ are the cross-section's effective elastic section moduli according to y and z -direction, $e_{y,N}$ and $e_{z,N}$ are the neutral axis variation according to y and z -axis, respectively, N_{Ed} is the design axial force, $M_{y,Ed}$ and $M_{z,Ed}$ are the design bending moments and γ_{M0} is a partial safety factor¹⁶. In the case of unstiffened plates (where plate-like behaviour prevails – column-like behaviour only is relevant for very small values of aspect ratio) the effective cross-section may be obtained simply by adding all sub-panels with a reduced width according to specific effective width formulae. For internal compressed plate elements the following equation is used

$$\left\{ \begin{array}{ll} \rho = 1 & \text{if } \lambda < 0.5 + \sqrt{0.085 - 0.055\psi} \\ \rho = \frac{\lambda - 0.055(3 + \psi)}{\lambda^2} & \text{if } \lambda \geq 0.5 + \sqrt{0.085 - 0.055\psi} \end{array} \right. \quad (3.49)$$

where ψ is the stress gradient and λ is the slenderness parameter given by Eq. (3.26); or, for outstand compressed plate elements

$$\left\{ \begin{array}{ll} \rho = 1 & \text{if } \lambda < 0.748 \\ \rho = \frac{\lambda - 0.188}{\lambda^2} & \text{if } \lambda \geq 0.748 \end{array} \right. \quad (3.50)$$

In the case of stiffened plates the process is more complex and an interpolation between plate-like behaviour and column-like behaviour is required¹⁷. This interpolation scheme is given in 4.5.4 of EN1993-1-5:2006 and requires several intermediate calculations (for a more complete description of EN1993-1-5:2006 procedures for stiffened plates the reader is invited to further investigate the

¹⁶ The recommended value for γ_{M0} is 1.

¹⁷ Beg *et al.* (2010) presented a study (see Beg *et al.* (2010), pp.72-75) where it is stated "at realistic aspect ratios, plate-like behaviour may be easily ignored for heavy stiffened and even for normally stiffened plates and column-like behaviour for unstiffened plates" (p. 75, Beg *et al.*, 2010).

works of Johansson *et al.* (2007), Beg *et al.* (2010), among others and the EN1993-1-5:2006 standard itself).

Another method present in EN1993-1-5:2006 is the reduced stress method. It uses the von Mises criterion and contrasts to the effective width method in the following aspects (Beg *et al.*, 2010):

- The reduced stress method assumes a linear stress distribution up to the limit of the plate element which buckles first;
- For steel plated cross-sections the reduced stress method does not take into account load shedding from highly stressed to less stressed plate elements. As a result, the weakest plate element governs the resistance of the cross-section;
- The reduced stress method leads to a single step resistance calculation, erasing the necessity of the verification of each load type followed by a combination of these load types by means of an interaction equation.

The basic idea of the reduced stress method is a limit definition to the stress average of the actual stress distribution (Figure 3.20).

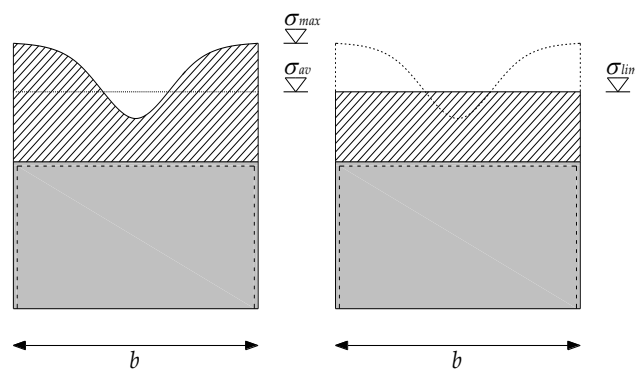


Figure 3.20: Basic notions of the reduced stress method

Furthermore, in those cases where the effective width method does not lead to a shift of the centre of gravity, *i.e.*, when the cross-section is symmetric and it is under pure compressive stress, it may be concluded that the two methods coincide.

The safety assessment of an element subjected only to compressive stresses in the x and z -directions by the reduced stress method needs to satisfy the following equation

$$\left(\frac{\sigma_{x,Ed}}{\rho_x f_y / \gamma_{M1}}\right)^2 + \left(\frac{\sigma_{z,Ed}}{\rho_z f_y / \gamma_{M1}}\right)^2 - \left(\frac{\sigma_{x,Ed}}{\rho_x f_y / \gamma_{M1}}\right) \left(\frac{\sigma_{z,Ed}}{\rho_z f_y / \gamma_{M1}}\right) \leq 1 \quad (3.51)$$

where ρ_x and ρ_z are reduction factors obtained from different sections of EN1993-1-5:2006. The reduced stress method is directly applicable to I- or box-girders where x -direction is the longitudinal direction, y -direction is the out-of-plane direction (strong axis) and z -direction is the transverse direction (weak axis). The reduction factors ρ_x and ρ_z are obtained from Eq. (3.49) or (3.50) (depending on the type of element – internal or outstanding). Alternatively, and as it is recommended by Beg *et al.* (2010), the calculation of ρ_z may be performed by the procedure given in annex B of EN1993-1-5:2006. This recommendation arises from the realisation that the “application of 4.5.4(1) [of EN1993-1-5:2006] and the interpolation between plate-like behaviour and column-like behaviour may lead to unsafe results as shown in Kuhlman *et al.* (2009)” (p. 165 Beg *et al.*, 2010).

3.14.2. DNV-RP-C201 design procedure for plated structures under in-plane stresses

DNV-RP-C201 (DNV, 2010a) gives design guidelines to assess the buckling strength of plated structures under several load arrangements. Here, the concern is set to unstiffened plates under longitudinal stresses and under biaxial loading.

For unstiffened plates under longitudinal stresses, the safety assessment is performed by verifying the following expression

$$\frac{\sigma_{Ed}}{\sigma_{x,Rd}} \leq 1 \quad (3.52)$$

where σ_{Ed} is the design applied stress and $\sigma_{x,Rd}$ is the design buckling resistance of an unstiffened plate under longitudinal stresses. Calculation of $\sigma_{x,Rd}$ is performed by direct application of the following equation

$$\sigma_{x,Rd} = \rho_x \frac{f_y}{\gamma_M} \quad (3.53)$$

where ρ_x is the reduction factor which is calculated exactly in the same way as in EN1993-1-5:2006, *i.e.* by Eq. (3.49) and Eq. (3.50). The main difference between DNV-RP-C201 and EN1993-1-5:2006 is that in the former ρ_x is seen as a resistance reduction factor, while for the latter it is seen as a width reduction factor. For the special case of uniform compression this difference is irrelevant, but for varying in-plane stresses it leads to distinct final values for the resistance. In sec. 8.5.2 this will be further addressed.

For an unstiffened plate under transverse compressive stresses (where shorter edges are loaded) safety is checked by verifying the following condition

$$\frac{\sigma_{Ed}}{\sigma_{z,Rd}} \leq 1 \quad (3.54)$$

where $\sigma_{z,Rd}$ is given by

$$\sigma_{z,Rd} = \left[\frac{1.3t}{a} \sqrt{\frac{E}{f_y}} + \kappa \left(1 - \frac{1.3t}{a} \sqrt{\frac{E}{f_y}} \right) \right] \frac{f_y}{\gamma_M} \quad (3.55)$$

It is brought to the attention of the reader that the above expression is an interpolation formula between plate-like buckling and column-like buckling where the column-like behaviour is accounted for by the factor κ , which is given by

$$\kappa = \begin{cases} 1 & \text{for } \lambda_c \leq 0.2 \\ \frac{1}{2\lambda_c^2} \left(1 + \mu + \lambda_c^2 - \sqrt{(1 + \mu + \lambda_c^2)^2 - 4\lambda_c^2} \right) & \text{for } 0.2 < \lambda_c < 2 \\ \frac{1}{2\lambda_c^2} + 0.07 & \text{for } \lambda_c \geq 2 \end{cases} \quad (3.56)$$

where λ_c and μ are given by

$$\mu = 0.21(\bar{\lambda}_c - 0.2) \quad (3.57)$$

$$\lambda_c = 1.1 \frac{b}{t} \sqrt{\frac{f_y}{E}} \quad (3.58)$$

It should be noted that Eq. (3.55) is suitable for plated structures in ships where large values of aspect ratio are common; on the other hand, it leads to wrong results when it is applied to plates approaching $a/b=1$ (Braun, 2010). A closer look to Eq. (3.56) reveals that it corresponds to the European Buckling Curve *a*.

Finally, in what concerns the safety assessment of unstiffened plates under biaxial loading, DNV-RP-C201 indicates Eq. (3.59) as the interaction formula

$$\left(\frac{\sigma_{x,Ed}}{\sigma_{x,Rd}} \right)^2 + \left(\frac{\sigma_{z,Ed}}{\sigma_{z,Rd}} \right)^2 - V \left(\frac{\sigma_{x,Ed}}{\sigma_{x,Rd}} \right) \left(\frac{\sigma_{z,Ed}}{\sigma_{z,Rd}} \right) \leq 1 \quad (3.59)$$

where V is given by

$$V = \begin{cases} 1 - \frac{b}{120t} & \text{for } \frac{b}{t} \leq 120 \\ 0 & \text{for } \frac{b}{t} > 120 \\ 1 & \text{if } \sigma_{x,Ed} \text{ or } \sigma_{z,Ed} \text{ is in tension} \end{cases} \quad (3.60)$$

and $\sigma_{x,Rd}$ and $\sigma_{z,Rd}$ are given by the already described expressions in this section.

3.14.3. DNV-RP-C202 design procedure for shell structures under membrane stresses

In DNV-RP-C202 (DNV, 2010b) the proof of safety for cylindrically curved panels under uniform compression is made according to the following expression

$$\frac{\sigma_{Ed}}{\sigma_{k,Rd}} \leq 1 \quad (3.61)$$

where σ_{Ed} is the design applied stress and $\sigma_{k,Rd}$ is the characteristic buckling strength. The design applied stress is obtained from the following expression

$$\sigma_{Ed} = \sqrt{\sigma_{x,Ed}^2 - \sigma_{x,Ed}\sigma_{z,Ed} + \sigma_{z,Ed}^2} \quad (3.62)$$

and the characteristic buckling strength of cylindrically curved panels under pure compression (with aspect ratio larger than 1) is given by (it should be noticed that in Eq. (3.64) if the acting stresses $\sigma_{0x,Ed}$ and $\sigma_{0z,Ed}$ are in tension they are considered to be equal to 0)

$$\sigma_{k,R} = \frac{f_y}{\sqrt{1 + \lambda^4}} \quad (3.63)$$

$$\lambda = \frac{f_y}{\sigma_{Ed}} \sqrt{\frac{\sigma_{0x,Ed}}{\sigma_{cr,x}} + \frac{\sigma_{0z,Ed}}{\sigma_{cr,y}}} \quad (3.64)$$

$$\sigma_{cr} = k_\sigma \frac{\pi^2 E}{12(1-\nu^2)} \left(\frac{t}{b}\right)^2 \quad (3.65)$$

$$k_\sigma = \Psi \sqrt{1 + \left(\frac{0.702Z \rho_i}{4}\right)^2} \quad (3.66)$$

where Ψ depends on the direction of the applied load (axial or circumferential) ρ_i translates the influence of initial imperfections on the characteristic buckling strength of the curved panel.

$$\Psi = \begin{cases} 4 & \text{for axial compression} \\ \left[1 + \left(\frac{b}{l}\right)^2\right]^2 & \text{for circumferential compression} \end{cases} \quad (3.67)$$

$$\rho_i = \begin{cases} \frac{0.5}{\sqrt{1 + \frac{R}{150t}}} & \text{for axial compression} \\ 0.6 & \text{for circumferential compression} \end{cases} \quad (3.68)$$

The design shell buckling strength is defined as

$$\sigma_{k,Rd} = \frac{\sigma_{k,R}}{\gamma_M} \quad (3.69)$$

where γ_M is material safety factor and it is defined according the following expressions

$$\gamma_M = \begin{cases} 1.15 & \text{if } \lambda < 0.5 \\ 0.85 + 0.6\lambda & \text{if } 0.1 < \lambda \leq 1.0 \\ 1.45 & \text{if } \lambda > 1.45 \end{cases} \quad (3.70)$$

It is pointed out that these formulas are applied to obtain the buckling strength of a particular buckling mode that may occur in a stiffened circular shell¹⁸. Therefore, boundary conditions are necessarily different from those that are considered further in this work (see 4.2.3).

3.15. Summary

In this chapter the characterisation of the behaviour of plates and cylindrically curved panels under several load arrangements was carried out. Particular attention was given to plates and cylindrically curved panels simply supported in all edges under axial compressive stresses and under biaxial compressive stresses.

Furthermore, this chapter is intended to gather essential information about previous works and standards, which will act as comparable data to the numerical analysis. For this purpose, the works from Tran (2012), Tran *et al.* (2012), Braun (2010) and the referred standards/design guidelines, namely, EN1993-1-5:2006 (CEN, 2006) are highlighted.

As a concluding remark, the reason why EN1993-1-6:2007 was not addressed in this chapter should be stated. In fact, it was mentioned that the scope of this

¹⁸ "The probable buckling modes of ring- and/or stringer-stiffened cylindrical shells can be sorted as follows: Local shell or curved panel buckling (i.e., buckling of the shell between adjacent stiffeners). The stringers remain straight and the ring stiffeners remain round. (...)" (p. 48, ABS, 2004)

European standard falls outside the scope of cylindrically curved panels. Nevertheless, the design guideline from Det Norske Veritas DNV-RP-C202 was addressed. This is due to the fact that DNV-RP-C202 incorporates in its design procedure for the determination of the ultimate resistance of shells of revolution a buckling collapse mode exclusively related to the buckling of the shell panel between longitudinal and ring stiffeners.

4. Numerical models of cylindrically curved panels under compressive stresses

4.1. Chapter overview

This chapter addresses all numerical models and numerical analyses that were carried out throughout this thesis. These analyses were performed using the FEA software ABAQUS FEA (Simulia, 2011). All data required to perform LBA and GMNIA (geometry, material properties, loading and boundary conditions, imperfections, finite element type and mesh discretisation) is described in sec. 4.2.

Sec. 4.3 describes the types of performed analysis highlighting the main cautions when using the finite element method. Specifically, LBA and GMNIA analysis are addressed.

The validation of the numerical model is carried out in sec. 4.4. The validation is achieved by comparing previous well-established results from the literature with results from numerical simulations. Both LBA and GMNIA are validated for flat and cylindrically curved panels.

Finally, a short study on the suitability of the curvature parameter as defined in Eq. (3.1) is presented.

4.2. Data for finite element analysis

4.2.1. Geometry

Since the models are all cylindrically curved panels, their geometry can be fully described by 4 parameters (see sec. 3.2 and Figure 3.1):

- a is the length of the panel;
- b is the width of the panel;
- t is the thickness of the panel;
- R is the radius of curvature of the panel.

The last 3 parameters are usually merged into 1 parameter called the curvature parameter Z given by Eq. (3.1). Since the finite element method requires the replacement of the real geometry of the structure by a discretised one, a sub-routine able to compute the coordinates of all points of a previously defined mesh discretisation was implemented.

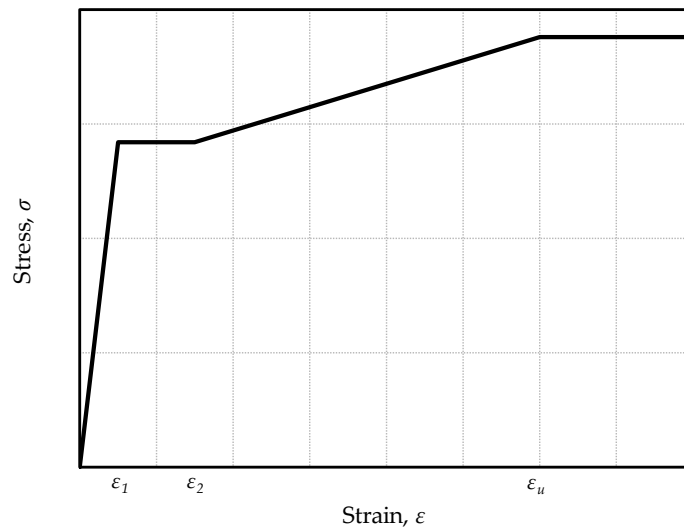
4.2.2. Material properties

The mechanical properties of steel are characterised by Young's modulus E , yield stress f_y and ultimate strength f_u given by EN10025-2:2004 (CEN, 2004), and strain hardening behaviour. The steel grade considered is S355 JR. Although recommendations for material models are given in Annex C of EN1993-1-5:2006 (CEN, 2006a) the one followed in this work is described in ECCS Publication no. 125 (Rotter & Schmidt, 2008) and it is represent in Figure 4.1.

For numerical simulations purposes ECCS recommendations (Rotter & Schmidt, 2008) state that it may be appropriate to disregard the plastic plateau (a plastic plateau with zero slope may cause numerical convergence problems). This comment was taken into account to model the material for numerical simulations purposes ($\varepsilon_1 = \varepsilon_2$). Table 4.1 summarises all information necessary to model the material.

Table 4.1: Material properties

<i>Young's modulus, E</i>	<i>Poisson's coefficient, ν</i>	<i>Yield stress, f_y</i>	<i>Ultimate stress, f_u</i>
210 GPa	0.3	355 MPa $t \leq 16\text{mm}$	470 MPa $3 < t \leq 80\text{mm}$

**Figure 4.1:** Material behaviour from Rotter & Schmidt (2008)

4.2.3. Loading and boundary conditions

Only simply supported panels are studied in this work. The boundary conditions are implemented in the shell model as shown in Figure 4.2. The following restraints are imposed: central point restrained in x -direction, points E and F restrained in z -direction; all edges restrained in y -direction. Additionally, the following restraints are defined:

- Boundary conditions type 1 (BC1): loaded edges and unloaded edges free-to-wave (unconstrained);
- Boundary conditions type 2 (BC2): loaded edges remain straight (constrained) and unloaded edges free-to-wave (unconstrained), actual representation in Figure 4.2 *b*) and *c*);
- Boundary conditions type 3 (BC3): loaded edges and unloaded edges remain straight (constrained), actual representation in Figure 4.2 *d*).

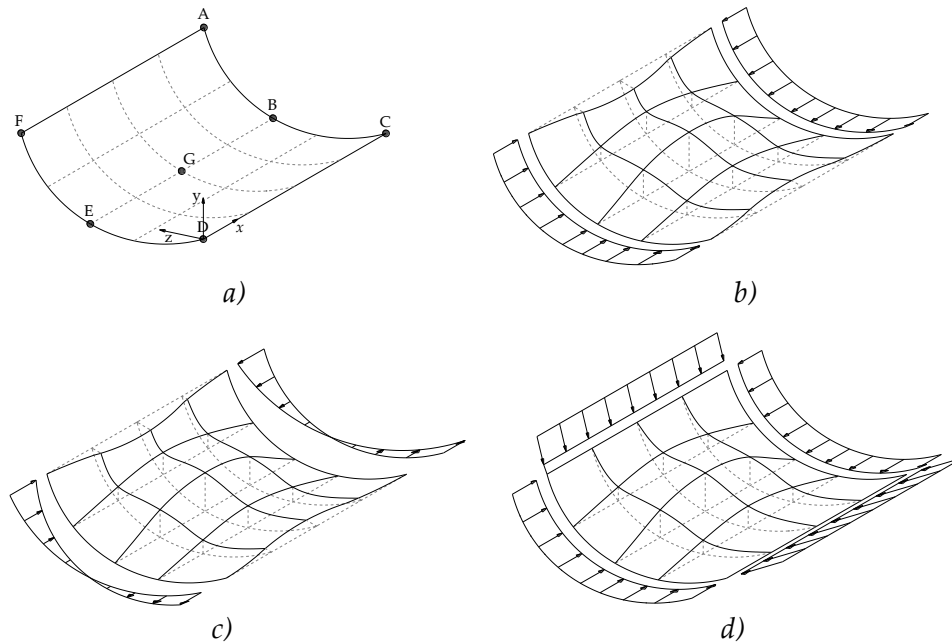


Figure 4.2: Loading and boundary conditions for cylindrically curved panels under uniaxial and biaxial stresses

Boundary conditions type 2 are the most common to use as they simulate approximately the boundary conditions of a bottom flange in a box-girder: web flexibility (unloaded edges free-to-wave) and rigid diaphragm (loaded edges constrained). Therefore, boundary conditions type 2 will be the basis of the parametric study for cylindrically curved panels under uniaxial stresses; while boundary conditions type 3 will be the basis of the parametric study for cylindrically curved panels under biaxial stresses (Chapter 5). Nevertheless, boundary conditions type 2 is still an approximation to real situation and, therefore, boundary conditions type 1 and type 3 are introduced as limiting scenarios. The intention is to sporadically make comparisons between the 3 different boundary conditions. Exception is made to the parametric study of cylindrically curved panels under biaxial loading where boundary conditions type 3 are used exclusively. In ABAQUS (Simulia, 2011) these boundary conditions are easily applied recurring to keyword **BOUNDARY*. To simulate the constrained edges in boundary conditions type 2 and 3, keyword **EQUATION* was used.

The load is applied as point loads at element nodes along the curved edges and varies from pure compression $\psi=1$, to pure in-plane bending $\psi=-1$. The stress gradient has the same definition as in EN1993-1-5:2006 (CEN, 2006a) being obtained from the following expression

$$\psi = \frac{\sigma_1}{\sigma_2} \quad (4.1)$$

The magnitude of the applied loads is not of the utmost importance since it is the maximum load factor (MLF) that will be evaluated and from where the ultimate strength will be computed. Nevertheless, in order to simplify computations and interpretation of results, the total magnitude of the applied loads equals *b.t.f_y*, *i.e.* the yielding strength.

4.2.4. Imperfections

In Europe, when numerically modelling plated structures, imperfections may be treated by Annex C of EN1993-1-5:2006 (CEN, 2006a). It is stated that both geometric and material related imperfections should be taken into account or, alternatively, in a more straightforward way, only equivalent geometric imperfections may be considered. If the first approach is chosen, the shape of geometric imperfections should follow the shape of relevant eigenmodes with a recommended amplitude of 80% of the fabrication tolerance limits (this recommendation is based on engineering judgement (Johansson *et al.*, 2007)) which are defined by EN1090-2:2002 (CEN, 2008), and the material related imperfections (residual stresses) should be represented by a stress field on the element and should translate the fabrication process (welding and forming). On the other hand, if the second approach is chosen, it is recommended to use an eigenmode shape or shapes defined in Figure C.1 of EN1993-1-5:2006 with amplitudes defined in Table C.2. In the case of unstiffened isolated plates or sub-panels the amplitude proposed by EN 1993-1-5:2006 is given by the following expression

$$\Delta w_{0,eq,EN1993-1-5} = \min(a/200; b/200) \quad (4.2)$$

where a is the panel's length and b is the panel's width. For shell structures (shells of revolution), recommendations on how to consider geometric imper-

fections are given in clause 8.7 of EN1993-1-6:2007, where it is stated that “imperfections should generally be introduced by means of equivalent geometric imperfections”. The amplitude of the equivalent geometric imperfections is given by the following expression

$$\Delta w_{0,eq,EN1993-1-6} = \max(l_g U_n, 25tU_n) \quad (4.3)$$

where l_g is the relevant gauge length according to the clause 8.4.4(2) in EN1993-1-6:2007, U_n is the dimple imperfection amplitude parameter which depends on the fabrication tolerance quality class, and t is the shell’s thickness. In contrast to what is considered for plates, EN1993-1-6:2007 only recommends the eigenmode affine shape for geometric imperfections unless no other more unfavourable pattern can be justified. Additionally, it is recommended that the imperfection’s maximum amplitude should always be applied inwards. The introduction of the imperfection shape into the numerical model is done using the keyword **IMPERFECTION* and referring it to the respective LBA results and defining the desired amplitude.

4.2.5. Finite element type and mesh discretisation

Since the FEM is an approximate method, it will yield results containing unavoidable errors. Therefore, before trying to validate the numerical model, some considerations and revision on numerical good practices should be made. According to Frey & Jirousek (2001) the modelling of a structure by finite elements requires that some information be previously gathered, like the type of element used and the level of discretisation for the mesh. Both these options must answer the problem’s complexity and prove to be accurate in simulating the structure’s real behaviour. Otherwise, a finite element and a mesh discretisation too complex may lead to unnecessary amount of time of analysis. Therefore, in the next paragraphs the justification for the type of finite element and level of discretisation for the mesh is done.

In what concerns the finite element type, a nine-node thin shell elements S9R5 (Simulia, 2011) is used as this element has been shown to perform well in applications involving the modelling of curved geometries (Gardner & Ministro,

2004; Moen & Schafer, 2006) and it has a faster convergence, as fewer elements are needed^{19,20} (Table 4.2). Overall, the finite element S9R5 is characterised by:

- Using quadratic shape functions;
- Being suitable for thin shells with small strains and large rotations;
- Having 5 degrees-of-freedom per node;
- Being shear deformable;
- Having reduced integration for shear stiffness.

Table 4.2: Mesh convergence study for LBA

<i>Curvature</i>	<i>Type of element</i>	<i>N=20</i>	<i>N=30</i>	<i>N=40</i>	<i>N=50</i>	<i>N=100</i>
Z=0	S4	0.214	0.214	0.214	0.214	-
	S4R	0.215	0.214	0.214	0.214	-
	S8R5/S9R5	0.214	0.214	0.214	0.214	-
Z=10	S4	0.274	0.274	0.273	0.273	0.273
	S4R	0.274	0.273	0.273	0.273	0.273
	S8R5/S9R5	0.272	0.272	0.272	0.272	0.272
Z=100	S4	2.102	2.041	2.013	1.994	1.940
	S4R	1.990	1.992	1.986	1.976	1.935
	S8R5/S9R5	1.847	1.845	1.845	1.844	1.844

¹⁹ The S9R5 element is a doubly curved thin shell element with nine nodes and it uses a quadratic shape function to estimate displacements. Consequently, S9R5 elements are able to simulate the half-sine wave of a buckled panel with just one element (while S4 and S4R require at least 3 elements) (Moen & Schafer, 2006).

²⁰ It should be noticed that, due to the fact that S4/S4R finite element has 20 degrees-of-freedom while S8R5 has 40 degrees-of-freedom and S9R5 has 45 degrees-of-freedom, the convergence speed is measured by comparing results obtained using S4/S4R with results obtained using S8R5/S9R5 and half the number of finite elements.

Table 4.3: Mesh convergence study for GMNIA

<i>Curvature</i>	<i>Type of element</i>	<i>N=10</i>	<i>N=15</i>	<i>N=20</i>	<i>N=25</i>	<i>N=50</i>
Z=0	S9R5	0.227	0.225	0.224	0.224	0.224
Z=10	S9R5	0.207	0.206	0.205	0.205	0.205
Z=100	S9R5	0.135	0.133	0.132	0.132	0.132

Mesh discretization studies were performed and the conclusion was that 50 square elements were enough to achieve numerical convergence for LBA and 25 for GMNIA. Table 4.2 and Table 4.3 show this study (which was made reading values of load factors, being the total load applied equal to the plastic load).

4.3. Types of analyses

4.3.1. Linear buckling analysis

LBA (linear buckling analysis, also known as eigenvalue analysis) are used to predict the elastic buckling strength of an imperfection free structure. This elastic buckling strength happens by bifurcation (see Figure 2.1). Since nonlinearities and imperfection free structures are an idealisation of the real imperfect structure with nonlinear responses, the elastic buckling strength is a theoretical value and its usefulness ends (for the majority of the problems in the field of structural mechanics) with the calculation of the slenderness of the structure (see Chapter 3).

4.3.2. Geometrically and materially nonlinear analysis with imperfections

The postbuckling response of the cylindrically curved panel requires performing a GNA (geometrically nonlinear analysis) and/or a GMNIA (geometrically and materially nonlinear analysis with imperfections). The main difference between GNA and GMNIA is that the latter includes initial geometric imperfections and material nonlinearity.

In this study only GMNIA were performed and they applied the arc-length method, namely the modified Riks method (implemented in ABAQUS (Simulia, 2011) and applied using the keyword **STATIC, RIKS*). The arc-length method is well suited for structures which are able to support elevated loads but are very prone to instability, *i.e.* it is appropriate for obtaining nonlinear static equilibrium solutions for unstable structures, where the load level and/or the displacement decrease along the loading path (Crisfield, 1997). Nonetheless, this method must be employed with great caution (Rotter & Schmidt, 2008):

- It may miss the true bifurcation point when the change between the fundamental and a descending postbuckling path is abrupt (typical shell problems) – to overcome this problem a constrained small arc-length was defined (Figure 4.3);
- In some cases (namely those with medium to high values for the curvature parameter) the arc-length routine may decide on the loading path as the postbuckling path – this was carefully verified by observing the load-displacement curves. This might happen at a primary bifurcation load (Figure 4.4) or at a secondary bifurcation load (Figure 4.5);
- The arc-length routine may maintain the primary path instead of opting for the new secondary path at the bifurcation point thus missing the true bifurcation load leading to an overestimation of the ultimate load (for a GMNIA the presence of a potential bifurcation point can be evaluated by searching for loss of positive definiteness of the tangent stiffness matrix).

In some rare cases the arc-length routine may jump to a non-realistic postbuckling path. For example, in Figure 4.6, it can be seen at a lower load level a convergence problem characterised by a jump to a higher postbuckling path and, at a higher load level, a convergence problem characterised by the decision of the arc-length routine to follow the loading path as the postbuckling path. Additionally, the definition of the buckling resistance is taken as in annex C of EN1993-1-5:2006 (CEN, 2006a):

- Maximum load factor on the load-deformation curve;
- Maximum of 5% for principal membrane strains.

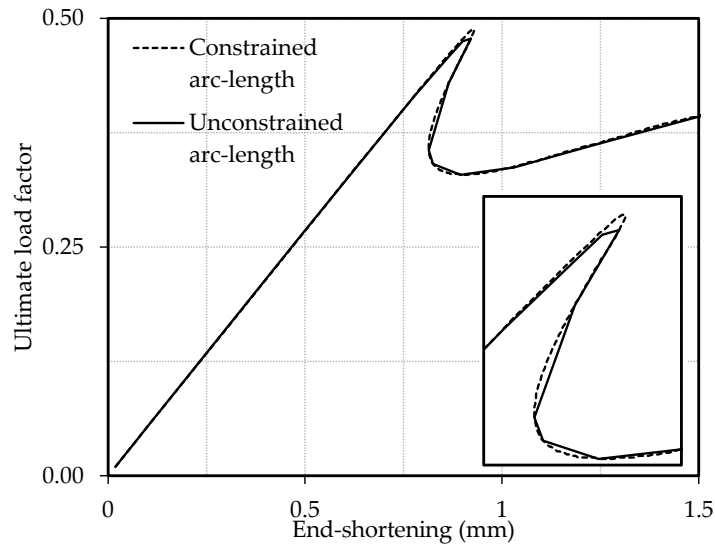


Figure 4.3: Example of a non-converged analysis ($Z=30$ and $\alpha=2.2$; imperfection pattern based on buckling mode 3 with maximum amplitude equal to 2 mm)

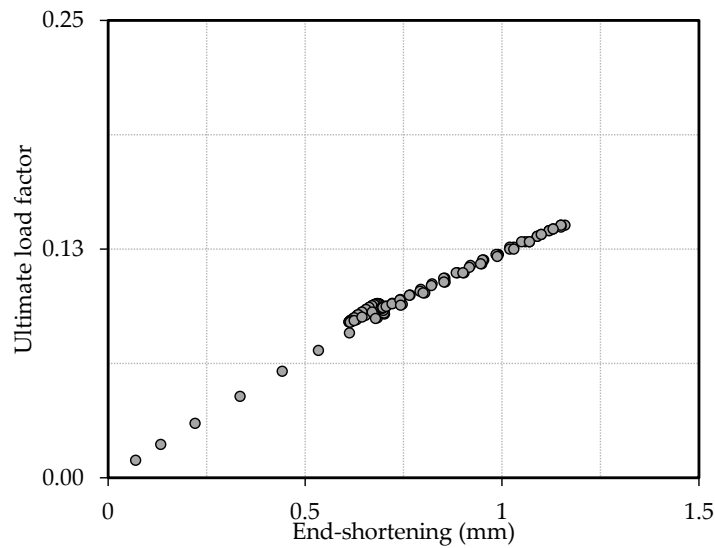


Figure 4.4: Example of a non-converged analysis ($Z=30$ and $\alpha=5.0$; imperfection pattern based on buckling mode 3 with maximum amplitude equal to 10 mm)

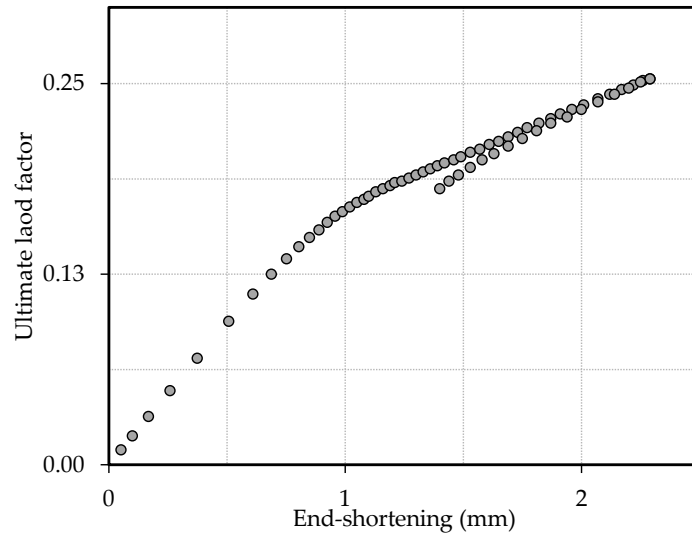


Figure 4.5: Example of a non-converged analysis ($Z=60$ and $\alpha=3.0$; imperfection pattern based on buckling mode 6 with maximum amplitude equal to 7 mm)

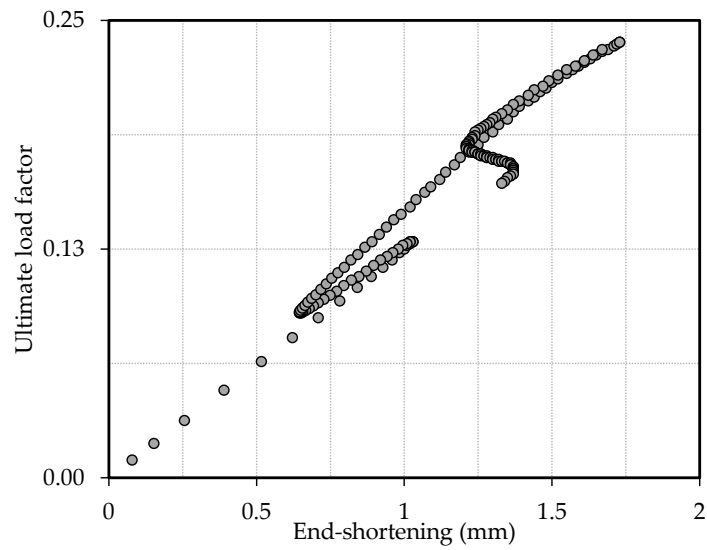


Figure 4.6: Example of a non-converged analysis ($Z=60$ and $\alpha=5.0$; imperfection pattern based on buckling mode 5 with maximum amplitude equal to 10 mm)

4.4. Validation of numerical models

4.4.1. Validation of LBA

The validation of flat panel's models is done by comparing numerical results with some analytical results from literature, namely from the classical Eq. (3.3) and from Timoshenko & Gere (1961), Table 3.2. Results are presented in Table 4.4 and the agreement is excellent (maximum error is equal to 0.4%).

In the case of cylindrically curved panels, the validation is done comparing numerical results with those obtained by Davaine & Tran (2010), Tran *et al.* (2012) and Tran (2012) (denoted by $k_{\sigma,Tran}$). Results are presented in Table 4.5 and agreement is very good (maximum absolute error is equal to 3.7 %).

Table 4.4: Validation of flat models for LBA

<i>Aspect ratio, α</i>	<i>Stress gradient, ψ</i>	<i>$k_{\sigma,Timoshenko}$</i>	<i>$k_{\sigma,num}$</i>	<i>Error (%)</i>
0.40	1	8.41	8.40	- 0.1
	0	15.10	15.13	+ 0.2
	-1	29.10	29.04	- 0.2
0.67	1	-	-	-
	0	-	-	-
	-1	23.90	23.87	- 0.1
1.00	1	4.00	4.00	0.0
	0	7.80	7.81	+ 0.1
	-1	25.60	25.50	- 0.4

Table 4.5: Validation of cylindrically curved models under uniform compressive stresses for LBA

<i>Stress gradient, ψ</i>	<i>Aspect ratio, α</i>	<i>Curvature, Z</i>	<i>$k_{\sigma, Tran}$</i>	<i>$k_{\sigma, num}$</i>	<i>Diff. (%)</i>
1	1	20	7.943	8.157	+ 2.6
		25	9.511	9.602	+ 0.9
		50	17.782	18.263	+ 2.6
		100	34.378	35.485	+ 3.1
	2	50	17.900	18.375	+ 2.6
		100	34.497	35.802	+ 3.6
		200	67.808	70.263	+ 3.5
		3	19	7.376	7.602
	50		17.426	17.974	+ 3.1
	100		34.378	35.339	+ 2.7
	200		67.927	70.503	+ 3.7

4.4.2. Validation of GMNIA

The validation procedure for flat models involves the evaluation of numerical results obtained by the modified Winter curve adopted by EN1993-1-5:2006 (CEN, 2006a) (Eq. (3.49) for $\psi=1$ and $\psi=-1$)²¹. According to Rusch & Lindner (2001) recommended values for the numerical recalculation of Winter curve for plates under pure compression are: *i*) equivalent geometric imperfection based on Eq. (3.4) ($n=1$) with amplitude equal to $b/420$ or, *ii*) geometric imperfection based on Eq. (3.4) ($n=1$) with amplitude equal to $b/500$ and residual stresses.

²¹ In case of pure in-plane bending, $\psi=-1$, equivalence between χ and ρ is not straightforward but it can be easily established by an iterative procedure given in sec. 8.3.

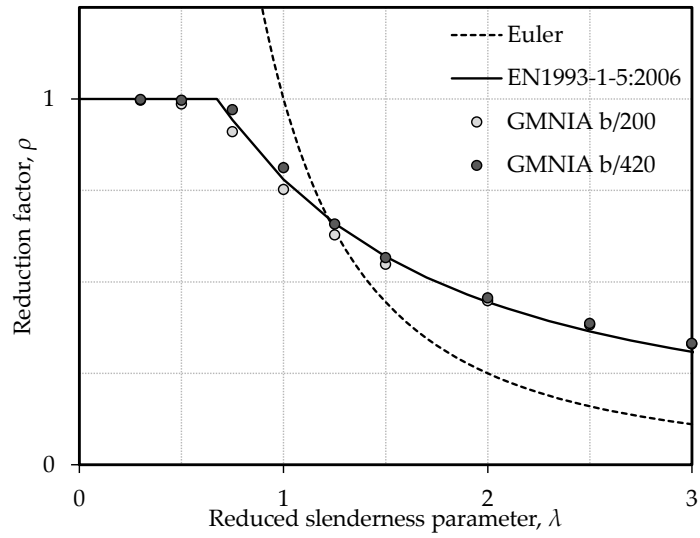


Figure 4.7: Comparison between numerical simulations and values from EN1993-1-5:2006, $\psi=1$

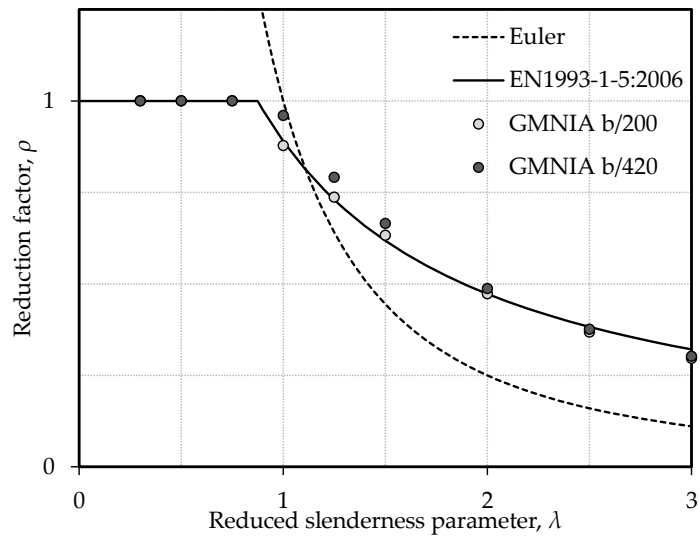


Figure 4.8: Comparison between numerical simulations and values from EN1993-1-5:2006, $\psi=-1$

The validation study was carried out considering imperfection shapes based on the first buckling mode with maximum amplitudes of $b/420$ and $b/200$ to cover EN1993-1-5:2006 (CEN, 2006a) recommendations. Figure 4.7 and Figure 4.8 show the results from Eq. (3.49) for uniform compression and pure bending plotted against numerical results (results plotted in those figures are from models with aspect ratios equal to 1 and boundary conditions type 2). Table 4.6 and Table 4.7 present detailed results for amplitudes $b/200$ and respective errors for 3 different values of the reduced slenderness parameter. From the analysis of these results, it is concluded that both equivalent geometric imperfections with amplitudes $b/420$ and $b/200$ are well adjusted to Eq. (3.49). The option fell on those recommended by EN1993-1-5:2006, *i.e.* amplitude $b/200$.

Table 4.6: Comparison between numerical results and EN1993-1-5:2006, $\psi=1$ (imperfection amplitude equal to $b/200$)

	$\lambda=1$	$\lambda=2$	$\lambda=3$
$\rho_{EN1993-1-5}$	0.780	0.445	0.309
ρ_{Num}	0.752	0.448	0.330
Diff. (%)	- 3.6	+ 0.7	+ 6.8

Table 4.7: Comparison between numerical results and EN1993-1-5:2006, $\psi=-1$ (imperfection amplitude equal to $b/200$)

	$\lambda=1$	$\lambda=2$	$\lambda=3$
$\rho_{EN1993-1-5}$	0.890	0.473	0.321
ρ_{Num}	0.878	0.473	0.296
Diff. (%)	- 1.3	+ 0.1	- 7.9

Additionally, it can be highlighted that the bigger differences between amplitudes $b/200$ and $b/420$ mainly occur for slenderness parameters between 0.673 and 1.22. This region of the reduced slenderness parameter is where imperfection sensitivity of compressed plates has more influence on the ultimate load. For higher values of the reduced slenderness parameter the differences become negligible (in that range the ultimate load is mainly driven by the elastic response and by the post-critical strength reserve). For lower values of the reduced slenderness parameter it is the yield strength of the material limiting the ultimate load.

Cylindrically curved panels under uniform compression are validated comparing numerical results with results from the method proposed by Tran in 2012 (see sec. 3.11.2; Tran, 2012; Tran *et al.*, 2012). From the analysis of Figure 4.9 to Figure 4.12, it is concluded that some non-negligible differences do exist. Several reasons emerge explaining these inconsistencies:

- Different material's law: linear unlimited strain-hardening (Tran's proposal) *vs.* more realistic strain-hardening with an ultimate stress plateau;
- Different type of finite element: four-node finite element (Tran's proposal) *vs.* nine-node finite element;
- Different software: ANSYS FEA (Tran's proposal) *vs.* ABAQUS FEA (own calculations);
- Definition of the reduced slenderness parameter: in fact, the normalised slenderness calculated based upon numerical results and from Tran's work are not the same. While in this study the slenderness parameter is defined using numerical results for the elastic critical stress, in Tran's works the elastic critical stress is obtained using Stowell's formula, which, as it will be seen in Chapter 8, returns non-negligible errors when compared to numerical results for the elastic critical stress.

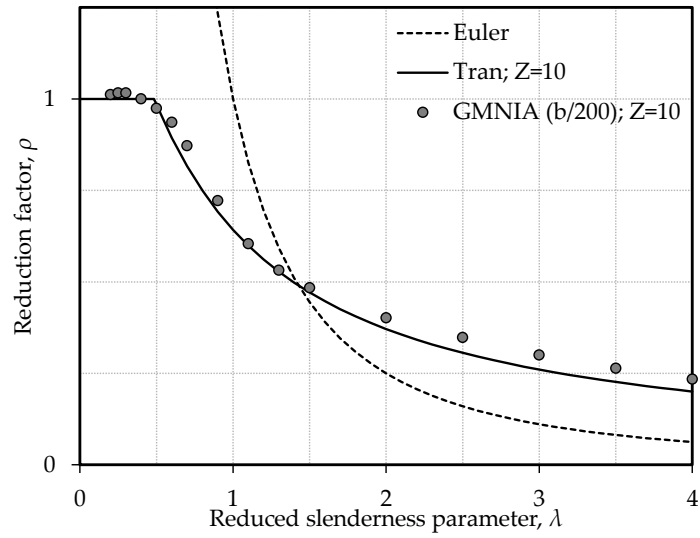


Figure 4.9: Comparison of numerical simulations and curves proposed by Tran *et al.* (2012) for $Z=10$ and $\psi=1$

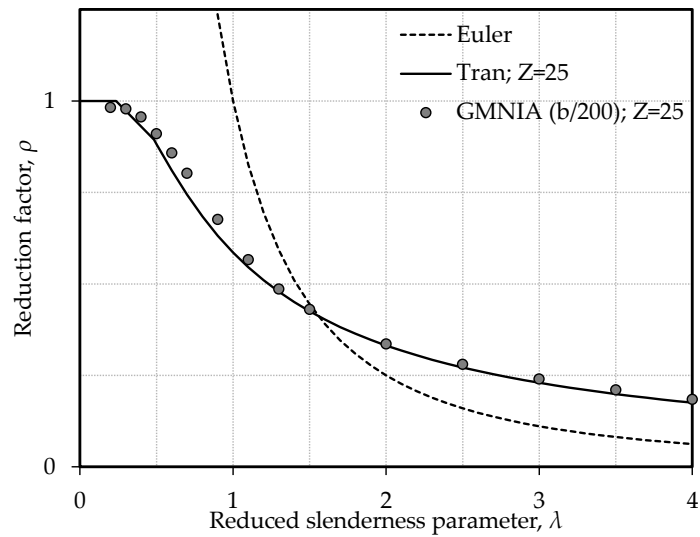


Figure 4.10: Comparison of numerical simulations and curves proposed by Tran *et al.* (2012) for $Z=25$ and $\psi=1$

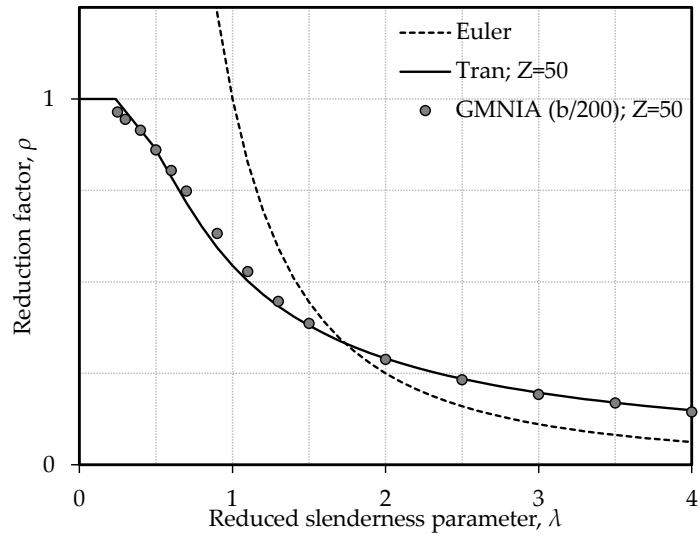


Figure 4.11: Comparison of numerical simulations and curves proposed by Tran *et al.* (2012) for $Z=50$ and $\psi=1$

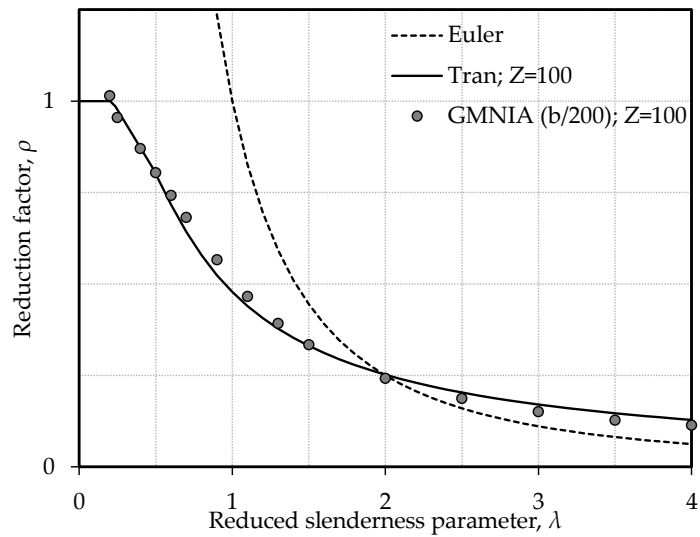


Figure 4.12: Comparison of numerical simulations and curves proposed by Tran *et al.* (2012) for $Z=100$ and $\psi=1$

The fact that the main differences occur for $Z=10$ is highlighted, since it is around this value that Stowell's formula (used by Tran in his method) returns the largest errors when compared to numerical results of the elastic critical stress. Therefore, it is expectable that the main errors between numerical results for the ultimate strength (that are based on slenderness parameters computed numerically, *i.e.* computed using a numerically obtained critical stress) and the curves from Tran's method occurs for the same values of Z .

In what concerns the validation of models of flat plates under biaxial loading (only square plates are considered in this validation), it can be seen in Figure 4.13 that the numerical results are almost in perfect accordance with numerical results from Braun (2010).

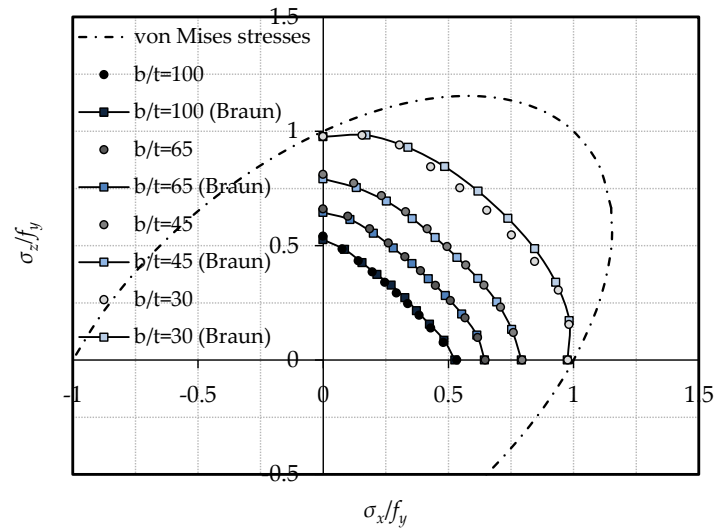


Figure 4.13: Comparison of own numerical simulations and numerical results from Braun (2010)

In fact, it is suggested by Figure 4.13 that only for stocky plates, specifically for plates with $b/t=30$, the differences start to be noticeable. This may be explained by numerical convergence strategies (*i.e.* differences due to user and/or software convergence strategies) which play a more important role for plasticity driven collapse modes rather than for elasticity driven collapse modes.

4.4.3. Brief study on the suitability of the curvature parameter

4.4.3.1. General

The majority of studies related to cylindrically curved panels suggest that the curvature parameter Z is a suitable parameter to characterise the geometry of cylindrically curved panels when computing its critical behaviour and ultimate load. In fact, as seen in Chapter 3, various formulae using the curvature parameter have been proposed to calculate the value of k_{σ} of cylindrically curved panels under uniform compression. Additionally, to compute the ultimate load of cylindrically curved panels under uniform compression the same parameter is seen as a key parameter (*e.g.* in Tran's proposal). In fact, Tran *et al.* (2012) did mention that the curvature parameter represents well the geometrical variability of the problem.

Nevertheless, further investigations are presented in the following sections trying to numerically verify this statement and, at the same time, validating Z as key parameter for loading conditions other than uniform compression (*i.e.* pure in-plane bending).

4.4.3.2. As a key parameter for the elastic critical stress

In order to verify to what extent is the assumption of using the curvature parameter accurate for computing the elastic critical stress of cylindrically curved panels under uniaxial stresses, a brief study performed by Martins *et al.* (2013) is presented and the results are discussed. The models have constant thickness ($t=10$ mm), aspect ratio ($\alpha=1$) and the same mesh discretisation (constant finite element size). The differences between results are measured taking as reference the models with $b=1000$ mm since those are the ones which will be used in the parametric study (Chapter 5). The results from this study are presented in Table 4.8 to Table 4.10. From the analysis of these tables it is possible to conclude that the sectorial angle θ may have some influence on the value of the critical stress of a cylindrically curved panel. Nevertheless, its influence will be disregarded for two reasons:

- In the domain of the parametric study (Chapter 5) the sectorial angle varies up to 1 rad and within this domain, all results show that the maximum error (which occurs for $\psi=-1$ and $Z=100$, therefore $\theta =1.333$ rad) is 1.83% (negligible error);
- The remaining cases show even lower errors leading to the conclusion that the curvature parameter, as it is defined in Eq. (3.1), is, in fact, a suitable parameter to fully characterise the geometry of cylindrically curved panels under compressive stresses.

Table 4.8: 1st justification for the utilisation of the curvature parameter, $\psi=1$

	<i>Width, b</i>	<i>0.75 m</i>	<i>1 m</i>	<i>1.25 m</i>	<i>1.5 m</i>	<i>1.75 m</i>	<i>2 m</i>	<i>5 m</i>	<i>7.5 m</i>
<i>Z=1</i>	k_{σ}	4.007	4.009	4.010	4.010	4.010	4.011	4.011	4.011
	<i>Diff. (%)</i>	<i>0.0</i>	-	<i>0.0</i>	<i>0.0</i>	<i>0.0</i>	<i>0.0</i>	<i>+0.1</i>	<i>+0.1</i>
	<i>R (m)</i>	56.25	100	156.25	225	306.25	400	2500	5625
	<i>θ (rad)</i>	0.0133	0.01	0.008	0.0067	0.0057	0.005	0.002	0.0013
<i>Z=25</i>	k_{σ}	9.602	9.602	9.602	9.601	9.601	9.602	-	-
	<i>Diff. (%)</i>	<i>+0.0</i>	-	<i>0.0</i>	<i>0.0</i>	<i>0.0</i>	<i>0.0</i>	-	-
	<i>R (m)</i>	2.25	4	6.25	9	12.25	16	100	225
	<i>θ (rad)</i>	0.3333	0.25	0.2	0.1667	0.1429	0.125	0.05	0.0333
<i>Z=100</i>	k_{σ}	34.532	34.497	34.488	34.487	34.486	34.485	-	-
	<i>Diff. (%)</i>	<i>+0.1</i>	-	<i>0.0</i>	<i>0.0</i>	<i>0.0</i>	<i>0.0</i>	-	-
	<i>R (m)</i>	0.5625	1	1.5625	2.25	3.0625	4	25	56.25
	<i>θ (rad)</i>	1.3333	1	0.8	0.6667	0.5714	0.5	0.2	0.1333

Table 4.9: 1st justification for the utilisation of the curvature parameter, $\psi=0$

	<i>Width, b</i>	<i>0.75 m</i>	<i>1 m</i>	<i>1.25 m</i>	<i>1.5 m</i>	<i>1.75 m</i>	<i>2 m</i>	<i>5 m</i>	<i>7.5 m</i>
<i>Z=25</i>	k_σ	17.899	17.902	17.903	17.904	17.905	17.905	-	-
	<i>Diff. (%)</i>	0.0	-	0.0	0.0	0.0	0.0	-	-
	<i>R (m)</i>	2.25	4	6.25	9	12.25	16	100	225
	θ (rad)	0.3333	0.25	0.2	0.1667	0.1429	0.125	0.05	0.0333
<i>Z=100</i>	k_σ	52.448	52.627	52.730	52.790	52.829	52.855	-	-
	<i>Diff. (%)</i>	-0.3	-	+0.2	+0.3	+0.4	+0.4	-	-
	<i>R (m)</i>	0.5625	1	1.5625	2.25	3.0625	4	25	56.25
	θ (rad)	1.3333	1	0.8	0.6667	0.5714	0.5	0.2	0.1333

Table 4.10: 1st justification for the utilisation of the curvature parameter, $\psi=-1$

	<i>Width, b</i>	<i>0.75 m</i>	<i>1 m</i>	<i>1.25 m</i>	<i>1.5 m</i>	<i>1.75 m</i>	<i>2 m</i>	<i>5 m</i>	<i>7.5 m</i>
<i>Z=25</i>	k_σ	33.916	33.992	34.029	34.050	34.062	34.070	-	-
	<i>Diff. (%)</i>	-0.2	-	+0.1	+0.2	+0.2	+0.2	-	-
	<i>R (m)</i>	2.25	4	6.25	9	12.25	16	100	225
	θ (rad)	0.3333	0.25	0.2	0.1667	0.1429	0.125	0.05	0.0333
<i>Z=100</i>	k_σ	72.524	73.460	73.927	74.189	74.350	74.459	74.759	74.791
	<i>Diff. (%)</i>	-1.3	-	+0.6	+1.0	+1.2	+1.4	+1.8	+1.8
	<i>R (m)</i>	0.5625	1	1.5625	2.25	3.0625	4	25	56.25
	θ (rad)	1.3333	1	0.8	0.6667	0.5714	0.5	0.2	0.1333

4.4.3.3. As a key parameter for the ultimate strength

In contrast to the previous section, models do not have constant thickness because the ultimate strength of cylindrically curved panels under uniaxial stresses depends also on the reduced slenderness parameter of the panels. Therefore, thickness is calculated setting the slenderness and curvature parameters constant. On the other hand, aspect ratio ($\alpha=1$), imperfection amplitude (5 mm) and the mesh discretisation (element size) are kept constant.

Table 4.11: 2nd justification for the utilisation of the curvature parameter, $\psi=1$

<i>Thickness, b</i>		<i>2 mm</i>	<i>5 mm</i>	<i>10 mm</i>	<i>15 mm</i>
	χ	0.546	0.546	0.546	0.546
Z=1;	<i>Diff. (%)</i>	0.0	0.0	-	0.0
$\lambda=1.5$	<i>b (m)</i>	0.139	0.347	0.693	1.040
	<i>R (m)</i>	9.618	24.045	48.089	72.134
	χ	0.368	0.386	0.368	0.368
Z=100;	<i>Diff. (%)</i>	0.0	0.0	-	0.0
$\lambda=1.5$	<i>b (m)</i>	0.381	0.953	1.906	2.858
	<i>R (m)</i>	0.726	1.816	3.631	5.447

Table 4.12: 2nd justification for the utilisation of the curvature parameter, $\psi=0$

<i>Thickness, b</i>		<i>2 mm</i>	<i>5 mm</i>	<i>10 mm</i>	<i>15 mm</i>
	χ	0.752	0.752	0.752	0.752
Z=1;	<i>Diff. (%)</i>	0.0	0.0	-	0.0
$\lambda=1.25$	<i>b (m)</i>	0.162	0.404	0.809	1.213
	<i>R (m)</i>	13.075	32.688	65.377	98.065
	χ	0.512	0.512	0.512	0.512
Z=100;	<i>Diff. (%)</i>	0.0	0.0	-	0.0
$\lambda=1.25$	<i>b (m)</i>	0.389	0.972	1.945	2.917
	<i>R (m)</i>	0.756	1.891	3.782	5.673

Table 4.13: 2nd justification for the utilisation of the curvature parameter, $\psi=-1$

<i>Thickness, b</i>		<i>2 mm</i>	<i>5 mm</i>	<i>10 mm</i>	<i>15 mm</i>
	χ	0.738	0.738	0.738	0.738
<i>Z=1;</i> <i>$\lambda=1.25$</i>	<i>Diff. (%)</i>	<i>0.0</i>	<i>0.0</i>	<i>-</i>	<i>0.0</i>
	<i>b (m)</i>	0.282	0.706	1.412	2.118
	<i>R (m)</i>	39.869	99.672	199.344	299.016
	χ	0.660	0.660	0.660	0.660
<i>Z=100;</i> <i>$\lambda=1.25$</i>	<i>Diff. (%)</i>	<i>0.0</i>	<i>0.0</i>	<i>-</i>	<i>0.0</i>
	<i>b (m)</i>	0.459	1.147	2.294	3.440
	<i>R (m)</i>	1.052	2.630	5.260	7.891

From the analysis of Table 4.11 to Table 4.13, it is concluded that the curvature parameter is suitable to fully describe the geometry of a cylindrically curved panel.

4.5. Summary

This chapter is intended to act as a foundation for parametric studies that were performed and which are presented in the next chapter (Chapter 5). Therefore, in order to make clear which were the main assumptions behind numerical studies they are thoroughly described and discussed throughout the entire chapter:

- The geometry of a generic cylindrically curved panel was carefully defined. All basic geometric parameters (width, length, thickness and radius) were visually identified;
- The material properties were characterised being adopted the ECCS recommended stress-strain curve (Rotter & Schmidt, 2008). This option is sustained by the fact that this stress-strain relation translates correctly the behaviour of structural carbon steels avoiding at the same time problems with the numerical convergence during computer analysis;
- The loading and boundary conditions were defined according to the

type of load arrangement under analysis – for cylindrically curved panels under uniaxial compression boundary conditions type 2 were adopted, while for cylindrically curved panels under biaxial loading it were the boundary conditions type 3;

The validation of the numerical models was also carried out, being the main conclusions about the accuracy of the numerical model addressed. Here it is highlighted the fact that, besides some minor identified and explained discrepancies, the results from the numerical model are in line with the results from literature.

Finally, the chapter ends with a brief, but pertinent, numerical investigation on the suitability of the curvature parameter Z . The conclusion of this study supports the preconceived idea that the curvature parameter as it is defined in Eq. (3.1) is a satisfactory parameter to describe the geometry of cylindrically curved panels.

5. Characterisation of the behaviour of cylindrically curved panels

5.1. Chapter overview

This chapter extensively describes all steps performed during the parametric studies. Relevant parameters are defined, studied and conclusions about their influence on several aspects related to cylindrically curved panels are drawn.

Firstly, in sec. 5.2 a parametric study on the elastic buckling behaviour of cylindrically curved panels is presented. In this study particular relevance is given to the following parameters: curvature, boundary conditions, aspect ratio and loading type. Their relation to the elastic critical stress and to the first buckling shape is analysed from the results and conclusions are made.

Secondly, in sec. 5.3 the study on the ultimate strength of short cylindrically curved panels is presented. In this study, the main parameters analysed are: curvature, boundary conditions and loading type. This study, together with the parametric study on the elastic buckling behaviour, is essential to create a model capable of accurately and safely predict the ultimate resistance of cylindrically curved panels. Following these studies, a complete study on the imperfection sensitivity study is performed in Chapter 6 (the option to set apart the parametric study on geometric imperfection sensitivity from the remaining ones is explained by the fact that its dimension and importance are enough to justify an entire chapter), where the studied parameters are (besides curvature and aspect ratio): the imperfection amplitude and the imperfection shape. It

should be mentioned that boundary conditions type 2 are given the main focus throughout all parametric studies. This is due to two reasons: firstly, boundary conditions type 2 are those which seem to be more appropriate to simulate the conditions of a lower flange in a box-girder (rigid diaphragms - loaded edges, and flexible thin webs - unloaded edges); and secondly, boundary conditions type 1 and 3 are, as it will be evident further on, limiting cases, *i.e.* numerical results from models with boundary conditions type 2 are limited by results from models with boundary conditions type 3 as an upper bound and limited by results from models with boundary conditions type 1 as a lower bound.

Thirdly, in sec. 5.4 a parametric study on the ultimate load of cylindrically curved panels under biaxial compressive stresses is performed. Here the boundary conditions for all curved panels are type 3.

Finally, the chapter ends with a summary where all main conclusions are highlighted and related to subsequent chapters.

5.2. Parametric study on the elastic buckling behaviour of cylindrically curved panels under uniaxial compressive stresses

5.2.1. Scope

This parametric study aims at characterising the elastic critical behaviour of simply supported cylindrically curved panels and to provide data to extrapolate the obtained results to new critical stress formulae. The parametric study comprises the following parameters:

- Curvature, Z (where thickness t and width b are kept constant);
- Boundary conditions;
- Aspect ratio, a ;
- Loading type, ψ .

As it can be concluded from Table 5.1, the total number of performed analyses is 276 942.

Table 5.1: Parametric study on the elastic buckling behaviour of cylindrically curved panels

<i>Load cases</i>	<i>Width, b</i>	<i>Thickness, t</i>	<i>Curvature, Z</i>	<i>Aspect Ratio, α</i>	
$\psi=1$					
to	1000 mm	10 mm	0 to 100	0.2 to 5.0	
$\psi=-1$					
Total for BC1	3 (step=1)	1	1	11 (step=10)	6 (0.5, 1 to 5 step=1)
Total for BC2	21 (step=0.1)	1	1	101 (step=1)	130 (0.2 to 2.1 step=0.02, 2.1 to 5 step=0.1)
Total for BC3	3 (step=1)	1	1	13 (0, 1, 5, 10 to 100 step=10)	26 (0.1 to 1 step=0.1, 1 to 4 step=0.2, 5)

5.2.2. Influence of boundary conditions on the elastic critical stress of cylindrically curved panels

In opposition to plates, the elastic critical stress of cylindrically curved panels under uniform compression is influenced by the boundary conditions. This happens because curvature adds nonlinearity to the prebuckling state of the panel, which is sensitive to boundary conditions. Figure 5.1 shows a perfect agreement between analytical results and numerical results for $Z=0$ and boundary conditions type 2. For boundary conditions type 1 and 3 this perfect agreement is verified as well (this is due to the fact that prebuckling state of flat panels is not sensitive to the differences between boundary conditions types 1, 2 and 3).

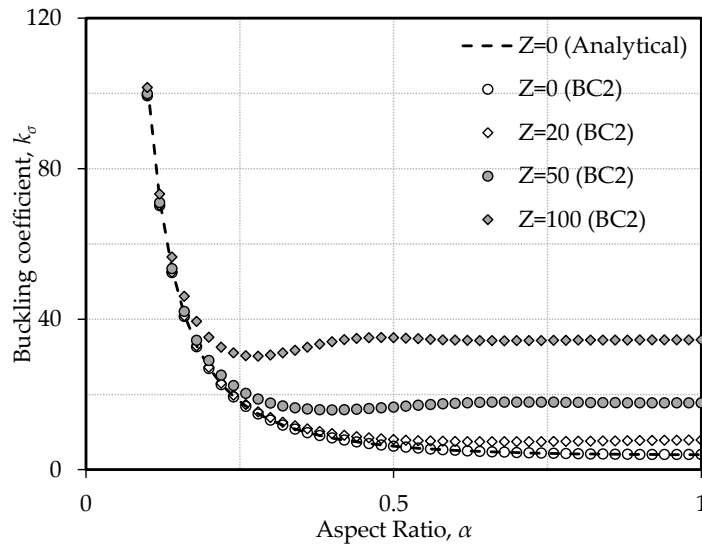


Figure 5.1: k_{σ} (1st buckling mode) vs. Z curves for panels with $\alpha \leq 1$ and $\psi = 1$ and boundary conditions type 2

Table 5.2 compares the three boundary conditions types, making clear that, in what concerns the elastic critical stress, boundary conditions of type 1 lead to the lowest values while boundary conditions of type 3 lead to the highest value.

Table 5.2: Comparison between boundary conditions type 1, 2 and 3 (values of the elastic critical stress for $\alpha = 1$ and $\psi = 1$)

	$Z=0$	$Z=10$	$Z=20$	$Z=50$	$Z=80$	$Z=100$
BC1	4.00	4.79	6.94	16.25	26.37	33.13
BC2	4.00	5.10	7.94	17.77	27.84	34.53
BC3	4.00	5.70	9.21	18.52	28.45	35.06
Diff. BC1 (%)	0	-6.1	-12.6	-8.5	-5.3	-4.0
Diff. BC3 (%)	0	11.8	16.0	4.2	2.2	1.5

As expected (since boundary conditions type 1 are the least rigid option and boundary conditions type 3 are the most rigid option), boundary conditions

type 2 lead to values limited by boundary conditions type 1 and 3. Surprisingly, Table 5.2 also shows that larger curvature does not mean larger differences between types of boundary conditions. This fact indicates that boundary conditions may be a critical parameter, within the elastic critical stress of cylindrically curved panels, for values of Z around 20 since it is for this value that the largest differences occur.

5.2.3. Influence of aspect ratio on the elastic critical stress of cylindrically curved panels

5.2.3.1. General

Aspect ratio plays an important role on critical behaviour of cylindrically curved panels. An earlier study on cylindrically curved panels (Martins *et al.*, 2011) has shown that the aspect ratio has a strong influence on the elastic critical stress value of cylindrically curved panels. This influence is quite distinct from the influence that aspect ratio has on flat plates.

In fact, for plates under uniform compression it is well known that the minimum elastic critical stress corresponds to an integer value of aspect ratio. For cylindrically curved panels and/or for types of loading other than pure compressive stresses (for plates see, for example Table 3.2), the minimum critical stress is obtained for a non-integer value of aspect ratio.

5.2.3.2. Short cylindrically curved panels with boundary conditions type 2

For plates subjected to pure compressive stresses ($\psi=1$) Eq. (3.5) gives the elastic buckling coefficient (function to the aspect ratio of the plate and the number of half-waves in each direction, m and n). For short cylindrically curved panels Eq. (3.5) is not able to predict the buckling coefficient accurately: the higher the aspect ratio and the higher the curvature the bigger the difference is, particularly for $\alpha>0.2$. Figure 5.1 shows exactly this statement for cylindrically curved panels with boundary conditions type 2. It also shows, as conveniently stated, a perfect agreement between Eq. (3.5) and numerical results. Figure 5.2 shows all numerical results for $\psi=1$ and $\psi=-1$. Essentially, Figure 5.2 *a*) it is an extended 3D representation of the same information in Figure 5.1.

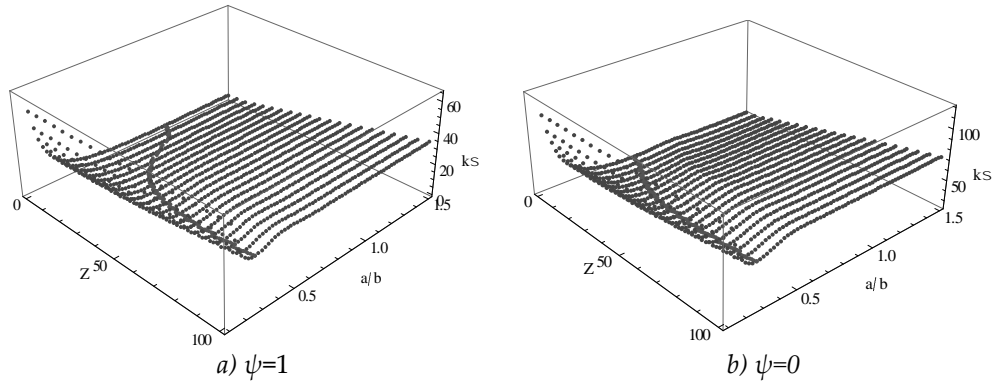


Figure 5.2: 3D plot of k_σ (1st buckling mode) vs. (Z, α) for $\psi=1$ and $\psi=-1$

Figure 5.2 is better understood realising that the plane $Z=0$ represents the classical behaviour of a plate described by Eq. (3.5) in $0 < \alpha \leq 1.5$ range. It is concluded that minimum values of k_σ , henceforth denote $k_{\sigma,min}$, are not independent from curvature (in Figure 5.2 these minimum values of k_σ are highlighted). Focusing on the plane defined by Z and α it is seen that for the different load cases plotted in Figure 5.2 the evolution of $k_{\sigma,min}$ is similar; for a clearer interpretation of results, these values are also plotted in 2D (Figure 5.3). It is also observed that aspect ratios which lead to $k_{\sigma,min}$ tend asymptotically to 0.28 for $Z=100$ with increasing curvature independently of ψ .

5.2.3.3. Long cylindrically curved panels ($\alpha \gg 1$)

Numerical results for long flat panels present perfect agreement with results from Table 4.1 of EN1993-1-5:2006 (*i.e.* numerical results for $Z=0$ tend asymptotically to values from Table 4.1 of EN1993-1-5:2006).

For long cylindrically curved panels the evolution of the elastic critical stress with the aspect ratio is highly influenced by boundary conditions. Figure 5.4 to Figure 5.7 show exactly this dependence and, also, how boundary conditions change the value of the elastic buckling coefficient with increasing aspect ratio. Taking into consideration only boundary conditions type 2, for long curved panels, as in flat panels, the minimum elastic buckling coefficient stabilises with the increase of aspect ratio and its influence becomes negligible (the higher the curvature, the higher the value of the elastic critical stress).

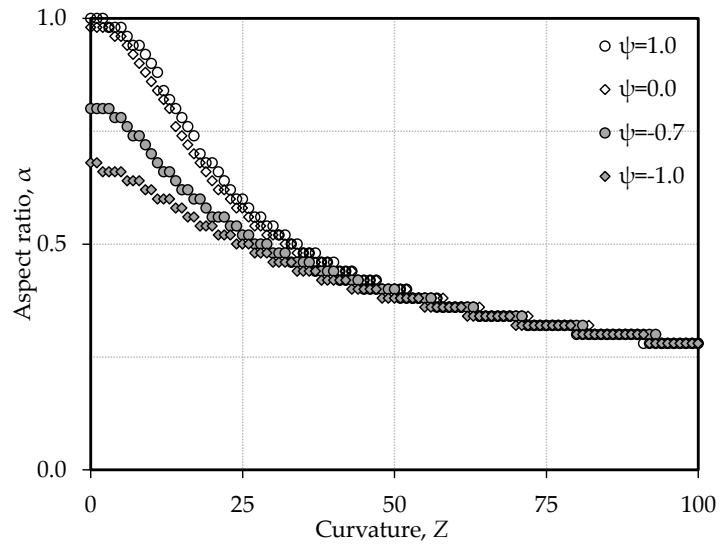


Figure 5.3: 2D plot Z vs. α inducing $k_{\sigma,min}$ for different loading cases

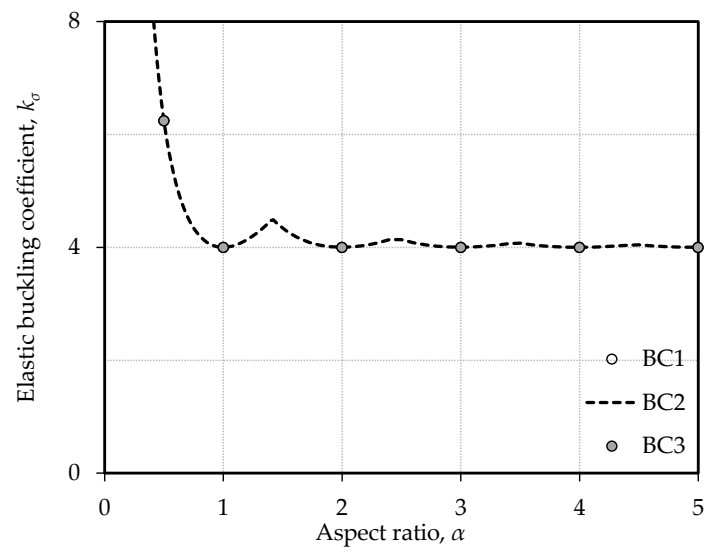


Figure 5.4: Plot of k_{σ} (1st buckling mode) vs. α for $Z=0$ and $\psi=1$ for boundary conditions type 1, 2 and 3

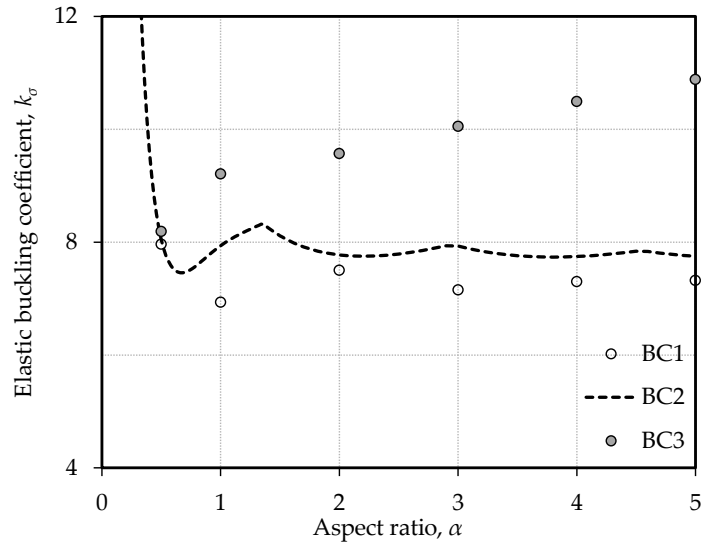


Figure 5.5: Plot of k_σ (1st buckling mode) vs. α for $Z=20$ and $\psi=1$ for boundary conditions type 1, 2 and 3

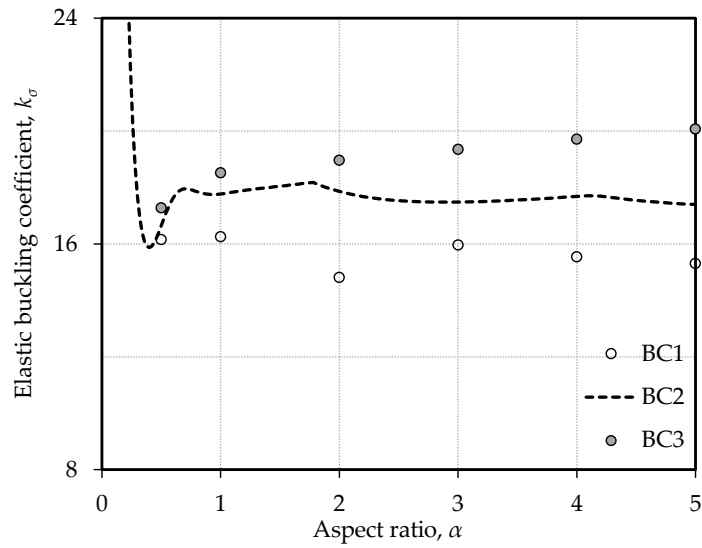


Figure 5.6: Plot of k_σ (1st buckling mode) vs. α for $Z=50$ and $\psi=1$ for boundary conditions type 1, 2 and 3

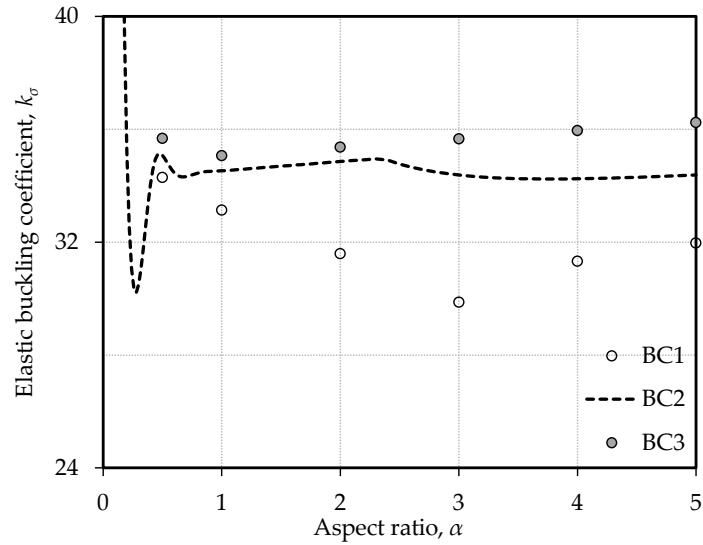


Figure 5.7: Plot of k_σ (1st buckling mode) vs. α for $Z=100$ and $\psi=1$

Table 5.3 shows the differences on the minimum values of the elastic buckling coefficient between short and long panels with boundary conditions type 2. The difference between absolute values of elastic critical stress for short and long curved panels is plotted in Figure 5.8.

Table 5.3: Differences between short and long panels with boundary conditions type 2

Loading type, ψ	Curvature, Z	$k_{\sigma, \min}$ for short panels	$k_{\sigma, \min}$ for long panels	Diff. (%)
	0	4.00 ($\alpha=1$)	4.00	0.0
1	50	15.87	17.40	+ 9.6
	100	30.21	34.23	+ 13.3
	0	7.81 ($\alpha=0.98$)	7.81	0.0
0	50	26.31	29.68	+ 12.8
	100	45.31	52.08	+ 14.9
	0	23.90 ($\alpha=0.66$)	23.90	0.0
-1	50	42.26	48.17	+ 14.0
	100	63.03	72.90	+ 15.7

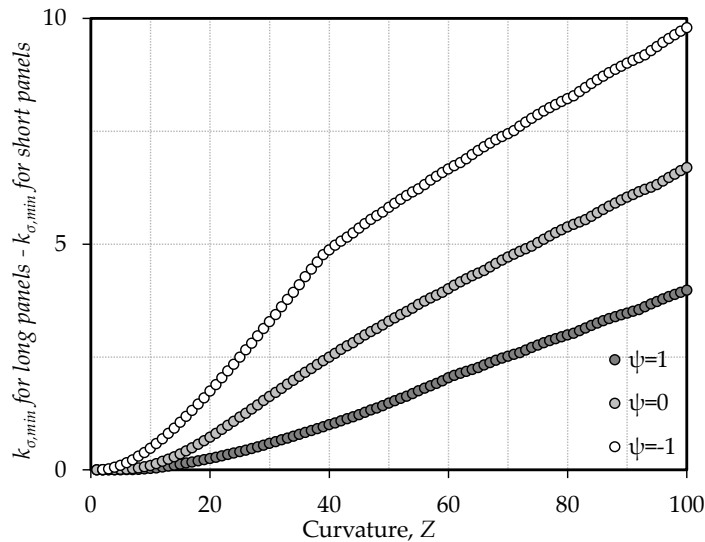


Figure 5.8: ($k_{\sigma,min}$ for long panels - $k_{\sigma,min}$ for short panels) vs. Z for panels with $\alpha > 1$ and boundary conditions type 2

5.2.4. Influence of loading conditions on the elastic critical stress of cylindrically curved panels

Considering only cylindrically curved panels having boundary conditions type 2 with aspect ratios that minimise k_{σ} (*i.e.* those aspect ratios of Figure 5.3), Figure 5.9 plots $k_{\sigma,min}$ for different loading cases showing that there is a perfect agreement between numerical results and the values given by EN1993-1-5:2006 (maximum absolute error equal to 0.7% for $\psi = -0.8$).

It is also observable that, with respect to the elastic critical stress of (short and long) cylindrically curved panels, EN1993-1-5:2006 assumption that curved panels characterised by a curvature parameter $Z \leq 1$ can be treated as plates is accurate (error less than 1%). Nonetheless, this conclusion does not have any added value by itself since it is the ultimate stress that can truly verify the accuracy of that limit.

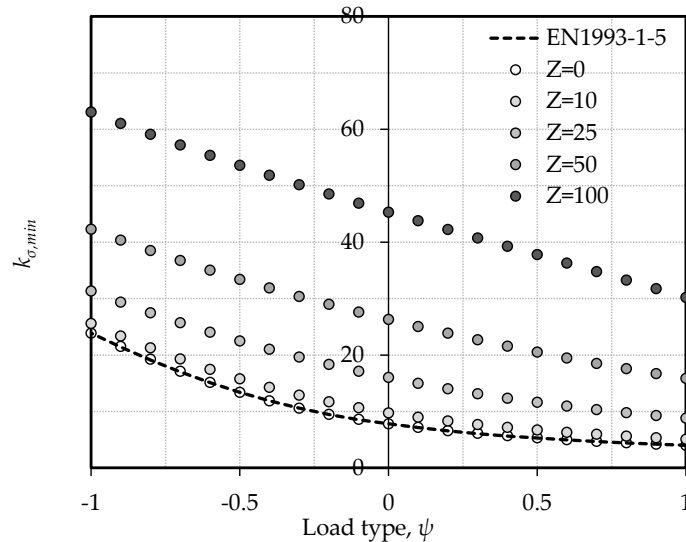


Figure 5.9: $k_{\sigma, min}$ for different values of ψ and curvatures and for short cylindrically curved panels with boundary conditions type 2

5.2.5. Influence of curvature and aspect ratio on the elastic buckling pattern of cylindrically curved panels with boundary conditions type 2

5.2.5.1. Square cylindrically curved panels under uniform compression ($\alpha=1$ and $\psi=1$)

When aspect ratio is fixed the curvature has a significant influence on the buckling pattern of a cylindrically curved panel. Figure 5.10 shows the buckling patterns for different values of the curvature parameter. From the numerical results it is possible to identify two main different types of buckling patterns which are related to curvature. The first type of buckling pattern occurs for low values of Z being very similar to the classical displacement field for plates with $m=1$ and $n=1$, Eq. (3.4). Its limits vary from $Z=0$ to $Z \approx 23$. The second type of buckling pattern is valid from $Z \approx 23$ to $Z=100$ (upper limit of the parametric study) and less agreement exists between classical and numerical displacement field for $m=1$ and $n=1$, Figure 5.11. Domb and Leigh (2001) also set this difference between two types of behaviour (the transition was fixed at

$Z \approx 24.27$). This odd behaviour may be explained by the fact that, together with the boundary conditions, the increase in curvature establishes a non-uniform transversal state of stress with relevant compressive stresses near the edges and less relevant at the centre of the panel.

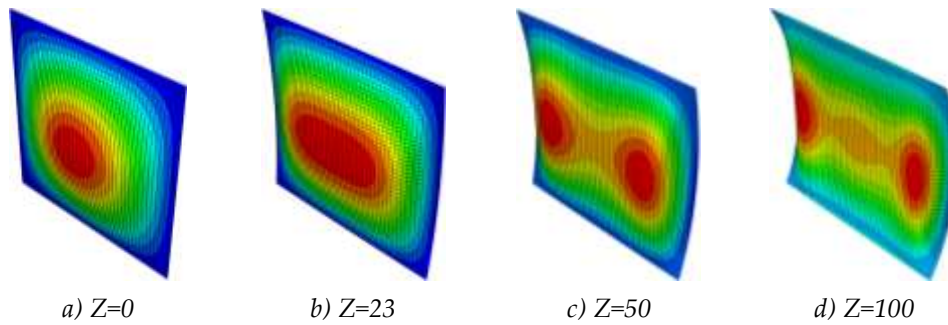


Figure 5.10: Buckling pattern for cylindrically curved panels with boundary conditions type 2 and with $\alpha=1$ and $\psi=1$

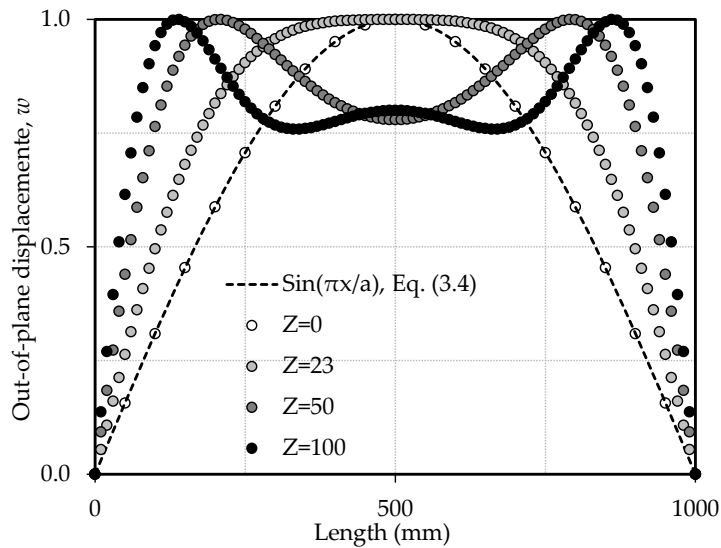


Figure 5.11: Comparison between Eq. (3.4) and the numerical displacement field at $y=b/2$ for cylindrically curved panels with boundary conditions type 2 and with $\alpha=1$ and $\psi=1$

5.2.5.2. Short cylindrically curved panels with α that minimises k_σ and under uniform compression ($\alpha \leq 1$ and $\psi=1$)

For curved panels with aspect ratios leading to minimum values of k_σ instead of constant aspect ratios, it is plausible to assume that the buckled pattern, Figure 5.12, is close to the product of sine functions in both x and y directions (as Eq. (3.4) with $m=1$ and $n=1$). Figure 5.13 demonstrates this statement by plotting Eq. (3.4) together with numerically obtained displacement fields.

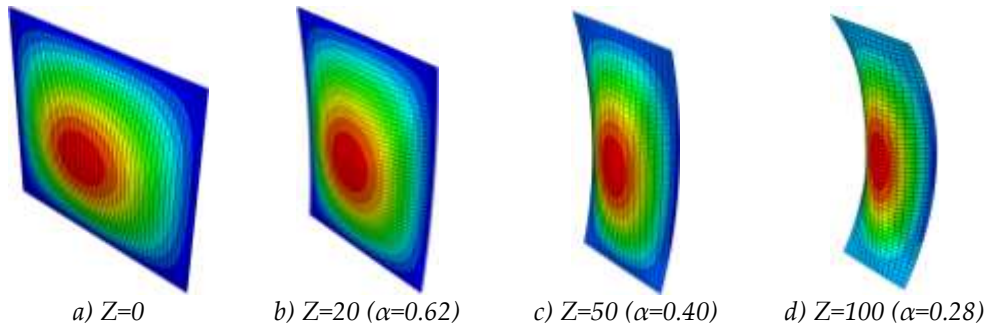


Figure 5.12: Buckling pattern for cylindrically curved panels with boundary conditions type 2 and with α minimising k_σ and $\psi=1$

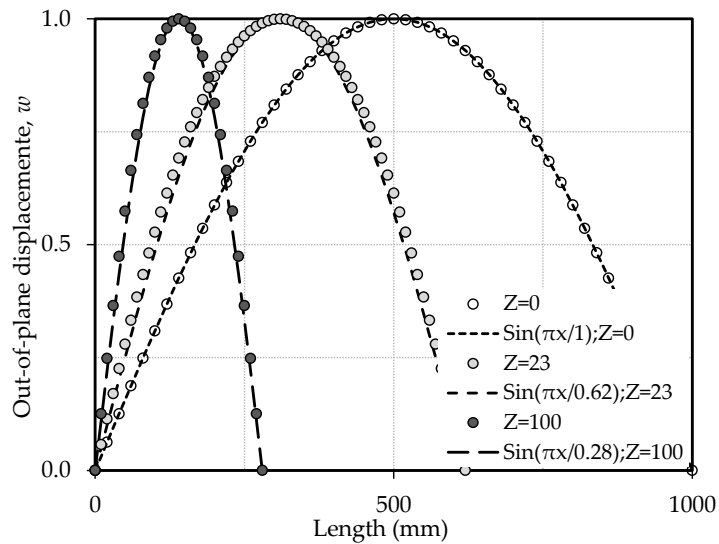


Figure 5.13: Comparison between Eq. (3.4) and the numerical displacement field at $y=b/2$ for cylindrically curved panels with boundary conditions type 2 and with α minimising k_σ and $\psi=1$

5.2.5.3. Square curved panels and varying loading conditions ($\alpha=1$ and $-1 \leq \psi \leq 1$) with boundary conditions type 2

Figure 5.14 represents the buckling pattern from a curved panel characterised by $Z=100$ and aspect ratio equal to 1 for different loading conditions.

As expected, the buckling pattern follows the compressive stresses, while in areas with tensile stresses the panel remain with little or zero deformation.

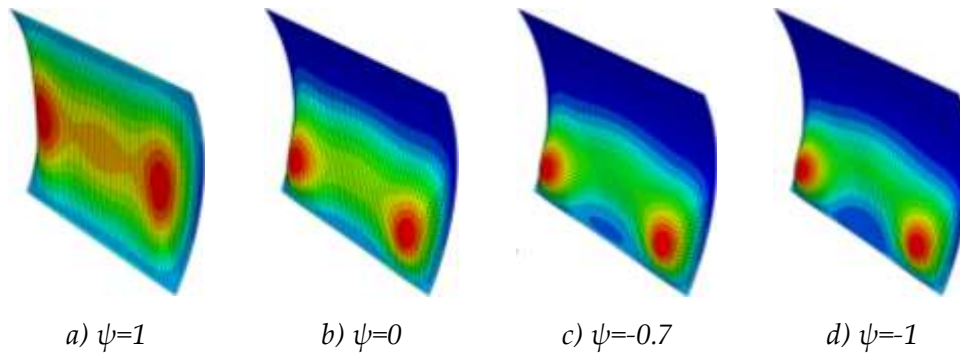


Figure 5.14: Buckling pattern for cylindrically curved panels with $Z=100$, with boundary conditions type 2 and with $\alpha=1$ and different loading conditions

5.2.5.4. Long cylindrically curved panels and ($\alpha \gg 1$ and $\psi=1$) with boundary conditions type 2

Figure 5.15 illustrates the effect of curvature on the buckling pattern of long cylindrically curved panels (in this example $\alpha=3$). In this case, curvature affects the number of half-waves (3 half-waves for $Z < 23$ and two for $Z \geq 23$) and thus the buckling mode. With the increase of curvature the maximum out-of-plane displacement moves towards the loaded edges. It is also pointed out that this change in the number of half-waves takes place approximately also for $Z=23$.

In Chapter 6 a comprehensive study on long cylindrically curved panels is performed. Not only the elastic buckling behaviour of long cylindrically curved panels is approached, but also, as previously mentioned, their ultimate strength and how they cope with different imperfection amplitudes and shapes.

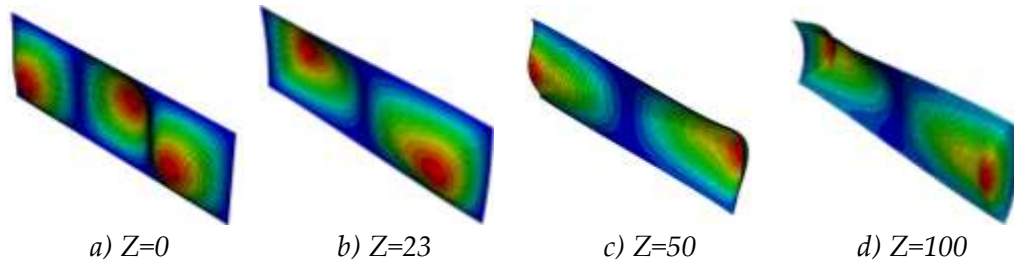


Figure 5.15: Buckling pattern for cylindrically curved panels with boundary conditions type 2 and with $\alpha=3$ and different curvature

5.2.6. Concluding remarks

It was shown that curvature plays an important role when predicting the elastic critical stress of cylindrically curved panels. Besides this obvious conclusion, a distinction on the buckling patterns due to curvature was identified: curved panels with $Z < 23$ buckle in a different manner when compared to curved panels with $Z \geq 23$.

Furthermore, in order to clarify the results from formulae obtained in the next chapters, it is important to stress out the fact that only models with aspect ratios such that the elastic buckling coefficient is a minimum value ($k_{\sigma, min}$) for a given value of curvature and loading were used in the calibration process (for short and long panels). Thus, the proposed formulae, besides the limits imposed by the parametric study, only returns minimum values for the elastic buckling coefficient. This approach is in line and consistent with the approach in EN1993-1-5:2006 (CEN, 2006a). Additionally, it was seen clearly that boundary conditions type 2 are limited by boundary conditions type 1 (which, for the same panel's geometry) return lower values for the elastic critical stress; and by boundary conditions type 3 (which, for the same panel's geometry) return the higher values for the elastic critical stress.

Finally, it was shown that the classical displacement field expressed by Eq. (3.4) ($m=n=1$) is only suitable for cylindrically curved panels with aspect ratio following the curves in Figure 5.13.

5.3. Parametric study on the ultimate strength of short cylindrically curved panels under uniaxial compressive stresses

5.3.1. Scope

Numerical results are obtained from GMNIA and represent the maximum load factor achieved (which may vary from 0 to 1, whereby 1 corresponds to the full plastic resistance of the panel). The following parametric study comprises the study of the parameters:

- Curvature, Z (where thickness t and width b are kept constant, sec. 4.4.3);
- Boundary conditions;
- Loading type, ψ .
- Slenderness, λ .




The cylindrically curved panels considered in this study have constant thickness ($t=10\text{mm}$), the remaining geometric characteristics being variable (Table 5.4). The thickness may be kept constant because the geometry of the panel is fully described by the curvature parameter. The width is taken as a dependent variable of the reduced slenderness parameter and it is calculated by Eq. (5.1) (which is obtained by solving Eq. (3.26) with respect to the width)

$$b = \lambda \frac{t\sqrt{k_\sigma E\pi}}{2\sqrt{3f_y(1-\nu^2)}} \quad (5.1)$$

Besides width, thickness and radius of curvature, length also influences the elastic critical stress of a cylindrically curved panel. Its influence is accounted for in the buckling coefficient k_σ (the previous parametric study proves that the minimum elastic critical stress is a function of the curvature parameter, the aspect ratio and the loading type). So, it is important to be aware that values of width are calculated taking into account specific, and not random, values of length (or such that the aspect ratio is equal to 1). Finally, for this parametric study geometric imperfections based on the first buckling mode with amplitudes given by expression (4.2) are used. The total number of analysis per-

formed for this parametric study is 31 455. It should be noticed that all models with boundary conditions other than type 2 may have aspect ratios which minimise k_σ different from those in Figure 5.3 but that influence was not accounted for in this study. Nevertheless, to simplify the comparison between the three types of boundary conditions, it was assumed aspect ratios according to the curves in Figure 5.3 independently from the boundary condition type. Additionally, models with constant b/t ratios were performed. These models allowed verifying the evolution of the resistance of a panel with constant material (constant cross-sectional area) with varying curvature over the slenderness (see grey-dashed lines in Figure 5.24 and Figure 5.25). In what concerns imperfections, it was considered an equivalent geometric imperfection based on the 1st eigenmode with amplitude equal to $b/200$ applied inwards.

Table 5.4: Parametric study on the ultimate behaviour of cylindrically curved panels

<i>Load cases</i>	<i>Slenderness, λ</i>	<i>Width, b</i>	<i>Thick-ness, t</i>	<i>Curva-ture, Z</i>	<i>Aspect Ratio, α</i>
	$\psi=1$				
	to	0.2 to 3.0	Eq. (5.1)	10 mm	0 to 100
	$\psi=-1$				
Total for BC1	3 (step=1)	6 (step=0.5)	1	1	11 (step=10)
Total for BC2	21 (step=0.1)	29 (step=0.1)	1	1	51 (step=2)
Total for BC3	3 (step=1)	6 (step=0.5)	1	1	11 (step=10)

See Figure 5.3

5.3.2. Influence of boundary conditions on the ultimate strength of short cylindrically curved panels ($\alpha \leq 1$)

In opposition to what happens for the elastic buckling behaviour, it is known that whether unloaded edges are or not constrained influences the postbuckling behaviour of plates (see sec. 0) and, therefore, influences their ultimate strength. Figure 5.16 and Figure 5.17 plot, respectively, on top of the Winter's curve and on top of Tran *et al.* (2010) proposal, numerical results from models with the three types of boundary conditions. As it is visible, the best fit is for models having boundary conditions type 2. Again, as for the parametric study on the elastic buckling of cylindrically curved panels, values from models having boundary conditions type 1 represent a lower bound of results, while models with boundary conditions type 3 represent an upper bound of results. For panels with curvature, numerical results from models with boundary conditions type 3, despite being an upper bound, they are close to Tran *et al.* (2010) proposal (Figure 5.17). This is obvious from the analysis of both figures: in Figure 5.16, Winter curve and numerical results from models with boundary conditions type 2 represent the middle bandwidth of results from models with boundary conditions type 1 and 3; in Figure 5.17 results from Tran *et al.* (2010) and numerical results from models with boundary conditions type 2 and 3 are almost on top of each other while results from models with boundary conditions type 1 are far apart on the lower part of the graph. Table 5.5,

Table 5.6 and Table 5.7 compare the three boundary conditions, showing that, in what concerns the ultimate load factor, boundary conditions type 1 lead to the lowest values while boundary conditions type 3 lead to the highest value.

Generally speaking, as expected, boundary conditions type 2 lead to values limited by boundary conditions type 1 and 3. However, as already seen and analysed in Figure 5.16 and Figure 5.17, it is pointed out that for panels with curvature, the bigger differences are between boundary conditions type 1 and type 2.

Table 5.5: Comparison between boundary conditions type 1, 2 and 3 (values of the ultimate strength for $\psi=1$ and $\lambda=1$)

	<i>Z=0</i>	<i>Z=10</i>	<i>Z=20</i>	<i>Z=50</i>	<i>Z=80</i>	<i>Z=100</i>
BC1	0.738	0.536	0.438	0.412	0.382	0.370
BC2	0.752	0.656	0.622	0.576	0.523	0.512
BC3	0.782	0.652	0.620	0.580	0.536	0.518
Diff. BC1 (%)	-1.9	-18.3	-29.6	-28.5	-27.9	-27.7
Diff. BC3 (%)	4.0	-0.6	-0.3	0.7	1.1	1.2

Table 5.6: Comparison between boundary conditions type 1, 2 and 3 (values of the ultimate strength for $\psi=1$ and $\lambda=2$)

	<i>Z=0</i>	<i>Z=10</i>	<i>Z=20</i>	<i>Z=50</i>	<i>Z=80</i>	<i>Z=100</i>
BC1	0.378	0.276	0.178	0.103	0.108	0.105
BC2	0.448	0.404	0.356	0.288	0.254	0.242
BC3	0.562	0.452	0.384	0.304	0.264	0.252
Diff. BC1 (%)	-15.6	-31.7	-50.1	-64.2	-57.4	-56.4
Diff. BC3 (%)	25.4	11.9	7.9	5.6	3.9	4.1

Table 5.7: Comparison between boundary conditions type 1, 2 and 3 (values of the ultimate strength for $\psi=1$ and $\lambda=3$)

	<i>Z=0</i>	<i>Z=10</i>	<i>Z=20</i>	<i>Z=50</i>	<i>Z=80</i>	<i>Z=100</i>
BC1	0.242	0.185	0.131	0.061	0.046	0.044
BC2	0.330	0.304	0.256	0.195	0.165	0.154
BC3	0.414	0.404	0.308	0.220	0.184	0.172
Diff. BC1 (%)	-26.7	-39.2	-49.7	-68.7	-72.4	-71.6
Diff. BC3 (%)	25.5	32.9	18.5	12.6	11.2	11.5

5.3.3. Influence of loading type on the ultimate strength of short cylindrically curved panels ($\alpha \leq 1$)

From the point of view of the ultimate strength the loading type is an essential parameter since depending on it the reduction factor changes are not negligible. As it is known from flat plates, the type of applied load influences the value of the reduction factor ρ . For this reason, as already mentioned in Chapter 3, EN1993-1-5:2006 proposes a modification of Winter's curve given by Eq. (3.49). Figure 5.18 to Figure 5.23 show the effect of the loading type for different curvature and slenderness. The global pattern showed by all of the graphs is the same: higher reductions for loading type closer to pure compression, for higher values of the curvature parameter and for higher values of slenderness.

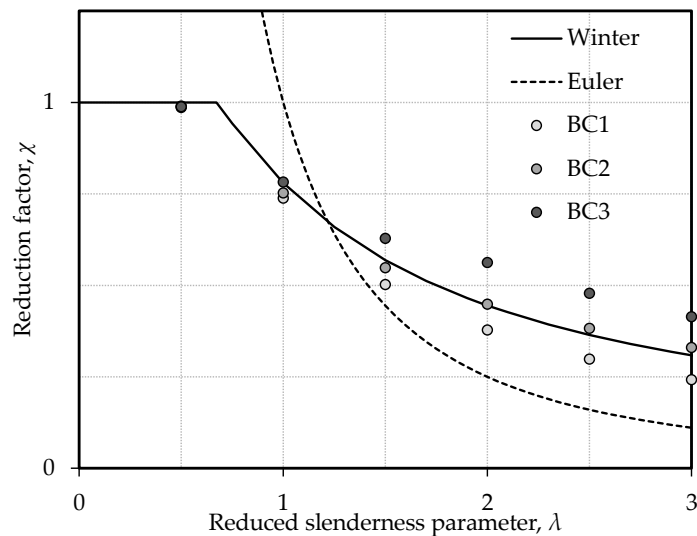


Figure 5.16: Comparison of numerical results assuming boundary conditions type 1, 2 and 3 and the Winter curve (pure compression)

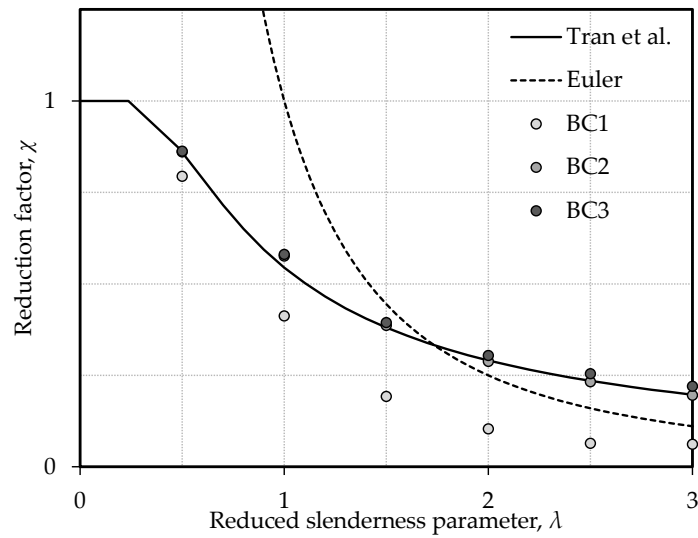


Figure 5.17: Comparison of numerical results assuming boundary conditions type 1, 2 and 3 and the Tran's *et al.* (2010) proposal for $Z=50$ (pure compression)

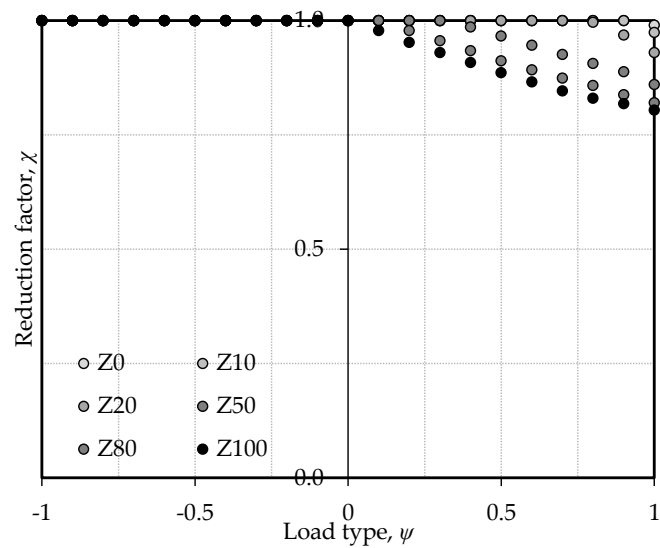


Figure 5.18: Influence of loading type for $\lambda=0.5$

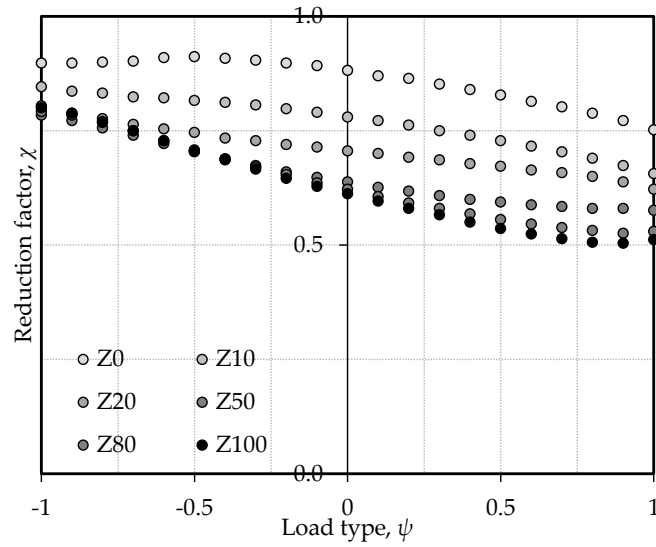


Figure 5.19: Influence of loading type for $\lambda=1$

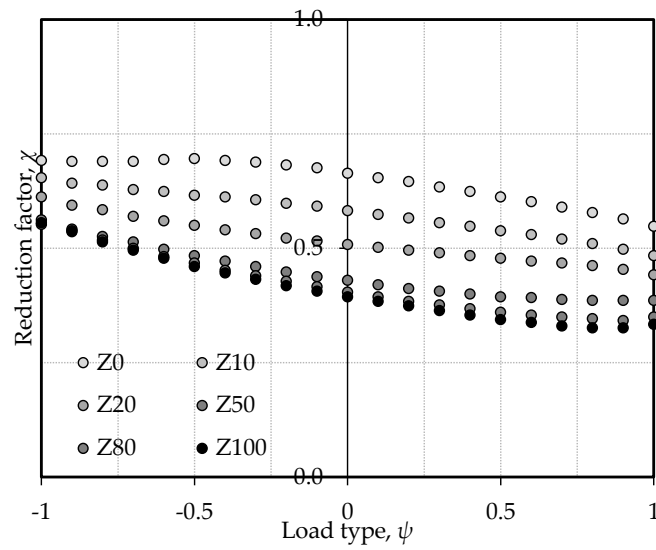


Figure 5.20: Influence of loading type for $\lambda=1.5$

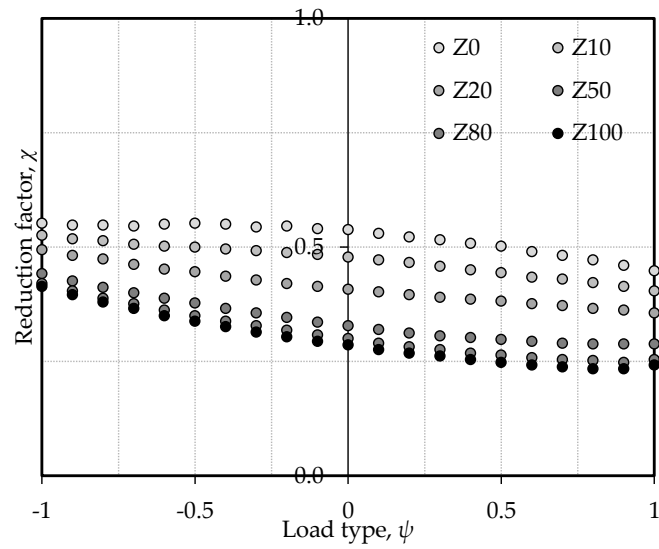


Figure 5.21: Influence of loading type for $\lambda=2$

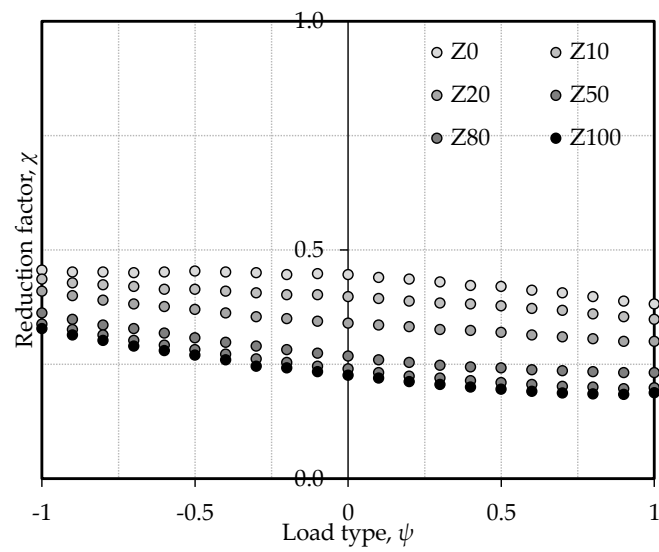


Figure 5.22: Influence of loading type for $\lambda=2.5$

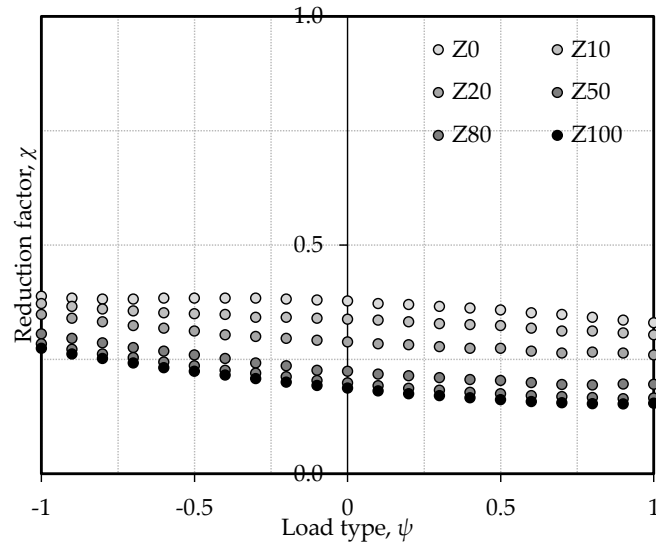


Figure 5.23: Influence of loading type for $\lambda=3$

It is brought to the attention of the reader that the values from the previous figures cannot be directly compared with the modified Winter formula (Eq. (3.49)). In fact, the resistance reduction factor, χ , only coincides with the width reduction factor, ρ , for pure compression. Otherwise, it is necessary to compute the equivalent value of ρ for each value of χ . The evaluation of the resistance reduction factor in terms of the width reduction factor is not straightforward and it requires an iterative process which is described in detail in sec. 8.5.2.

It should be also pointed out the fact that a cylindrically curved panel by presenting a higher value of the curvature parameter does not necessarily mean that it is less resistant. In fact, previous figures do not compare panels with the same width but with the same reduced slenderness parameter.

As it will be shown in the next section, with the exception of combinations of low curvature parameter with stocky panels, the higher the curvature parameter the more resistant a cylindrically curved panel is.

5.3.4. Influence of slenderness on the ultimate strength of short cylindrically curved panels under pure compression and pure in-plane bending

Figure 5.24 and Figure 5.25 show that the reduction in the resistance of cylindrically curved panels follows the same trend as flat panels do when plotted against slenderness and, when moving from uniform compression to pure in-plane bending, the gap between flat panels and curved panels (in this study the curvature limit is set as $Z=100$) becomes smaller. Furthermore, Figure 5.24 and Figure 5.25 also may induce the wrong conclusion that a cylindrically curved panel is always less resistant than a flat panel with equal cross-sectional area. The opposite is proved by the grey-dashed curves which show the variations of χ for panels with constant area (different b/t ratios). An increase of χ with Z is noted, the resistance reduction factor exhibiting a minimum for small values of curvature in some cases, as clearly shown in Figure 5.26 and Figure 5.27. The minimum is more pronounced for stockier panels, disappearing for more slender panels whereby the flat plate exhibits the lowest resistance.

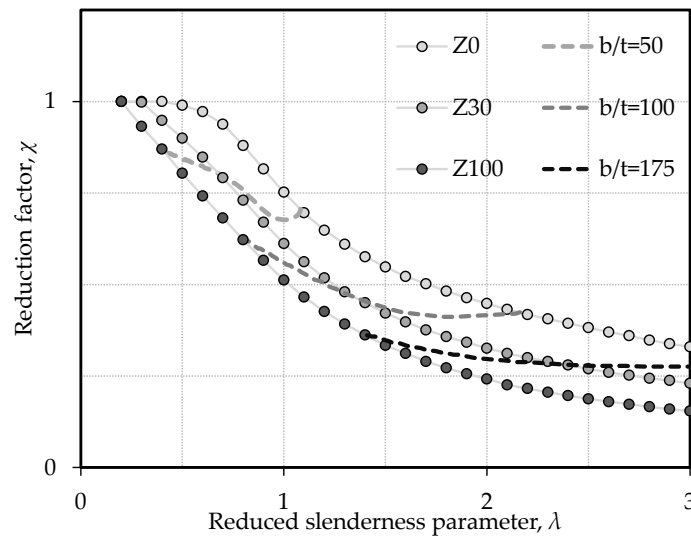


Figure 5.24: Numerical results for the resistance reduction factor for $\psi=1$

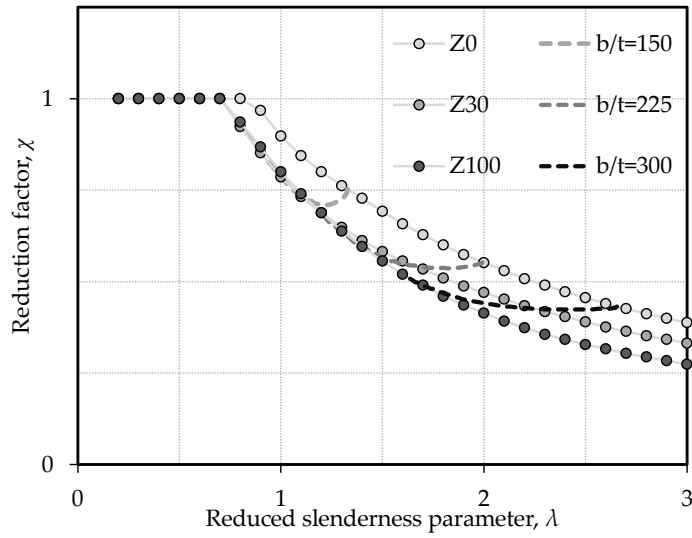


Figure 5.25: Numerical results for the resistance reduction factor for $\psi=-1$

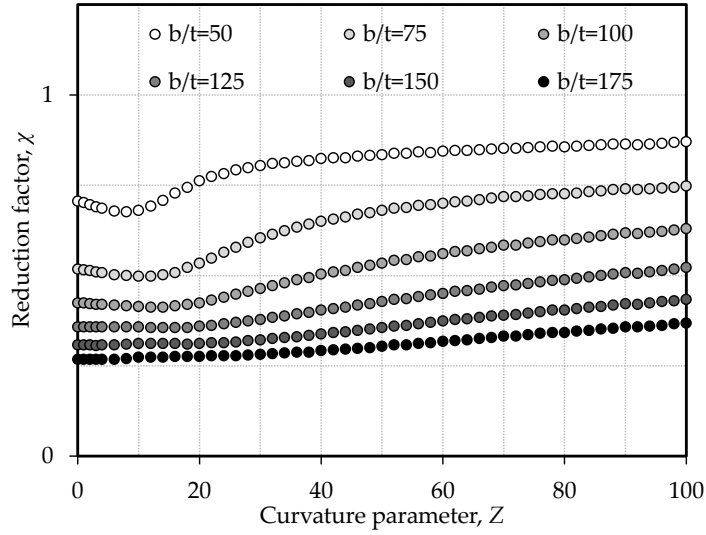


Figure 5.26: Relation between curvature and the resistance reduction factor for $\psi=1$

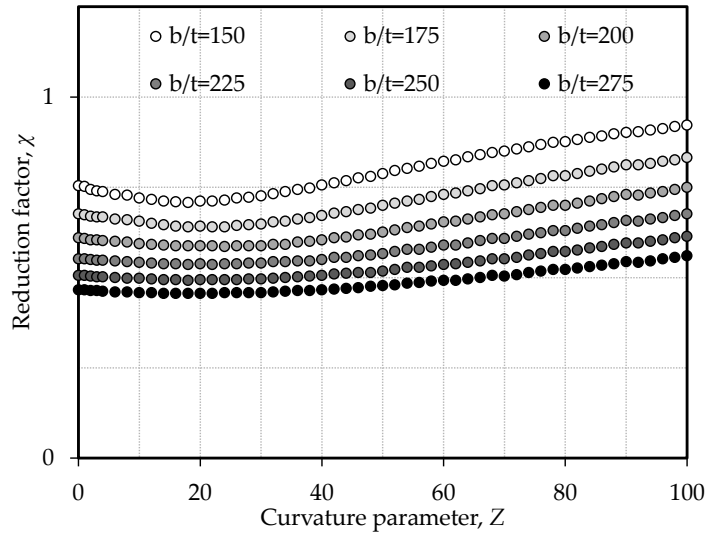


Figure 5.27: Relation between curvature and the resistance reduction factor for $\psi=-1$

5.3.5. Concluding remarks

In this section, it has been proven that curvature has a large influence on the ultimate strength of short cylindrically curved panels. In fact, the curvature parameter together with the slenderness seems to govern their behaviour. This realisation will lead in following chapters to a proposal to compute the ultimate strength of cylindrically curved panels based on Winter's formula which explicitly introduces the curvature parameter. Adding to these main conclusions, the numerical results also show that:

- Boundary conditions type 2 are always limited by boundary conditions type 1 (lower bound) and by boundary conditions type 3 (upper bound);
- The evolution of the reduction factor with the reduced slenderness parameter is similar to what is observed for plates. The main difference lies on the magnitude of the reduction: the bigger the curvature the smaller the width/resistance reduction factor (*i.e.* the bigger the reduction is);
- For panels with b/t ratio constant, an increase of the reduction factor with the increase of curvature is noted. The resistance reduction factor takes a minimum value for small values of curvature for stockier panels, disappearing for more slender panels. This means that introducing

curvature in an initially flat plate may add a resistance reserve, especially if it is introduced a high curvature; the downside is that it also may change the plate's postbuckling behaviour from stable to unstable.

Additionally, the numerical results allow validating the assumption present in EN1993-1-5:2006 (CEN, 2006a): $b^2/(R.t) < 1$ (i.e. $Z < 1$) (see Figure 5.28 and Figure 5.29 and Table 5.8 and Table 5.9). Therefore, it is concluded that, within the range of the parametric study, the limit for the curvature parameter imposed by EN1993-1-5:2006 is on the safe side.

Table 5.8: Validation of the limit for the curvature parameter in EN1993-1-5:2006 ($\psi=1$)

	$\lambda=0.2$	$\lambda=1$	$\lambda=1.5$	$\lambda=2$	$\lambda=2.5$	$\lambda=3$
EN1993-1-5	1.000	0.780	0.569	0.445	0.365	0.309
Z=1	1.000	1.000	0.548	0.448	0.382	0.330
Z=2	1.000	0.738	0.540	0.444	0.380	0.328
Z=4	1.000	0.718	0.526	0.436	0.374	0.324
EN1993-1-5 vs. Z=1 (%)	+0.0	-4.4	-4.4	+0.2	+4.2	+6.9
EN1993-1-5 vs. Z=4 (%)	+0.0	-7.9	-7.5	-2.0	+2.5	+4.9

Table 5.9: Validation of the limit for the curvature parameter in EN1993-1-5:2006 ($\psi=-1$)

	$\lambda=0.2$	$\lambda=1$	$\lambda=1.5$	$\lambda=2$	$\lambda=2.5$	$\lambda=3$
EN1993-1-5	1.000	0.890	0.618	0.473	0.362	0.292
Z=1	1.000	0.873	0.630	0.471	0.368	0.296
Z=2	1.000	0.861	0.623	0.469	0.366	0.294
Z=4	1.000	0.854	0.619	0.464	0.362	0.292
EN1993-1-5 vs. Z=1 (%)	+0.0	-1.9	+2.0	-0.3	-3.2	-7.8
EN1993-1-5 vs. Z=4 (%)	+0.0	-4.0	+0.2	-1.8	-4.7	-9.1

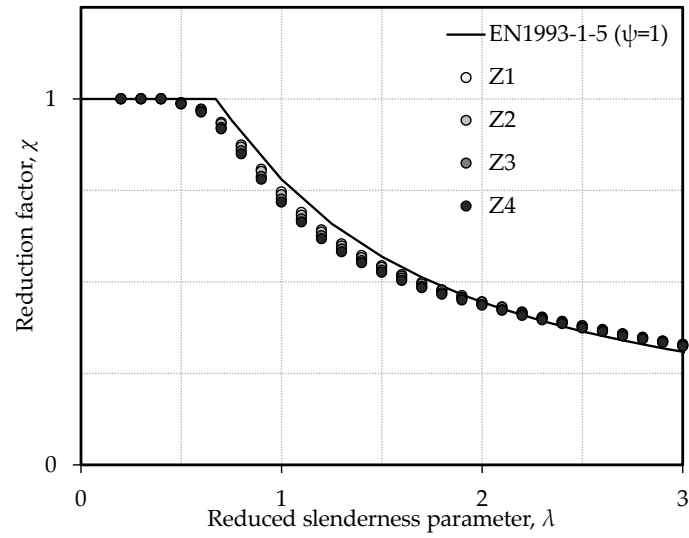


Figure 5.28: Validation of the limit for the curvature parameter in EN1993-1-5:2006, $\psi=1$

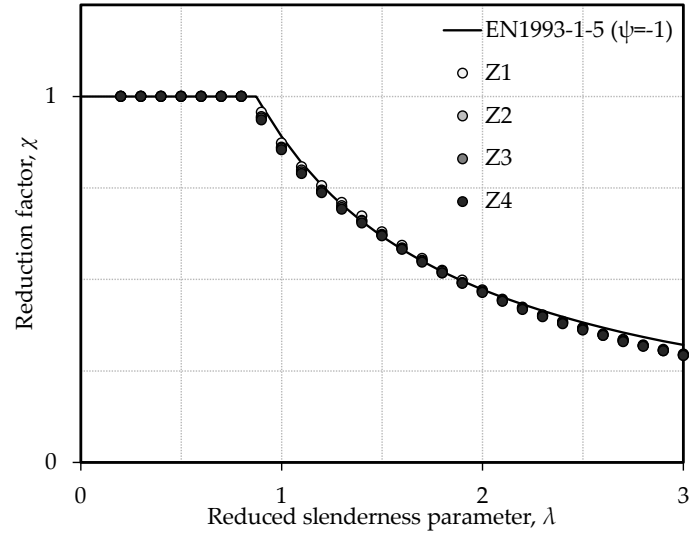


Figure 5.29: Validation of the limit for the curvature parameter in EN1993-1-5:2006, $\psi=-1$

5.4. Parametric study on the ultimate strength of short cylindrically curved panels under biaxial compressive stresses

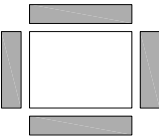
5.4.1. Scope

This parametric study aims at characterising the ultimate strength behaviour of cylindrically curved panels under biaxial loading. Numerical results are obtained from GMNIA analyses and represent the maximum load factor obtained (which may vary from 0 to the normalised von Mises stress). The following parametric study comprises the study of the parameters:

- Curvature, Z ;
- ratio between longitudinal and circumferential stresses, defined by θ_{bl} (see Figure 5.30);
- Slenderness, whereby defined by the b/t ratio.

From the information given by Table 5.10 it is concluded that 1760 analyses have been performed within this parametric study.

Table 5.10: Parametric study on the ultimate behaviour of cylindrically curved panels under biaxial loading

<i>Load cases, θ_{bl}</i> <i>(see Figure 5.30)</i>	<i>Width, b</i>	<i>Thickness, t</i>	<i>Curvature, Z</i>	<i>Aspect Ratio, α</i>	<i>Geometric imperfection</i>	
	300, 450, 650 and 1000 mm	10 mm	0 to 10 (step=1) 20 to 100 (step=10)	1.0	Inwards and outwards	
Total for BC3	11 (step= $\pi/20$)	4	1	20	1	2

The cylindrically curved panels studied in this section have constant thickness ($t=10\text{mm}$) and an imperfection shape based on the first eigenmode of a cylindrically curved panel under uniaxial compressive stresses (see Figure 5.10). The

maximum amplitude for the geometric imperfection shape is $b/200$ and it is applied both inwards and outwards. The use of the first buckling mode for the shape of the geometric imperfections in this parametric study is justified by the fact that, for square panels (*i.e.* aspect ratio equal to 1), one half-wave in both directions (longitudinal and transversal) is appropriate to “catch” the lower bound resistance of plates under biaxial loading (Braun, 2010). Here, it is assumed that this trend is still true for square cylindrically curved panels under biaxial loading. In what concerns the maximum amplitude of the geometric imperfections, again recommendations from Braun (2010) are followed, *i.e.* maximum amplitude equal to $b/200$.

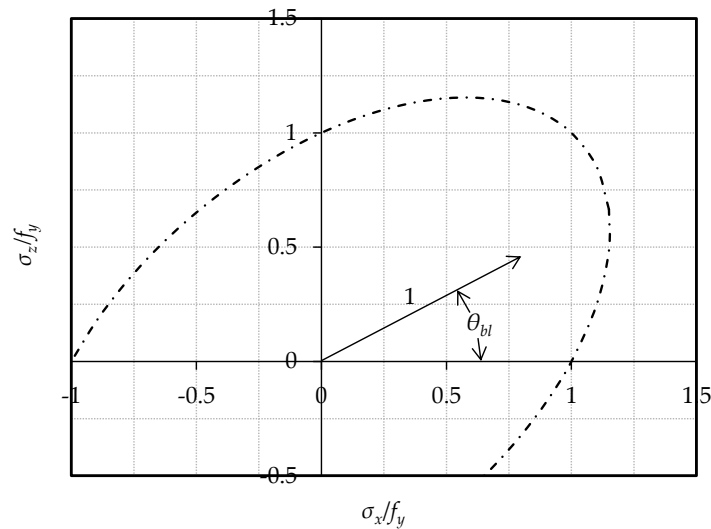


Figure 5.30: Definition of θ_{bl}

5.4.2. Influence of geometry (curvature and geometric imperfections) on the ultimate strength of cylindrically curved panels

In opposition to what was observed for cylindrically curved panels under uniaxial compressive stresses, the ultimate resistance of cylindrically curved panels under biaxial loading generally decreases with the increase of curvature.

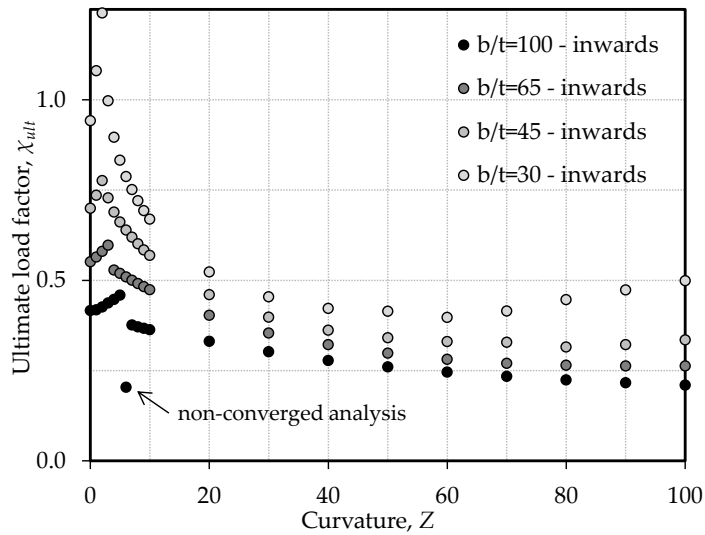


Figure 5.31: Ultimate load factor for cylindrically curved panels under biaxial loading (geometric imperfections applied inwards and $\theta_{bi}=\pi/4$)

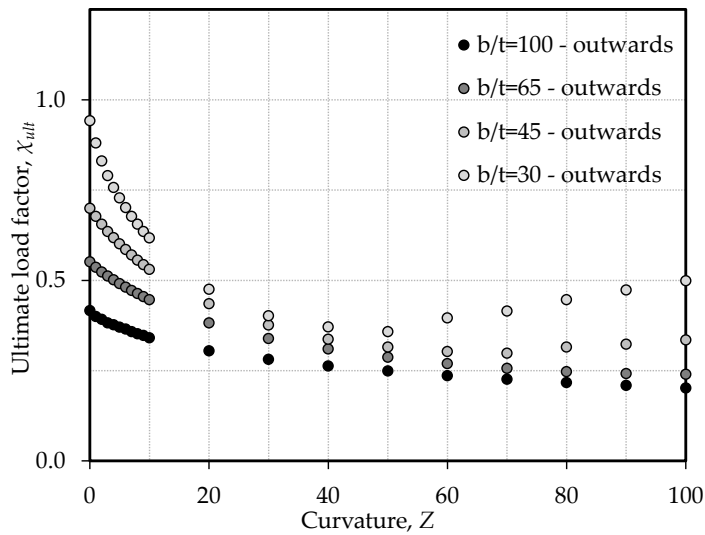


Figure 5.32: Ultimate load factor for cylindrically curved panels under biaxial loading (geometric imperfections applied outwards and $\theta_{bi}=\pi/4$)

The last statement is supported by information gathered from Figure 5.31 and Figure 5.32. However, from Figure 5.31 it is seen that for low values of curvature the trend is an increasing on the ultimate resistance followed by an abrupt drop around values of $Z=3$ to $Z=5$. The referred increase in the ultimate resistance is explained by the fact that, for low values of curvature (high values of radius of curvature and low values of total depth), the maximum amplitude for the geometric imperfection is greater than the total depth of the cylindrically curved panel and, therefore, the applied load compels the panel to increase the amplitude in the same direction as the geometric imperfection, *i.e.*, inwards. For values of curvature around 3 to 6 (depending on the b/t ratio) the geometric imperfection becomes smaller than the total depth of the panel which means that the applied load is no longer able to force the panel to follow the geometric imperfection (Figure 5.33 and Figure 5.34). In this case the panel's deflection starts increasing into the outwards direction right from the beginning of the load-displacement curve.

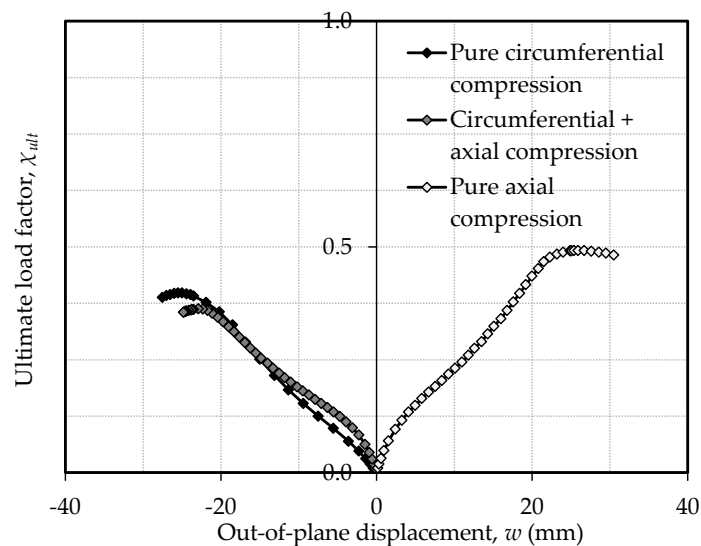


Figure 5.33: Out-of-plane displacement of a cylindrically curved panel with geometric imperfections applied inwards ($Z=10$ and $b/t=100$)

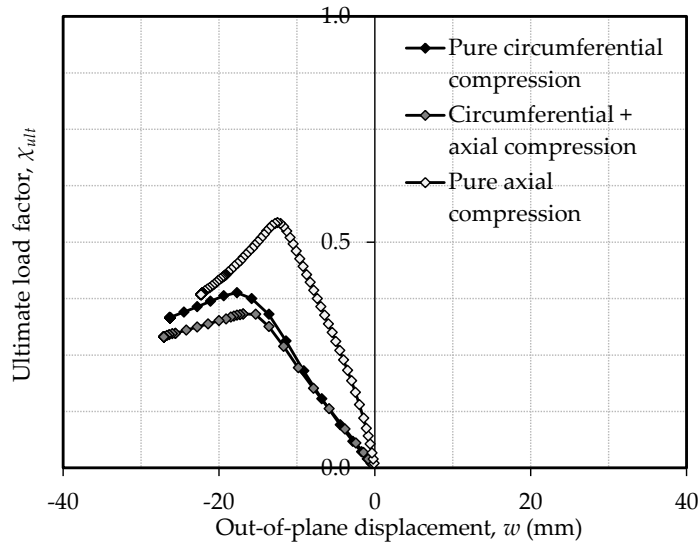


Figure 5.34: Out-of-plane displacement of a cylindrically curved panel with geometric imperfections applied outwards ($Z=10$ and $b/t=100$)

In conclusion, it is seen that the ultimate resistance for high values of curvature and geometric imperfections applied inwards tend to the ultimate resistance of cylindrically curved panels where the geometric imperfection is applied outwards (Figure 5.35 and Figure 5.36).

5.4.3. Influence of the ratio between longitudinal and circumferential stresses on the ultimate strength of cylindrically curved panels

As already discussed in sec. 3.4 and 3.13, the ratio between longitudinal and circumferential stresses (expressed by θ_{bl}) has a strong influence on the behaviour of cylindrically curved panels. Here, that influence is studied with more detail and with emphasis on the specific influence of the curvature parameter and on the direction of the applied geometric imperfections. Figure 5.37 to Figure 5.40 show that these parameters are in fact the most important to accurately characterise the behaviour of square cylindrically curved panels under biaxial loading.

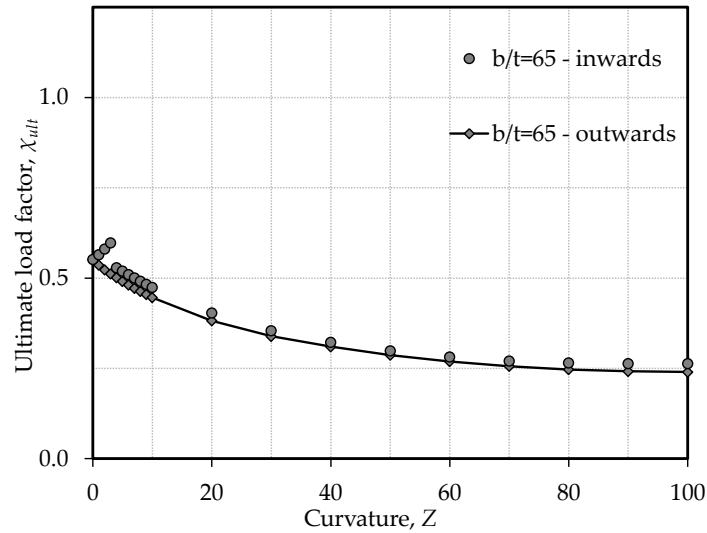


Figure 5.35: Ultimate load factor for cylindrically curved panels under biaxial loading (geometric imperfections applied outwards *vs.* geometric imperfections applied outwards; $\theta_{bl}=\pi/4$ and $b/t=65$)

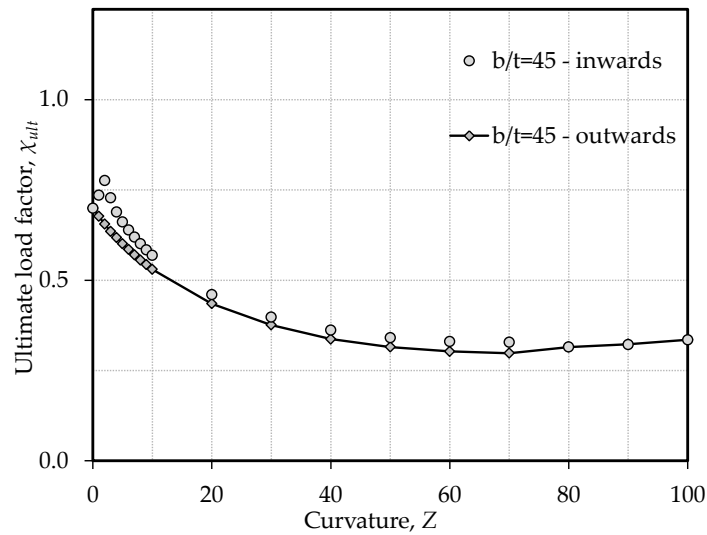


Figure 5.36: Ultimate load factor for cylindrically curved panels under biaxial loading (geometric imperfections applied outwards *vs.* geometric imperfections applied outwards; $\theta_{bl}=\pi/4$ and $b/t=45$)

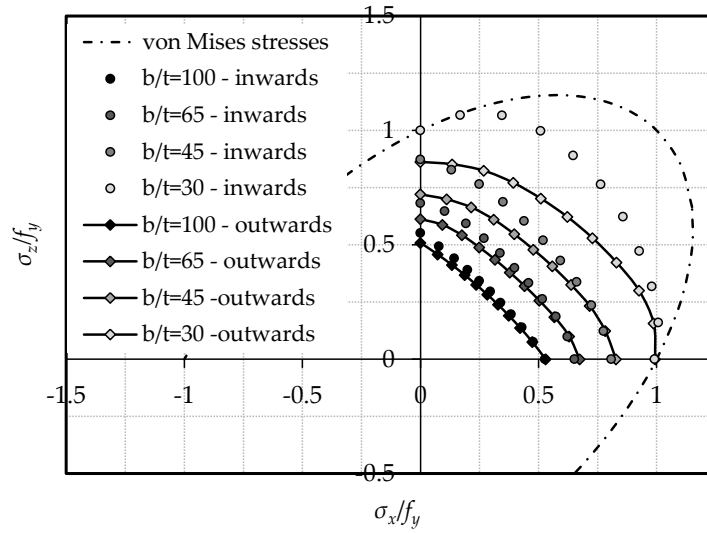


Figure 5.37: Ultimate load factor for cylindrically curved panels under biaxial loading ($Z=1$)

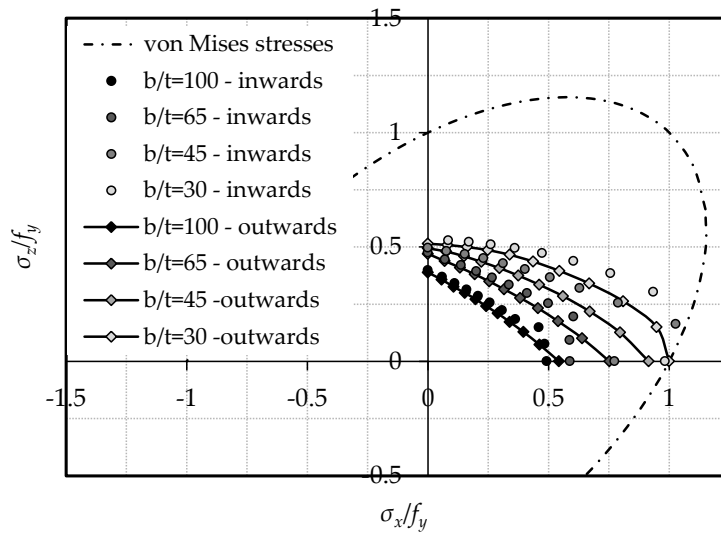


Figure 5.38: Ultimate load factor for cylindrically curved panels under biaxial loading ($Z=10$)

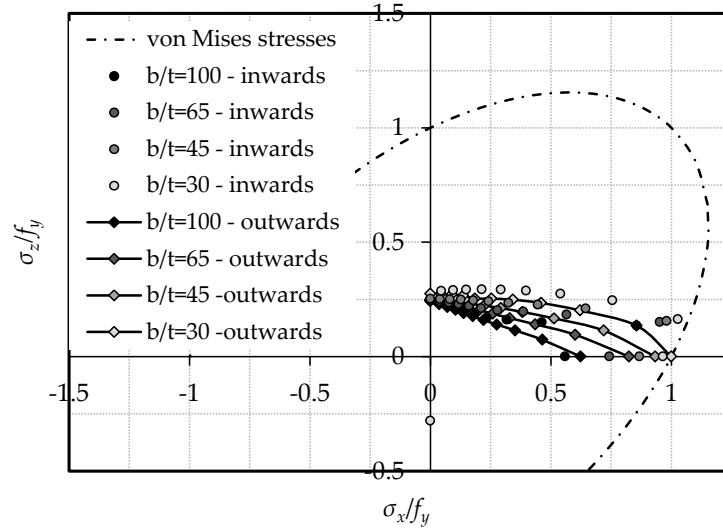


Figure 5.39: Ultimate load factor for cylindrically curved panels under biaxial loading ($Z=50$)

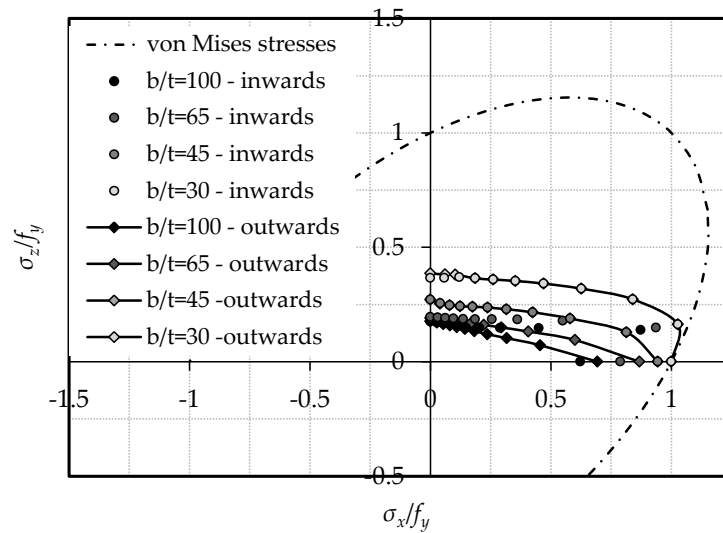


Figure 5.40: Ultimate load factor for cylindrically curved panels under biaxial loading ($Z=100$)

A direct conclusion from Figure 5.37 to Figure 5.40 is that for cylindrically curved panels under pure circumferential stresses the reduction on the ultimate strength with the increase in curvature is quite abrupt, especially for slender curved panels ($b/t=100$); for stockier curved panels ($b/t=30$) it is seen a slight increase in the ultimate load factor from curvature around 50-60 to 100 (this is also patent in Figure 5.31 and Figure 5.32 for $b/t=45$ and $b/t=30$).

In what concerns the direction of geometric imperfections (inwards *vs.* outwards), from the analysis of Figure 5.41 it is seen that models with geometric imperfection applied inwards only return lower values of ultimate resistance when σ_x is dominant ($\theta_{bl} \leq \pi/10$, *i.e.*, low values of circumferential stresses). Although, Figure 5.41 only shows the results for $Z=9$ and $b/t=65$ this trend is noticeable for other combinations of Z and b/t ratios.

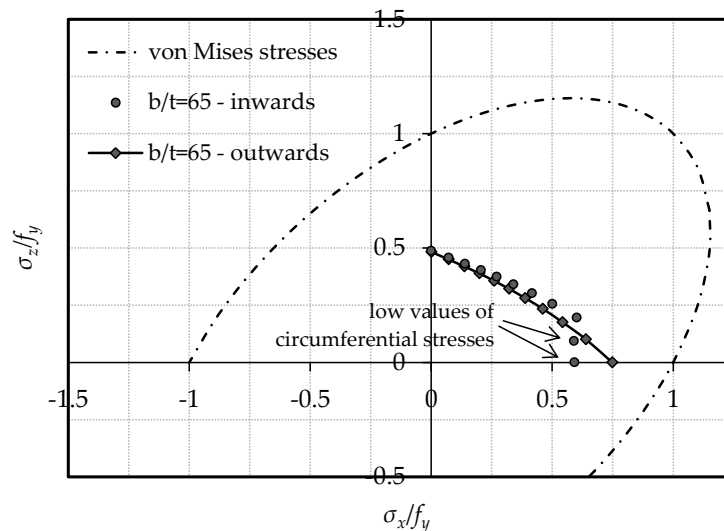


Figure 5.41: Ultimate load factor for cylindrically curved panels under biaxial loading ($Z=9$ and $b/t=65$)

5.4.4. Concluding remarks

In this section, the influence of an additional loaded direction was studied being concluded that it has a strong influence on the ultimate response of cylindrically curved panels. In fact, it is seen that the reduction on the ultimate

strength of cylindrically curved panels is greater when stresses in the circumferential direction are dominant. This is in line to what was expected: as the circumferential direction is less stiff than the longitudinal direction the reduction is bigger in the circumferential direction.

Another important conclusion is that the most unfavourable direction of geometric imperfections changes from inwards for very low curvatures and when longitudinal stresses are dominant to outwards for medium to high curvatures and for low values of circumferential stresses (Figure 5.41).

Finally, it should be said that the postbuckling behaviour is also different whether the geometric imperfections are applied inwards or outwards. Seemingly, comparing Figure 5.33 to Figure 5.34, it is seen that the initial stiffness is higher (higher slope of the initial segment of the postbuckling path) when geometric imperfections are applied outwards.

5.5. Summary

In this chapter the numerical results (except those related to the imperfection sensitivity study) were shown and interpreted. It was shown, numerically and in a thoroughly way, that curvature is a central parameter that must be taken into account when evaluating the overall behaviour of cylindrically curved panels under compressive stresses (uniaxial and biaxial compressive stresses). Furthermore, it was shown that the definition of boundary conditions is more important than it is for flat plates. In fact, on one hand, for flat plates the results for the elastic critical stress are exactly the same whether boundary conditions type 1, 2 or 3 are used; on the other hand, the elastic buckling stress is influenced by curvature.

Another important outcome of this chapter is the awareness of the evolution of the shape of the first buckling mode of axially compressed cylindrically curved panels with the curvature parameter: the higher the curvature the more different from the classical displacement field the eigenmode is. This outcome is of extreme importance for the interpretation of analytical derivations in Chapter 7 and also it responsible for the development of the study

presented in Chapter 6: the study of the influence of different shapes (and amplitudes) based upon the panel's buckling mode playing the role of geometric imperfections.

Finally, it should be said that results from sec. 5.2 and sec. 5.3 are the core of the calibration of proposed formulae (for computing the elastic critical stress and the ultimate strength of cylindrically curved panels under axial compressive stresses) in Chapter 8.

6. Imperfection sensitivity of cylindrically curved panels under uniaxial compression

6.1. Chapter overview

In the field of plate and shell stability, imperfections (geometric, residual stresses and eccentricities) are known to be the cause of poor correlation between theoretical and experimental results. Generally speaking, the presence of imperfections decreases the ultimate load that a structure can support (Figure 2.1).

Classically, design formulae were calibrated exclusively with experimental results (*e.g.* Winter's formula) where the measurement of imperfections was not important since the goal was, after identifying relevant parameters, to establish a large scatter of points representing the ultimate resistance of a certain structural component and later perform a regression to obtain an expression capable of predicting the structural element ultimate load on the safe side. Nowadays, experimental campaigns are complemented with numerical simulations of the structural component being studied, allowing a much larger scatter of points in a much shorter time period. The downside of numerical approaches is that it becomes crucial to know and to model imperfections accurately.

Additionally, high-performance software tools (almost exclusively based on the finite element and on the finite strip methods) are widespread and are used in most design offices around the world. Therefore, definition and guidelines on how to model imperfections is an urgent task. As already mentioned

in sec. 4.2.4, at the European level imperfections are treated in Annex C of EN1993-1-5:2006 (CEN, 2006a) for plated structures and in clause 8.7 of EN1993-1-6:2007 (CEN, 2007). Additionally, since cylindrically curved panels are neither flat panels nor shells of revolution, the following question is raised: what standard should be followed to define imperfections in cylindrically curved panels? If neither of the options is appropriate, definition rules for estimating equivalent geometric imperfections are missing from European standards. On top of this problem, preliminary results confirm that unstiffened cylindrically curved panels are highly sensitive to initial geometric imperfections.

In order to tackle the above referred problems, sec. 6.2 describes a parametric study organised to include all parameters that have an important role in what concerns geometric imperfections, namely maximum amplitude and pattern. In sec. 6.3 a very detailed analysis of the influence of the geometric imperfection on the postbuckling response and on the ultimate strength is made. Finally, in sec. 6.4 the main conclusions are highlighted.

6.2. Parametric study

6.2.1. Scope

A total of 24 120 GMNIA's were carried out. The range of all parameters which intervene in the parametric study is presented in Table 6.1. The parametric study is centred on imperfect cylindrically curved panels with b/t ratios equal to 100. This choice is related to the belief that this ratio is the most representative of practical applications. As shown in Figure 5.24 whereby b/t ratios equal to 100 are equivalent to non-dimensional slenderness parameters between 0.75 and 2, which is a comprehensive range and also where imperfections plays a larger role in the determination of the ultimate load (for lower non-dimensional slenderness parameters the ultimate strength is driven by plasticity and for higher values the ultimate load is driven by stability). Nevertheless, additional b/t ratios are also analysed ($b/t=150$ and $b/t=200$). It is highlighted that this additional results are only used to compare higher b/t ratios equal to 100 in sec. 6.3.3.4.

6.2.2. Definition of equivalent geometric imperfections: pattern and amplitude

Since the main goal of this paper is to characterise the imperfection sensitivity of cylindrically curved panels, the definition of equivalent geometric imperfections requires a more complete description. Ten different imperfection shapes (based on the ten first buckling modes) are considered which are combined with eight different amplitudes (from 20% to 200% of $b/200$, and two additional values representing a modified approach by EN1993-1-5:2006 (CEN, 2006a) and EN1993-1-6:2007 (CEN, 2007)).

Table 6.1: Range of the imperfect sensitivity study parametric study

<i>Width, b</i>	<i>Thickness, t</i>	<i>Curvature, Z</i>	<i>Aspect ratio, α</i>	<i>Imp. shape</i>	<i>Imp. amplitude</i>
1000 mm	10 mm	1, 10 to 100 step=10	0.4 to 5.0 step=0.2	Buckling modes 1 to 10	2, 3, 4, 5, 7, 10mm
					$\Delta w_{0,eq,EN1993-1-5}^{mod}$
					$\Delta w_{0,eq,EN1993-1-6}^{mod}$
1500 mm	10 mm	1, 10 to 100 step=10	1.0 to 5.0 step=1.0	Buckling modes 1 to 10	$b/200$
2000mm					$\Delta w_{0,eq,EN1993-1-5}^{mod}$
					$\Delta w_{0,eq,EN1993-1-6}^{mod}$

In what concerns the pattern of the equivalent geometric imperfections, the ten first buckling modes were considered. As an example, these buckling modes are shown in Figure 6.1 for a cylindrically curved panel with a curvature parameter $Z=50$ and an aspect ratio $\alpha=2$. As it is patent in Figure 6.1 the order of the buckling mode is not appropriate to identify a specific buckling mode by its wave number (*e.g.* the buckling mode with one half-wave in the longitudinal direction is buckling mode number seven, while for a cylindrically curved panel $Z=1$ and $\alpha=1$, the buckling mode with one half-wave is the first one), buckling modes are classified according to their shape instead. The following geometrical aspects are considered to classify the buckling modes:

- Number of half-waves in the longitudinal direction: one half-wave is defined as the deflected part of the panel delimited by zero deformation lines;
- Number of peaks, *i.e.* maxima and minima, in the longitudinal direction;
- Number of transverse half-waves.

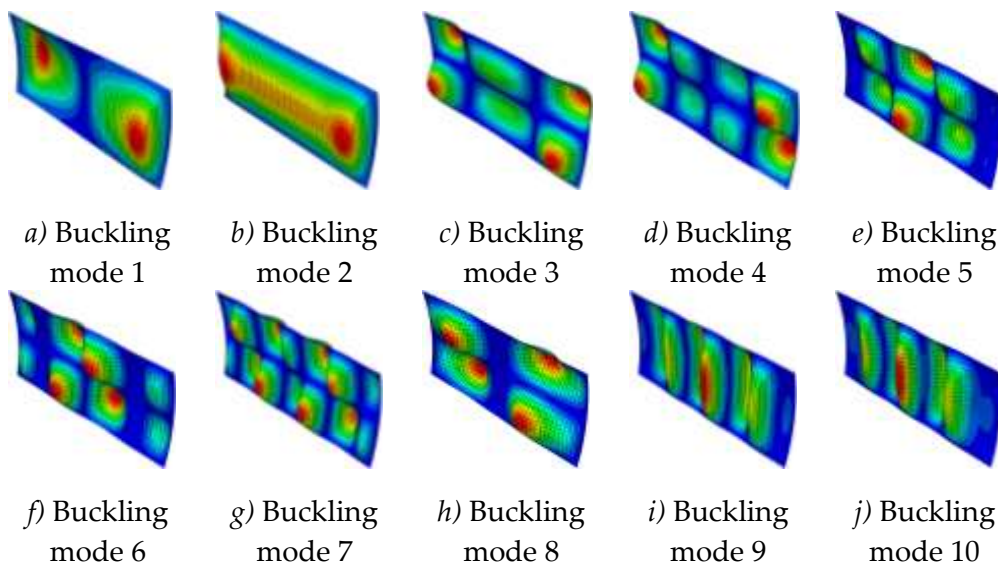


Figure 6.1: Buckling modes for a cylindrically curved panel with $Z=50$ and $\alpha=2$

Considering buckling mode number 2 of Figure 6.1, it is clear that it has one longitudinal half-wave and one transverse half-wave. Concerning the number of peaks, a deeper analysis must be done.

Analysing Figure 6.2 (section at $b/2$) it is concluded that the number of peaks is equal to seven. Therefore, the name of this buckling mode is $1.7LW_1TW$ (where LW means longitudinal half-wave and TW means transverse half-wave). For instance, $3.11LW_2TW$ is referring to a buckling mode with three longitudinal half-waves with eleven peaks and two transverse half-waves.

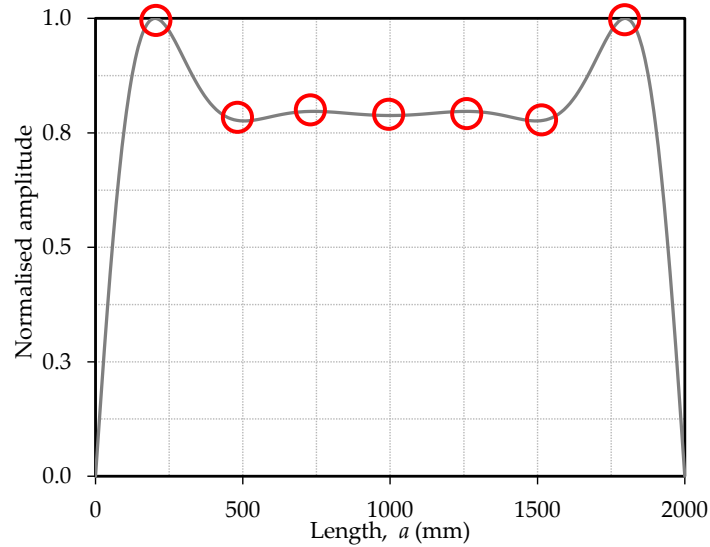


Figure 6.2: Shape of buckling mode 2 at $b/2$ for a cylindrically curved panel with $Z=50$ and $\alpha=2$

Another important parameter related to the equivalent geometric imperfections is their maximum amplitude. As already mentioned, besides predefined amplitudes, the parametric study considers amplitudes based on two modified approaches based on methodologies for computing equivalent geometric imperfections given by EN1993-1-5:2006 (CEN, 2006a) and EN1993-1-6:2007 (CEN, 2007). These modified approaches are based on the dimensions of the largest half-wave of the buckled shape, l_{Lw} in the longitudinal direction, and l_{Tw} in the transverse direction (see Figure 6.3), and the amplitudes are given by Eqs. (6.1) and (6.2).

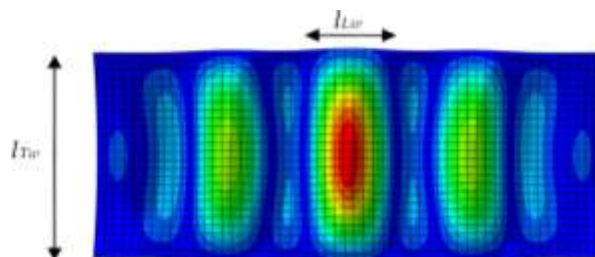


Figure 6.3: Definition of l_{Lw} and l_{Tw}

$$\Delta w_{0,eq,EN1993-1-5}^{\text{mod}} = \min(l_{LW}/200; l_{TW}/200) \text{ - based on EN1993-1-5:2006} \quad (6.1)$$

$$\Delta w_{0,eq,EN1993-1-6}^{\text{mod}} = \max \left\{ \begin{array}{l} \min(l_{LW}U_n; l_{TW}U_n) \\ 25tU_n \end{array} \right\} \text{ - based on EN1993-1-6:2007} \quad (6.2)$$

Eq. (6.1) is directly obtained from Eq. (4.2) by substituting a by l_{Lw} and b by l_{Tw} . Eq. (6.2) is less intuitive, but it is obtained from Eq. (4.3) by assuming the lowest value between $l_{Lw}.U_n$ and $l_{Tw}.U_n$ for $l_g.U_n$ with a lower limit set to $25.t.U_n$. The use of the length of the largest half-wave of the buckled shape as relevant length to compute the imperfection's amplitude instead of the plate's length, a , or width, b (as it is done for plates) and instead of predefined lengths, l_g , given by EN1993-1-6:2007 (as it is done for shells) is justified by the fact that it would be to unfavourable (*i.e.* the reduction of resistance would be unrealistically high) to use $\min(a/200; b/200)$ or $\max(l_g.U_n; 25.t.U_n)$ for a panel with geometric imperfections based on an eigenmode-affine shape with a large number of half-waves along the plate's length.

6.3. Results and discussion

6.3.1. Preliminary remarks

From a preliminary analysis, based on engineering judgement, it was seen that some buckling modes were "unrealistic" as imperfection shapes (not necessarily giving the lowest value of the ultimate load). The idea that some buckling modes should not be considered came from the realisation that at some point a buckling shape would have so many half-waves that the membrane resistant behaviour would disappear (especially for high values of the maximum amplitude) becoming a bending resistance behaviour, which is clearly unrealistic when dealing with this type of elements.

Examples of such buckling modes are given in Figure 6.4. Obviously, the definition of "unrealistic" needs to be clarified and, again based on engineering judgement, some criteria were established to define whether a buckling shape should or should not be considered suitable as imperfection shape:

- Buckling modes with longitudinal half-wave lengths lower than $\min(a/4; 2.b/3)$ are considered unrealistic;
- Buckling modes with transverse half-wave lengths lower than $b/2$ are considered unrealistic.

As an example, Figure 6.5 and Figure 6.6 shows numerical results for $Z=40$ and $Z=100$ where the “realistic” patterns are separated from the “unrealistic” patterns. It is seen that for $Z=40$ some “unrealistic” shapes were found as the most critical while for $Z=100$ “unrealistic” shapes defined according to the previously defined criteria are never the most unfavourable ones. It is pointed out that in Figure 6.5 and in Figure 6.6 higher values for “unrealistic” shapes are related to shapes with three or more transverse half-waves. It is also highlighted that, for $Z=40$, the points with the lowest values of the ultimate load factor are exactly those with a large number of longitudinal half-waves where the behaviour might no longer be characterised by the presence of a membrane resistant mechanism but by a bending resistant mechanism.

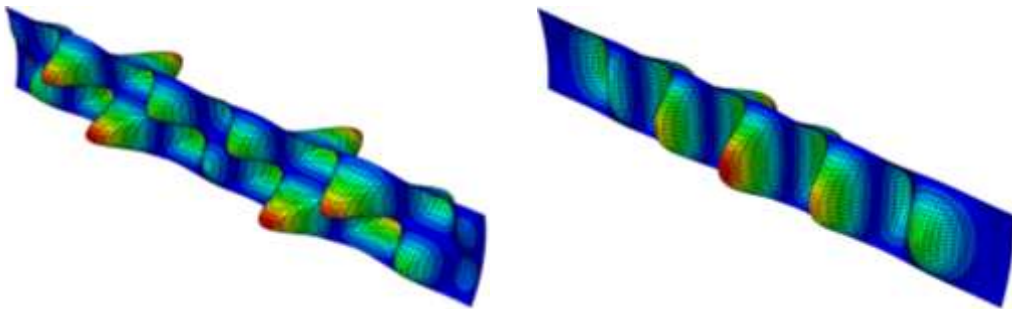


Figure 6.4: Examples of “unrealistic” imperfection shapes according to previously defined criteria

Finally, it is again brought to the attention of the reader that the discussion of results in the next sections is centred on results from models with b/t ratios equal to 100. The comparison between results with different b/t ratios is performed at sec. 6.3.3.4.

6.3.2. Postbuckling behaviour response to geometric imperfections

6.3.2.1. Influence of amplitude

Generally speaking, it can be concluded from a first analysis of Figure 6.7 to Figure 6.10, that the postbuckling behaviour is strongly influenced by the imperfection's amplitude. In particular, Figure 6.7 to Figure 6.10 plot the load-displacement curves for models with curvature parameters $Z=10, 30, 50$ and 100 , aspect ratios $\alpha=1.0, 1.2, 1.6$ and 2.2 and for models with one longitudinal half-wave and one transverse half-wave as the geometric imperfection pattern. It is noticed that other shapes may induce different behaviours and responses. This aspect will be treated in the next section. From a more refined analysis, it is concluded that the postbuckling behaviour changes its characteristics with the curvature parameter and with the increase of the aspect ratio.

For example, from Figure 6.7 it is clear that the postbuckling path resembles the behaviour of a plate for all aspect ratios, progressing to a completely different postbuckling path in Figure 6.8, specially for $\alpha=2.2$, which resemble a classical shell behaviour. Moreover, this tendency seems to be lost, or weakened, for curvature parameters higher than 40 , where the pattern of imperfections seems to have less influence (see also sec. 6.3.2.2).

It is also pointed out that this resemblance to classical shell behaviour coincides with bigger errors when comparing numerical results to previously calibrated expressions for the ultimate load of cylindrically curved panels (see sec. 8.5.4). Additionally, for all cases it is fair to conclude that lower imperfection amplitudes generally lead to higher peaks of the postbuckling path. However, the panel characterised by $Z=10$ shows a very low sensitivity of initial amplitudes of geometric imperfections, and for the case with $\alpha=2.2$ clearly presents a higher peak for initial amplitude equal to 10 mm. The evolution of the ultimate load (peak of the postbuckling path) with the amplitude of geometric imperfections will be discussed in more detail in sec. 6.3.3 where it will be proven that $Z=10$ is not an isolated case.

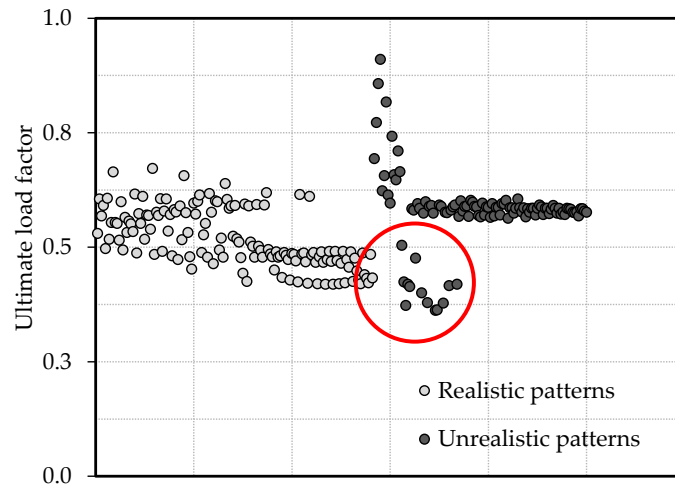


Figure 6.5: Realistic *vs.* unrealistic shapes for $Z=40$

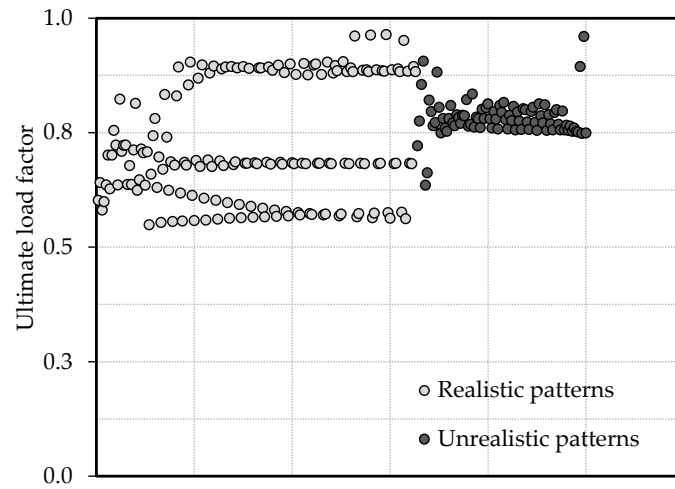


Figure 6.6: Realistic *vs.* unrealistic shapes for $Z=100$

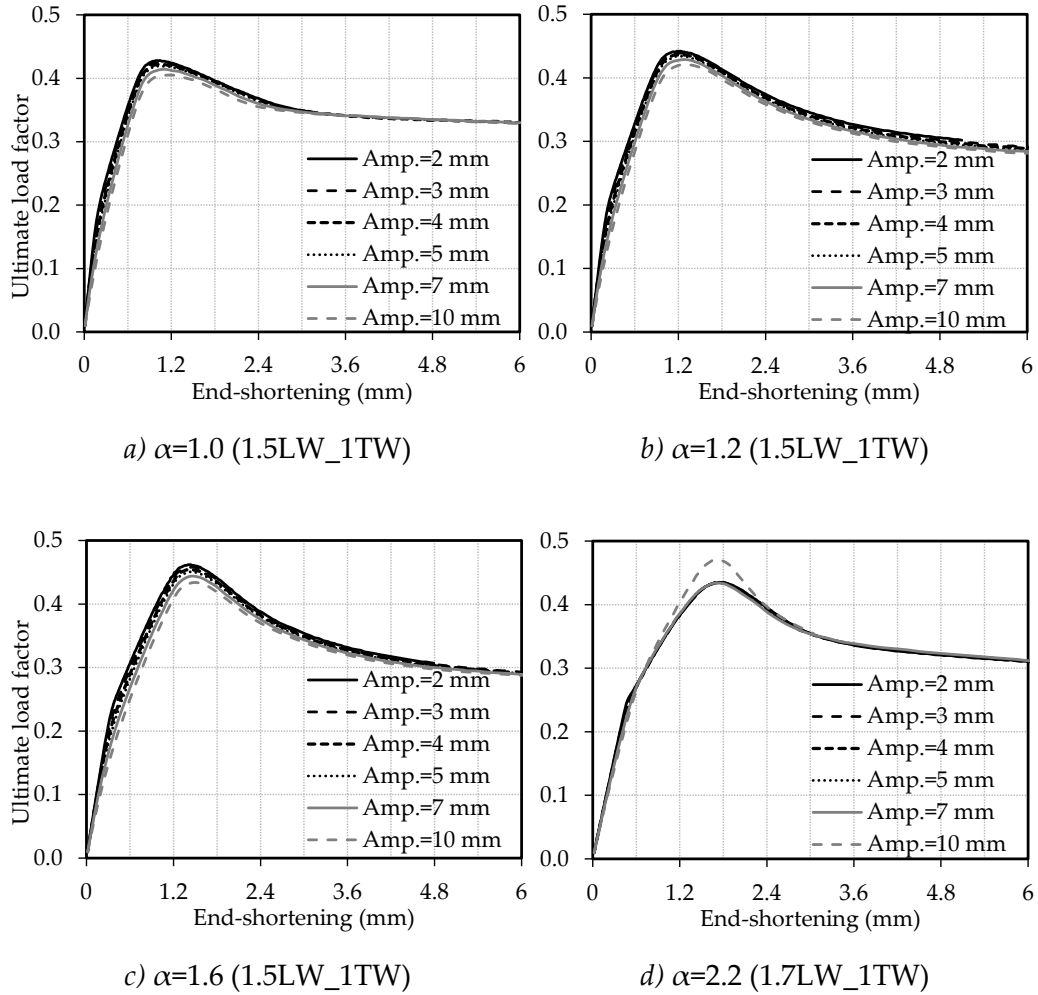


Figure 6.7: Load-displacement curves (end-shortening) curves $Z=10$

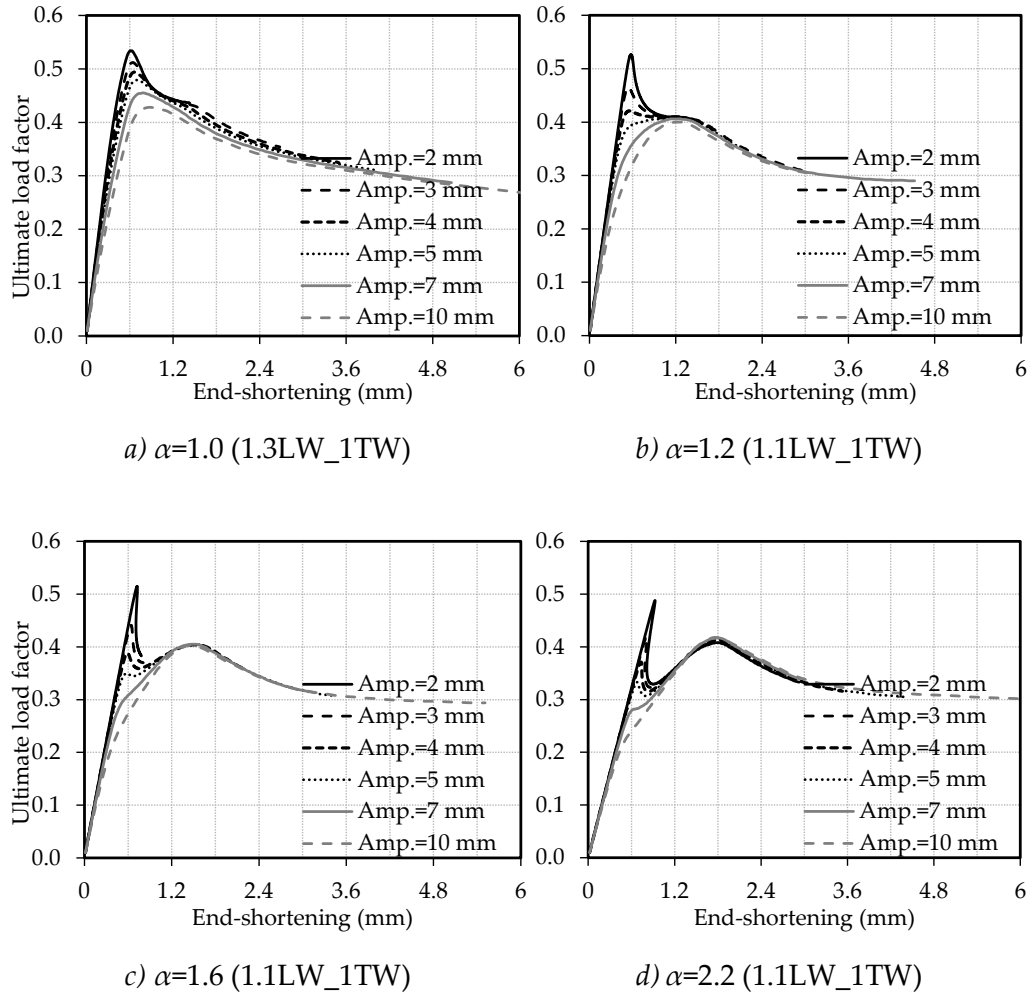


Figure 6.8: Load-displacement curves (end-shortening) curves $Z=30$

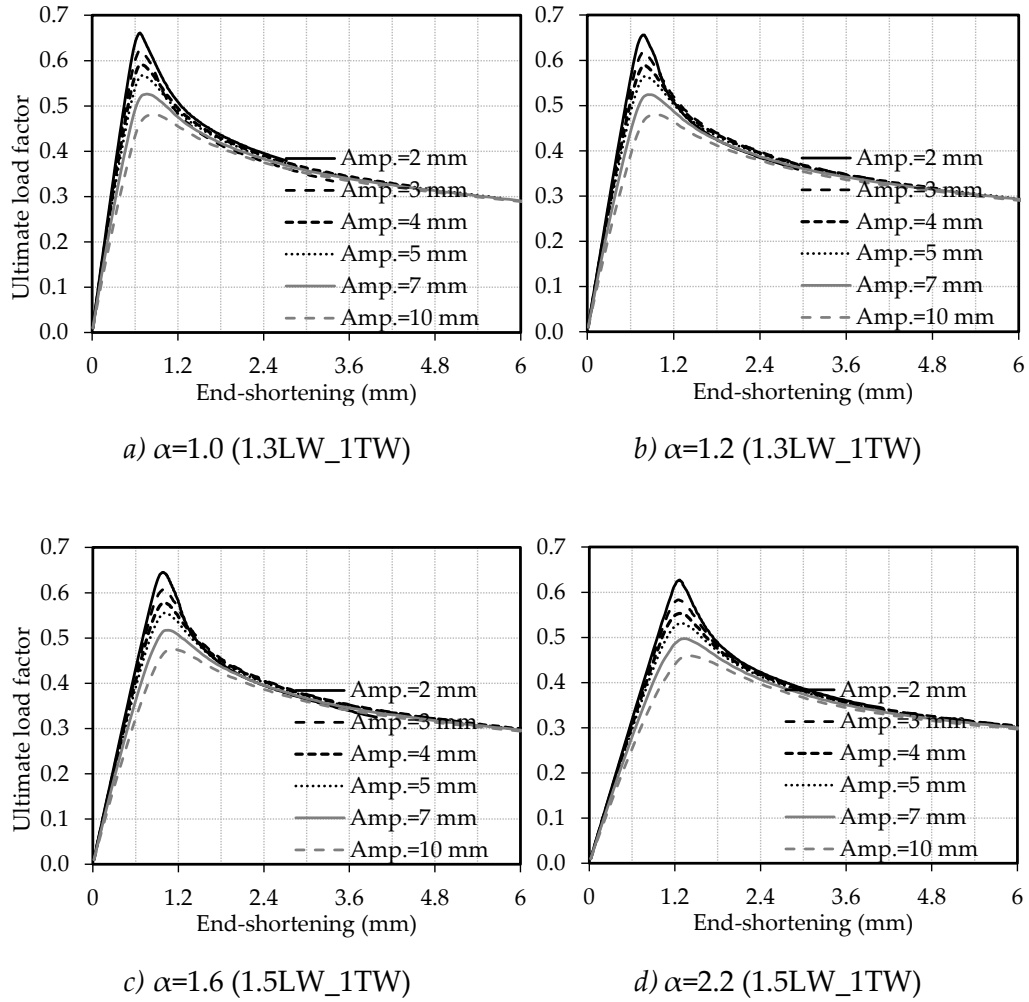


Figure 6.9: Load-displacement curves (end-shortening) curves $Z=50$

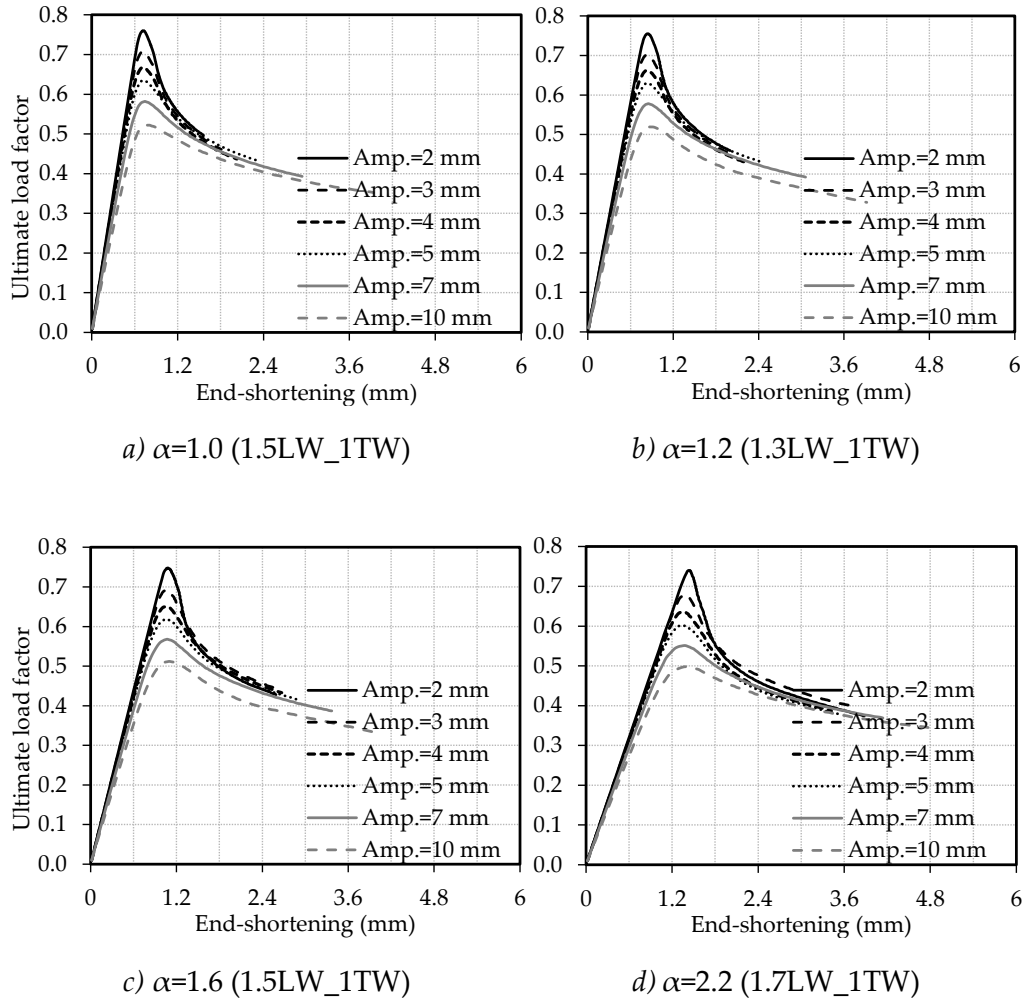


Figure 6.10: Load-displacement curves (end-shortening) curves $Z=100$

6.3.2.2. Influence of the imperfection pattern

The pattern of geometric imperfections is another parameter of the utmost importance in the definition of the load-displacement curve. In fact, initial geometric imperfections used in the parametric study stimulate ten different buckling modes, thus being expectable a strong influence of this parameter. Figure 6.11 to Figure 6.14 shows the load-displacement curves for cylindrically curved panels with equal curvature parameters as those in Figure 6.7 to Figure 6.10 but with aspect ratios and imperfection patterns yielding a minimum value for the ultimate load, *i.e.* Figure 6.11 to Figure 6.14 are a minimum envelope of results presented in Figure 6.7 to Figure 6.10.

It is interesting to notice that all *worst case scenarios*, except for $Z=100$, occur for panels with geometric imperfection patterns characterised by the presence of many longitudinal half-waves. The influence of the pattern of the geometric imperfections will be thoroughly analysed further in secs. 6.3.3.2 and 6.3.3.3.

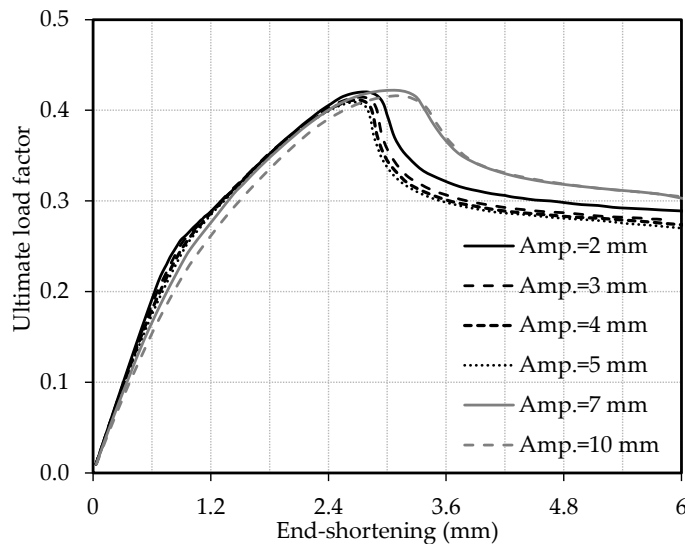


Figure 6.11: Load-displacement curve (end-shortening) curves $Z=10$
(*worst case scenario: $\alpha=3.6$ (6.6LW_1TW)*)

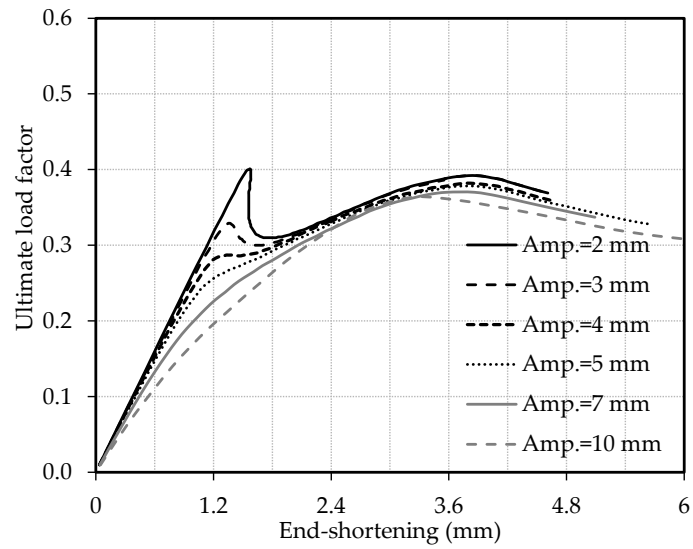


Figure 6.12: Load-displacement curve (end-shortening) curves $Z=30$
(worst case scenario: $\alpha=4.4$ (8.8LW_1TW))

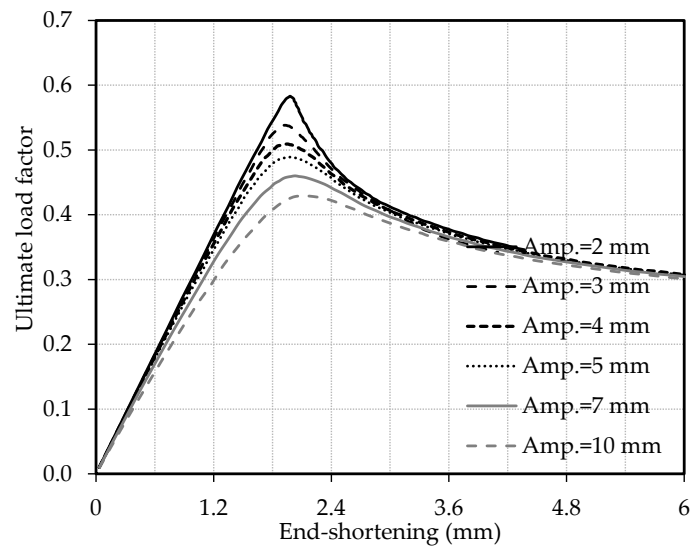


Figure 6.13: Load-displacement curve (end-shortening) curves $Z=50$
(worst case scenario: $\alpha=3.8$ (8.8LW_1TW))

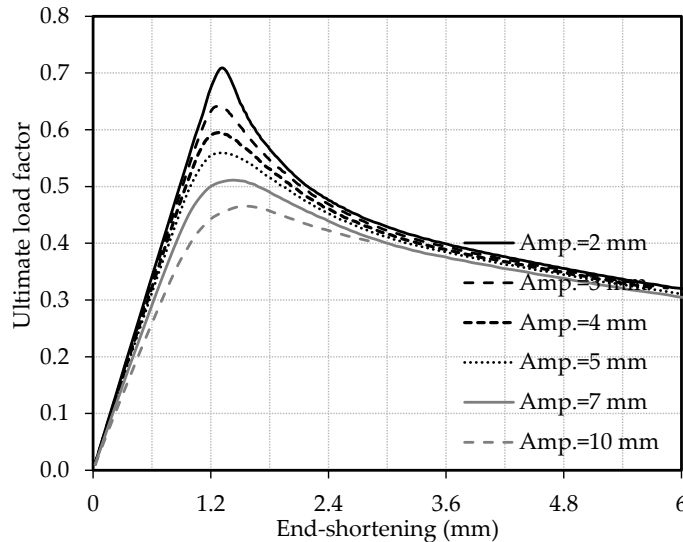


Figure 6.14: Load-displacement curve (end-shortening) curves $Z=100$
(*worst case scenario: $\alpha=2.0$ (2.2LW_1TW)*)

After analysing Figure 6.11 to Figure 6.14 and comparing them to Figure 6.7 to Figure 6.10, the main conclusion is that all cases referred to as *worst case scenario* the linear part of the load-displacement curve has a significantly lower slope when compared to the remaining load-displacement curves of the respective cylindrically curved panel. This suggests that those cylindrically curved panels (with *worst case scenario* patterns as geometric imperfections) have, generally, less membrane stiffness and are not able to cope with axial loads as efficiently as cylindrically curved panels with other buckling modes as imperfection shape.

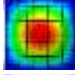
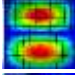
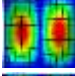
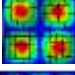
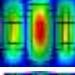
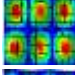
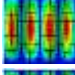
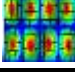
6.3.3. Ultimate behaviour response to geometric imperfections

6.3.3.1. Influence of the amplitude

As already established, amplitude is an ultimate load defining parameter. In Figure 6.15 to Figure 6.31 the evolution of the ultimate load factor with the maximum amplitude for “realistic” shapes is plotted for cylindrically curved panels with curvature parameters $Z=10, 30, 50$ and 100 and aspect ratio $\alpha=1$. Additionally, values of the ultimate load factor for amplitudes based on Eqs. (6.1) and

(6.2) for each imperfection shape are also plotted and information about the ultimate load factor given by EN1993-1-5:2007 (*i.e.* the ultimate load factor disregarding the effect of curvature) is added. In order to aid in the interpretation of Figure 6.15 to Figure 6.31, Table 6.2 to Table 6.5 shows the buckling shapes and imperfection amplitudes used in each respective graph. The first conclusion drawn is that the general trend is the decreasing of the ultimate load factor with the increasing of the imperfection's amplitude. Nevertheless, and as already stated for the panel characterised by $Z=10$ and $\alpha=2.2$, the panel with $Z=10$ and $\alpha=1.0$ for the imperfection shape *1.1LW_2TW* (Figure 6.15) also returns higher ultimate load factor for amplitude equal to 10 mm. The same is true for the panel with $Z=30$ and $\alpha=1.0$ for the imperfection shape *1.1LW_2TW* (Figure 6.29).

Table 6.2: Amplitudes based on Eqs. (6.1) and (6.2) for each buckling shape presented in Figure 6.15 to Figure 6.18 ($Z=10$ and $\alpha=1.0$)

<i>Imperfection's shape</i>	$\Delta w_{0,eq,EN1993-1-5}^{mod}$	$\Delta w_{0,eq,EN1993-1-6}^{mod}$
<i>1.1LW_1TW</i> 	5.00 mm	10.00 mm
<i>1.1LW_2TW</i> 	5.00 mm	10.00 mm
<i>2.2LW_1TW</i> 	2.50 mm	5.00 mm
<i>2.2LW_2TW</i> 	2.50 mm	5.00 mm
<i>3.3LW_1TW</i> 	1.85 mm	3.69 mm
<i>3.3LW_2TW</i> 	1.68 mm	3.37 mm
<i>4.4LW_1TW</i> 	1.27 mm	2.53 mm
<i>4.4LW_2TW</i> 	1.26 mm	2.52 mm

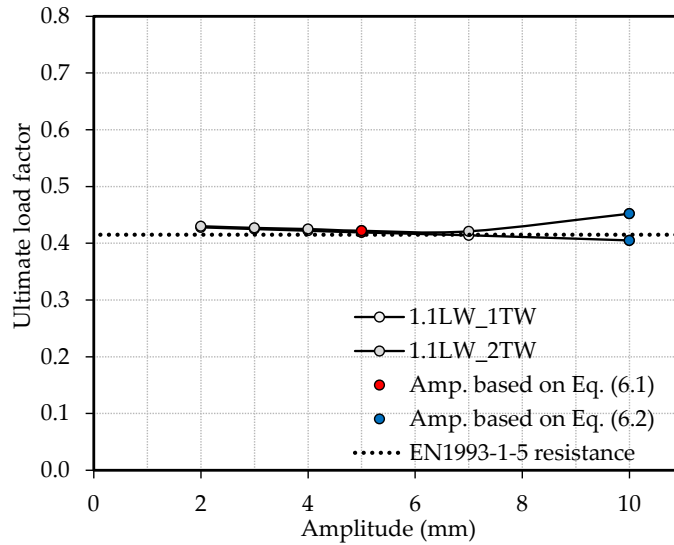


Figure 6.15: Imperfection amplitude *vs.* ultimate load factor for $Z=10$ and $\alpha=1.0$ (imperfection shapes 1.1LW_1TW and 1.1LW_2TW)

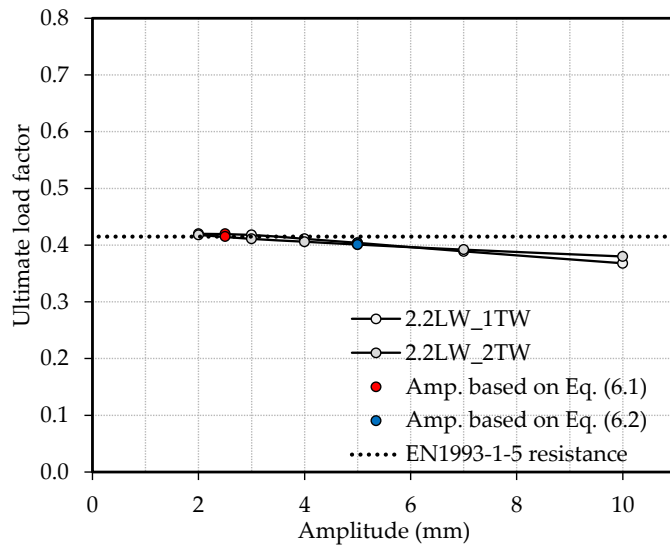


Figure 6.16: Imperfection amplitude *vs.* ultimate load factor for $Z=10$ and $\alpha=1.0$ (imperfection shapes 2.2LW_1TW and 2.2LW_2TW)

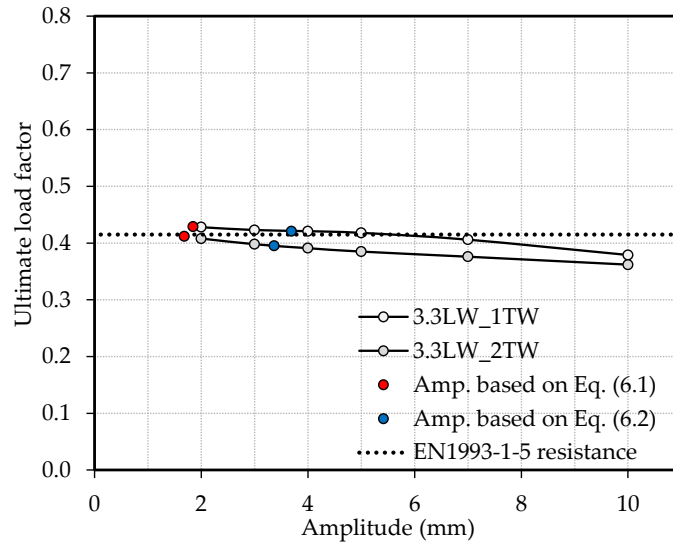


Figure 6.17: Imperfection amplitude *vs.* ultimate load factor for $Z=10$ and $\alpha=1.0$ (imperfection shapes 3.3LW_1TW and 3.3LW_2TW)

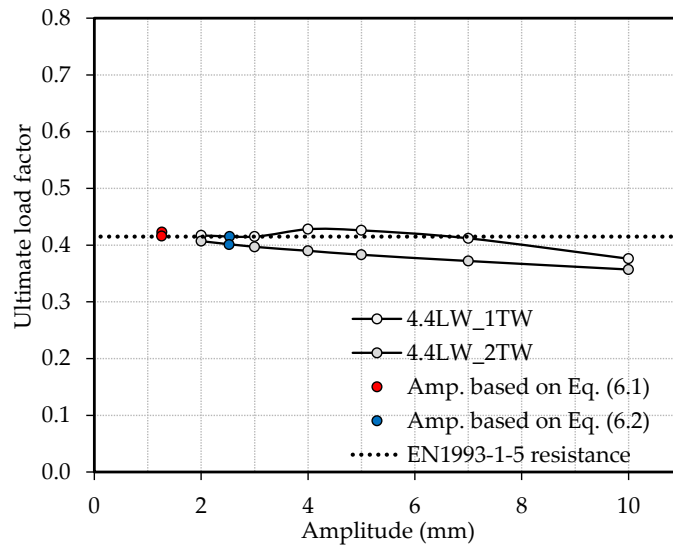
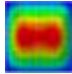
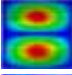
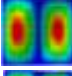
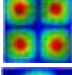
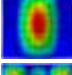
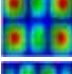
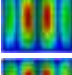
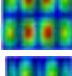
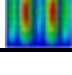


Figure 6.18: Imperfection amplitude *vs.* ultimate load factor for $Z=10$ and $\alpha=1.0$ (imperfection shapes 4.4LW_1TW and 4.4LW_2TW)

Table 6.3: Amplitudes based on Eqs. (6.1) and (6.2) for each buckling shape presented in Figure 6.19 to Figure 6.23 ($Z=30$ and $\alpha=1.0$)

<i>Imperfection's shape</i>	$\Delta w_{0,eq,EN1993-1-5}^{mod}$	$\Delta w_{0,eq,EN1993-1-6}^{mod}$
1.3LW_1TW 	5.00 mm	10.00 mm
1.1LW_2TW 	5.00 mm	10.00 mm
2.2LW_1TW 	2.50 mm	5.00 mm
2.2LW_2TW 	2.50 mm	5.00 mm
3.3LW_1TW 	3.34 mm	6.68 mm
3.3LW_2TW 	1.83 mm	3.66 mm
4.4LW_1TW 	1.42 mm	2.85 mm
4.4LW_2TW 	1.35 mm	2.70 mm
5.5LW_1TW 	1.26 mm	2.53 mm

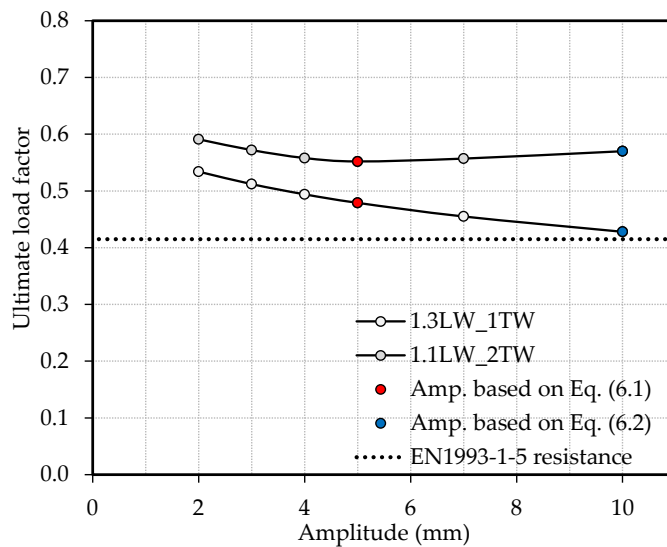


Figure 6.19: Imperfection amplitude *vs.* ultimate load factor for $Z=30$ and $\alpha=1.0$ (imperfection shapes 1.3LW_1TW and 1.1LW_2TW)

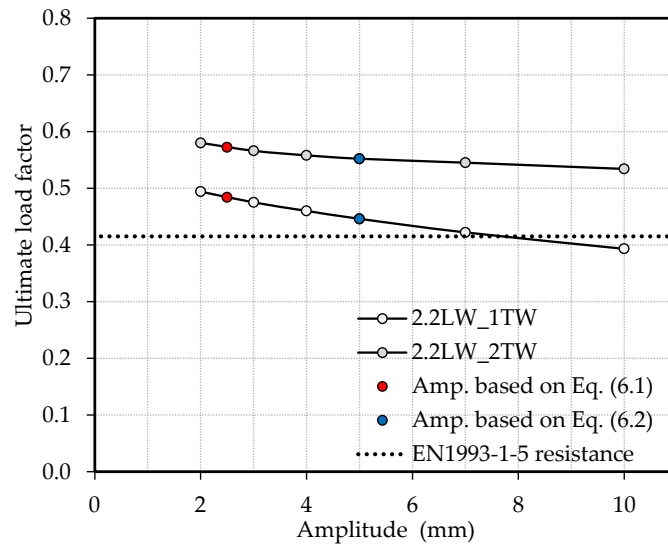


Figure 6.20: Imperfection amplitude *vs.* ultimate load factor for $Z=30$ and $\alpha=1.0$ (imperfection shapes 2.2LW_1TW and 2.2LW_2TW)

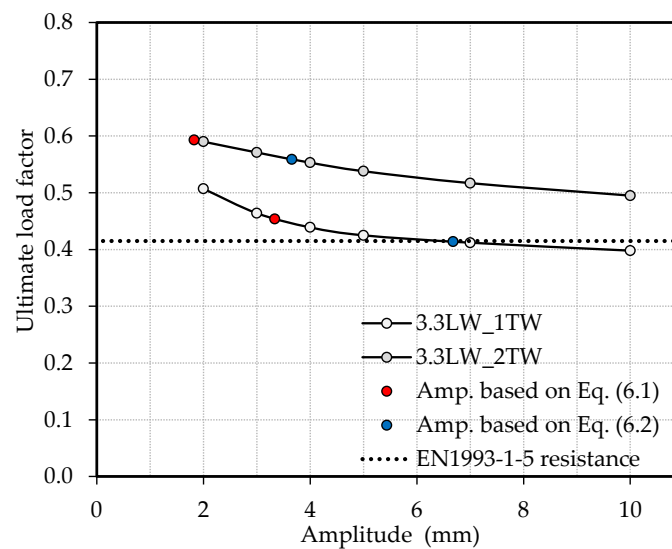


Figure 6.21: Imperfection amplitude *vs.* ultimate load factor for $Z=30$ and $\alpha=1.0$ (imperfection shapes 3.3LW_1TW and 3.3LW_2TW)

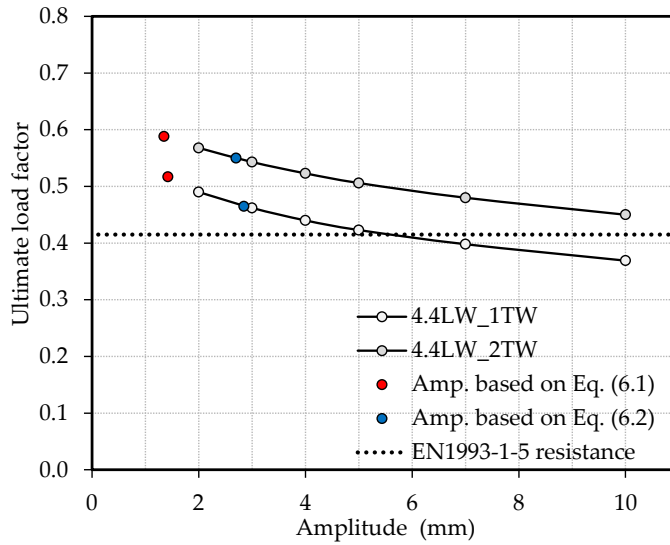


Figure 6.22: Imperfection amplitude *vs.* ultimate load factor for $Z=30$ and $\alpha=1.0$ (imperfection shapes 4.4LW_1TW and 4.4LW_2TW)

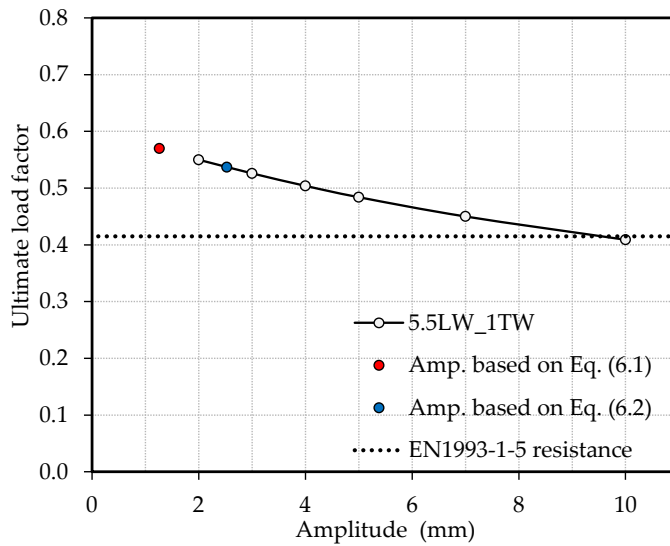

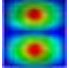
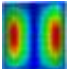
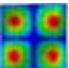
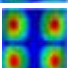
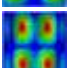
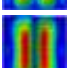
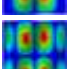
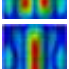
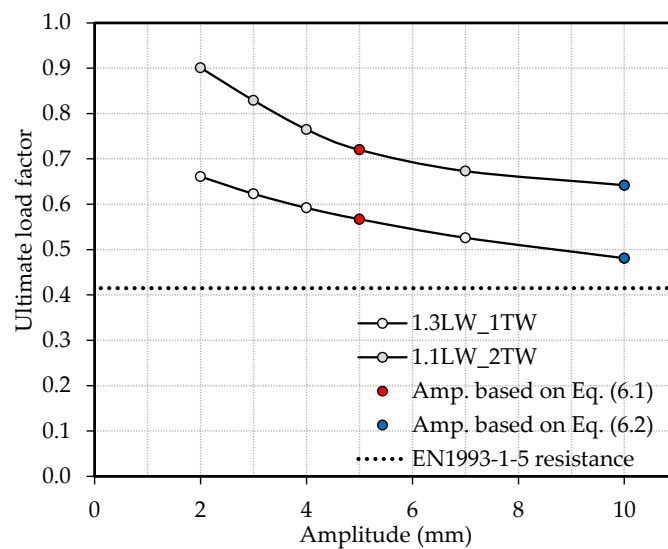


Figure 6.23: Imperfection amplitude *vs.* ultimate load factor for $Z=30$ and $\alpha=1.0$ (imperfection shape 5.5LW_1TW)

Table 6.4: Amplitudes based on Eqs. (6.1) and (6.2) for each buckling shape presented in Figure 6.24 to Figure 6.28 ($Z=50$ and $\alpha=1.0$)

<i>Imperfection's shape</i>	$\Delta w_{0,eq,EN1993-1-5}^{mod}$	$\Delta w_{0,eq,EN1993-1-6}^{mod}$
1.3LW_1TW 	5.00 mm	10.00 mm
1.1LW_2TW 	5.00 mm	10.00 mm
2.2LW_1TW 	2.50 mm	5.00 mm
2.2LW_2TW 	2.50 mm	5.00 mm
3.3LW_2TW 	2.35 mm	4.70 mm
3.5LW_2TW 	3.63 mm	7.23 mm
4.4LW_1TW 	1.78 mm	3.57 mm
4.4LW_2TW 	1.53 mm	3.05 mm
5.5LW_1TW 	1.69 mm	3.39 mm

**Figure 6.24:** Imperfection amplitude vs. ultimate load factor for $Z=50$ and $\alpha=1.0$ (imperfection shapes 1.3LW_1TW and 1.1LW_2TW)

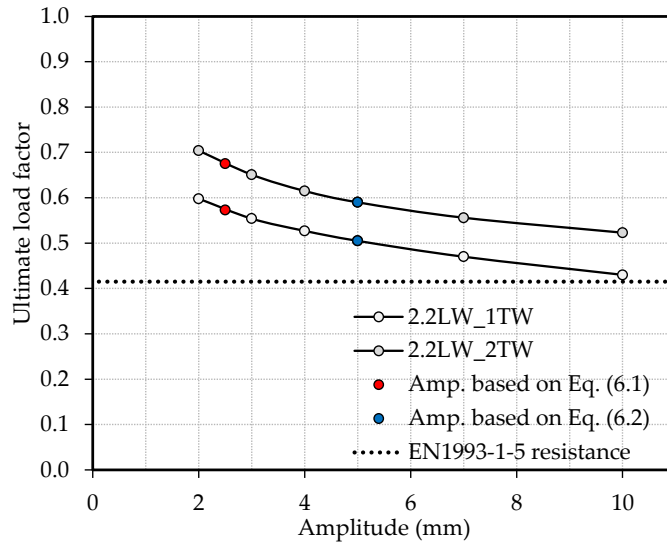


Figure 6.25: Imperfection amplitude *vs.* ultimate load factor for $Z=50$ and $\alpha=1.0$ (imperfection shapes 2.2LW_1TW and 2.2LW_2TW)

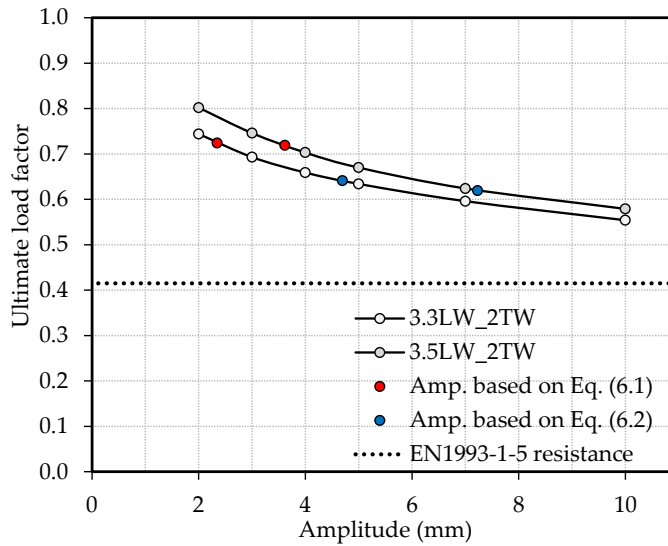


Figure 6.26: Imperfection amplitude *vs.* ultimate load factor for $Z=50$ and $\alpha=1.0$ (imperfection shapes 3.3LW_2TW and 3.5LW_2TW)

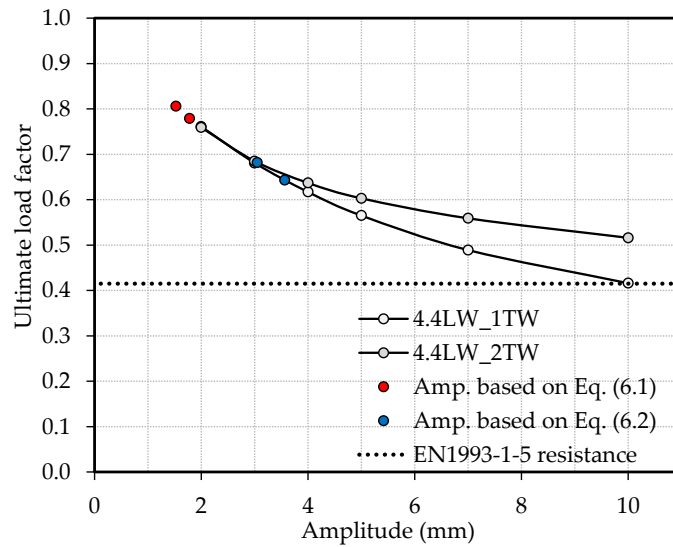


Figure 6.27: Imperfection amplitude *vs.* ultimate load factor for $Z=50$ and $\alpha=1.0$ (imperfection shapes 4.4LW_1TW and 4.4LW_2TW)

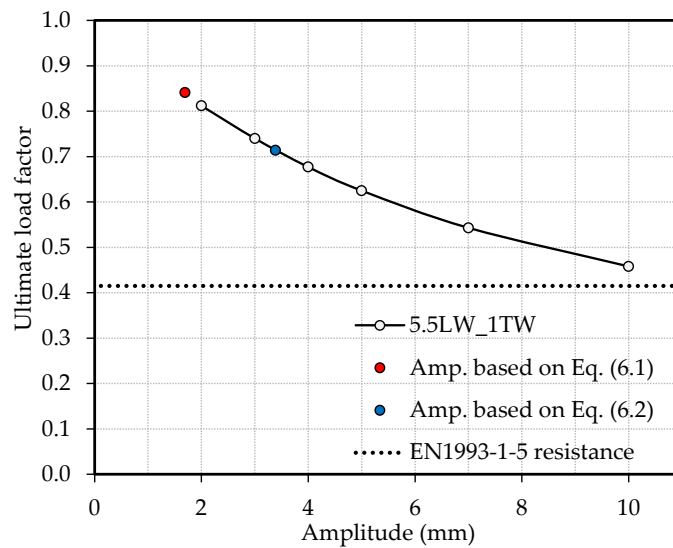
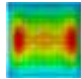
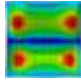
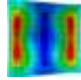
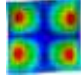
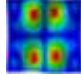
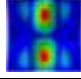


Figure 6.28: Imperfection amplitude *vs.* ultimate load factor for $Z=50$ and $\alpha=1.0$ (imperfection shapes 5.5LW_1TW)

Table 6.5: Amplitudes based on Eqs. (6.1) and (6.2) for each buckling shape presented in Figure 6.29 to Figure 6.31 ($Z=100$ and $\alpha=1.0$)

<i>Imperfection's shape</i>	$\Delta w_{0,eq,EN1993-1-5}^{mod}$	$\Delta w_{0,eq,EN1993-1-6}^{mod}$
1.5LW_1TW 	5.00 mm	10.00 mm
1.3LW_2TW 	5.00 mm	10.00 mm
2.2LW_1TW 	2.50 mm	5.00 mm
2.2LW_2TW 	2.50 mm	5.00 mm
2.2LW_2TW 	2.50 mm	5.00 mm
5.5LW_2TW 	1.86 mm	3.72 mm

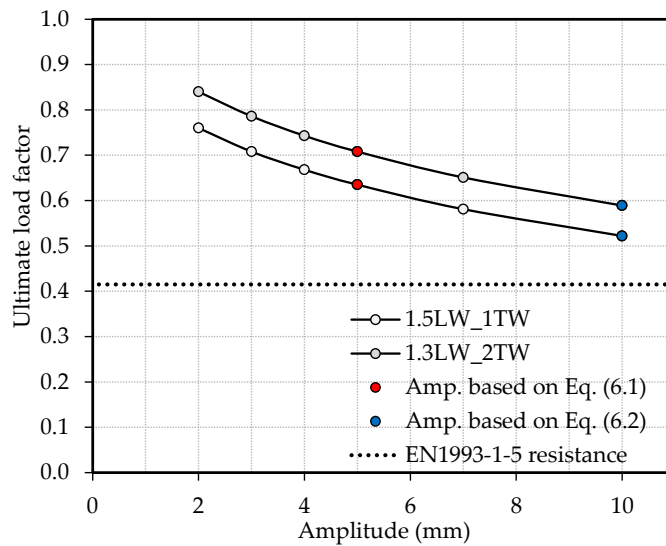


Figure 6.29: Imperfection amplitude vs. ultimate load factor for $Z=100$ and $\alpha=1.0$ (imperfection shapes 1.5LW_1TW and 1.3LW_2TW)

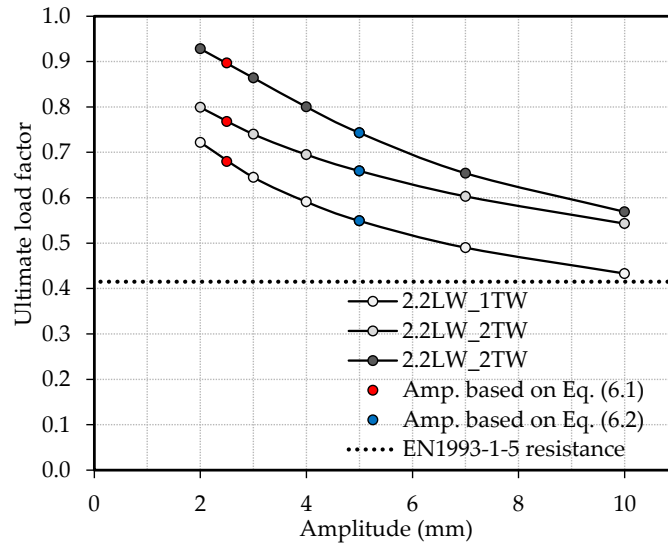


Figure 6.30: Imperfection amplitude *vs.* ultimate load factor for $Z=100$ and $\alpha=1.0$ (imperfection shapes 2.2LW_1TW and 2.2LW_2TW)

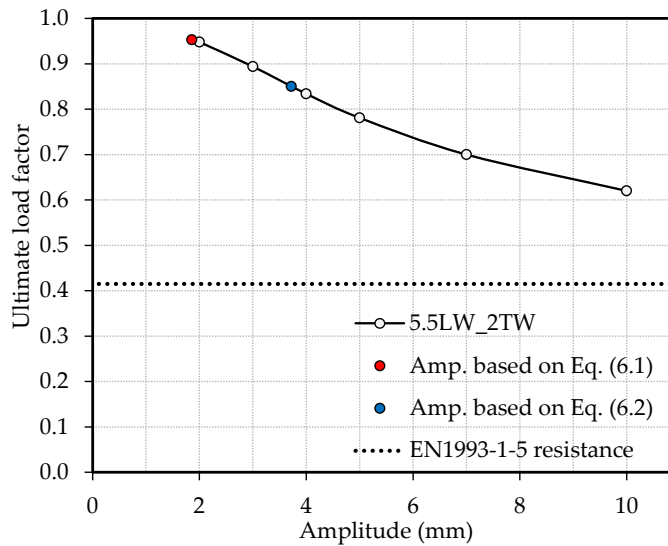


Figure 6.31: Imperfection amplitude *vs.* ultimate load factor for $Z=100$ and $\alpha=1.0$ (imperfection shapes 5.5LW_2TW)

To more strongly support the idea that an increase in the amplitude correspond a decrease in the ultimate load factor, Figure 6.32 shows the average value of the minimum values obtained for all different imperfection shapes and for each aspect ratio.

Another important conclusion is the overall effect of curvature on the ultimate load factor for different values of amplitude. In fact, it is seen that for amplitudes equal to 2 mm the difference between $Z=10$ and $Z=100$ takes the highest value, while for amplitudes equal to 10 mm the difference is the smallest. A better way to express this conclusion is to say that panels with smallest curvature are the least sensitive to geometric imperfection's amplitude; or, by increasing the curvature parameter the ultimate resistance becomes more sensitive to initial imperfection amplitude.

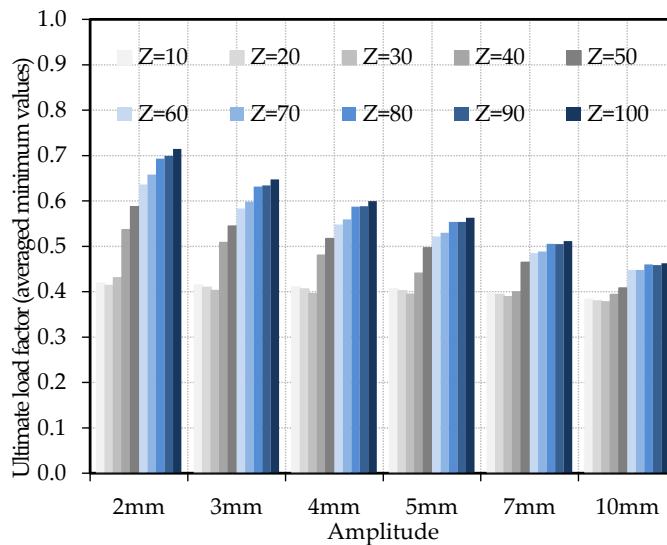


Figure 6.32: General trend of the ultimate load factor with the geometric imperfections' amplitude

6.3.3.2. Influence of the pattern

From every analysis made so far, it is easily accepted that geometric imperfections' pattern is of the utmost importance for the value of the ultimate load factor. This statement is specially sustained by analysing Figure 6.15 to Figure

6.32. Now, the search is for the most unfavourable pattern for geometric imperfections. Figure 6.33 compares the average value of the ultimate load factor for all models with one transverse half-wave and two transverse half-waves (geometric imperfections' amplitude equal to 5 mm). It is concluded that, independently from curvature, shapes with two transverse half-waves tend to higher values of the ultimate load factor.

Concerning the global tendency with respect to the number of longitudinal waves, Figure 6.34 compares the average value of the ultimate load factor for all models with one to five longitudinal half-waves (geometric imperfections' amplitude equal to 5 mm; models with two transverse half-waves were excluded based on the previous conclusion). In this case, it is not possible to claim a general trend independent from the curvature parameter. In fact, for $Z=30$ it is seen that the tendency for the ultimate load factor is decreasing by increasing the number of longitudinal half-waves, while for $Z=60$ the opposite is true (trend lines in Figure 6.34).

Once more, it is highlighted the fact that these conclusions are drawn based on average values for the ultimate load factor, *i.e.* these conclusions should be seen only as general trends and should not be extrapolated blindly to every particular case analysed in the parametric study.

6.3.3.3. Discussion on the order of the buckling mode

The first buckling mode is commonly used as imperfection shape. This is due the belief that, when used as imperfection shape, it will always yield the lowest ultimate load factor (as the first buckling mode is associated to the lowest bifurcation load and, therefore, associated to lowest energy necessary to change the state of equilibrium of a given system). This may be true for some types of structures (*e.g.* unstiffened plated structures), but it may also be an unsafe approach for others. Thus, it is the aim of this section to prove that, for cylindrically curved panels, the option for the first buckling mode may be unsafe.

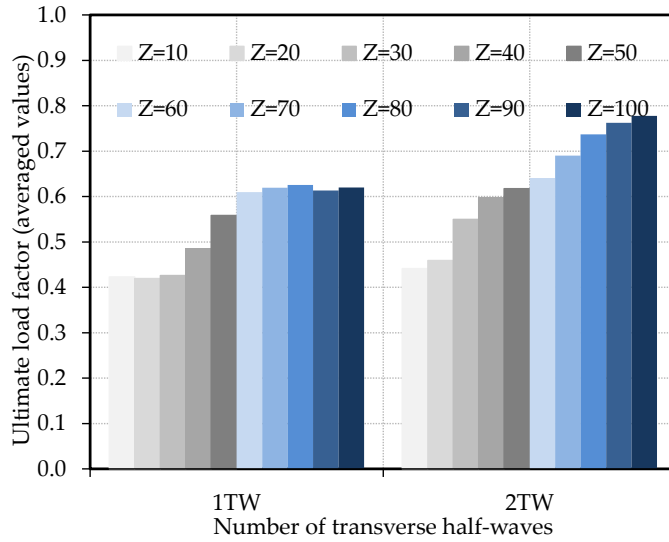


Figure 6.33: General trend of the ultimate load factor with the number of transverse half-waves

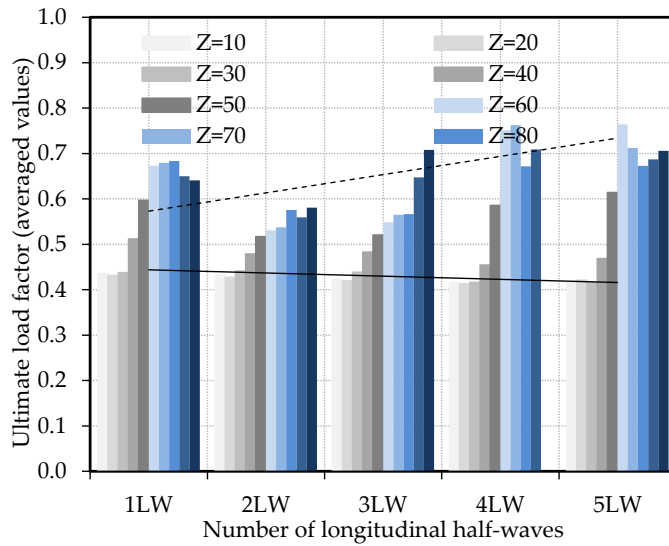


Figure 6.34: General trend of the ultimate load factor with the number of longitudinal half waves

For example, Figure 6.35 shows that for a panel with $Z=30$ and $\alpha=4.8$ the first buckling mode is the one to which the highest value for the ultimate load factor is obtained and the difference to the lowest ultimate load factor (associated to the seventh buckling mode) is 11.6%. This is a representative case of many in the parametric study and, as it will be further in this section, depending on the aspect ratio, the use of the first buckling mode as imperfection shape do not always yield the minimum value of the ultimate load factor.

Figure 6.36 shows the frequency distribution of the ten buckling modes corresponding to minimum values for the ultimate load factor for all panels with different curvature parameters and aspect ratios. The buckling mode that more often corresponds to a minimum value of the ultimate load factor is the second one (34%). The first buckling mode corresponds to a minimum value of the ultimate load factor 30% of the times.

Once more, a general trend can be drawn: the first two buckling modes are those which more likely will return a lowest value of the ultimate load factor (the possibility of getting the lowest value of the ultimate load factor is over 60%).

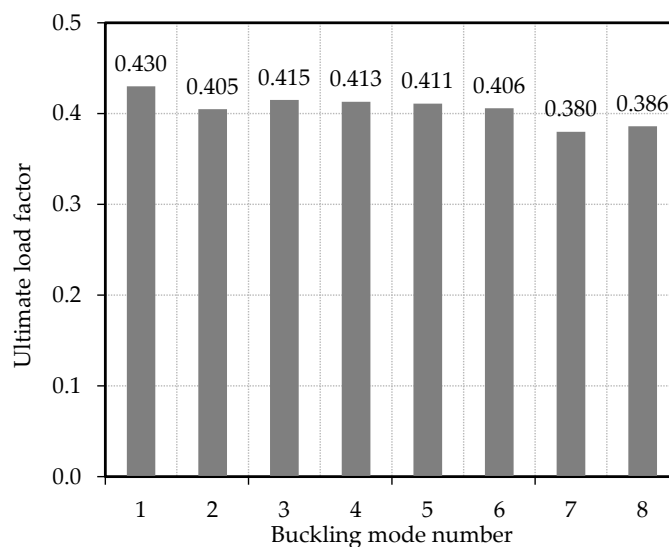


Figure 6.35: Ultimate load factor for a cylindrically curved panel with $Z=30$ and $\alpha=4.8$

However, if the results are divided in different sets of aspect ratio, more refined conclusions may be drawn:

- For short cylindrically curved panels ($\alpha \leq 1$), the first buckling mode most often returns the minimum value of the ultimate load factor (Figure 6.37). Additionally, it is stated that the fourth buckling mode, although not as often as the first one, returns the minimum value ultimate load factor 24 % of the times;
- For long cylindrically curved panels ($1.2 \leq \alpha \leq 5$), the second buckling mode is clearly the one that more times returns the lowest value of the ultimate load factor (Figure 6.38 and Figure 6.39). This is even more clear for cylindrically curved panels with $1.2 < \alpha \leq 2.4$ as it is visible in Figure 6.38.

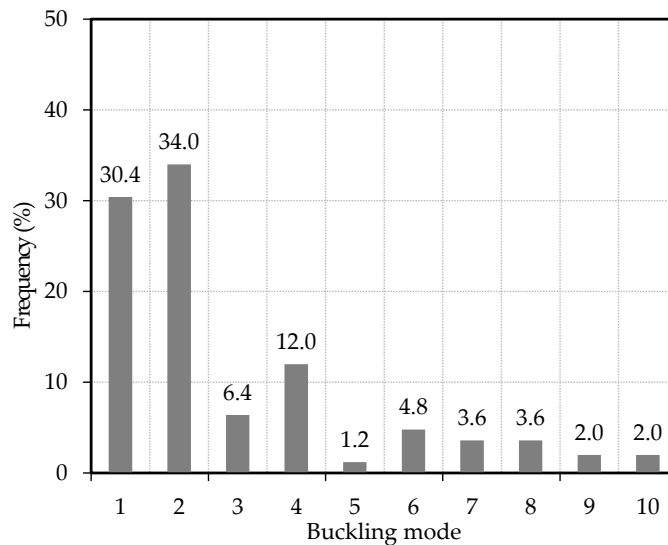


Figure 6.36: Distribution of the frequency of buckling modes corresponding to minimum values for the ultimate load factor (all aspect ratios)

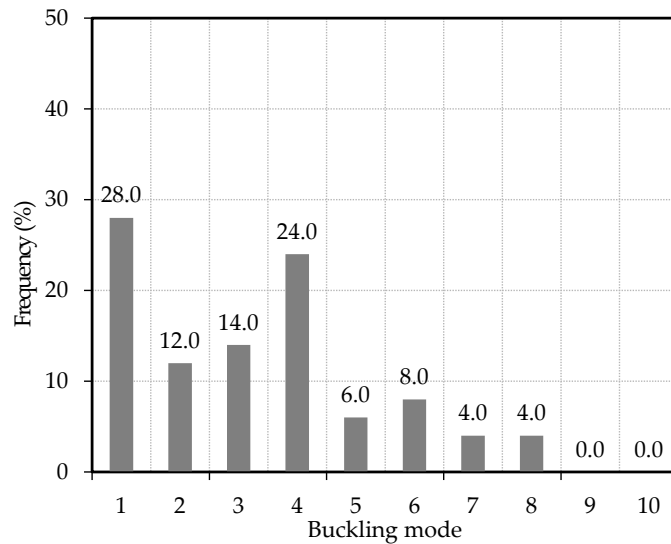


Figure 6.37: Distribution of the frequency of buckling modes corresponding to minimum values for the ultimate load factor (panels with $\alpha \leq 1.0$)

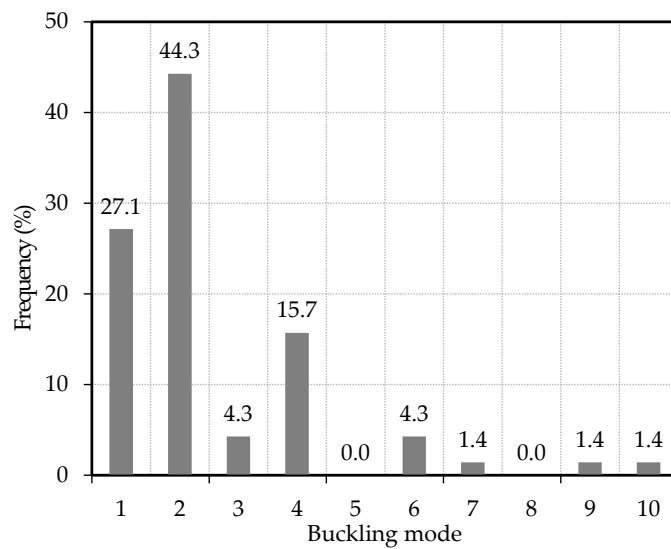


Figure 6.38: Distribution of the frequency of buckling modes corresponding to minimum values for the ultimate load factor (panels with $1.2 \leq \alpha \leq 2.4$)

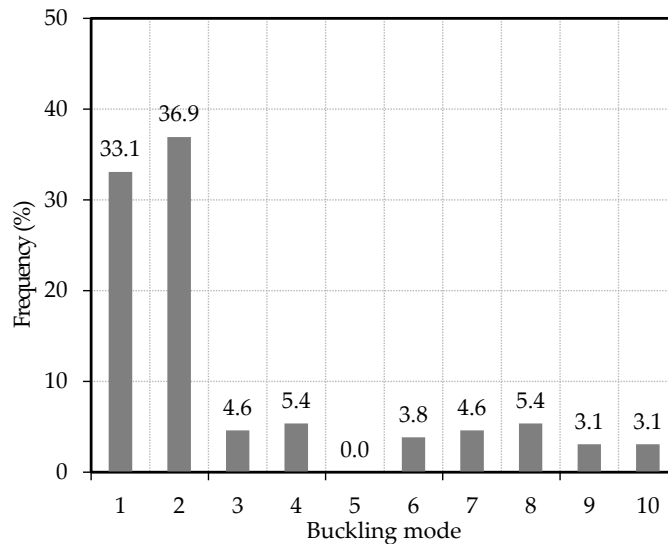


Figure 6.39: Distribution of the frequency of buckling modes corresponding to minimum values for the ultimate load factor (panels with $2.6 \leq \alpha \leq 5.0$)

6.3.3.4. Influence of the b/t ratio

In this section models with b/t ratios equal to 150 and 200 are studied and their results are compared to the results from models with b/t equal to 100. In Figure 6.40 it is seen that, as expected, higher b/t ratios lead to lower values of the ultimate load factor. This is in line with conclusion from previous chapters, namely with Chapter 5 (see sec. 5.3.4) where it can be seen the influence of the slenderness parameter on the resistance of cylindrically curved panels.

It is also pointed out an unexpected outcome: minimum numerical results for the ultimate load factor (for amplitudes based on Eq. (6.1)) decrease between $Z=1$ and $Z=30$ when, based on the results for short cylindrically curved panels, it was expected that they would always increase. This indicates that long cylindrically curved panels characterised by a curvature parameter between these values have a very high sensitivity to geometric imperfections. It also raises the question of which exact combination of Z and b/t is the most sensitive to geometric imperfection and therefore the most unfavourable one. Again, from the analysis of Figure 6.40, it is concluded that independently from the value of b/t , the minimum value of the ultimate load factor is obtained for models with $Z=30$.

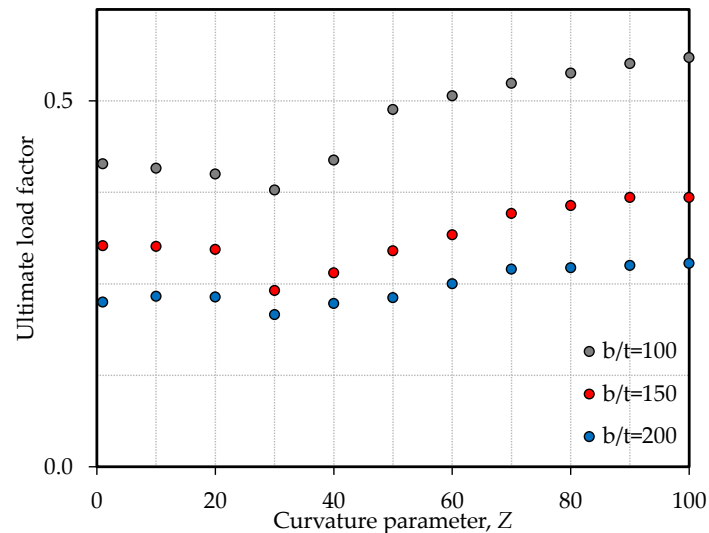


Figure 6.40: Minimum values of the ultimate load factor for models with $b/t=100$, 150 and 200 and maximum amplitude of the imperfection shape based on Eq. (6.1)

6.4. Summary

This chapter focused on the response of imperfect cylindrically curved panels. Specifically, geometric initial imperfections were studied and fundamental characteristics of the behaviour of imperfect cylindrically curved panels were described, namely:

- The postbuckling path is very sensitive to imperfections' amplitude and pattern and it also depends on the curvature parameter and aspect ratio value;
- The postbuckling path presents a less steep linear part for some combinations of shapes (not necessarily based on the first buckling mode) and amplitudes. These combinations of shape and amplitudes yields the lowest value of the ultimate load factor and for that reason are called *worst case scenarios*;
- Generally, the ultimate load factor value decreases with the increase in the imperfection's amplitude (Figure 6.32). However, there are cases where this is not true and where higher amplitude corresponds to higher ultimate load factors (Figure 6.15 and Figure 6.19 for example);

- Additionally, the smaller the curvature the less sensitive to the imperfection's amplitude cylindrically curved panels are, *i.e.* by increasing the curvature parameter the ultimate resistance becomes more sensitive to initial imperfection amplitude.
- Imperfection shapes with one transverse half-wave has generally a lower ultimate load factor than cylindrically curved panels with imperfection's shapes with two transverse half-waves (Figure 6.33);
- On the other hand, no global trend is possible to establish in what concerns the evolution of the ultimate load factor with the number of longitudinal half-waves. In fact, Figure 6.34 shows that for $Z=30$ the trend has a positive slope, while for $Z=60$ has a negative slope;
- The first buckling mode used as imperfection shape does not return always the lowest value for the ultimate load factor. In fact, within the limits of the parametric study the first buckling mode returns the lowest value for the ultimate load factor only for 30% of the times, while the second returns for 34% of the times (Figure 6.36);
- If the parametric study is divided into three different ranges of aspect ratio, it is concluded that imperfection shapes simulating the first buckling mode yield more often the lowest value of the ultimate load factor for short cylindrically curved panels (*i.e.* $\alpha \leq 1$); for panels with $1.2 \leq \alpha \leq 2.4$ and $2.6 \leq \alpha \leq 5$ the second buckling mode is the one that most often returns the lowest value of the ultimate load factor (see Figure 6.37, Figure 6.38 and Figure 6.39);
- The highest sensitivity to geometric imperfections (amplitude and pattern) is obtained for long cylindrically curved panels characterised by a curvature parameter, Z , around 30 (Figure 6.40).

Additionally, the definition of criteria for admitting a buckling mode as a "realistic" pattern for geometric imperfections for local buckling assessment is proposed (assuming uniaxial compressive stresses):

- Buckling modes with longitudinal half-wave lengths lower than $\min(a/4; 2.b/3)$ are considered unrealistic and

- Buckling modes with transverse half-wave lengths lower than $b/2$ are considered unrealistic.

It is also concluded that current standards do not cover accurately enough the problematic of geometric imperfections in what concerns cylindrically curved panels. In fact, it was proven that cylindrically curved panels are highly sensitive to initial geometric imperfections and, on top of that, the difference of using amplitudes given by EN1993-1-5:2006 (CEN, 2006) for plates and given by EN1993-1-6:2007 (CEN, 2007) for shells of revolution is significant. In order to fill the void in European standards Eqs. (6.1) and (6.2) are proposed for computing the amplitude of imperfections.

7. Energy based analytical model of cylindrically curved panels

7.1. Chapter overview

This chapter covers all analytical studies performed within the goals of this thesis. Specifically, the analytical tools used were the formulation of the total potential energy function of cylindrically curved panels under pure compressive stresses.

In sec. 7.2 the energy formulation is described from a general point of view. General assumptions are enunciated, the degrees-of-freedom and the displacement functions are defined and, finally, from the strain-displacement relations the strain energy and the potential energy are derived.

In sec. 7.3 the energy formulation derived in sec. 7.2 is used to obtain, whenever feasible, simple expressions or, otherwise, values of the elastic critical stress of cylindrically curved panels under pure compressive stresses for boundary conditions type 2 and 3. A discussion on the number of degrees-of-freedom necessary to obtain good results is also started. The analytical results are compared to numerical results gathered from the first parametric study in Chapter 5.

Finally, a short summary is performed at the end of this chapter where the most relevant contributions are listed and addressed in a concise way.

7.2. Energy formulation

7.2.1. General

The semi-analytical study presented herein is based on a previous study by Thompson & Hunt (1984), and later followed by Simões da Silva (1988) to introduce his work on modal interactions in sandwich plates, and where the effect of initial curvature is added at the strain-displacement relations level. Fundamentally, the approach followed by Simões da Silva (1988) ignores the transverse and shear membrane stresses. From a physical point of view, this assumption means that the panel is seen as an infinite group of infinitely thin strips unable to transfer shear and/or membrane stresses to each other, but acting together during the deformation imposed by the external applied loads. Although this is a rather crude assumption, this energy formulation is still able to incorporate the main features of the plate's buckling and postbuckling behaviour (Simões da Silva, 1988).

However, in this chapter, this simplification is dropped making the panel able to transfer shear and membrane stresses in both directions. It should be mentioned that while for flat panels accounting for nonlinear terms in the y -direction does not play any role in obtaining the elastic critical stress, the same is not true for curved panels, where the consideration for these extra nonlinear terms is crucial to obtain accurate results for both the elastic critical stress and the postbuckling path.

7.2.2. Degrees-of-freedom and boundary conditions

The cylindrically curved panel studied in this section is simply supported along all edges with longitudinal edges unconstrained and constrained (boundary conditions type 2 and 3, see Chapter 4) and it is under pure axial compression. In order to build an energy formulation of such a panel, three generic degrees-of-freedom (a_1 , $a_{2,i}$ and $a_{3,i}$) corresponding to the three principal directions (x , y , and z) are considered (Figure 7.1).

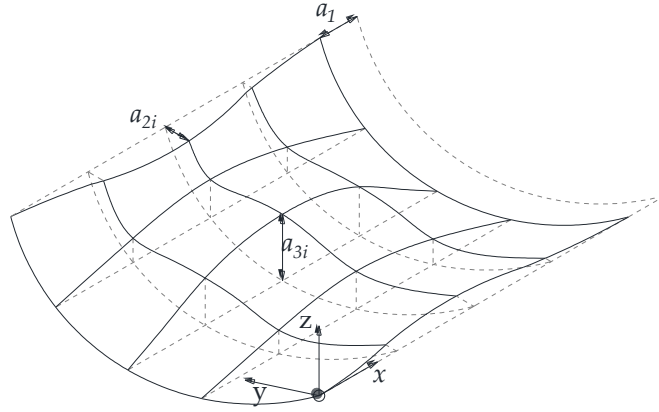


Figure 7.1: Degrees-of-freedom considered in the analysis

The degree-of-freedom in x -direction, a_1 , consists of the end-shortening of the panel (pre- and postbuckling path) and it is assumed to be constant along the width, corresponding to a constrained loaded edge and it is associated with the following displacement field

$$u(x, y) = a_1 x \quad (7.1)$$

In the y -direction, for boundary conditions type 2, the following function was assumed

$$v(x, y) = a_{2,1} \cos\left(\frac{\pi y}{b}\right) + a_{2,2} \left[1 - \sin\left(\frac{\pi x}{a}\right)\right] \cos\left(\frac{\pi y}{b}\right) \quad (7.2)$$

This displacement function has two terms: the first reflects the sinusoidal displacement along the width and the second is required to model the displacement of unconstrained edges along their length. For boundary conditions type 3, the displacement function is obtained from Eq. (7.2) dropping the second term (*i.e.*, $a_{2,2}=0$).

At last, the degree-of-freedom in the z -direction describes the out-of-plane displacement of the panel during buckling. This out-of-plane displacement is assumed to adopt a similar shape to a plate, *i.e.* a sinusoidal shape with one

half-wave across the width and a number i of longitudinal across the length, given by

$$w(x, y) = \sum_{i=1} a_{3,i} \sin\left(\frac{i\pi x}{a}\right) \sin\left(\frac{\pi y}{b}\right) \quad (7.3)$$

7.2.3. Strain-displacement relations and strain energy expressions

The strain-displacement relations are derived directly from the nonlinear shallow shell theory presented in sec. 2.5. This means that when the shallowness of the cylindrically curved panels starts to disappear (*i.e.* the conditions expressed by Eqs. (2.33) and (2.34) are no longer verified), the curved panel geometry will differ noticeably from the plane geometry, *i.e.*, the very basic assumption of the shallow shell theory will become less and less accurate leading to more and more non-negligible errors.

The strain-displacement relations are obtained from Eqs. (2.57) to (2.62) substituting R_x by ∞ and R_y by R . Additionally, since the nonlinear terms in the y -direction are taken into consideration, it is necessary to account also for an extra term in the transverse direction which is originated by the Poisson's effect.

$$\varepsilon_{x,0} = \frac{\partial u}{\partial x} - \frac{1}{2} \left(-\frac{\partial w}{\partial x} \right)^2 \quad (7.4)$$

$$\varepsilon_{y,0} = -\nu \frac{\partial u}{\partial x} + \frac{\partial v}{\partial y} + \frac{w}{R} - \frac{1}{2} \left(-\frac{\partial w}{\partial y} \right)^2 \quad (7.5)$$

$$\gamma_{xy,0} = \frac{\partial v}{\partial x} + \frac{\partial u}{\partial y} + \frac{\partial w}{\partial x} \frac{\partial w}{\partial y} \quad (7.6)$$

$$\chi_x = -\frac{\partial^2 w}{\partial x^2} \quad (7.7)$$

$$\chi_y = -\frac{\partial^2 w}{\partial y^2} \quad (7.8)$$

$$\chi_{xy} = -\frac{\partial^2 w}{\partial x \partial y} \quad (7.9)$$

The strain energy expression for this system is obtained substituting Eqs.(7.4) to (7.9) into Eqs. (2.75) and (2.76) yielding two expressions: one representing the membrane strain energy and another representing the bending strain energy.

7.2.4. Potential energy function and passive degree-of-freedom elimination

The total potential function, Eq. (7.10), is obtained by adding to the two components of the strain energy and the work done by the line load P , Eq. (7.11)

$$V = U_m + U_b - W \quad (7.10)$$

$$W = P \int_0^a \int_0^b \frac{\partial u}{\partial x} dx dy = a_1 P ab \quad (7.11)$$

The degree-of-freedom associated with the total end-shortening can be eliminated from further consideration by using the corresponding equilibrium equation and solving it with respect to a_1

$$\frac{\partial V}{\partial a_1} = 0 \quad (7.12)$$

Replacing the result back into Eq. (7.10) gives an expression for the total potential energy of the curved panel function to $a_{2,i}$ and $a_{3,i}$.²²

7.3. Elastic critical stress

7.3.1. General procedure to obtain the elastic critical stress

The elastic critical stress is obtained by setting to zero the determinant of the matrix formed by the quadratic terms with respect to each of the $a_{2,i}$ and $a_{3,i}$, of

²² The expressions which result from the application of the steps now described are very long and complex. For that reason, they are not shown in this work. Nevertheless, to the readers seeking deeper understanding of the developed formulation, two examples using the developed Mathematica (Wolfram, 2010) code are given in annex A.

the total potential energy function written in general form and evaluated on the fundamental path, and solve the resulting expression in order to P .

$$|V_{aj,i}| = 0 \quad \text{with } j = 2,3 \text{ and } i = 1, \dots, 10 \quad (7.13)$$

In the next sub-sections, some examples in which the elastic critical stress of cylindrically curved panels are obtained are shown.

7.3.2. Boundary conditions type 3 and 3 degrees-of-freedom

In the case of an energy formulation for a cylindrically curved panel with boundary conditions type 3 and with 3 degrees-of-freedom the displacement functions are as follows

$$u(x, y) = a_1 x \quad (7.14)$$

$$v(x, y) = a_{2,1} \cos\left(\frac{\pi y}{b}\right) \quad (7.15)$$

$$w(x, y) = a_{3,1} \sin\left(\frac{m\pi x}{a}\right) \sin\left(\frac{\pi y}{b}\right) \quad (7.16)$$

It should be noted that, in Eq. (7.16) the letter m is added to the argument of the first sine function. This indicates that, although only one degree-of-freedom is considered for the function displacement in z -direction, several longitudinal half-waves may be considered. Therefore, in Eq. (7.16) m represents the number of longitudinal half-waves.

In these conditions the expression of the quadratic terms of the total potential energy written in general form evaluated on the fundamental path is given by

$$V_2 = \frac{1}{2} V_{a_{2,1}^2} + \frac{1}{2} V_{a_{3,1}^2} + V_{a_{2,1} \cdot a_{3,1}} \quad (7.17)$$

$$V_{a_{2,1}^2} = \frac{a\pi^2 E}{2(1-\nu^2)} \frac{t}{b} \quad (7.18)$$

$$V_{a_{3,1}^2} = -\frac{\pi^2 b}{4a} m^2 P + \frac{(a^2 + m^2 b^2)^2 \pi^4 E}{48a^3 (1-\nu^2)} \left(\frac{t}{b}\right)^3 + \frac{a E}{4(1-\nu^2)} \left(\frac{t}{b}\right)^3 Z^2 \quad (7.19)$$

$$V_{a_{2,1}.a_{3,1}} = \frac{(-1 + (-1)^m)}{m} \frac{a E}{2(1-\nu^2)} \left(\frac{t}{b}\right)^2 Z \quad (7.20)$$

The determinant which allows obtaining the elastic critical stress is

$$\begin{vmatrix} V_{a_{2,1}} & V_{a_{2,1}.a_{3,1}} \\ V_{a_{2,1}.a_{3,1}} & V_{a_{3,1}} \end{vmatrix} = 0 \quad (7.21)$$

Solving this equation with respect to P and then dividing the solution by t gives an expression for the elastic critical stress of a cylindrically curved panel with boundary conditions type 3

$$\sigma_{cr} = \frac{\pi^2 E}{12(1-\nu^2)} \left(\frac{t}{b}\right)^2 \left[\frac{(a^2 + m^2 b^2)^2}{a^2 b^2 m^2} + \frac{12m^2 \pi^2 - 24(1 - (-1)^m)^2}{\pi^6 m^4} \left(\frac{a}{b}\right)^2 Z^2 \right] \quad (7.22)$$

It is easy to conclude that the first term of Eq. (7.22) is the classical expression for the elastic critical stress of plates. The second term is the additional contribution given by curvature.

This expression is deduced based on a simplified displacement function for the out-of-plane direction. In fact, it is easy to conclude that Eq. (7.16) is not suitable to describe eigenmodes like those in Figure 5.10. Therefore, the presented expression is only valid in those cases where Eq. (7.16) accurately describes the out-of-plane displacements at the critical point (*e.g.* those in Figure 5.12). Figure 7.2 to Figure 7.6 show the accuracy of the above deduced expression by comparing it to numerically obtained buckling coefficients.

It is seen that for low values of the curvature parameter ($Z \leq 5$), it is reasonable to use Eq. (7.22) to compute the elastic critical stress of a cylindrically curved panel under pure compression with boundary conditions type 3. For higher values of the curvature parameter, it is seen that only by setting $m=1$ (buckling mode with one longitudinal half-wave) and for low values of aspect ratio (short panels) it is possible to obtain reasonable values for the elastic critical stress.

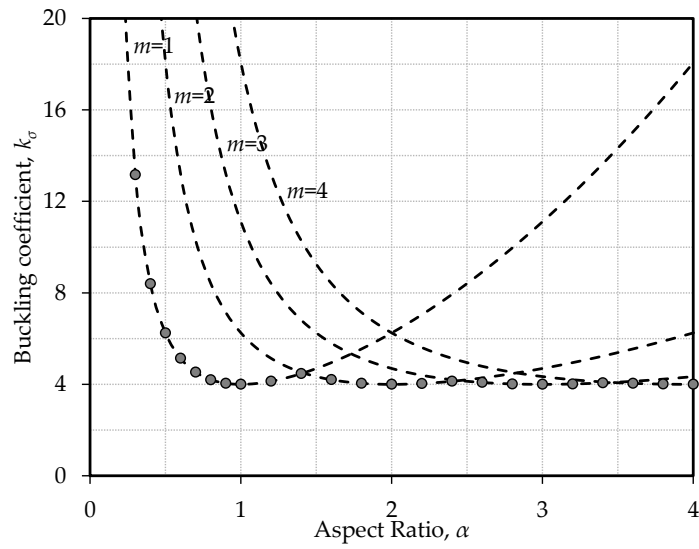


Figure 7.2: Comparison between numerical results of elastic critical stress and Eq. (7.22) for $Z=0$ and BC3

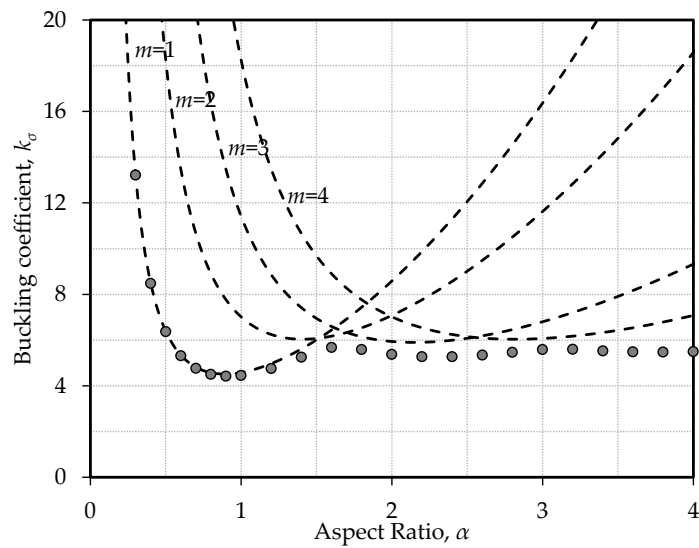


Figure 7.3: Comparison between numerical results of elastic critical stress and Eq. (7.22) for $Z=5$ and BC3

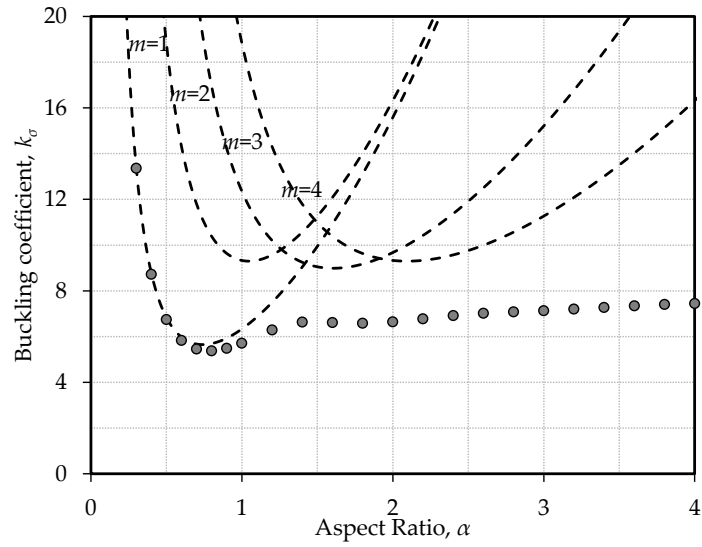


Figure 7.4: Comparison between numerical results of elastic critical stress and Eq. (7.22) for $Z=10$ and BC3

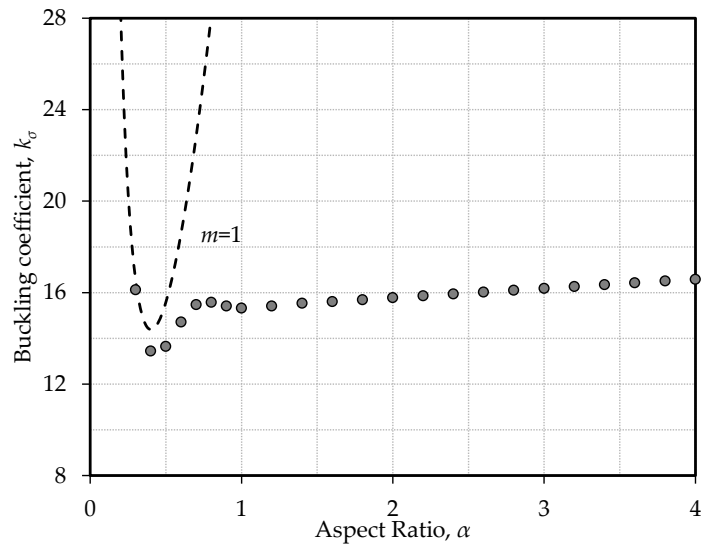


Figure 7.5: Comparison between numerical results of elastic critical stress and Eq. (7.22) for $Z=40$ and BC3

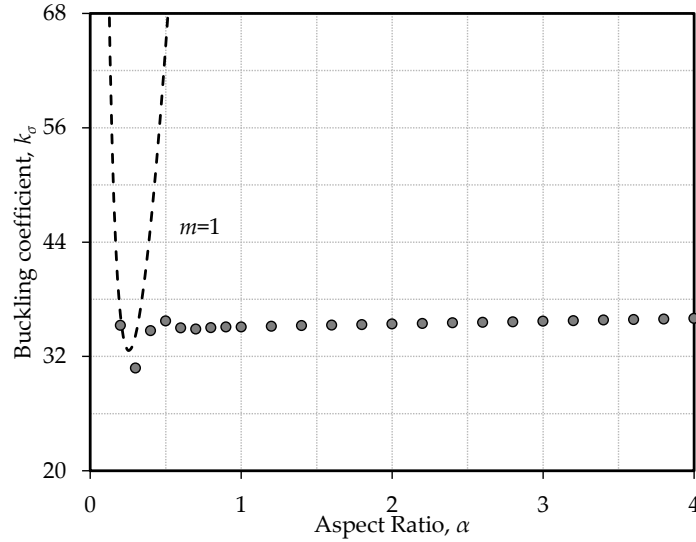


Figure 7.6: Comparison between numerical results of elastic critical stress and Eq. (7.22) for $Z=100$ and BC3

Thus, after some reworking, a simplified version of Eq. (7.22) where $m=1$ is presented

$$\sigma_{cr,m=1} = \frac{\pi^2 E}{12(1-\nu^2)} \left(\frac{t}{b}\right)^2 \left[\frac{(a^2 + b^2)^2}{a^2 b^2} + \frac{12(\pi^2 - 8)}{\pi^6} \left(\frac{a}{b}\right)^2 Z^2 \right] \quad (7.23)$$

Additionally, further simplification can be made by minimising the second factor of Eq. (7.23) (which represents the elastic buckling coefficient) with respect to aspect ratio ($\alpha=a/b$)

$$\sigma_{cr,\min} = \frac{\pi^2 E}{6(1-\nu^2)} \left(\frac{t}{b}\right)^2 \left[1 + \frac{\sqrt{\pi^6 + 12(\pi^2 - 8) Z^2}}{\pi^3} \right] \quad (7.24)$$

Finally, from Eq. (7.24) it is possible to isolate the elastic buckling coefficient, resulting in an expression to compute minimum values of the elastic buckling coefficient of short cylindrically curved panels under pure compression with boundary conditions type 3

$$k_{\sigma, \min} = 2 \left[1 + \frac{\sqrt{\pi^6 + 12(\pi^2 - 8) Z^2}}{\pi^3} \right] \quad (7.25)$$

Figure 7.7 compares numerically obtained minimum values for the elastic buckling coefficient with Eq. (7.25). As also patent in Figure 7.2 to Figure 7.6 the biggest differences are found for high values of the curvature parameter, where the biggest difference is 6.96% obtained for $Z=80$.

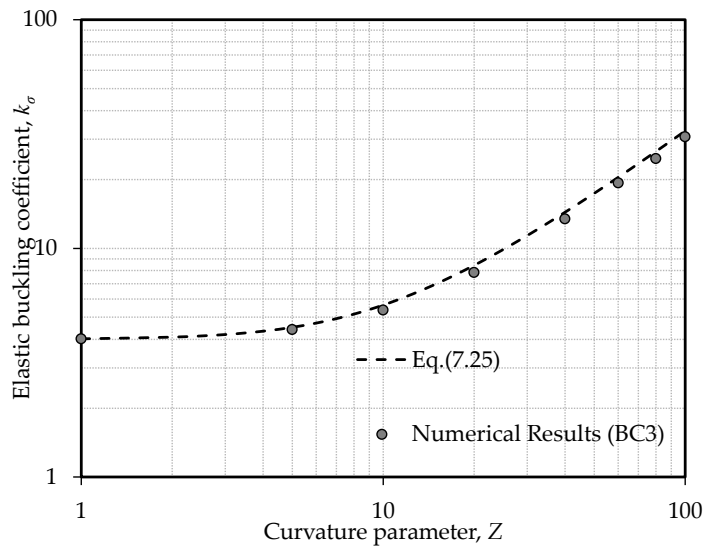


Figure 7.7: Comparison between numerical results of elastic critical stress and Eq. (7.25) for BC3

7.3.3. Boundary conditions type 2 and 4 degrees-of-freedom

Similarly to the previous section, the energy formulation for a cylindrically curved panel with boundary conditions type 2 is now deduced. In this case an extra degree-of-freedom is required. This extra degree-of-freedom allows the consideration of nonhomogeneous transverse displacements along the length of the panel, *i.e.* it allows the consideration of unconstrained longitudinal edges. Thus, the energy formulation presented in this subsection has 4 degrees-of-freedom and the displacements functions are given by Eq. (7.26) to Eq. (7.28).

$$u(x, y) = a_1 x \quad (7.26)$$

$$v(x, y) = a_{2,1} \cos\left(\frac{\pi y}{b}\right) + a_{2,2} \left[1 - \sin\left(\frac{\pi x}{a}\right)\right] \cos\left(\frac{\pi y}{b}\right) \quad (7.27)$$

$$w(x, y) = a_{3,1} \sin\left(\frac{\pi x}{a}\right) \sin\left(\frac{\pi y}{b}\right) \quad (7.28)$$

Here, following the conclusions of the previous subsection on the number of longitudinal half-waves, the out-of-plane displacement function is simplified setting $m=1$. In these conditions the expression of the quadratic terms of the total potential energy written in general form evaluated on the fundamental path is given by

$$V_2 = \frac{1}{2} V_{a_{2,1}^2} + \frac{1}{2} V_{a_{2,2}^2} + \frac{1}{2} V_{a_{3,1}^2} + V_{a_{2,1} \cdot a_{2,2}} + V_{a_{2,1} \cdot a_{3,1}} + V_{a_{2,2} \cdot a_{3,1}} \quad (7.29)$$

$$V_{a_{2,1}^2} = \frac{a \pi^2 E}{2(1-\nu^2)} \frac{t}{b} \quad (7.30)$$

$$V_{a_{2,2}^2} = \frac{\pi E}{8 a (1-\nu^2)} \frac{t}{b} [a^2 (16 - 6\pi) + b^2 \pi (1 - \nu^2)] \quad (7.31)$$

$$V_{a_{3,1}^2} = -\frac{\pi^2 b}{4 a} P + \frac{(a^2 + b^2)^2 \pi^4 E}{48 a^3 (1-\nu^2)} \left(\frac{t}{b}\right)^3 + \frac{a E}{4(1-\nu^2)} \left(\frac{t}{b}\right)^3 Z^2 \quad (7.32)$$

$$V_{a_{2,1} \cdot a_{2,2}} = \frac{a \pi E}{2(1-\nu^2)} \frac{t}{b} (\pi - 2) \quad (7.33)$$

$$V_{a_{2,1} \cdot a_{3,1}} = \frac{a E}{(1-\nu^2)} \left(\frac{t}{b}\right)^2 Z \quad (7.34)$$

$$V_{a_{2,2} \cdot a_{3,1}} = \frac{a E}{4(1-\nu^2)} \left(\frac{t}{b}\right)^2 Z (\pi + 4) \quad (7.35)$$

The determinant which allows obtaining the elastic critical stress is

$$\begin{vmatrix} V_{a_{2,1}^2} & V_{a_{2,1} \cdot a_{2,2}} & V_{a_{2,1} \cdot a_{3,1}} \\ V_{a_{2,1} \cdot a_{2,2}} & V_{a_{2,2}^2} & V_{a_{2,2} \cdot a_{3,1}} \\ V_{a_{2,1} \cdot a_{3,1}} & V_{a_{2,2} \cdot a_{3,1}} & V_{a_{3,1}^2} \end{vmatrix} = 0 \quad (7.36)$$

Solving this equation with respect to P and then dividing the solution by t gives, after some reworking, an expression for the elastic critical stress of a cylindrically curved panel with boundary conditions type 2

$$\sigma_{cr,m=1} = \frac{\pi^2 E}{12(1-\nu^2)} \left(\frac{t}{b}\right)^2 \left[\frac{(a^2 + b^2)^2}{a^2 b^2} + \frac{12a^2(1-\nu)(\pi^2 - 8)}{\pi^6 b^2(1-\nu) + 2a^2 \pi^4 (\pi^2 - 8)} Z^2 \right] \quad (7.37)$$

Again, the first term of Eq. (7.37) is the classical expression for the elastic critical stress of plates and the second term is the additional contribution given by curvature. Figure 7.8 to Figure 7.12 show the accuracy of the above deduced expression by comparing it with numerically obtained buckling coefficients (this comparison is made for minimum values of both analytical and numerical results).

Additionally, in opposition to Eq. (7.23), obtaining a simplified expression from Eq. (7.37) for minimum values of the elastic critical stress is much more complex. Nevertheless, it is possible to compute those values (see examples in annex A) and compare them to numerical ones (Figure 7.13). The biggest difference is 6.08% obtained for $Z=20$.

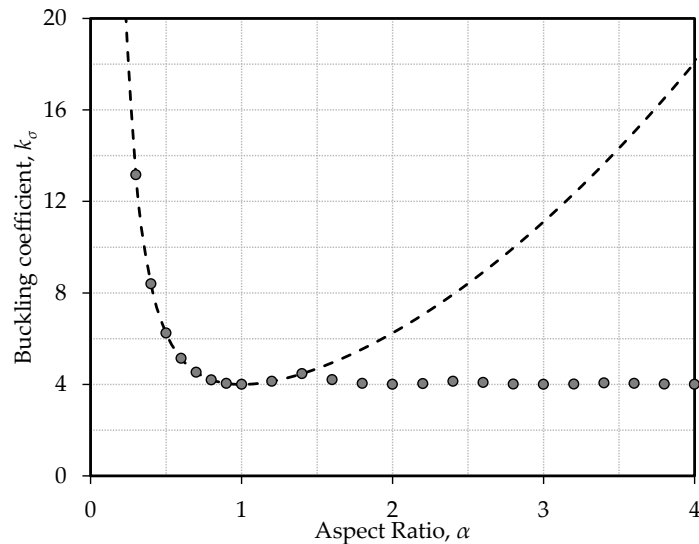


Figure 7.8: Comparison between numerical results of elastic critical stress and Eq. (7.37) for $Z=0$ and BC2

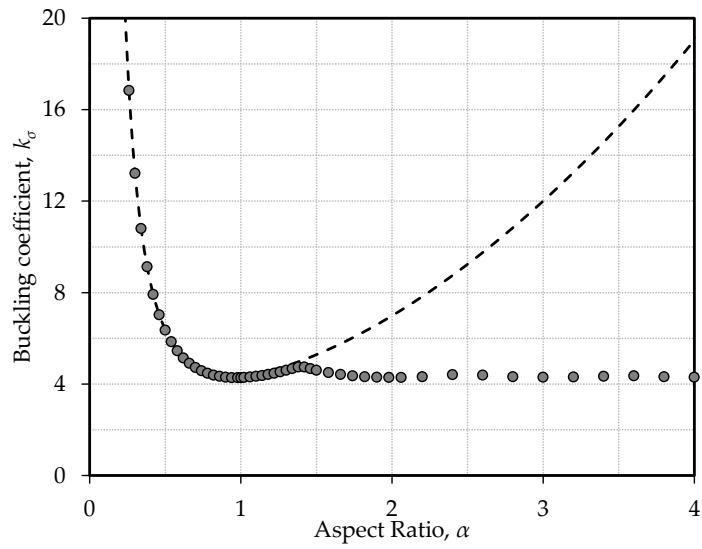


Figure 7.9: Comparison between numerical results of elastic critical stress and Eq. (7.37) for $Z=5$ and BC2

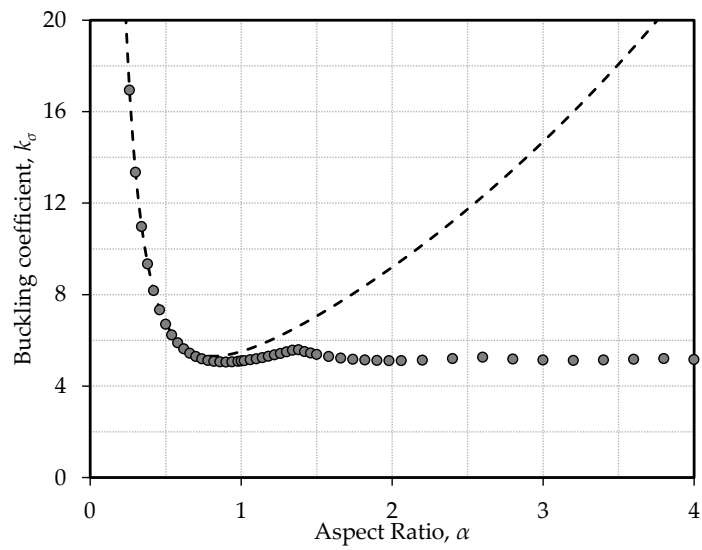


Figure 7.10: Comparison between numerical results of elastic critical stress and Eq. (7.37) for $Z=10$ and BC2

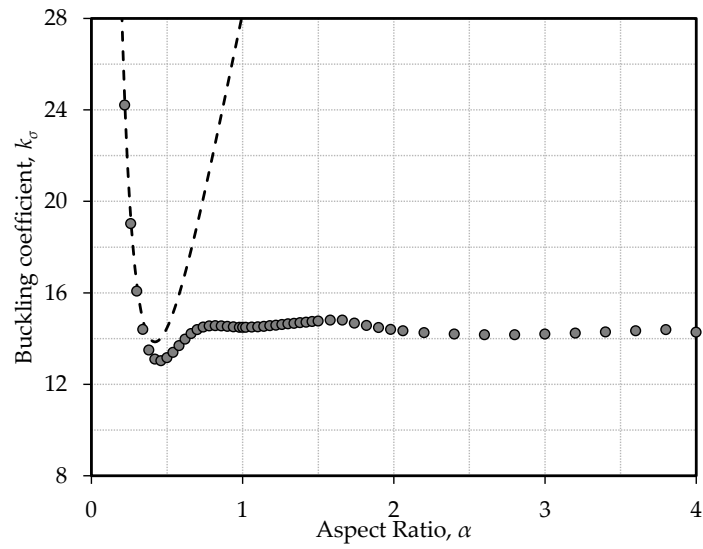


Figure 7.11: Comparison between numerical results of elastic critical stress and Eq. (7.37) for $Z=40$ and BC2

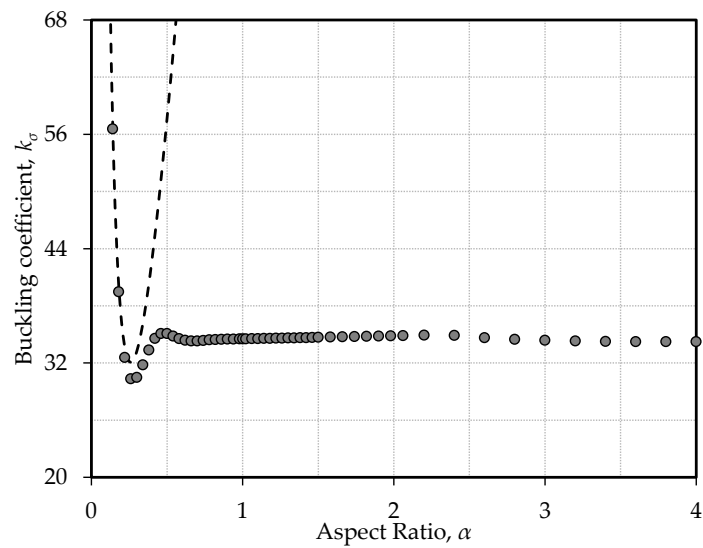


Figure 7.12: Comparison between numerical results of elastic critical stress and Eq. (7.37) for $Z=100$ and BC2

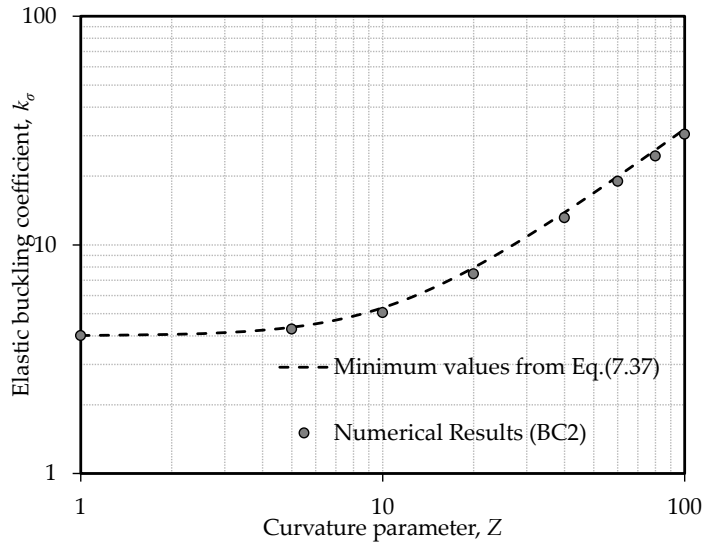


Figure 7.13: Comparison between numerical results of elastic critical stress and analytical results obtained from minimising Eq. (7.37) with respect to the aspect ratio for BC2

7.3.4. Boundary conditions type 3 and 5, 7 and 9 degrees-of-freedom

As it was concluded in sec. 7.3.2, an energy formulation with only three degrees-of-freedom is not able capture the elastic critical stress of curved panels for a wide range of aspect ratio values. This is due to the fact that, as previously mentioned, the consideration of only one degree-of-freedom in the out-of-plane displacement function is not sufficient to describe accurately more complex shapes (Figure 5.10). Therefore, in this section, the effect of introducing extra degrees-of-freedom at the out-of-plane displacement function level is studied. Since the complexity of the energy formulation grows with the number of degrees-of-freedom, the expressions are not shown (the reader is invited to consult the examples in annex A for deeper information). It was found that, even with seven degree-of-freedom in the out-of-plane displacement function, the elastic critical stress of cylindrically curved panels with high values curvature and aspect ratio is not accurately obtained (Figure 7.17 and Figure 7.18). In contrast, for low values of curvature, agreement between numerical results and analytical results is satisfactory (Figure 7.14 to Figure 7.16).

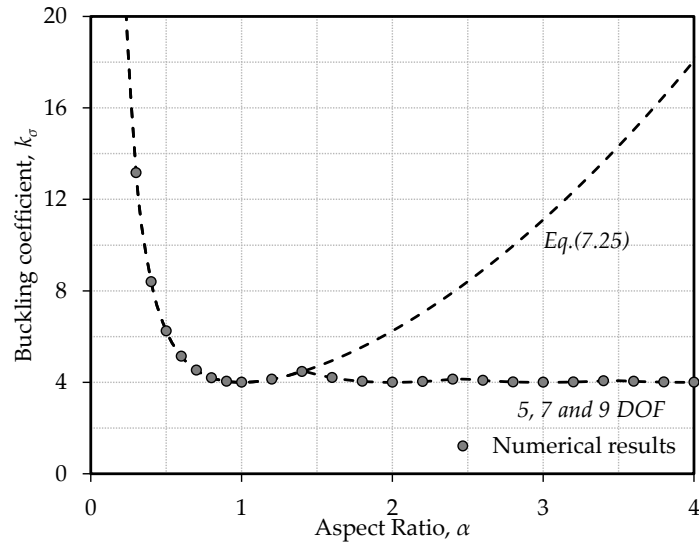


Figure 7.14: Comparison between numerical results of elastic critical stress and analytical results from energy formulations with extra degrees-of-freedom for $Z=0$ and BC3

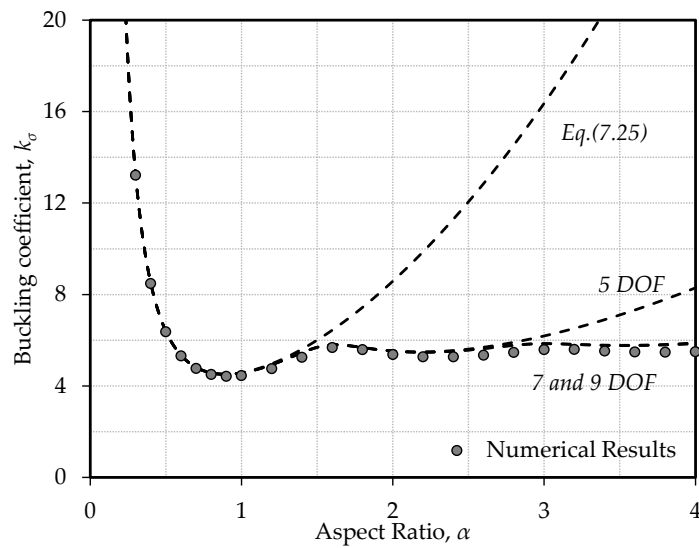


Figure 7.15: Comparison between numerical results of elastic critical stress and analytical results from energy formulations with extra degrees-of-freedom for $Z=5$ and BC3

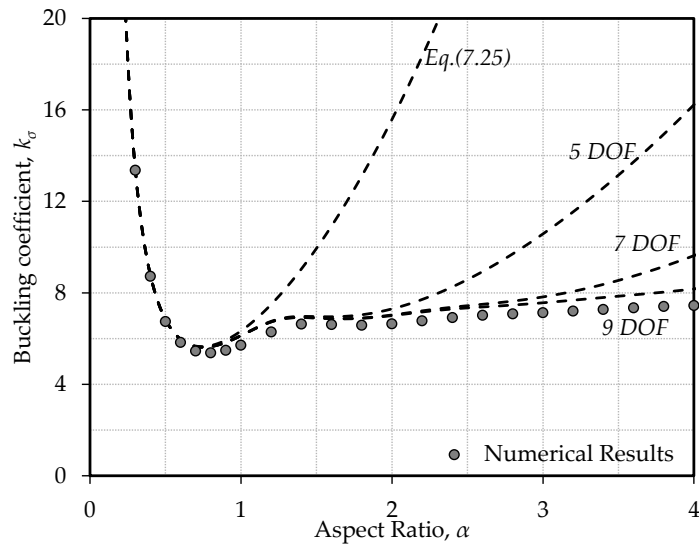


Figure 7.16: Comparison between numerical results of elastic critical stress and analytical results from energy formulations with extra degrees-of-freedom for $Z=10$ and BC3

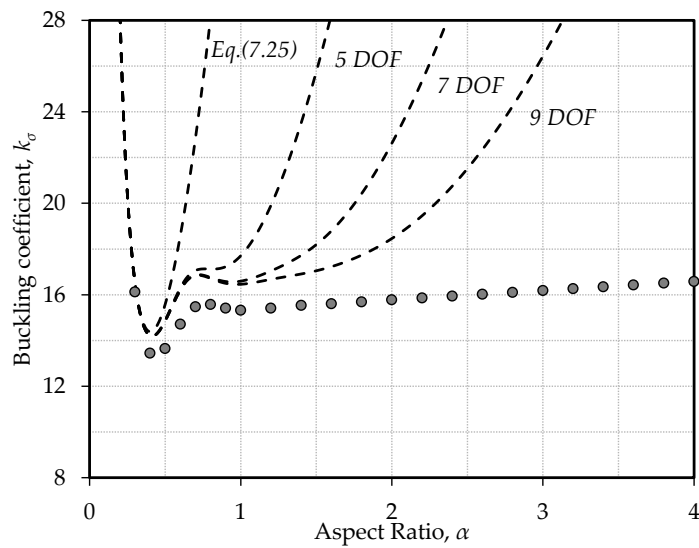


Figure 7.17: Comparison between numerical results of elastic critical stress and analytical results from energy formulations with extra degrees-of-freedom for $Z=40$ and BC3

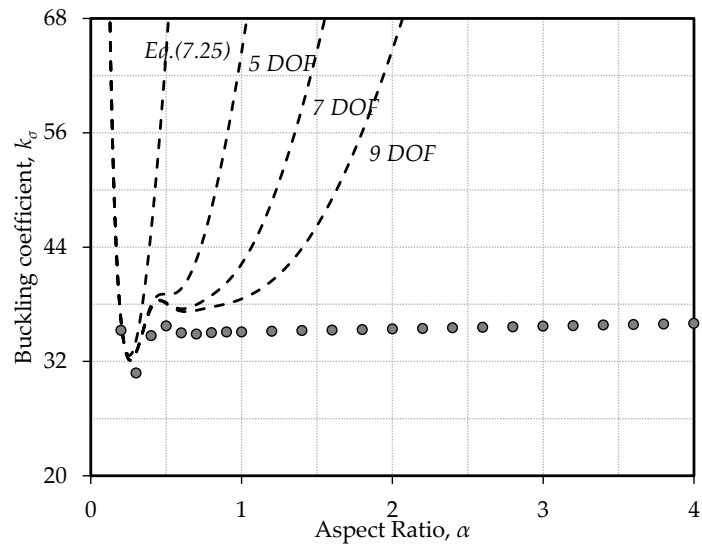


Figure 7.18: Comparison between numerical results of elastic critical stress and analytical results from energy formulations with extra degrees-of-freedom for $Z=100$ and BC3

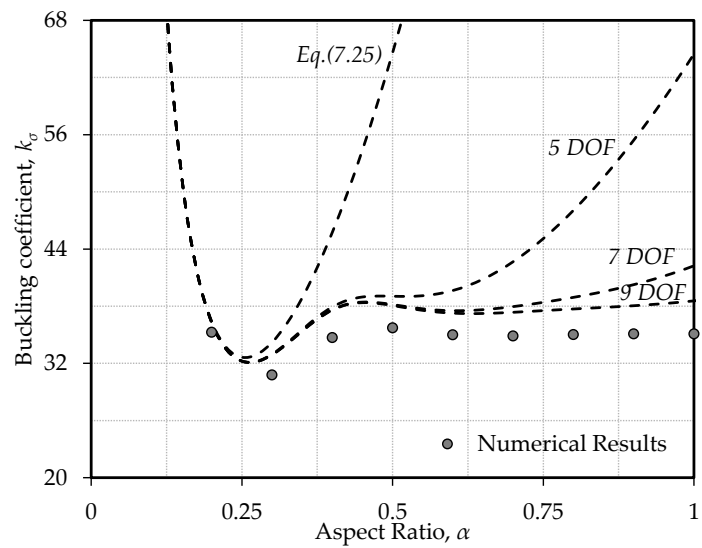


Figure 7.19: Comparison between numerical results of elastic critical stress and analytical results from energy formulations with extra degrees-of-freedom for $Z=100$ (short cylindrically curved panels) and BC3

Nevertheless, focusing only on results for short cylindrically curved panels ($\alpha \leq 1$), it is seen that this analytical model reproduces reasonably accurate results (Figure 7.19). In this case, the maximum absolute error between the analytical model and the numerical results is approximately 7% and it is obtained for $Z=100$ and $\alpha=1.0$. It is believed that additional degrees-of-freedom would allow having the same accuracy for higher values of aspect ratio. Additionally, the errors are surely related to the fact that approximate displacement functions are being considered. These introduce extra stiffness to the system that ultimately results in higher values of the elastic critical stress.

7.3.5. Boundary conditions type 2 and 6, 8 and 10 degrees-of-freedom

Following the same idea that extra degrees-of-freedom are required to more accurately capture the correct out-of-plane displacement, in this section results for the elastic critical stress of cylindrically curved panels with boundary conditions type 2 under pure compression are presented. As in the previous subsection, it was found that, even with seven degrees-of-freedom in the out-of-plane displacement function, the elastic critical stress of cylindrically curved panels characterised by high values of aspect ratio is not accurately obtained (Figure 7.21 to Figure 7.24). Again, focusing only on results for short cylindrically curved panels ($\alpha \leq 1$), it is seen that this analytical model reproduces also reasonably accurate results (Figure 7.25).

In the range of short cylindrically curved panels, the maximum absolute error between the analytical model and the numerical results is, now for curved panels with boundary conditions type 2, approximately 9% and it is obtained for $Z=100$ and $\alpha=1.0$. As it was stated for cylindrically curved panels with boundary conditions type 3, more degrees-of-freedom would allow more accurate results for high values of aspect ratio. Additionally, the errors are surely related to the fact that approximate displacement functions are being considered.

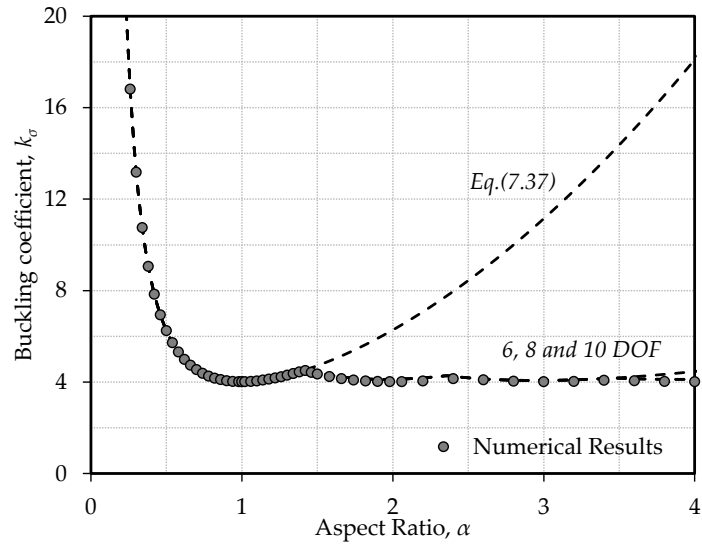


Figure 7.20: Comparison between numerical results of elastic critical stress and analytical results from energy formulations with extra degrees-of-freedom for $Z=0$ and BC2

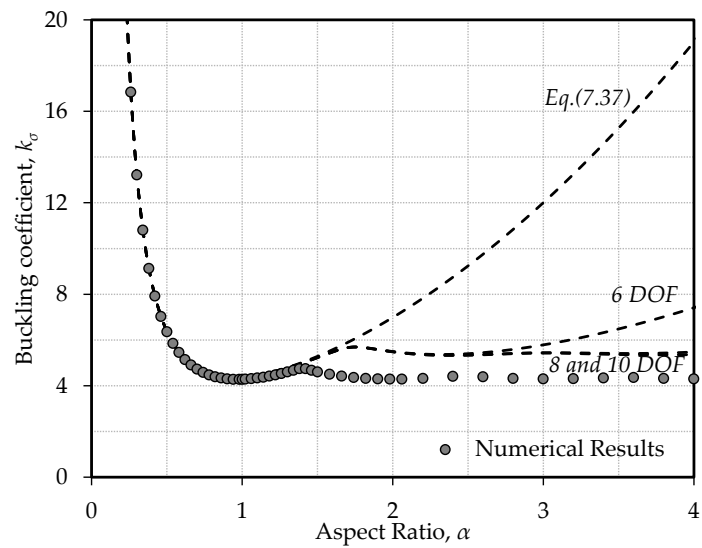


Figure 7.21: Comparison between numerical results of elastic critical stress and analytical results from energy formulations with extra degrees-of-freedom for $Z=5$ and BC2

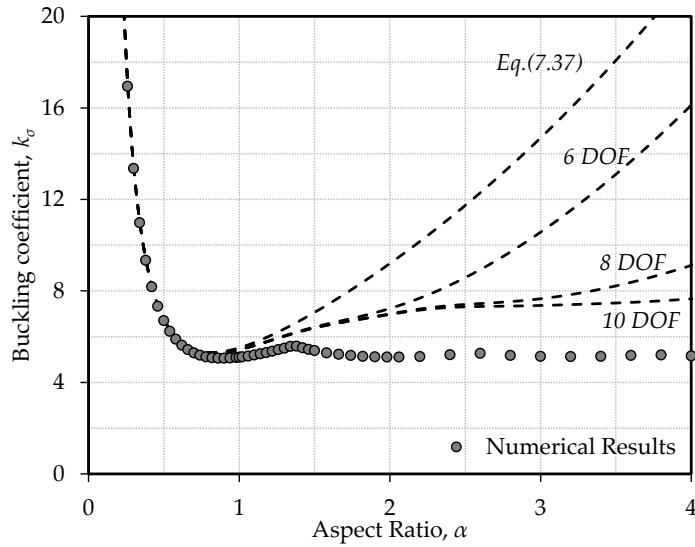


Figure 7.22: Comparison between numerical results of elastic critical stress and analytical results from energy formulations with extra degrees-of-freedom for $Z=10$ and BC2

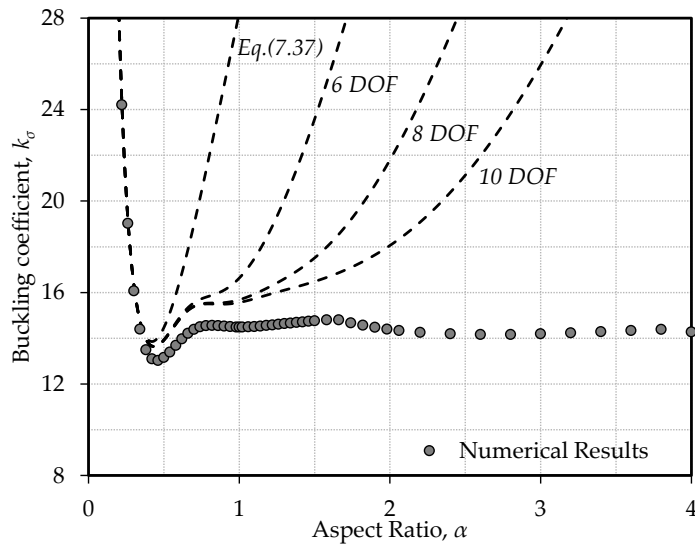


Figure 7.23: Comparison between numerical results of elastic critical stress and analytical results from energy formulations with extra degrees-of-freedom for $Z=40$ and BC2

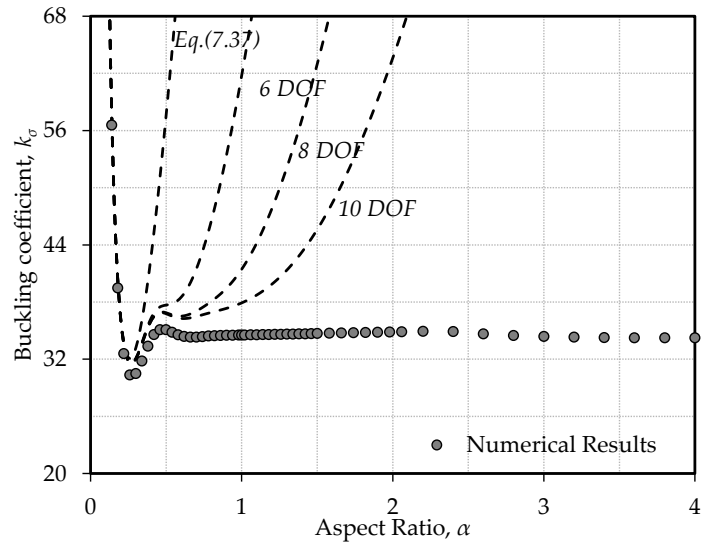


Figure 7.24: Comparison between numerical results of elastic critical stress and analytical results from energy formulations with extra degrees-of-freedom for $Z=100$ and BC2

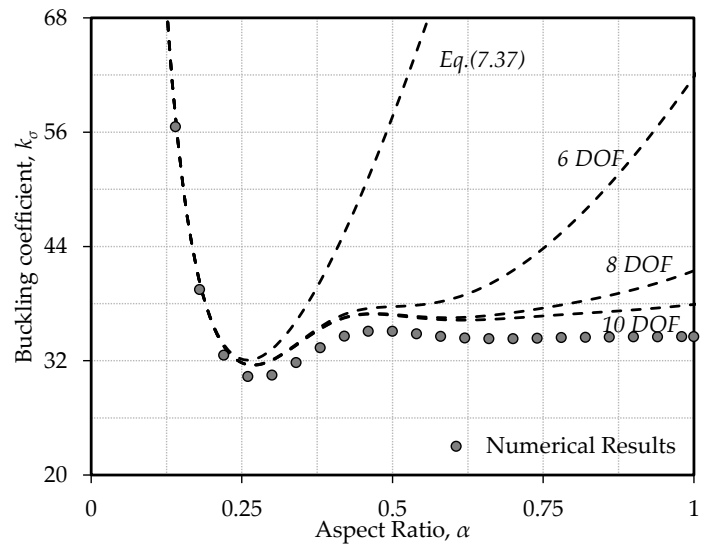


Figure 7.25: Comparison between numerical results of elastic critical stress and analytical results from energy formulations with extra degrees-of-freedom for $Z=100$ (short cylindrically curved panels) and BC2

7.4. Summary

This chapter focused on an energy formulation to study the behaviour of cylindrically curved panels. Specifically, the following achievements were made:

- Derivation of simple expressions capable of accurately predicting the elastic critical stress of cylindrically curved panels with different boundary conditions and with values of aspect ratio ranging from 0.2 to 1;
- Derivation of a simple expression to compute the minimum value of the elastic critical stress of cylindrically curved short panels with boundary conditions type 3;
- Derivation of complex total potential energy function whose quadratic term may be used to obtain accurate values of the elastic critical stress of cylindrically curved panels with different boundary conditions and with values of aspect ratio ranging from 0.2 to 4;

Additionally, it is worth to further investigate the origin of some observed unavoidable errors between analytical and numerical results (*e.g.* see Figure 7.19 and Figure 7.25). In order to do so, the presence of the transverse state of stress mentioned in sec. 5.2 is again highlighted: it may be seen as part of the reason why there are those errors between analytical and numerical results; specifically it explains why even with extra degrees-of-freedom and high curvatures those unavoidable errors still occur. It should be noticed that this transverse state of stress is ignored based on the *shallow shell* assumption made in Chapter 2. Consequently, it can be concluded that there is a value of Z that sets the difference between shallow and non-shallow curved panels. Based on Figure 5.10 and on the previous considerations, it is reasonable to set that value around 23.

Finally it is highlighted the fact that the expressions of the potential energy derived in this chapter may be used to obtain the equilibrium equations and, consequently, the postbuckling behaviour of cylindrically curved panels.

8. Design proposals for cylindrically curved steel panels

8.1. Chapter overview

This chapter comprises all calibration processes and presents the proposed methodologies for computing the elastic critical stress and ultimate strength of cylindrically curved panels. The background for all proposed formulae presented in this chapter is the numerical results from the parametric studies presented in Chapter 5 and Chapter 6 and the theoretical derivation of Chapter 7. It should also be emphasised that only boundary conditions type 2 are addressed by the developed methodologies leaving out of their scope boundary conditions type 1 and 3.

The chapter starts, in sec. 8.2, with the description of the steps that were taken from the first analyses of the numerical results of the elastic critical stress of cylindrically curved panels (performed in sec. 5.2) to the proposal of a set of expressions allowing an accurate evaluation of the elastic critical stress of cylindrically curved panels. At the end of this section, a comparison with existing proposals is made.

In sec. 8.3, an alternative to the proposed formulae in sec. 8.2 is presented. This formula is proposed based on the analytical studies performed in Chapter 7 and, on one hand, is considerable simpler to implement, and on the other, an extended version, allows to compute the elastic critical stress for varying values of the aspect ratio.

Sec. 8.4 is devoted to a detailed comparison between the two proposals and formulae found in literature and already presented in Chapter 3 (namely, Stowell (1943) and Domb & Leigh (2001)).

In sec. 8.5, an effective width approach is developed and presented. It is also based on numerical results from Chapter 5 as background and, additionally, in order to propose a correction factor for the evaluation of the ultimate strength of long cylindrically curved panels, numerical results from the imperfection sensitivity study performed in Chapter 6 are used. Additionally, in sec. 8.6 the ultimate strength of cylindrically curved panels under direct stresses is assessed by an interaction formula and its level of safety is verified against numerical results.

Subsequently, sec. 8.7 illustrates the application of the design formulae for curved panels for the evaluation of the resistance check of cross-sections built-up with curved panels.

Finally, the chapter ends with a short summary highlighting the main conclusions and contributions to the understanding and design of cylindrically curved panels under direct in-plane stresses.

8.2. Numerical evaluation of the elastic critical stress of cylindrically curved panels under uniaxial compressive stresses

8.2.1. General

The effect of curvature on the elastic critical stress of cylindrically curved panel is taken into account by means of calibrating numerical results of $k_{\sigma,min}$ and $0.2 \leq \alpha \leq 1$ for short panels and $1 < \alpha \leq 5$ for long panels. Proposed formulae are equivalent to those in Table 4.1 of EN1993-1-5:2006 (CEN, 2006a) for flat panels, *i.e.* $Z=0$. In fact, the aim was to provide an extension of formulae from the European standard from plates to cylindrically curved panels, thus the chosen mathematical framework is similar. Furthermore, the set of proposed formulae is divided into four subsets of panels: short ($\alpha \leq 1$) and long panels ($\alpha > 1$) and low curvature ($Z \leq 23$) and high curvature ($Z > 23$). This is necessary due to the already discussed facts that minimum elastic critical stress occurs for pan-

els with $\alpha \leq 1$ (the higher the curvature the shorter the panel is for a minimum value of k_σ) and that there is a distinction in the buckling behaviour for $Z=23$. Additionally, for panels with $\alpha > 1$ the minimum values of k_σ are higher than for panels with $\alpha < 1$.

8.2.2. Calibration methodology

Numerical results retrieved from parametric studies are not directly applicable to calibrate the elastic buckling factor for cylindrically curved panels. In fact, numerical results of linear buckling analysis are critical multipliers of the applied load. Since the applied load is the product of the sectional area of the panels by the yield stress of the steel, numerical values of the elastic buckling coefficient k_σ are obtained by Eq. (8.1), where $\alpha_{cr,num}$ is the critical multiplier directly read from numerical results.

$$k_\sigma = \frac{\alpha_{cr,num} f_y}{\frac{\pi^2 E}{12(1-\nu^2)} \left(\frac{t}{b}\right)^2} \quad (8.1)$$

After this first step, minimum values of k_σ are isolated since those are the ones used for formulae calibration (see sec. 5.2.3.2). The next step consists on obtaining numerical values of parameters A , B , C and D of Eq. (8.2) and Eq. (8.3). These expressions are exactly those given by EN1993-1-5:2006 (CEN, 2006a) for $A=8.2$, $B=1.05$, $C=-6.29$ and $D=9.78$ (see Table 8.1).

$$\frac{A}{B + \psi} \quad (8.2)$$

$$\frac{A}{B} + C \psi + D \psi^2 \quad (8.3)$$

Numerical values of A and B are obtained using numerical values of the elastic buckling stress for $\psi=1$ and $\psi=0$

$$\begin{aligned} \psi = 0 \Rightarrow & \begin{cases} \frac{A_{num}}{B_{num}} = k_{\sigma,num}^{\psi=0} \\ \frac{A_{num}}{B_{num} + 1} = k_{\sigma,num}^{\psi=1} \end{cases} \Leftrightarrow \begin{cases} A_{num} = \frac{k_{\sigma,num}^{\psi=0} k_{\sigma,num}^{\psi=1}}{k_{\sigma,num}^{\psi=0} + k_{\sigma,num}^{\psi=1}} \\ B_{num} = \frac{k_{\sigma,num}^{\psi=1}}{k_{\sigma,num}^{\psi=0} - k_{\sigma,num}^{\psi=1}} \end{cases} \end{aligned} \quad (8.4)$$

Numerical values of C and D are obtained using A_{num}/B_{num} and numerical values of the elastic buckling stress for $\psi=-0.5$ and $\psi=-1$

$$\begin{aligned} \psi = -1 &\Rightarrow \left\{ \begin{array}{l} \frac{A_{num}}{B_{num}} - C_{nym} + D_{num} = k_{\sigma,num}^{\psi=-1} \\ \frac{A_{num}}{B_{num}} - 0.5C_{nym} + 0.25D_{num} = k_{\sigma,num}^{\psi=-0.5} \end{array} \right. \Leftrightarrow \\ \psi = -0.5 &\Rightarrow \left\{ \begin{array}{l} C_{num} = 3 \frac{A_{num}}{B_{num}} - 4k_{\sigma,num}^{\psi=-0.5} + k_{\sigma,num}^{\psi=-1} \\ D_{num} = 2 \frac{A_{num}}{B_{num}} - 4k_{\sigma,num}^{\psi=-0.5} + 2k_{\sigma,num}^{\psi=-1} \end{array} \right. \end{aligned} \quad (8.5)$$

The last step comprises the calibration expressions depending on the curvature. The calibration was divided into two subsets defined for $Z=23$ (see sec. 5.2.5). The calibration is made recurring to a quadratic regression through the least squares method with two constraints:

- Value for $Z=0$ is fixed and is given by EN1993-1-5:2006 (CEN, 2006a);
- Value for $Z=23$ is fixed to guarantee continuity between the two branches of the proposed curve.

The proposed formulae resulting from this calibration process is given in sec. 8.2.3 and the respective statistical evaluation is made in sec. 8.2.4.

8.2.3. Proposed formulae for short curved panels

Following the structure of EN1993-1-5:2006, the elastic critical stress is given by multiplying the buckling coefficient obtained by the method in Table 8.1 and Table 8.2 by the classic critical Euler stress, σ_E

$$\sigma_{cr} = k_{\sigma} \sigma_E = k_{\sigma} \frac{\pi^2 E}{12(1-\nu^2)} \left(\frac{t}{b} \right)^2 \quad (8.6)$$

It is now possible to compute different formulae for different combinations of Z and ψ and plot them as curves in charts similar to Figure 3.11 as in Figure 8.1 that shows the variation of the critical stress coefficient with curvature for different values of ψ . Agreement with numerical simulations is very good, the

maximum absolute error (MAE) when comparing the suggested approach to numerical results being 3.79%.

Table 8.1: Elastic buckling coefficient for short cylindrically curved panels

ψ	$1 \geq \psi > 0$	$0 \geq \psi \geq -1$
EN1993-1-5:2006	$\frac{8.2}{1.05 + \psi}$	$7.81 - 6.29\psi + 9.78\psi^2$
New Approach	$\frac{A}{B + \psi}$ $A = a_1 + a_2Z + a_3Z^2$ $B = b_1 + b_2Z + b_3Z^2$	$\frac{A}{B} + C\psi + D\psi^2$ $C = d_1 + d_2Z + d_3Z^2$ $D = d_1 + d_2Z + d_3Z^2$

Table 8.2: a_i , b_i , c_i and d_i coefficients

ψ	$1 \geq \psi > 0$		$0 \geq \psi \geq -1$	
$0 < Z \leq 23$	$a_1 = 8.2$	$b_1 = 1.05$	$c_1 = -6.29$	$d_1 = 9.78$
	$a_2 = 0.074$	$b_2 = -0.0002$	$c_2 = -0.1971$	$d_2 = -0.2174$
	$a_3 = 0.0163$	$b_3 = 0.0003$	$c_3 = 0.0004$	$d_3 = -0.0002$
$23 < Z \leq 100$	$a_1 = 3.214$	$b_1 = 0.961$	$c_1 = -9.124$	$d_1 = 5.843$
	$a_2 = 0.5976$	$b_2 = 0.0104$	$c_2 = -0.0646$	$d_2 = -0.0556$
	$a_3 = 0.0028$	$b_3 = 0$	$c_3 = 0$	$d_3 = 0.0002$

8.2.4. Statistical evaluation for short curved panels

The comparison of the proposed formulae for short cylindrically curved panels with the numerical results (corresponding to all the numerical models with $k_{\sigma, min}$) leads to the results of Figure 8.2 and Table 8.3 (a total of 2121 numerical models – Z from 0 to 100 and loading from pure compression to pure in-plane bending) were used for the global statistical evaluation.

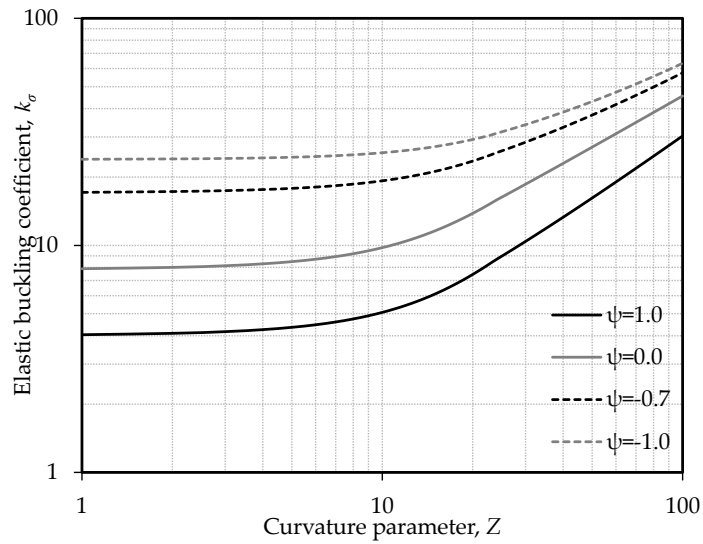


Figure 8.1: $k_{\sigma, proposed}$ Eq. (8.6) curves for $\psi=1$, $\psi=0$, $\psi=-0.7$ and $\psi=-1$

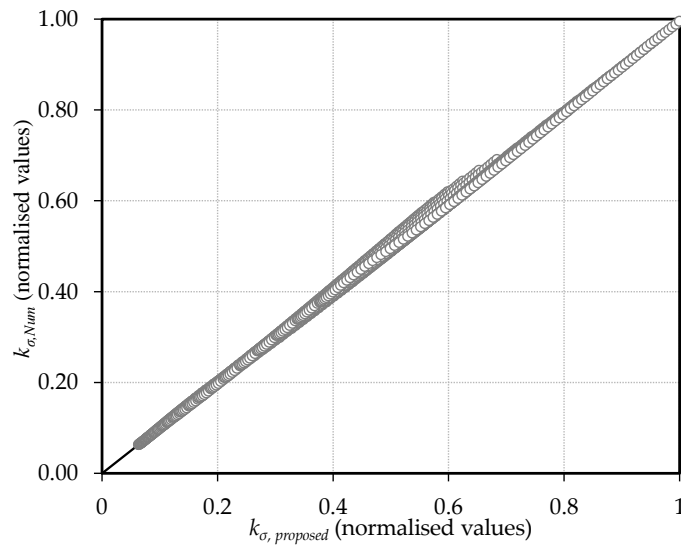


Figure 8.2: Correlation of the proposed formulae (Eq. (8.6)) for short cylindrically curved panels with numerical results (normalised values)

Since the formulae from Stowell (1943) and Domb & Leigh (2001) only allow computing the buckling coefficient of cylindrically curved panels under pure compression, Table 8.4 shows the comparison between the proposed formula and other formulae only for $\psi=1$. It can be concluded that the proposed formula is a better fit to the numerical results than Stowell's and Domb & Leigh's formulae for short cylindrically curved panels.

It should be mentioned again that long cylindrically curved panels have a higher elastic critical stress (the higher the curvature the bigger the difference for short curved panels, see Figure 5.4 to Figure 5.7). Therefore, the proposed formula to compute the elastic critical stress of cylindrically curved panels does not apply for long cylindrically curved panels.

Here, for the sake of simplicity, the work presented by Martins *et al.* (2013) where a correction factor is proposed, is omitted and the correction of results will be exclusively performed at the ultimate strength level (see sec. 8.5.4).

Table 8.3: Statistical evaluation concerning the ratios $k_{\sigma, \text{proposed Eq. (8.6)}}/k_{\sigma, \text{num}}$ for short cylindrically curved panels (normalised values)

<i>No. of analyses</i>	<i>Mean</i>	<i>CoV (%)</i>	<i>MAE (%)</i>
2121	1.0037	1.5	3.79

Table 8.4: Statistical evaluation concerning the ratios $k_{\sigma, \text{proposed Eq. (8.6)}}/k_{\sigma, \text{num}}$; $k_{\sigma, \text{Stowell}}/k_{\sigma, \text{num}}$ and $k_{\sigma, \text{Domb\&Leigh}}/k_{\sigma, \text{num}}$ for short cylindrically curved panels subjected only to pure compression (normalised values)

<i>No. of analyses</i>	<i>Proposed formulae Eq. (8.6)</i>			<i>Stowell (1943)</i>			<i>Domb & Leigh (2001)</i>		
	<i>Mean</i>	<i>CoV (%)</i>	<i>MAE (%)</i>	<i>Mean</i>	<i>CoV (%)</i>	<i>MAE (%)</i>	<i>Mean</i>	<i>CoV (%)</i>	<i>MAE (%)</i>
101	1.0113	0.80	2.07	1.1763	3.44	17.03	1.1712	4.26	18.34

8.3. Extended evaluation of the elastic critical stress of cylindrically curved panels under uniaxial compressive stresses: analytical closed-form solution

8.3.1. General

The scope of the formulae presented in the previous section is limited to cylindrically curved panels with an aspect ratio leading to minimum values of the elastic critical stress and it is exclusively calibrated with numerical results. Attempting to overcome this limitation and to obtain an expression with a physical meaning, in Chapter 7, an energy formulation was used to derive closed-form solutions for computing the elastic critical stress of curved panels under uniaxial compressive stresses with varying aspect ratios and with different boundary conditions (boundary conditions type 2 and 3).

As concluded in Chapter 7, these closed-form solutions allow to accurately predict the elastic critical stress of curved panels with aspect ratios up to 4 and with boundary conditions type 2 and 3. However, this achievement is bound to an analytical model with several degrees-of-freedom and characterised by a complex quadratic term of the total potential energy expression, making it impossible to propose a reasonably simple expression. Still, the quadratic terms and the corresponding determinant are easily programmed in a spreadsheet (a fully developed example of the analytical formulation for boundary conditions type 3 with 9 degrees-of-freedom and with the quadratic terms is shown in Annex A).

8.3.2. Proposed formulae for short curved panels

Nonetheless, in this section Eq. (8.7), which is based on Eq. (7.25) (derived in Chapter 7 from a simple analytical model with only 3 degrees-of-freedom for boundary conditions type 3), is proposed to compute minimum values of the elastic buckling factor of cylindrically curved panels under pure compression for boundary conditions type 2. This option is justified by the fact that Eq. (7.25) is very simple and, as concluded in Chapter 7, a similar expression for bounda-

ry conditions is rather difficult to obtain. Albeit the following proposed analytical expression is derived based on an energy formulation suitable to describe the critical behaviour of cylindrically curved panels with boundary conditions type 3, it will be seen that with a slight modification, it fits quite accurately also to minimum values of numerical results for boundary conditions type 2.

This modification, performed in Eq. (7.25) is seen in the following expression where the value 12 is replaced by α_{BC} . This small modification allows obtaining good results when compared to numerical results also for boundary conditions type 2, maintaining the physical meaning of Eq. (7.25).

$$k_{\sigma} = 2 \left[1 + \frac{\sqrt{\pi^6 + \alpha_{BC} (\pi^2 - 8)} Z^2}{\pi^3} \right] \quad (8.7)$$

The parameter α_{BC} was calibrated with numerical results through the least squares method and, for boundary conditions type 2 the value 9.6 is recommended; for boundary conditions type 3 the value 12 is kept unchanged from the analytical derivation.

Alternatively, for low values of curvature ($Z \leq 10$), Eq. (8.8) is proposed to obtain accurate values of the elastic buckling factor for cylindrically curved panels with aspect ratios from 0.2 to 1. This expression is directly obtained from Eq. (7.37) and it reflects the dependence of the elastic critical stress with α .

$$k_{\sigma} = \left[\frac{(a^2 + b^2)^2}{a^2 b^2} + \frac{12a^2(1-\nu)(\pi^2 - 8)}{\pi^6 b^2(1-\nu) + 2a^2 \pi^4 (\pi^2 - 8)} Z^2 \right] \quad (8.8)$$

8.3.3. Statistical evaluation for short curved panels

The comparison with the numerical results and the global statistical evaluation of the proposed formulae in Eq. (8.7) and Eq. (8.8) for short cylindrically curved panels leads, respectively, to the results of Figure 8.3 and Table 8.5 and Figure 8.4 and Table 8.6 where a total of 101 numerical models for Eq. (8.7) (corresponding to numerical models with $k_{\sigma, min}$ and pure compression) and 506

for Eq. (8.8) (corresponding to numerical models with $Z \leq 10$ and $0.2 \leq \alpha \leq 1$ and pure compression) were used.

It should be pointed out that, when comparing Table 8.4 and Table 8.6, although presenting poorer results than Eq. (8.6) when compared to numerical results, Eq. (8.7) still presents better results than proposals by Stowell (1943) and Domb & Leigh (2001). Additionally, the fact that Eq. (8.8) gives accurate results independently of the aspect ratio value is also highlighted. The downside of this expression is that it is only valid for values of curvature lower or equal to 10.

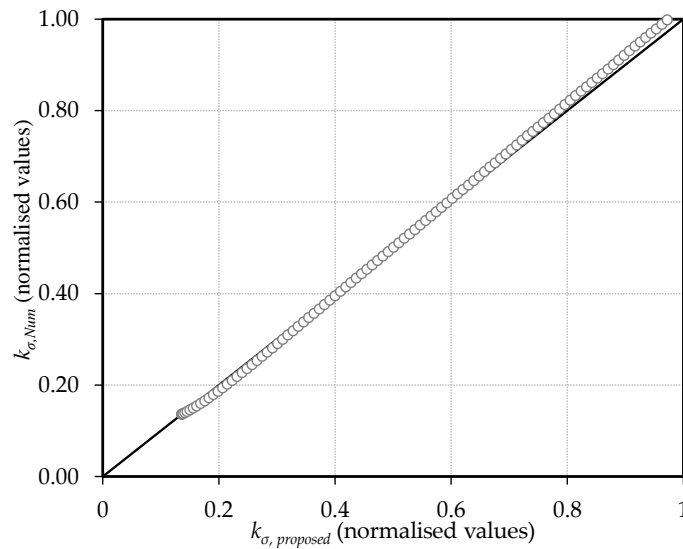


Figure 8.3: Correlation of the proposed formulae (Eq. (8.7)) for short cylindrically curved panels with numerical results (normalised values)

Table 8.5: Statistical evaluation concerning the ratios $k_{\sigma, proposed Eq. (8.7)} / k_{\sigma, num}$ for short cylindrically curved panels (normalised values)

<i>No. of analyses</i>	<i>Mean</i>	<i>CoV (%)</i>	<i>MAE (%)</i>
101	1.0052	2.89	6.79

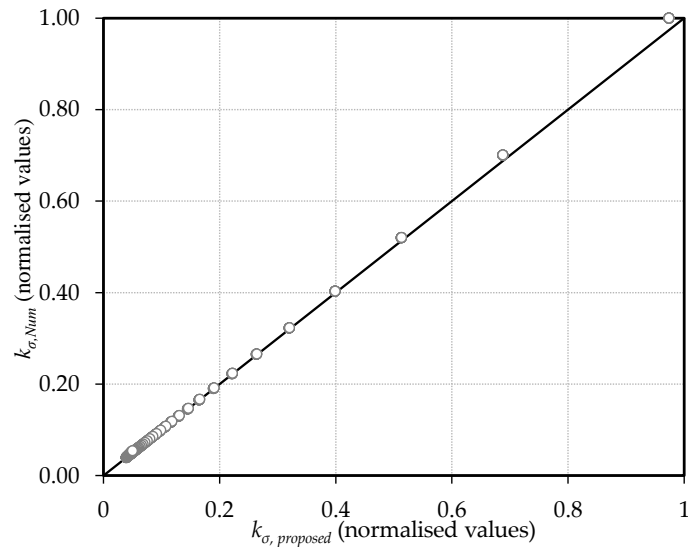


Figure 8.4: Correlation of the proposed formulae (Eq. (8.8)) for short cylindrically curved panels with numerical results (normalised values)

Table 8.6: Statistical evaluation concerning the ratios $k_{\sigma, proposed \text{ Eq. (8.8)}}/k_{\sigma, num}$ for short cylindrically curved panels (normalised values)

<i>No. of analyses</i>	<i>Mean</i>	<i>CoV (%)</i>	<i>MAE (%)</i>
506	0.9897	1.33	7.56

Finally, as it was concluded in Chapter 7 and already mentioned in this section, the alternative to Eq. (8.7) and Eq. (8.8) is to set up the total potential energy function (based on an energy formulation with several degrees-of-freedom) and to set the determinant composed by its quadratic terms to zero (see Annex A).

8.4. Detailed comparison between numerical results of the elastic buckling factor and proposed set of formulae for pure compression

In this section a detailed comparison between the proposed set of formulae in Eqs. (8.6) and (8.7) and current proposals from literature to compute the elastic

critical stress of cylindrically curved panels is performed. The proposed set of formulae is only compared with formulae developed by Stowell (1943) and Domb & Leigh (2001) because those are the ones that describe panels with similar boundary conditions and, therefore, those are the ones that truly can be compared.

Table 8.7: Comparison between Stowell's and Domb & Leigh's formula and proposed formulae in Eq. (8.6) and (8.7)

<i>Curvature, Z</i>	<i>Z=0</i>	<i>Z=10</i>	<i>Z=20</i>	<i>Z=30</i>	<i>Z=50</i>	<i>Z=75</i>	<i>Z=100</i>
$k_{\sigma,num}$	4.00	5.05	7.46	10.21	15.87	23.02	30.21
$k_{\sigma,Stowell}$	4.00	5.90	8.99	12.24	18.86	27.19	35.54
Error (%)	0.0	+14.6	+17.0	+16.6	+15.9	+15.3	+15.0
$k_{\sigma,Domb\&Leigh}$	-	6.16	8.30	11.37	18.71	27.77	36.76
Error (%)	-	+18.0	+10.1	+10.2	+15.2	+17.1	+17.8
$k_{\sigma,proposed\ Eq.\ (8.6)}$	4.00	5.07	7.45	10.41	16.16	23.28	30.32
Error (%)	0.0	+0.3	-0.2	+2.0	+1.8	+1.1	+0.4
$k_{\sigma,proposed\ Eq.\ (8.7)}$	4.00	5.39	7.82	10.44	15.81	22.59	29.40
Error (%)	0.0	+6.59	+4.85	+2.27	-0.38	-1.86	-2.70

Table 8.7 and Figure 8.5 show the comparison of the proposed formulae with Stowell's and Domb & Leigh's formulae. It is easily concluded that Stowell's and Domb & Leigh's formulae significantly differ from the proposed formulae and that this one is the best fit to the numerical results (this same conclusion can already be drawn from the analysis of Table 8.4 and Table 8.5).

It should be pointed out that Eq. (8.8) is not comparable to the proposals of Stowell (1943) and Domb & Leigh (2001) since their scope differs: while Stowell's and Domb & Leigh's proposals (as well as Eqs. (8.6) and (8.7)) do not take the aspect ratio into consideration, Eq. (8.8) does.

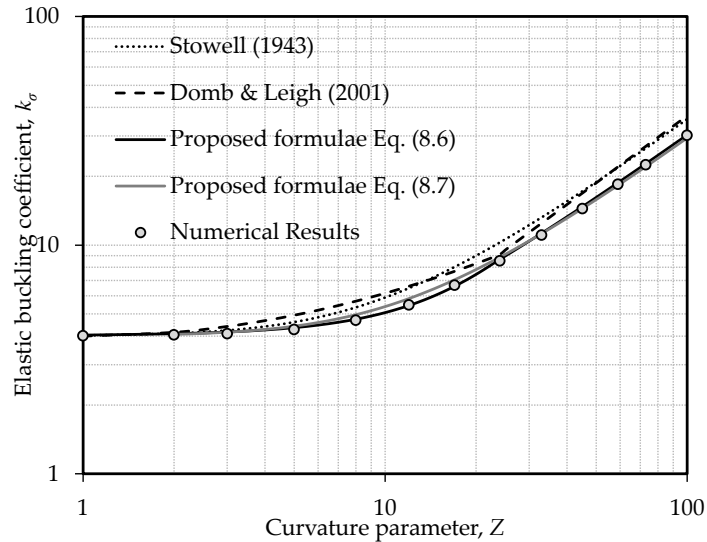


Figure 8.5: Comparison between Stowell's and Domb & Leigh's formula and proposed formulae in Eq. (8.6) and (8.7)

8.5. Ultimate strength of cylindrically curved panels under uniaxial compressive stresses by the effective width method

8.5.1. General

The proposed formulae in this section are based on the effective width concept, *i.e.* a width reduction factor is calibrated instead of a resistance reduction factor. In order to achieve this goal, numerical results from the parametric study presented in sec. 5.3 are used to calibrate a width reduction factor for short cylindrically curved panels. A correction factor allowing extending the defined formulae from short cylindrically curved panels to long panels is set based on the numerical results from the imperfection sensitivity study presented in Chapter 6.

8.5.2. Numerical evaluation of the effective width reduction factor for short curved panels and calibration methodology

Results of the numerical analysis directly provide a reduction factor on the reference loading applied on the panel (the first order plastic resistance),

$$N_{Rd} = \chi_{Num} A f_y \quad (8.9)$$

$$M_{Rd} = \chi_{Num} W_y f_y \quad (8.10)$$

The effective width concept reduces the width of the panel by an appropriate effective width reduction factor ρ , leading to effective cross-sectional properties that result in the same ultimate resistance of the cross-section

$$N_{Rd} = A_{eff} f_y = \rho b t f_y \quad (8.11)$$

$$M_{Rd} = W_{y,eff} f_y = W_{y,eff}(\rho) f_y \quad (8.12)$$

Comparing Eq. (8.9) and Eq. (8.11) leads to the following equality

$$\chi_{Num}^{N_{Rd}} = \rho^{N_{Rd}} \quad (8.13)$$

However, because the effective modulus ($W_{y,eff}$) for a non-uniform membrane stress distribution is not linearly dependent on ρ ($W_{y,eff} \neq \rho W_y$), it follows that for all in-plane applied stress other than uniform compression

$$\chi_{Num}^{M_{Rd}} \neq \rho^{M_{Rd}} \quad (8.14)$$

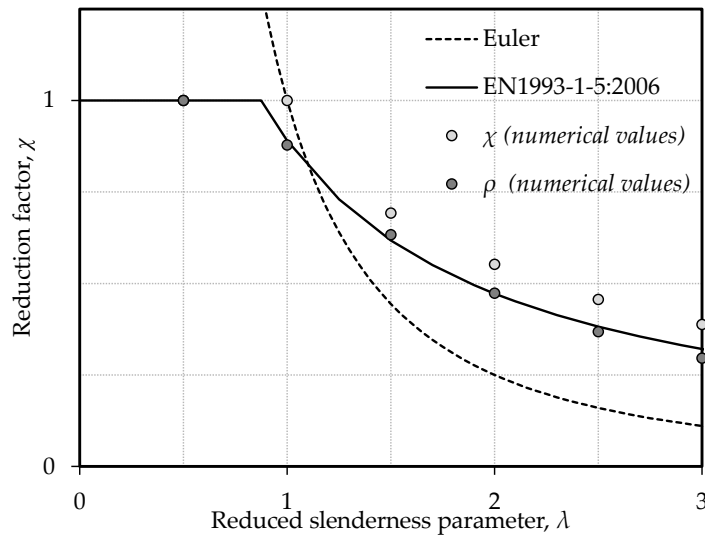


Figure 8.6: Comparison between χ - λ and ρ - λ approaches for $\psi=-1$

This conclusion is valid both for flat and cylindrically curved panels. Figure 8.6 confirms this conclusion by illustrating the two approaches (χ - λ and ρ - λ approaches) for $\psi=-1$.

Hence, it is necessary to translate the numerical resistance reduction factor χ_{Num} into the corresponding effective width reduction factor ρ_{Num} . Following the notation for b_{e1} , b_{e2} and b_t of Table 4.1 of EN1993-1-5:2006 (internal members), the effective width reduction factor is obtained by solving the following equations

$$\chi_{Num} \left(\frac{N_{Ed}}{A_{eff} f_y} \right) = 1 \quad (8.15)$$

$$\chi_{Num} \left(\frac{M_{y,Ed}}{W_{y,eff} f_y} \right) = 1 \quad (8.16)$$

where the maximum stress due to N_{Ed} and $M_{y,Ed}$ is f_y , A_{eff} is the effective area, $W_{y,eff}$ is the effective elastic section modulus and χ_{Num} is the maximum load factor obtained from numerical analysis. Thus, the goal is to obtain a value for ρ which results in values for A_{eff} and for $W_{y,eff}$ which together with χ_{Num} verify Eq. (8.15) and Eq. (8.16). Since obtaining direct solutions for these equations, for both load cases and curvatures, is not a straightforward process, an iterative procedure was implemented that comprised a sub-routine that calculated accurately the effective cross-section properties of the section (see Annex A in Nakai & Yoo (1988) for further information). The structure of this sub-routine is illustrated in Figure 8.7.

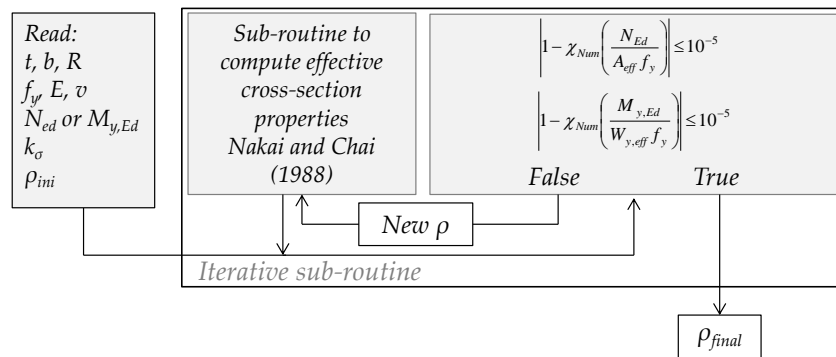


Figure 8.7: Iterative procedure to compute the width reduction factor ρ (acc. Martins *et al.*, 2014)

Based on the numerically calculated values of ρ obtained according to the previously described procedure, the set of formulae in Eq. (8.20) is proposed for the evaluation of the effective width reduction factor for cylindrically curved panels subject to non-uniform in-plane stress. The proposed formulae follow the format and incorporate EN1993-1-5:2006 for $Z=0$ as a particular case. As for the rules to compute the elastic buckling coefficient (see previous section), the aim of these set of equations is also to provide an extension of the effective width formula for internal elements from the European standard from plates to cylindrically curved panels (internal elements). Additionally, the set of proposed equations uses the concept of EN1993-1-6:2007 (CEN, 2007) according to which the formulae are divided into three branches ($\lambda < \lambda_{0,z}$; $\lambda_{0,z} \leq \lambda < \lambda_{0,p}$; $\lambda \geq \lambda_{0,p}$) as it is visible in Figure 8.8, where λ is the slenderness parameter, $\lambda_{0,p}$ is the length of the initial plateau for flat panels, $\lambda_{0,z}$ is the length of the initial plateau (general case), $\rho_{0,z}$ is given by the last branch of Eq. (8.20) setting $\lambda = \lambda_{0,p}$; α_z , c_z and S_z are parameters calibrated with numerical results that reflect the effect of curvature in the shape of the ρ - λ curves.

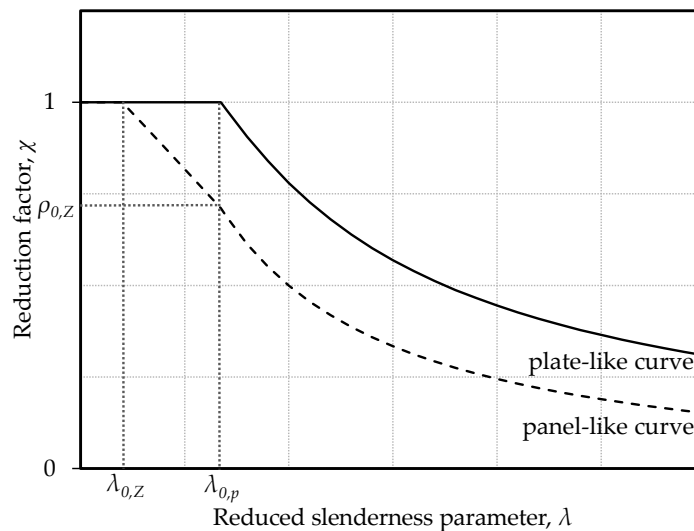


Figure 8.8: Generic output of proposed method

The numerical value of the initial plateau's length (the first branch of the proposed formulae) for curved panels was obtained by intersecting numerical val-

ues with the equation $\rho=1$. For pure compression ($\psi=1$), the lengths of the initial plateaus $\lambda_{0,p}$ and $\lambda_{0,z}$ are taken from EN1993-1-5:2006 (CEN, 2006a), Eq. (8.17), and from the work of Tran *et al.* (2012), Eq. (3.37) (see Figure 8.9). For pure in-plane bending ($\psi=-1$), the length $\lambda_{0,p}$ is taken from EN1993-1-5:2006 (CEN, 2006a), Eq. (8.17), and the length $\lambda_{0,z}$ is numerically calibrated, Eq. (8.18) (see Figure 8.10). It should be noted that in Eq. (8.18) ϕ_1 , ϕ_2 and ϕ_3 are dependent on the loading type. The regression is done by means of the method of the least squares by an algorithm developed in Mathematica (Wolfram, 2010).

$$\lambda_{0,p} = 0.5 + \sqrt{0.085 - 0.055 \psi} \quad (8.17)$$

$$\lambda_{0,z} = \phi_0 + \phi_1 \phi_2^Z \quad (8.18)$$

The length of the initial plateau $\lambda_{0,z}$ gives the upper limit for the first branch of the proposed formulae. Here, the reduction factor is always limited to 1 (the hardening effect is disregarded as in EN1993-1-5:2006). The second branch of the proposed formulae is a linear interpolation between the point $(\lambda_{0,z}, 1)$ and the point $(\lambda_{0,p}, \rho_{0,z})$. The last branch is given by a modification of the formulae in EN1993-1-5:2006 for computing the reduction factor, Eq. (8.19). This modification incorporates the already mentioned numerical parameters, α_z , c_z and S_z , reflecting the effect of curvature in the ultimate resistance cylindrically curved panels. After isolating, for each curvature and loading type, the numerical values that fall inside the limits of the third branch, the parameters α_z , c_z and S_z are calibrated by means of a regression done using the method of the least squares by an algorithm developed in Mathematica (Wolfram, 2010).

$$\rho = \frac{\lambda - 0.055 \alpha_z (3 + \psi)}{c_z \lambda^2} + S_z \quad (8.19)$$

The proposed formulae resulting from this calibration process is given in sec. 8.5.3 and the respective statistical evaluation is made in sec. 8.5.5.

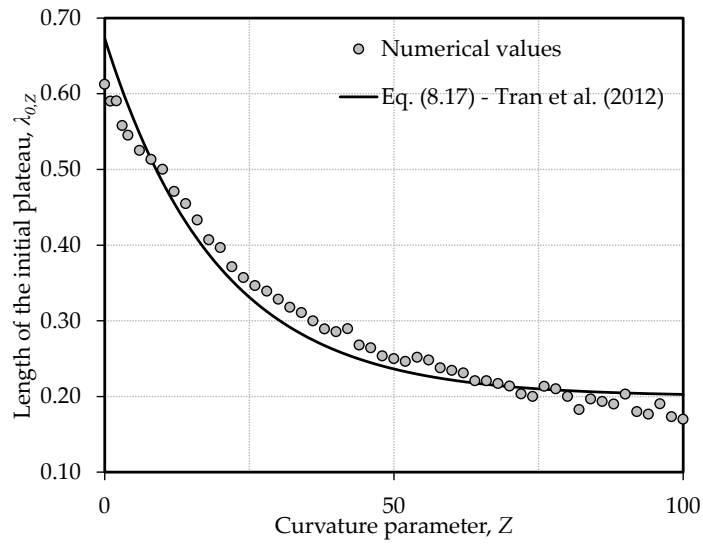


Figure 8.9: Tran *et al.* (2010) expression for the length of the initial plateau, $\lambda_{0,z}$ ($\psi=1$)

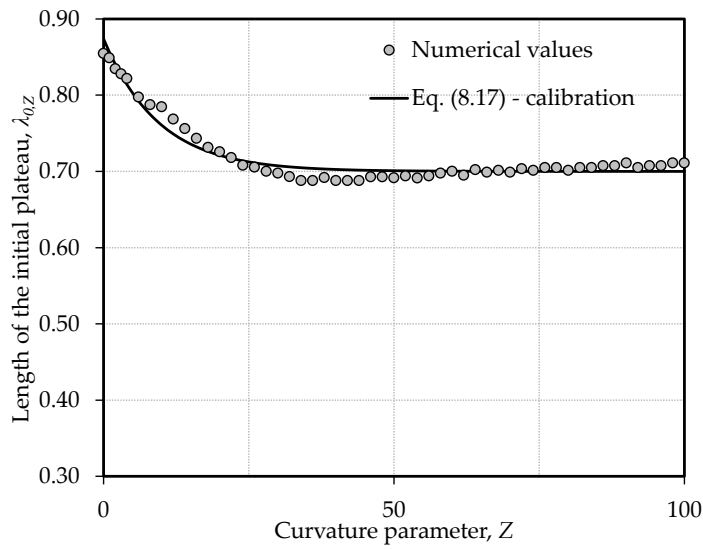


Figure 8.10: Calibration of parameters in Eq. (8.18) for the length of the initial plateau, $\lambda_{0,z}$ ($\psi=-1$)

8.5.3. Proposed formulae for short panels

The general form of the proposed formulae (with three branches) is represented by Eq. (8.20)

$$\left\{ \begin{array}{ll} \rho = 1 & \text{if } \lambda \leq \lambda_{0,Z} \\ \rho = \frac{\lambda_{0,p} - \lambda + \rho_{0,Z}(\lambda - \lambda_{0,Z})}{\lambda_{0,p} - \lambda_{0,Z}} & \text{if } \lambda_{0,Z} < \lambda < \lambda_{0,p} \\ \rho = \frac{\bar{\lambda} - 0.055\alpha_z(3 + \psi)}{c_z\lambda^2} + S_z & \text{if } \lambda \geq \lambda_{0,p} \end{array} \right. \quad (8.20)$$

The calibration of parameters carried out in the previous section results in the values for all parameters given by Table 8.8, Table 8.9 and Table 8.10.

Table 8.8: Values of numerical parameters α_z , c_z and S_z for pure compression ($\psi=1$)

	Z=0	Z=10	Z=23	Z=100
α_z	1	1	1	0.545
c_z	1	1.290	1.150	1.700
S_z	0	0.060	-0.040	-0.040

Table 8.9: Values of numerical parameters α_z , c_z and S_z for pure in-plane bending ($\psi=-1$)

	Z=0	Z=10	Z=23	Z=100
α_z	1	1	1	-3.182
c_z	1	1.025	1.125	1.650
S_z	0	-0.040	-0.040	-0.040

Table 8.10: Values of ϕ_1 , ϕ_2 and ϕ_3

	$\psi=1$ (<i>Tran et al., 2012</i>)	$\psi=-1$
ϕ_0	0.2	0.7
ϕ_1	0.473	0.174
ϕ_2	0.95	0.9

8.5.4. Correction factor for long curved panels under pure compressive stresses

8.5.4.1. General

In this section, numerical results from the imperfection sensitivity study (see Chapter 6) are compared with the previously proposed effective width formulae developed for short cylindrically curved panels under axial loads and a correction factor is calibrated.

The need for a correction factor for long cylindrically curved panels is justified by the influence that geometric imperfections (pattern and amplitude) have in the ultimate load factor of long cylindrically curved panels (see Chapter 6). In order to clarify this need, Figure 8.11 to Figure 8.14 compares numerical results (models with $b/t=100$) from sec. 6.2 (with imperfection amplitudes based on Eq. (6.1) and Eq. (6.2)) with the proposed formulae. The scope of the previously proposed formulae (short panels, *i.e.* $\alpha \leq 1$) is represented with a shadowed background ($0 < \alpha \leq 1.0$).

Generally, it is seen that the proposed formulae is accurate within the limits for which they were calibrated (it is also important to notice that the proposed formulae were calibrated for imperfection shapes corresponding to the first buckling mode only).

On the other hand, Figure 8.11 to Figure 8.14 show non-negligible errors for cylindrically curved panels with aspect ratio higher than 1. Additionally, and

in line with the general trends observed in Chapter 6, it is seen that results from models with amplitudes given by Eq. (6.2) are lower than results with amplitudes given by Eq. (6.1). This suggests that, generally, higher amplitudes will return lower values of the ultimate load factor. This is more obvious for higher values of the curvature parameter (see Figure 8.13 and Figure 8.14).

Summarised results are presented in Table 8.11. The largest error considering amplitudes given by Eq. (6.1) occurs for $Z=30$ for an aspect ratio equal to 4.4 and for an imperfection shape based on buckling mode number 8.

Table 8.11: Comparison between the minimum numerical values ($b/t=100$) and the proposed formulae

<i>Amplitude</i>	Z=10	Z=30	Z=40	Z=50	Z=60	Z=70	Z=80	Z=90	Z=100
<i>Proposed Formulae</i>	0.417	0.484	0.512	0.533	0.549	0.563	0.574	0.585	0.595
<i>Amp. based on Eq. (6.1)</i>	0.408	0.378	0.419	0.488	0.507	0.524	0.538	0.551	0.559
<i>Error (%)</i>	-2.2	-21.9	-18.2	-8.4	-7.7	-6.9	-6.3	-5.8	-6.1
<i>Amp. based on Eq. (6.2)</i>	0.393	0.364	0.371	0.383	0.437	0.443	0.449	0.455	0.460
<i>Error (%)</i>	-5.8	-24.8	-27.5	-28.1	-20.4	-21.3	-21.8	-22.2	-22.7

It is highlighted that values of the ultimate load factor decrease from $Z=10$ to $Z=30$. This conclusion was already made in sec. 6.3.3.4, where a detailed analysis and enlightenment of this phenomenon is given. Here the intention is only to justify the need of a correction factor for long cylindrically curved panels.

8.5.4.2. Correction factor

The correction factor is calibrated with results from the models of the imperfection sensitivity study performed in Chapter 6. Only those with maximum amplitude calculated with Eq. (6.1) are considered.

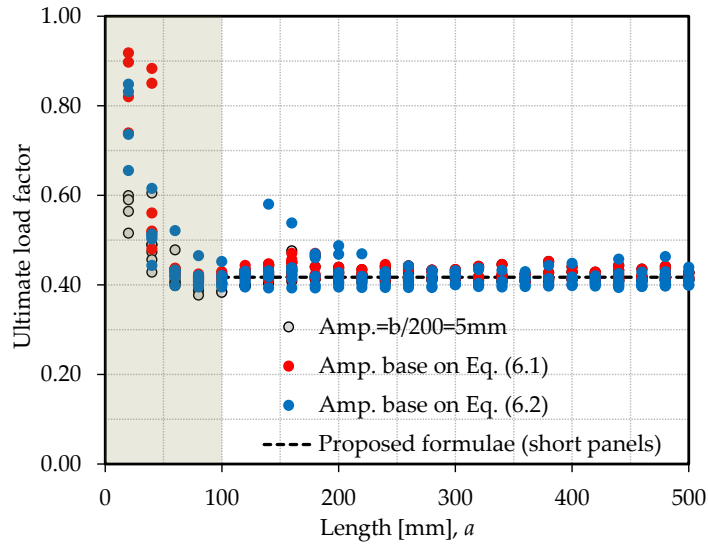


Figure 8.11: Comparison between numerical results and proposed formulae for $Z=10$ and $b/t=100$

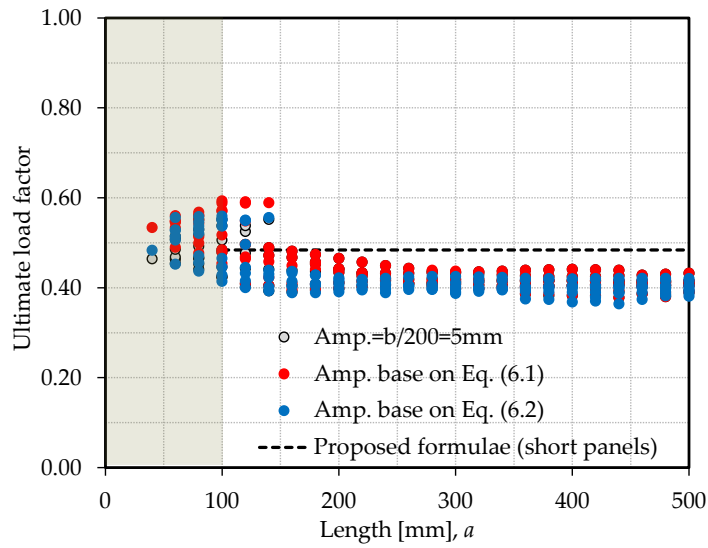


Figure 8.12: Comparison between numerical results and proposed formulae for $Z=30$ and $b/t=100$

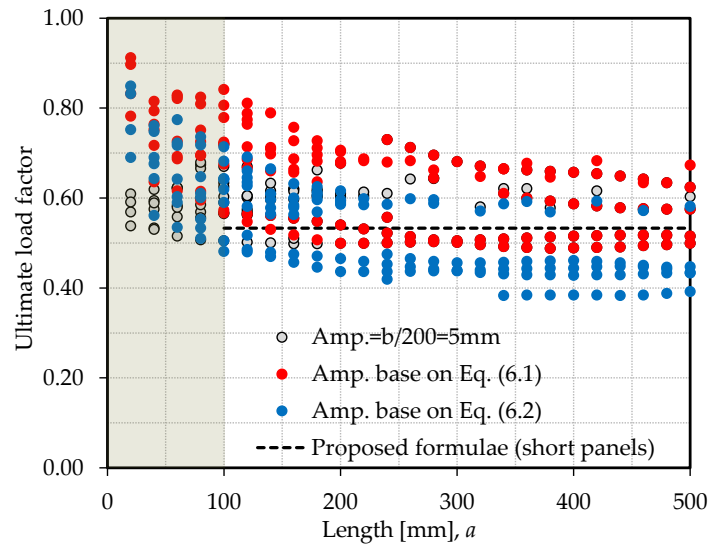


Figure 8.13: Comparison between numerical results and proposed formulae for $Z=50$ and $b/t=100$

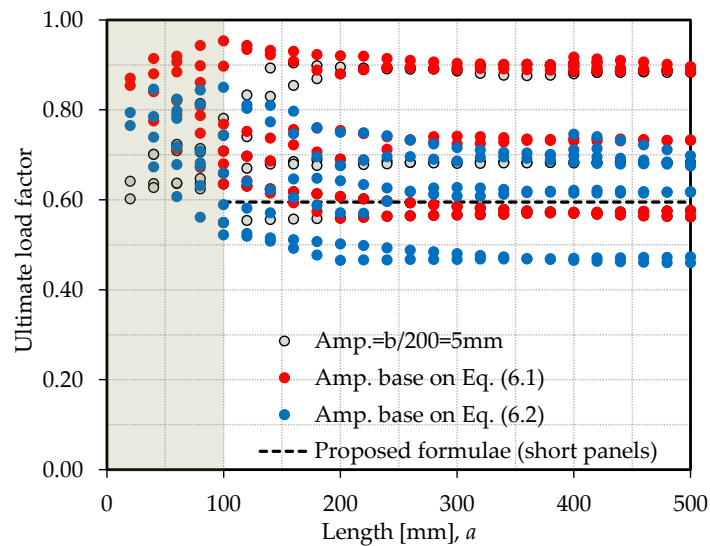


Figure 8.14: Comparison between numerical results and proposed formulae for $Z=100$ and $b/t=100$

This choice was prompted by the belief that Eq. (6.1), based on EN1993-1-5:2006, is more appropriate for cylindrically curved steel panels typically used in bridges; Eq. (6.2), based on EN1993-1-6:2007, would be more suitable for very high values of the reduced slenderness parameter (difficult to cope with more stringent fabrication tolerances) and for the presence of high circumferential stresses.

In Figure 8.15 the scatter relates to the ratio $\rho_{long,Num,min}/\rho_{short,proposed}$ for panels with $b/t=100, 150$ and 200 and the straight lines are linear regressions between the points $Z=1, Z=30, Z=70$ and $Z=100$ constrained to form a continuous line giving the proposed value for C_{ult} . The extreme values obtained by these linear regressions are given in Table 8.12. The ultimate strength of cylindrically curved panels under pure compression is given by

$$\rho_{long} = C_{ult} \rho \quad (8.21)$$

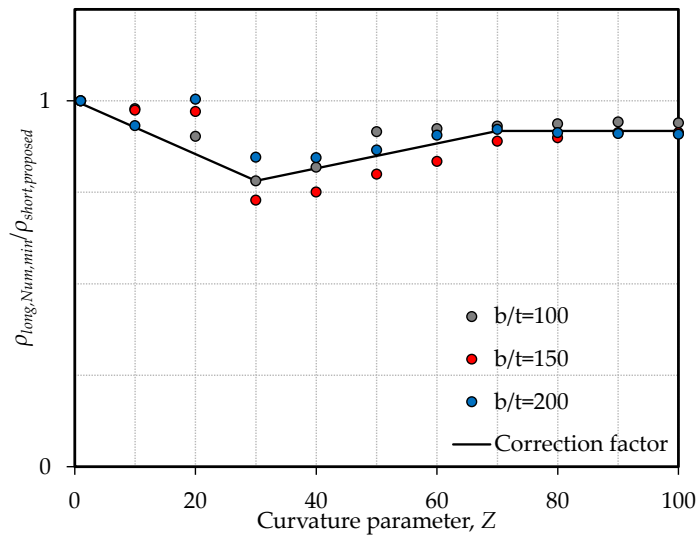


Figure 8.15: Correction factor for long cylindrically curved panels, C_{ult}

Table 8.12: Correction factor for long cylindrically curved panels, C_{ult}

	$Z=1$	$Z=30$	$Z=70$	$Z=100$
C_{ult}	1	0.782	0.912	

Figure 8.16 to Figure 8.20 shows that, when numerical values are obtained from models with maximum amplitudes computed from Eq. (6.1) (*i.e.* maximum amplitudes computed from a modified approach based on EN1993-1-5:2006) using the correction factor C_{ult} leads generally to values higher than the numerical values of the ultimate load factor, *i.e.* on the “safe side”.

Additionally, Figure 8.19 to Figure 8.21 shows that opting by computing maximum amplitudes for the geometric imperfections by Eq. (6.2) (*i.e.* maximum amplitudes computed from a modified approach based on EN1993-1-6:2007) a great amount of results fall inside the “unsafe zone”. This is sustained by the proven fact that, as a general trend, higher amplitudes lead to lower values of the ultimate load factor (see sec. 6.3.3.1 and Figure 6.32). Table 8.13 summarises all the relevant information that can be read from Figure 8.16 to Figure 8.21. It should be highlighted that the results from models which have “unrealistic” imperfection patterns (see sec. 6.3.1) are removed from Figure 8.15 to Figure 8.21 and Table 8.13 and, therefore, are not taken into account for the correction factor.

For amplitudes given by Eq. (6.1) it is concluded that C_{ult} corrects accurately the ultimate load factor from short cylindrically curved panels giving a lower bound for the ultimate load factor of long cylindrically curved panels.

Table 8.13: Summarised results from Figure 8.16 to Figure 8.21

	<i>No. of cases in the “unsafe zone”</i>			<i>Error of the lowest value (%)</i>		
	<i>b/t=100</i>	<i>b/t=150</i>	<i>b/t=200</i>	<i>b/t=100</i>	<i>b/t=150</i>	<i>b/t=200</i>
<i>Eq. (6.1)</i>	1 out of 1748	25 out of 413	4 out of 370	-0.1	-7.8	-0.4
<i>Eq. (6.2)</i>	339 out 1748	64 out of 413	44 out of 370	-15.2	-24.9	-21.2

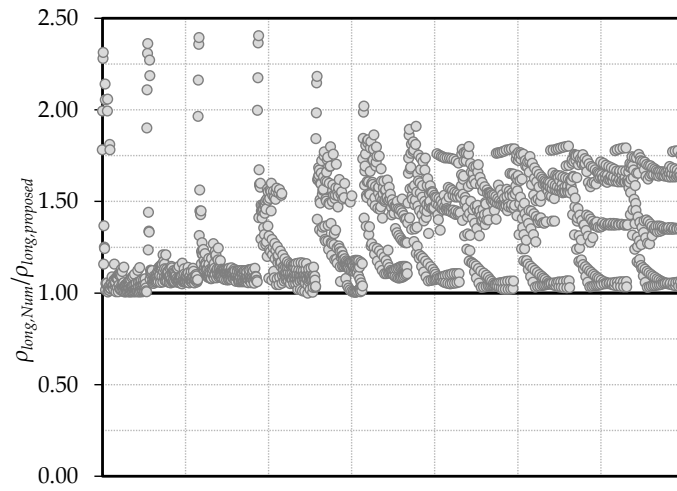


Figure 8.16: $\rho_{long,num,Eq.(6.1)}/\rho_{long,proposed}$ for $b/t=100$

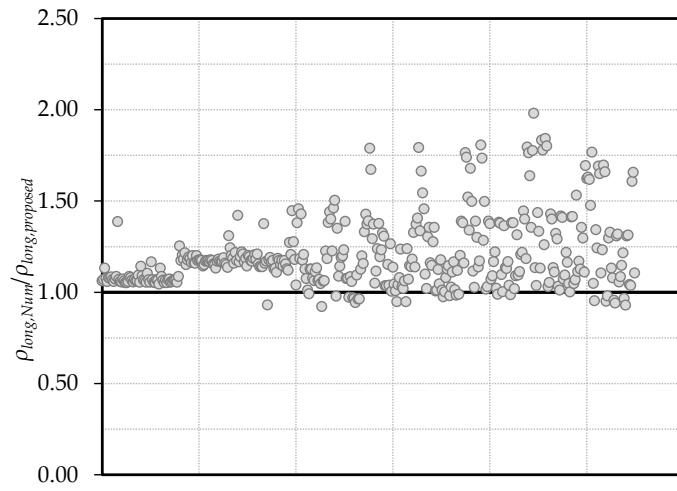


Figure 8.17: $\rho_{long,num,Eq.(6.1)}/\rho_{long,proposed}$ for $b/t=150$

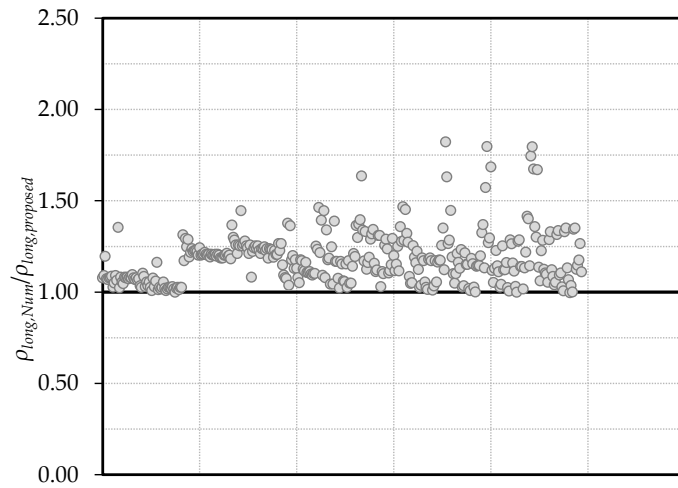


Figure 8.18: $\rho_{long,num,Eq.(6.1)}/\rho_{long,proposed}$ for $b/t=200$

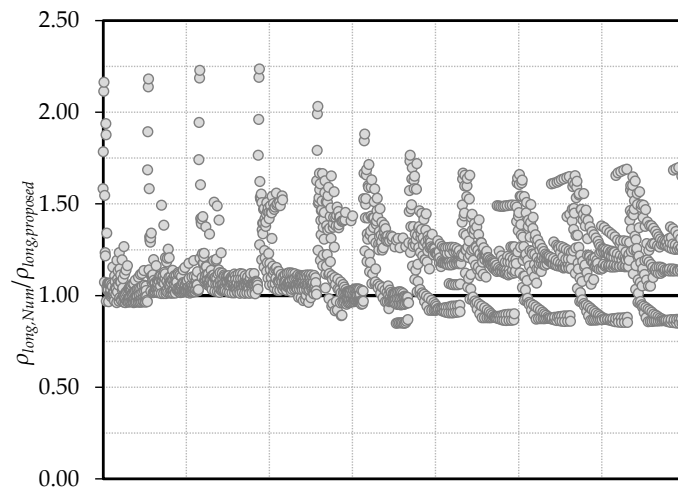


Figure 8.19: $\rho_{long,num,Eq.(6.2)}/\rho_{long,proposed}$ for $b/t=100$

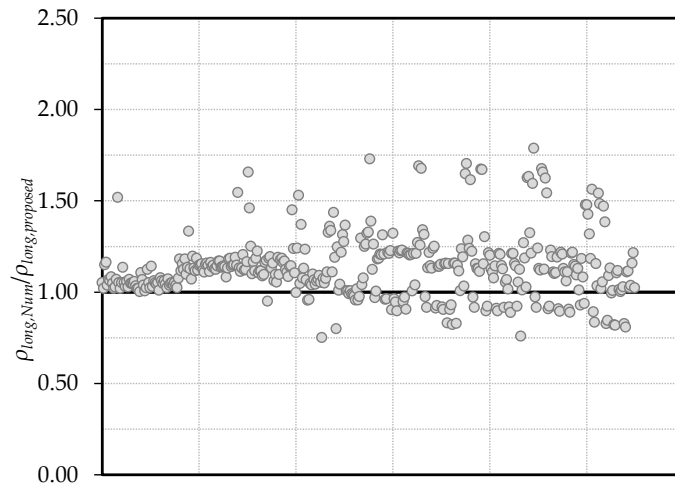


Figure 8.20: $\rho_{long,num,Eq.(6.2)}/\rho_{long,proposed}$ for $b/t=150$

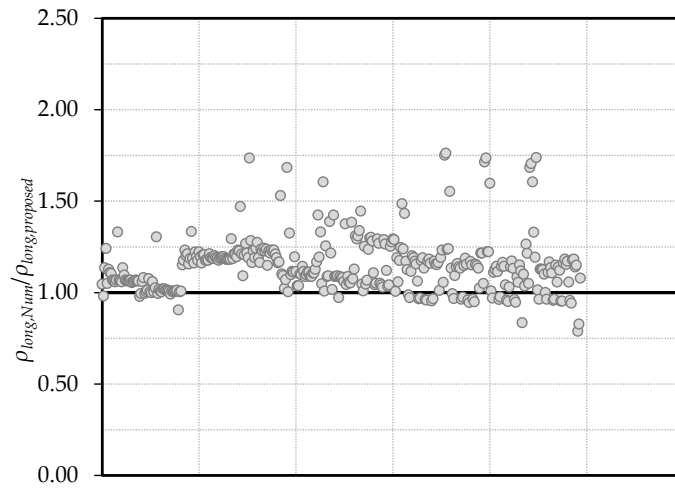


Figure 8.21: $\rho_{long,num,Eq.(6.2)}/\rho_{long,proposed}$ for $b/t=200$

8.5.5. Statistical evaluation for short curved panels

8.5.5.1. General

The following statistical evaluations are made using only results from the parametric study in sec. 5.3, *i.e.* where the effect of imperfection amplitudes other than $b/200$, imperfections shapes other than based on the first buckling mode and panels with aspect ratios other than those following Figure 5.3, were not used. Numerical results from the imperfection sensitivity study were used in sec. 8.5.4 to calibrate a correction factor to compute the ultimate strength of long cylindrically curved panels.

8.5.5.2. Pure compression

Comparison of the proposed formulae with the numerical results leads to the results of Figure 8.22 and Figure 8.23 (a total of 1537 numerical models were used for the global statistical evaluation for pure compression). It can be concluded that a good correlation between numerical and proposed results exists (all results are “inside” the zone delimited by the lines at $\pm 10\%$). In Figure 8.22 and Table 8.15 it is concluded that current proposed formulae replicate better the numerical results than the proposals by Tran *et al.* (2012), Tran (2012) and Tran *et al.* (2014) do. On the other hand, the proposal by Tran (2012) is the one that most poorly reproduces the numerical results as it is characterised by a relatively high value of the coefficient of variation and presents the highest value for the maximum absolute error.

8.5.5.3. Pure in-plane bending

The comparison of the proposed formulae with the numerical results (Figure 8.23 and Table 8.16 – a total of 1537 numerical models were used for the global statistical evaluation for pure bending). The agreement is very good.

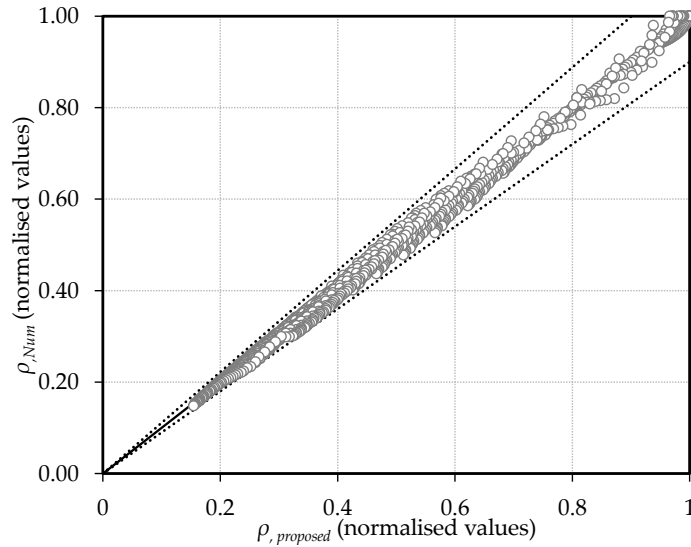


Figure 8.22: Correlation of the proposed formulae with FEM results for pure compression (normalised values)

Table 8.14: Statistical evaluation concerning the ratios $\rho_{proposed}/\rho_{Num}$, for pure compression (normalised values)

<i>No. of analyses</i>	<i>Proposed formulae</i>		
	<i>Mean</i>	<i>CoV (%)</i>	<i>MAE (%)</i>
1537	0.9994	2.7	8.0

Table 8.15: Statistical evaluation concerning the ratios $\rho_{Tran et al. (2012)}/\rho_{Num}$, ρ_{Tran}/ρ_{Num} , $\rho_{Tran et al. (2014)}/\rho_{Num}$ for pure compression (normalised values)

<i>No. of analyses</i>	<i>Tran et al. (2012)</i>			<i>Tran (2012)</i>			<i>Tran et al. (2014)</i>		
	<i>Mean</i>	<i>CoV (%)</i>	<i>MAE (%)</i>	<i>Mean</i>	<i>CoV (%)</i>	<i>MAE (%)</i>	<i>Mean</i>	<i>CoV (%)</i>	<i>MAE (%)</i>
1537*	0.9817	4.6	16.8	1.0106	6.5	17.1	1.0671	5.0	13.5

* Due to the limitation of the parametric range of the work by Tran *et al.* (2014) (see sec. 3.11.3), the number of analysis in this case is 212.

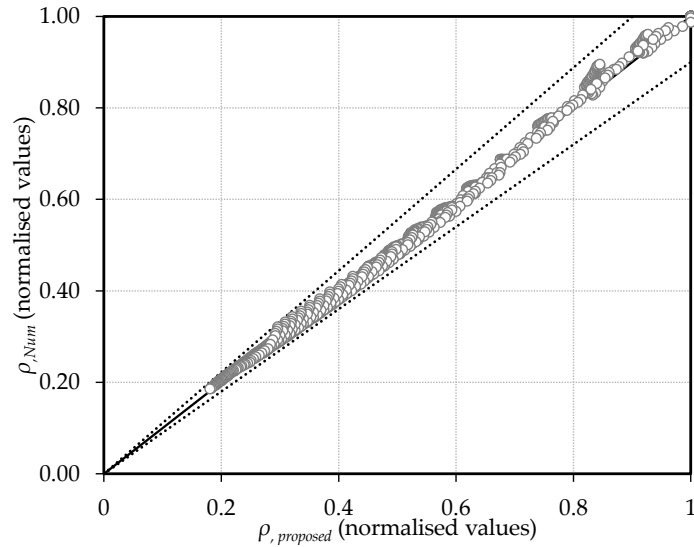


Figure 8.23: Correlation of the proposed formulae with FEM results for pure in-plane bending (normalised values)

Table 8.16: Statistical evaluation concerning the ratios $\rho_{proposed}/\rho_{Num}$ for pure in-plane bending (normalised values)

<i>No. of analyses</i>	<i>Proposed formulae</i>		
	<i>Mean</i>	<i>CoV (%)</i>	<i>MAE (%)</i>
1537	0.9993	2.0	7.8

8.6. Ultimate strength of cylindrically curved panels under generalised axial stresses

8.6.1. General

The last section dealt over the calibration of width reduction factors for cylindrically curved panels under pure compressive stresses and pure in-plane bending. For combinations of axial force and bending moment the option fell on the simplified approach of EN1993-1-5:2006 (CEN, 2006a) which stipulates that the safety of plated elements under these conditions may be checked using the ef-

fective properties calculated for axial force and bending moment acting separately. Using numerical results from sec. 5.3 and the effective properties calculated with the formulae proposed in the previous section, the level of safety of the design method of EN1993-1-5:2006 will be assessed.

8.6.2. Proposed formulae

The proposed expression to verify the level of safety of cylindrically curved panels under generalised in-plane stresses (combined effect of compression and bending) follows Eq. (8.22).

$$\eta_1 = \frac{N_{Ed}}{f_y A_{eff}} + \frac{M_{y,Ed}}{f_y W_{y,eff}} \leq 1 \quad (8.22)$$

where A_{eff} is cross section's effective area, $W_{y,eff}$ is the cross section's effective elastic section moduli according to y -direction, N_{Ed} is the design axial force and $M_{y,Ed}$ is the design bending moment. Since it is at the element level (in opposition to built-up sections), eccentricities do not participate in Eq. (8.22). As the account for eccentricities would increase the value η_1 , this option is on the safe side.

8.6.3. Statistical evaluation for short curved panels

Similarly to sec. 8.5.5, in order to evaluate whether Eq. (8.22) is or is not appropriate to evaluate the strength of cylindrically curved panels, it is compared to numerical results from the parametric study in sec. 5.3. Since in Eq. (8.22) it is required to input N_{Ed} and $M_{y,Ed}$, these values were calculated beforehand taking into account the geometry of the panels of the referred parametric study and in such a way that $\sigma_t=1$ (Eq. (8.23)). Finally, the inverse of the result given by Eq. (8.22) is compared to the respective numerical one.

$$\left\{ \begin{array}{l} \sigma_N = \frac{f_y (1 + \psi)}{2} \\ \sigma_M = \frac{f_y (1 - \psi)}{2} \end{array} \right. \quad (8.23)$$

In these previous equations, the cross-sectional effective area is calculated for the axial force acting alone and the effective elastic modulus around y -axis is calculated for the bending moment acting alone. In Figure 8.24 and in Table 8.17 the overall statistical evaluation results are shown.

It is possible to conclude that the majority of the results given by Eq. (8.22) are on the safe side (the maximum error on the unsafe side is equal to 5.9%). This is in line to what was expected: since the effective area A_{eff} is determined assuming that the cross-section is subject only to stresses due to uniform axial compression and the effective section modulus $W_{y,eff}$ is determined assuming the cross-section is subject only to bending stresses, the proposed methodology is a simplified one and, as for plates, it yields results generally on the safe side.

For a more detailed comparison of results, Figure 5.25 to Figure 8.27 show the statistical evaluation of results for $\psi=0.5$, $\psi=0$, $\psi=-0.5$. The comparison of results for $\psi=1$ and $\psi=-1$ is not shown here since it coincides with the comparison performed in sec. 8.5.5.3. Table 8.18 summarises all statistical data for all loading types (from $\psi=1$ to $\psi=-1$).

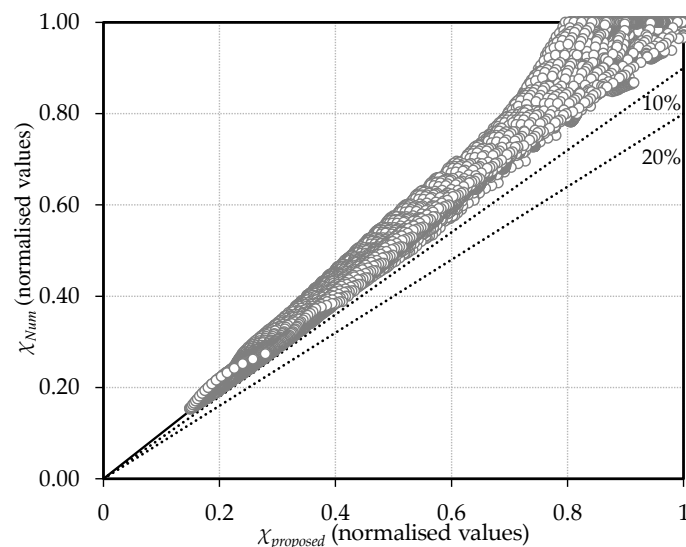


Figure 8.24: Correlation of Eq. (8.22) with FEM results for $-1 \leq \psi \leq 1$ (normalised values)

Table 8.17: Statistical evaluation concerning the ratios $\eta_{1,Eq.(8.22)}/\eta_{1,Num}$, $-1 \leq \psi \leq 1$
(normalised values)

<i>Proposed formulae</i>			
<i>No. of analyses</i>	<i>Mean</i>	<i>CoV (%)</i>	<i>Maximum error on unsafe side (%)</i>
32277	0.9606	4.7	5.9

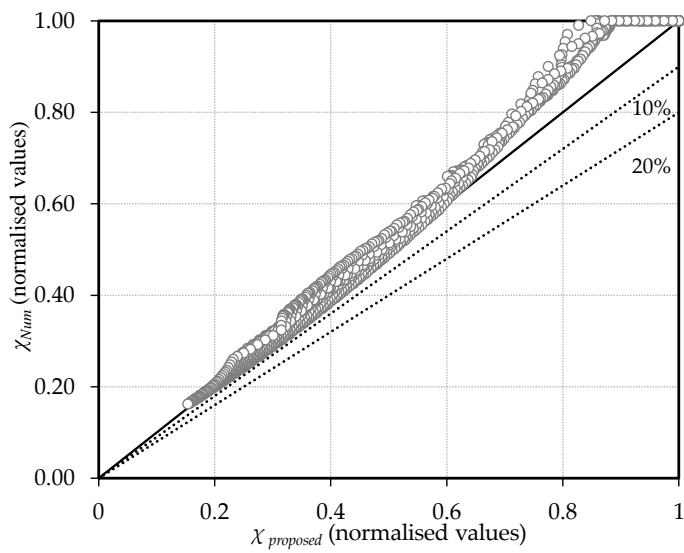


Figure 8.25: Correlation of Eq. (8.22) with FEM results for $\psi=0.5$
(normalised values)

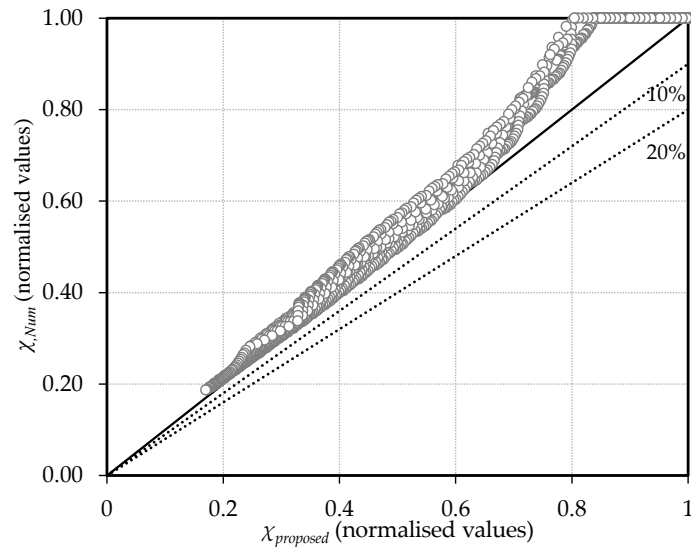


Figure 8.26: Correlation of Eq. (8.22) with FEM results for $\psi=0$ (normalised values)

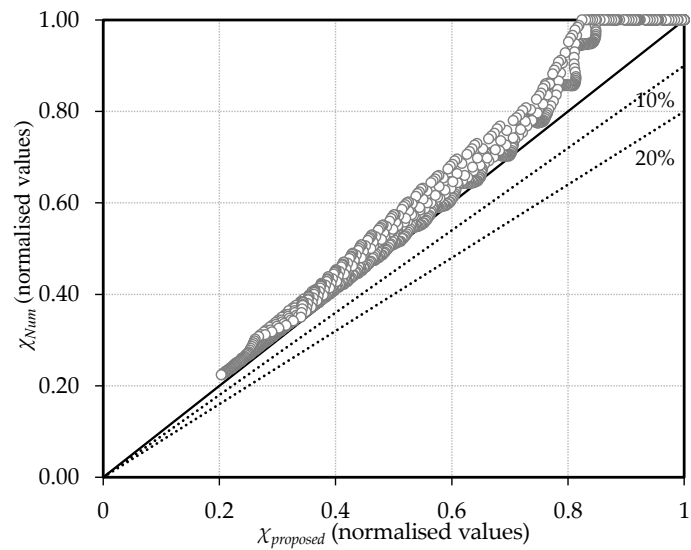


Figure 8.27: Correlation of Eq. (8.22) with FEM results for $\psi=-0.5$ (normalised values)

Table 8.18: Statistical evaluation concerning the ratios $\chi_{Eq. (8.22)}/\chi_{Num}$, $-1 \leq \psi \leq 1$
(normalised values)

<i>Type of loading, ψ</i>	<i>No. of analyses</i>	<i>Eq. (8.22)</i>		
		<i>Mean</i>	<i>CoV (%)</i>	<i>Maximum error on unsafe side (%)</i>
1	1537	0.9994	2.7	5.9
0.9	1537	0.9987	3.1	5.4
0.8	1537	0.9925	3.6	5.5
0.7	1537	0.9856	4.0	5.3
0.6	1537	0.9784	4.3	5.0
0.5	1537	0.9695	4.5	4.5
0.4	1537	0.9633	4.7	3.8
0.3	1537	0.9564	4.8	3.1
0.2	1537	0.9497	4.8	2.4
0.1	1537	0.9440	4.8	1.5
0	1537	0.9379	4.7	0.9
-0.1	1537	0.9349	4.6	0.1
-0.2	1537	0.9321	4.5	0.0
-0.3	1537	0.9308	4.3	0.0
-0.4	1537	0.9316	4.1	0.0
-0.5	1537	0.9335	3.9	0.0
-0.6	1537	0.9401	3.4	0.0
-0.7	1537	0.9487	2.9	0.0
-0.8	1537	0.9614	2.3	0.3
-0.9	1537	0.9794	1.7	1.4
-1	1537	0.9993	2.0	5.8

8.7. Detailed comparison between numerical results and proposed set of formulae for pure compression

Similarly to the study performed in 8.4, this section presents the comparison between the proposed formulae and formulae from literature for the ultimate strength of cylindrically curved panels. Once again, only formulae calibrated with results from panels having similar boundary conditions are chosen for this comparative analysis. In these conditions are the proposed formulae from Tran *et al.* (2012), Tran (2012) and Tran *et al.* (2014).

It is highlighted that this detailed analysis is limited to loading cases corresponding to pure compression (as already stated before none of the proposed formulae in the literature predicts the ultimate strength of cylindrically curved panels for loading cases other than pure compression).

The comparison between numerical results and the approaches proposed by Tran *et al.* (2012) (based on the Ayrton-Perry approach), Tran (2012) (based on EN1993-1-6:2007) and the one proposed in this study for panels with $\alpha \leq 1$ is made in Table 8.19 to Table 8.21, where detailed results are shown, and in Figure 8.28 to Figure 8.31.

As it was already concluded in Chapter 4, there are non-negligible errors between Tran's proposal, numerical results and the proposed formulae. However, the investigation of Figure 8.28 to Figure 8.31 indicates that the numerical results and the proposed formulae and Tran's proposals all have the same general trend. Here, the main reason that is thought to be the cause of the non-negligible errors is the fact that Tran's formula is calibrated with numerical results from models with $\alpha=1$, while in this study the models' aspect ratio varies with the curvature parameter. Additionally, for the second approach proposed by Tran, besides the already discussed reasons that may lead to non-negligible errors, it is pointed out the only possible conclusion: the framework of formulae from EN1993-1-6:2007 is not suitable for applications to the ultimate behaviour of cylindrically curved panels.

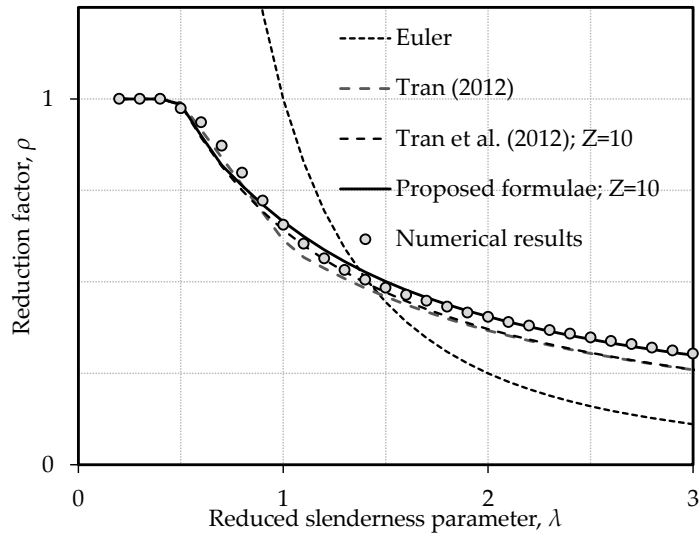


Figure 8.28: Comparison between curves proposed by Tran *et al.* (2012), Tran (2012) and proposed formulae for $Z=10$ and $\psi=1$

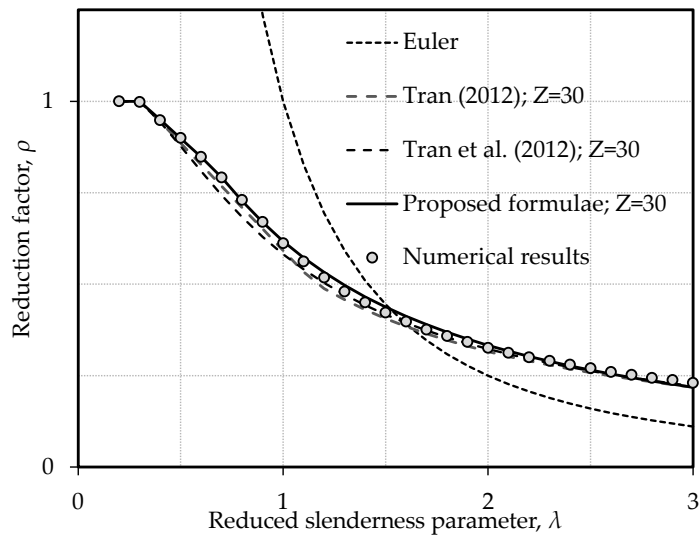


Figure 8.29: Comparison between curves proposed by Tran *et al.* (2012), Tran (2012) and proposed formulae for $Z=30$ and $\psi=1$

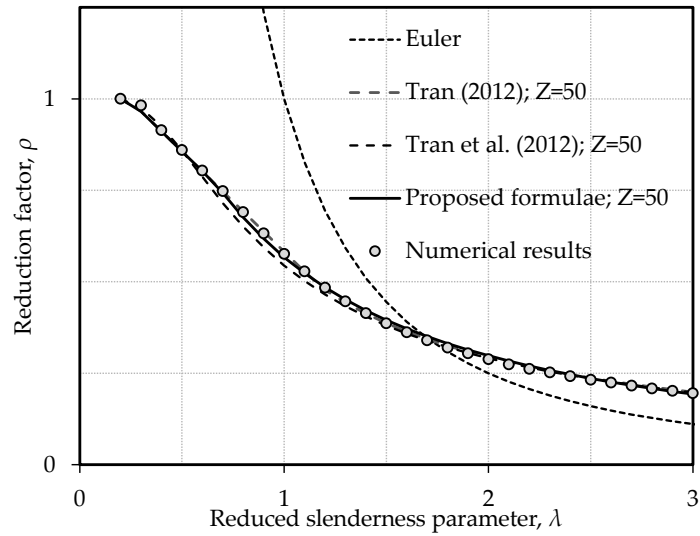


Figure 8.30: Comparison between curves proposed by Tran *et al.* (2012), Tran (2012) and proposed formulae for $Z=50$ and $\psi=1$

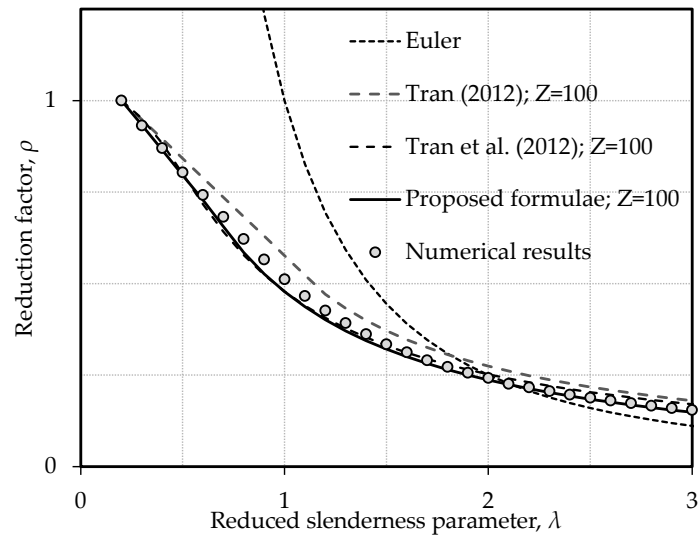


Figure 8.31: Comparison between curves proposed by Tran *et al.* (2012), Tran (2012) and proposed formulae for $Z=100$ and $\psi=1$

Table 8.19: Comparison between the approaches by Tran *et al.* (2012), Tran (2012) and proposed formulae for $\lambda=1$ and $\psi=1$

Curvature, Z	Z=10	Z=30	Z=50	Z=80	Z=100
χ_{Num}	0.656	0.612	0.576	0.530	0.512
$\chi_{Proposed}$	0.665	0.618	0.567	0.508	0.478
Error (%)	+1.3	+0.9	-1.6	-4.2	-7.2
$\chi_{Tran\ et\ al.\ (2012)}$	0.642	0.582	0.544	0.494	0.478
Error (%)	-2.1	-5.2	-5.8	-7.3	-7.0
$\chi_{Tran\ (2012)}$	0.614	0.592	0.582	0.578	0.576
Error (%)	-6.8	-3.4	+1.1	+8.2	+11.2

Table 8.20: Comparison between the approaches by Tran *et al.* (2012), Tran (2012) and proposed formulae for $\lambda=2$ and $\psi=1$

Curvature, Z	Z=10	Z=30	Z=50	Z=80	Z=100
χ_{Num}	0.404	0.326	0.288	0.254	0.242
$\chi_{Proposed}$	0.405	0.333	0.298	0.258	0.236
Error (%)	+0.2	+2.0	+3.3	+1.4	-2.4
$\chi_{Tran\ et\ al.\ (2012)}$	0.371	0.323	0.291	0.261	0.252
Error (%)	-8.9	-1.0	+1.0	+2.7	+3.9
$\chi_{Tran\ (2012)}$	0.367	0.316	0.294	0.279	0.274
Error (%)	-10.1	-3.2	+2.0	+8.9	+11.8

Table 8.21: Comparison between the approaches by Tran *et al.* (2012), Tran (2012) and proposed formulae for $\lambda=3$ and $\psi=1$

Curvature, Z	Z=10	Z=30	Z=50	Z=80	Z=100
χ_{Num}	0.304	0.230	0.195	0.165	0.154
$\chi_{Proposed}$	0.299	0.218	0.193	0.164	0.148
Error (%)	-1.5	-5.4	-1.3	-1.1	-4.2
$\chi_{Tran\ et\ al.\ (2012)}$	0.260	0.222	0.197	0.177	0.170
Error (%)	-16.8	-3.8	+0.9	+6.3	+9.3
$\chi_{Tran\ (2012)}$	0.260	0.218	0.198	0.184	0.180
Error (%)	-17.1	-5.3	+1.5	+10.3	+14.3

Table 8.22: Comparison between the approach by Tran *et al.* (2014) and proposed formulae

Slender-ness, λ	Curvature, Z	Aspect ratio, α	Numerical results	Proposed formulae	Error (%)	Tran <i>et al.</i> (2014)	Error (%)
1.0	10	0.9	0.656	0.665	+1.3	0.730	+10.1
	30	0.54	0.612	0.618	+0.9	0.593	-3.3
	50	0.4	0.576	0.567	-1.6	0.526	-9.5
	80	0.3	0.530	0.508	-4.2	0.484	-9.6
	100	0.28	0.512	0.478	-7.2	0.477	-7.4
2.0	10	0.9	0.484	0.501	+0.2	0.558	+13.2
	30	0.54	0.422	0.437	+2.0	0.438	+3.6
	50	0.4	0.386	0.395	+3.3	0.379	-1.8
	80	0.3	0.350	0.346	+1.4	0.340	-3.0
	100	0.28	0.334	0.321	-2.4	0.332	-0.5
3.0	10	0.9	0.404	0.405	-1.5	0.455	+11.3
	30	0.54	0.326	0.333	-5.4	0.350	+6.7
	50	0.4	0.288	0.298	-1.3	0.297	+3.0
	80	0.3	0.254	0.258	-1.1	0.260	+2.4
	100	0.28	0.242	0.236	-4.2	0.253	+4.5

The approach developed by Tran *et al.* (2014), besides accounting for the curvature and the slenderness (represented by the thickness to width ratio), allows accounting for the influence of the aspect ratio (Eq. (3.45)). For that reason in Table 8.22 the value of aspect ratio is presented. Since the manner to express the panel's slenderness is different from the proposed formulae, the geometric parameter defined by the thickness to width ratio is also presented.

It is concluded, similarly to the two previous methods for computing the ultimate strength of cylindrically curved panels, that there are non-negligible errors between Tran *et al.* (2014) proposal and numerical results. These errors are thought to be originated from the fact that many examples given in Table 8.22 fall outside the parametric range in Tran *et al.* (2014) work (see sec. 3.11.3).

8.8. Application of proposed methodology to the design of cross-sections using the effective width method

8.8.1. General

In order to determine the ultimate strength of cross-sections built-up with slender cylindrically curved panels subject to direct stresses by the effective²³ width method, the effective widths of all plate/panel elements in compression and or in bending are determined separately using the proposed approach in sec. 8.2 (or sec. 8.3) and 8.5. From these effective widths the effective geometric properties (*i.e.* effective position of the centre of gravity, effective cross-section area A_{eff} , effective second moment of area I_{eff} and effective elastic section modulus W_{eff}) are obtained. Finally, similarly to what is advocated by EN1993-1-5:2006, the resistance check is performed determining the utilisation factor using Eq. (8.24)

$$\eta_1 = \frac{N_{Ed}}{f_y A_{eff}} + \frac{M_{y,Ed} + N_{Ed} e_{y,N}}{f_y W_{y,eff}} + \frac{M_{z,Ed} + N_{Ed} e_{z,N}}{f_y W_{z,eff}} \leq 1 \quad (8.24)$$

²³ In this study shear lag effects are discarded and only local buckling phenomena are considered.

In short, Figure 8.32 presents schematically the design of cross-sections built-up with cylindrically curved panels subject to axial compression and uniaxial bending.

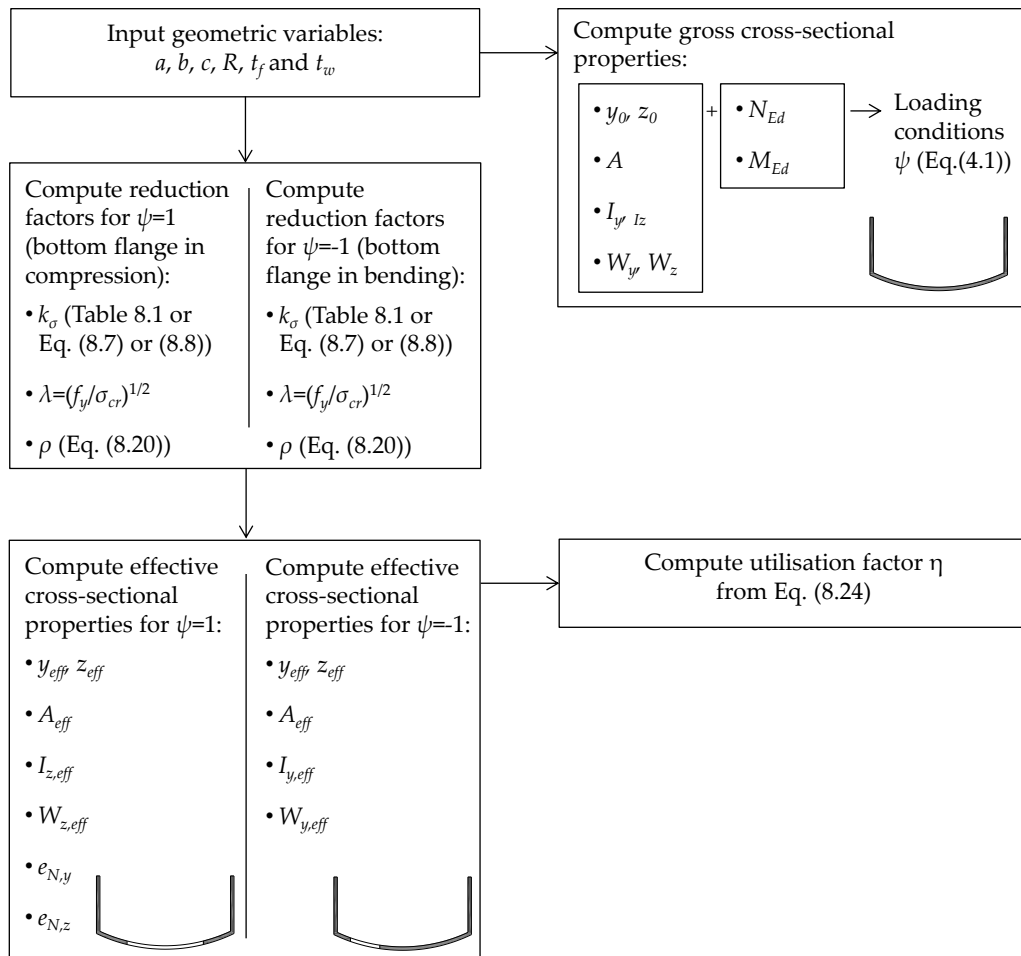


Figure 8.32: Design flowchart for cross-sections built-up with cylindrically curved panels

8.8.2. Box-girder bridge design examples

In this section, five different cross-sections having curved bottom flanges with increasing curvature (from $Z=0$ to $Z=100$) under four loading conditions are analysed. The analysed sections are part of possible box-girder bridge configu-

rations as suggested by Figure 8.33. It is assumed that the box-girder is being launched (therefore not having the benefit of the composite action) and, for the sake of simplicity, it is assumed also that the upper flanges are not accounted for in calculations. It is also assumed that a horizontal wind load is acting on the box-girder. The wind load (which is responsible for the curved bottom flange in bending, $\psi=-1$) together with the gravity load (which is responsible for the curved bottom flange in compression, $\psi=1$) produce a state-of-stress of combined direct stresses in a cross-section incorporating a curved element.

Additionally, in order to evaluate only the effect of the width reduction of the bottom cylindrically curved steel panel, webs are sized to be at least class 3²⁴ therefore not having any width reduction due to local buckling phenomena. The geometry of the design examples is fully described by Figure 8.33 and Table 8.23.

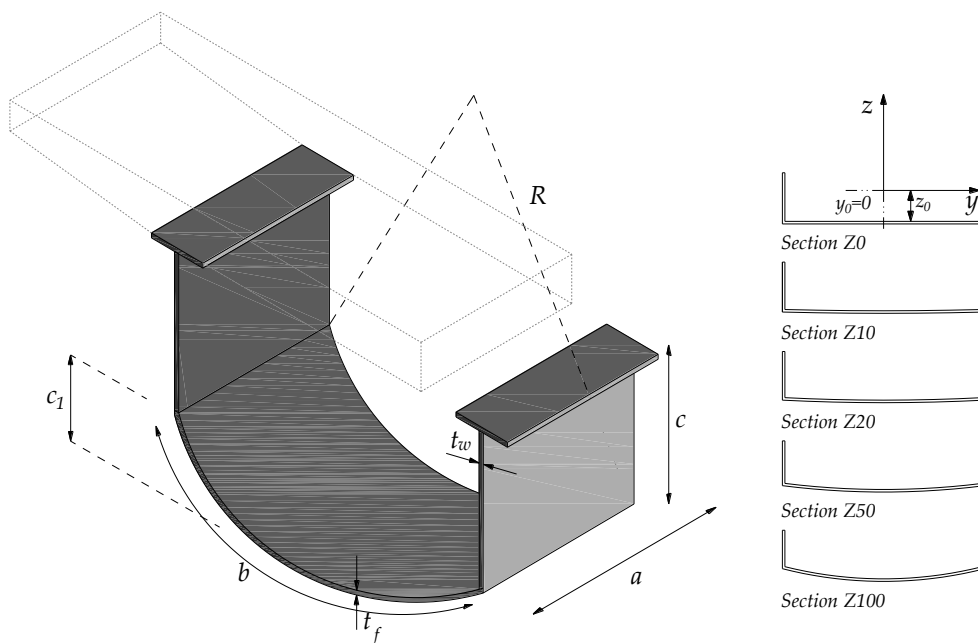


Figure 8.33: Generic cross-section under analysis

²⁴ Class 3 of outstand compression elements is defined in EN1993-1-1:2005 (CEN, 2005).

Following the notation in the Eurocodes, namely the notation in clause 1.7 of EN1993-1-1:2005 (CEN, 2005), the x -direction is defined as the direction along the member, y -direction is parallel to the flanges and z -direction is perpendicular to the flanges.

Table 8.23: Cross-section dimensions

	<i>Section Z0</i>	<i>Section Z10</i>	<i>Section Z20</i>	<i>Section Z50</i>	<i>Section Z100</i>
b	2000 mm	2000.8 mm	2003.3 mm	2020.6 mm	2079.2 mm
a			1000 mm		
R	-	20016.7 mm	10033.3 mm	4082.6 mm	2161.6 mm
Z	0	10	20	50	100
t_f			20 mm		
c	500 mm	475 mm	450 mm	375.6 mm	254.8 mm
c_t	0 mm	25 mm	50 mm	124.4 mm	245.2 mm
t_w			50 mm		

Following the flowchart in Figure 8.32, the design starts with the input of the basic geometric dimensions (width b , length a , radius of curvature R , thickness of the flange t_f , width of the webs c and thickness of the webs t_w) given in Table 8.23. It is pointed out the fact that with these dimensions the gross cross-sections' total width and depth are constant in all analysed cross-sections (*i.e.* the alignment of both webs is fixed varying their height; this means that the width of the curved element is also variable). This allows performing a direct comparison between all different cross-sections based on the utilisation factor given by Eq. (8.24) (where the utilisation factor is divided by the gross area).

As the flowchart indicates (Figure 8.32), the gross cross-sectional properties are calculated first. These properties were calculated using an iterative procedure that was implemented following Nakai & Yoo (1988) and are given in Table 8.24.

Table 8.24: Gross cross-sectional properties

	<i>Section Z0</i>	<i>Section Z10</i>	<i>Section Z20</i>	<i>Section Z50</i>	<i>Section Z100</i>
<i>Centroid, y_0</i>			0.00 mm		
<i>Centroid, z_0</i>	138.9 mm	146.3 mm	153.1 mm	171.9 mm	192.7 mm
<i>Area, A</i>	9.00 E+04 mm ²	8.75 E+04 mm ²	8.51 E+04 mm ²	7.80 E+04 mm ²	6.71 E+04 mm ²
<i>Second moment of area, I_y</i>	2.43 E+09 mm ⁴	2.30 E+09 mm ⁴	2.18 E+09 mm ⁴	1.92 E+09 mm ⁴	1.69 E+09 mm ⁴
<i>Second moment of area, I_z</i>	6.34 E+10 mm ⁴	6.09 E+10 mm ⁴	5.84 E+10 mm ⁴	5.12 E+10 mm ⁴	3.98 E+10 mm ⁴
<i>Elastic section modulus, W_y (bottom)</i>	6.73 E+06 mm ³	6.50 E+06 mm ³	6.30 E+06 mm ³	5.87 E+06 mm ³	5.51 E+06 mm ³
<i>Elastic section modulus, W_z</i>	6.34 E+07 mm ³	6.09 E+07 mm ³	5.84 E+07 mm ³	5.12 E+07 mm ³	3.98 E+07 mm ³

The next steps are to compute the effective with reduction factors for pure compression and pure in-plane bending (around z -axis, see Figure 8.33) using the methods described in the previous sections.

Specifically, to compute the elastic critical stress and slenderness parameter, the method proposed in sec. 8.2 was followed; in what concerns the reduction factor, the method proposed in sec. 8.5 was followed. Table 8.25 and Table 8.26 show the reduction factors for the curved panel element obtained for pure compression and pure in-plane bending, respectively. Figure 8.34 shows generic effective cross-sections resulting from the application of the computed reduction factors for the curved panel element.

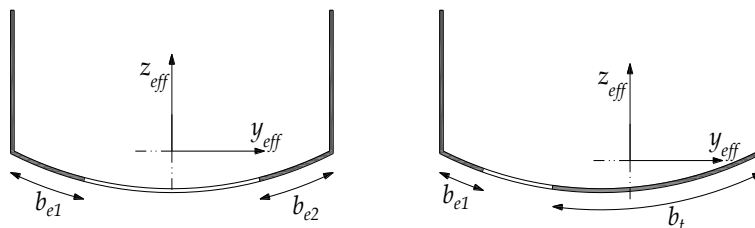
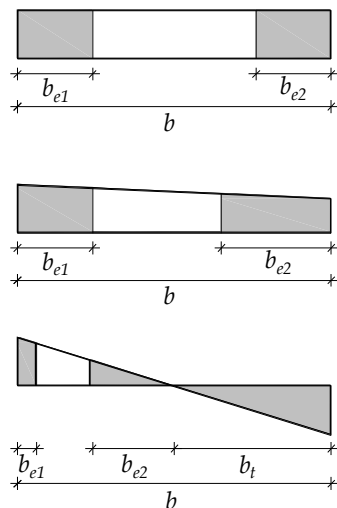
**Figure 8.34:** Generic effective cross-section for $\psi=1$ and $\psi=-1$

Table 8.25: Cylindrically curved panel reduction factors for $\psi=1$

	Section Z0	Section Z10	Section Z20	Section Z50	Section Z100
k_{σ} , Table 8.1	4.00	5.07	7.45	16.16	30.31
λ	2.163	1.922	1.588	1.087	0.817
$\rho_{Eq. (8.20)}$ (reduction of bottom flange)	0.415	0.417	0.442	0.529	0.575

Table 8.26: Cylindrically curved panel reduction factors for $\psi=-1$

	Section Z0	Section Z10	Section Z20	Section Z50	Section Z100
k_{σ} , Table 8.1	23.88	25.58	29.26	42.99	63.33
λ	0.885	0.855	0.801	0.665	0.565
$\rho_{Eq. (8.20)}$ (reduction of bottom flange)	0.989	0.946	0.931	1.000	1.000



$$\psi = 1$$

$$b_{eff} = \rho b$$

$$b_{e1} = b_{e2} = 0.5 b_{eff}$$

$$0 \leq \psi < 1$$

$$b_{eff} = \rho b$$

$$b_{e1} = \frac{2}{5 - \psi} b_{eff} \quad b_{e2} = b_{eff} - b_{e1}$$

$$\psi < 0$$

$$b_{eff} = \rho b_c = \frac{\rho b}{1 - \psi}$$

$$b_{e1} = 0.4 b_{eff} \quad b_{e2} = 0.6 b_{eff}$$

Figure 8.35: Internal effective widths according to EN1993-1-5:2006 (CEN, 2006a)

Having the effective dimensions of the bottom curved flange (b_{e1} , b_{e2} and b_t are computed following Table 4.1 of EN1993-1-5:2006 and Figure 8.35) it is possible to compute the properties of the effective cross-section which are given in Table 8.27 and Table 8.28 for pure compression and pure in-plane bending, respectively.

Finally, the utilisation factor is obtained from Eq. (8.24) and it is given in Table 8.29 for the four different load cases and it is plotted in Figure 8.36.

Table 8.27: Effective cross-sectional properties for $\psi=1$

	<i>Section Z0</i>	<i>Section Z10</i>	<i>Section Z20</i>	<i>Section Z50</i>	<i>Section Z100</i>
<i>Centroid, $y_{0,eff}$</i>			0.00 mm		
<i>Centroid, $z_{0,eff}$</i>	187.64 mm	198.4 mm	206.1 mm	224.5 mm	256.3 mm
<i>Effective elastic section modulus, $W_{y,eff}$</i>	5.83 E+06 mm ³	5.45 E+06 mm ³	5.16 E+06 mm ³	4.56 E+06 mm ³	3.82 E+06 mm ³

Table 8.28: Effective cross-sectional properties for $\psi=-1$

	<i>Section Z0</i>	<i>Section Z10</i>	<i>Section Z20</i>	<i>Section Z50</i>	<i>Section Z100</i>
<i>Centroid, $y_{0,eff}$</i>	1.5 mm	7.4 mm	9.8 mm	0.0 mm	0.0 mm
<i>Centroid, $z_{0,eff}$</i>	139.2 mm	148.0 mm	155.6 mm	171.9 mm	192.7 mm
<i>Effective elastic section modulus, $W_{z,eff}$</i>	6.32 E+07 mm ³	6.00 E+07 mm ³	5.73 E+07 mm ³	5.12 E+07 mm ³	3.98 E+07 mm ³

Table 8.29: Utilisation factor according to Eq. (8.24) for different load cases

	<i>Loading type 1</i>	<i>Loading type 2</i>	<i>Loading type 3</i>	<i>Loading type 4</i>
	$M_{y,Ed} = 1500\text{kNm}$	$M_{y,Ed} = 2000\text{kNm}$	$M_{y,Ed} = 1000\text{kNm}$	$M_{y,Ed} = 0\text{kNm}$
	$M_{z,Ed} = 0\text{kNm}$	$M_{z,Ed} = 450\text{kNm}$	$M_{z,Ed} = 1000\text{kNm}$	$M_{z,Ed} = 9500\text{kNm}$
	$\eta^l, \text{Eq. (8.24)}$	$\eta^l, \text{Eq. (8.24)}$	$\eta^l, \text{Eq. (8.24)}$	$\eta^l, \text{Eq. (8.24)}$
<i>Section Z0</i>	0.725	0.986	0.528	0.424
<i>Section Z10</i>	0.775	1.054	0.564	0.446
<i>Section Z20</i>	0.818	1.113	0.595	0.467
<i>Section Z50</i>	0.927	1.261	0.673	0.523
<i>Section Z100</i>	1.105	1.506	0.808	0.673

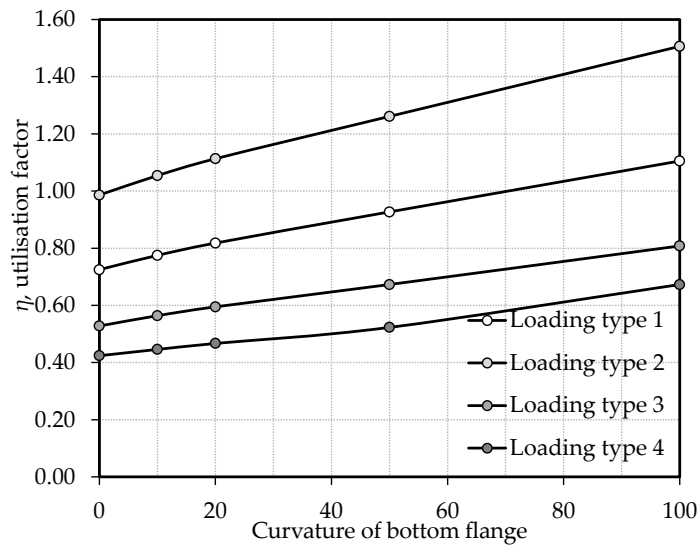


Figure 8.36: Evolution of the utilisation factor according to Eq. (8.24) with the increase of the curvature of the bottom flange

From the analysis of both Figure 8.36 and Table 8.29 it is possible to infer that the higher the curvature, the higher the utilisation factor is (*i.e.* the less resistance the section is). At a first glance, it may appear curvature has a negative

effect on the resistance of cross-sections. In fact, the analysed cross-sections' area is not constant and therefore the comparison is biased. In an attempt to solve this issue, the results given in Table 8.29 are normalised to the area of the Z0 section (Table 8.30).

Table 8.30: Normalised utilisation factor according to Eq. (8.24) for different load cases

	<i>Loading type 1</i>	<i>Loading type 2</i>	<i>Loading type 3</i>	<i>Loading type 4</i>
	$M_{y,Ed} = 0 \text{ kNm}$	$M_{y,Ed} = 450 \text{ kNm}$	$M_{y,Ed} = 1000 \text{ kNm}$	$M_{y,Ed} = 9500 \text{ kNm}$
	$M_{z,Ed} = 1500 \text{ kNm}$	$M_{z,Ed} = 2000 \text{ kNm}$	$M_{z,Ed} = 1000 \text{ kNm}$	$M_{z,Ed} = 0 \text{ kNm}$
	$\eta_{1,Eq. (8.24)} \frac{A_{Zi}}{A_{Z0}}$	$\eta_{1,Eq. (8.24)} \frac{A_{Zi}}{A_{Z0}}$	$\eta_{1,Eq. (8.24)} \frac{A_{Zi}}{A_{Z0}}$	$\eta_{1,Eq. (8.24)} \frac{A_{Zi}}{A_{Z0}}$
<i>Section Z0</i>	0.725	0.986	0.528	0.424
<i>Section Z10</i>	0.753	1.025	0.548	0.434
<i>Section Z20</i>	0.773	1.052	0.563	0.442
<i>Section Z50</i>	0.803	1.093	0.583	0.453
<i>Section Z100</i>	0.824	1.123	0.602	0.502

From the analysis of Table 8.30 it may be concluded that, in fact, curvature as a negative effect on the resistance of cross-sections but not as severe as at initially perceived. Additionally, concerning the ultimate strength of cross-sections, the following two aspects are worth to be mentioned:

- Firstly, at the same time curvature is increased all the properties of the gross cross-section decrease (Table 8.24), meaning that for the same load level, cross-sections with curved bottom flange will typically present higher utilisation factors;
- Secondly, as already discussed in sec. 5.3 for curved elements (see Figure 5.24 to Figure 5.27). In these graphs it is seen that for constant b/t ratio the ultimate strength decreases from $Z=0$ to $Z=10-20$, reversing this trend in the range from $Z=10-20$ to $Z=100$. Since in the examples webs are sized to be at least class 3, it is fair to assume that, if the cross-sectional area is

constant, then the ultimate strength of cross-sections will follow the same trend.

Finally, it should be highlighted that the use of steel box-girders with cylindrically curved bottom flanges has some advantages like enhanced aerodynamic behaviour (*e.g.* Stonecutters bridge (Janjic, 2008)), aesthetics, etc.

8.9. Summary

In this chapter the new proposals to compute the elastic critical stress and the ultimate load of cylindrically curved steel panels were presented.

Firstly, a new methodology for computing the elastic critical stress of cylindrically curved panel under generalised axial compressive stresses (from pure axial compression to pure in-plane bending) was proposed. This new expressions were derived with the same structure as those currently proposed by EN1993-1-5:2006 (CEN, 2006*a*). It is assumed that non-negligible errors arise when the aspect ratio increases. Nevertheless, these errors will vanish during the calibration process of the new expressions proposed for computing the ultimate load of cylindrically curved steel panels. In parallel, simple closed-formed analytical solutions obtained from the study performed in Chapter 7 were also proposed to compute the elastic critical stress of cylindrically curved panels. These expressions have the advantage of considering the aspect ratio and allowing a physical interpretation of results as they are directly derived from an exact energy formulation (the only source of error is intrinsic to the choice of the displacement functions, as already discussed in Chapter 7). The downside of these expressions is that, even though they are quite simple to implement, they yield considerably larger errors than the numerically calibrated proposed methodology.

Secondly, new expressions for computing the ultimate load of cylindrically curved steel panels under pure axial compression and pure in-plane bending are proposed based on the effective width method. They are also based on the

slenderness parameter computed through the previously proposed numerically calibrated method for the elastic critical stress.

It should be mentioned that, while for curved panels under pure axial compressive stresses these new methods are an improvement of previously proposed ones, for curved panels under combinations of pure compression and in-plane bending they are entirely innovative. Additionally, as it has been shown, the use of Eq. (8.22) allows a safe evaluation of the ultimate strength of cylindrically curved panels.

In what concerns the design of cross-sections incorporating cylindrically curved panels by the effective width method, simple examples were solved and explained in detail. In what concerns their accuracy, it is expected that in the near future, these results will be validated against numerical and experimental studies.

Finally, it should be highlighted that both methods to evaluate the elastic critical stress and the method to evaluate the ultimate strength of curved panels under generalised axial compression have been statistically evaluated against own numerical results and compared to previous works of other authors.

9. Summary and future research

9.1. Conclusions

Overall, the stability behaviour of cylindrically curved panels under direct stresses was studied. In fact, the performed research is the first to comprehensively incorporate a large range of key parameters that influence the behaviour of cylindrically curved panels. Specifically, the following aspects were thoroughly analysed throughout the thesis:

- **Influence of the boundary conditions type** on the elastic critical and ultimate behaviour: firstly, in opposition to plates, the elastic critical stress depends on whether the edges are or not constrained; secondly, it was concluded that while boundary conditions type 1 represent the lower bound of results for both the elastic critical stress and the ultimate stress, boundary conditions type 3 represent the upper bound;
- **Influence of aspect ratio** on the eigenmode, elastic critical and ultimate behaviour: together with curvature, this parameter is one of the most important parameters due to the fact that, firstly, in the range of short panels, for each value of the curvature parameter there is a value of aspect ratio that minimises the elastic buckling factor ($k_{\sigma,min}$); secondly, if only square panels are considered it was concluded that curved panels with a curvature parameter lower than 23 buckle in a different manner when compared to those with a curvature parameter more higher than 23 (one longitudinal half-wave *vs.* many longitudinal half-waves); and finally, it should be said that another important stud-

ied parameter, geometric imperfections, is closely related to the aspect ratio as the pattern is directly determined by the combination of aspect ratio and curvature;

- **Influence of the loading type** (direct stresses ranging from pure axial compression to pure in-plane bending and biaxial compression) on the elastic critical and ultimate behaviour;
- **Influence of the pattern and amplitude of geometric imperfections** on ultimate behaviour: to this parameter an entire chapter was devoted where an extensive parametric study allowed to conclude that, for cylindrically curved panels, geometric imperfections have a strong impact on their ultimate strength (in fact, cylindrically curved panels characterised by a curvature parameter equal to 30 present the highest sensitivity to geometric imperfections); additionally, it was concluded that, if the lowest resistance possible is intended to be obtained, the choice for the first buckling mode is not a correct one the majority of times (the first buckling mode returns the lowest value for the ultimate load factor only for 30% of the times, while the second returns for 34% of the times); finally, as a general trend it can be concluded that cylindrically curved panels characterised by higher curvature parameter are more sensitive to the amplitude of initial imperfection amplitude;
- **Influence of the curvature** on the overall behaviour of cylindrically curved panels: curvature is the most important parameter in this research; in fact all other parameters are studied together with curvature. The main conclusions about the effect of curvature on the behaviour of cylindrically curved panels are: firstly, curvature dictates the buckling shape (which is crucial for the imperfection sensitivity study); secondly, the higher the curvature parameter is the higher the elastic critical stress and the lower the reduction curve ($\rho-\lambda$ or $\chi-\lambda$) is. Nevertheless, as concluded at the end of sec. 5.3, the higher the curvature, the higher the resistance of cylindrically curved panels with the same b/t ratio is.

To reach the initially proposed objectives, early chapters shed light into the topics that this research involves. Supported by those chapters where the numeri-

cal, parametric and analytical studies are defined, new design methodologies, which significantly improve the accuracy of previous ones and establish new expressions to deal with some particular load cases (namely pure compression combined with pure in-plane bending), were proposed. The adopted strategy was to follow as closely as possible the rules proposed in EN1993-1-5:2006. In fact, one of the conclusions is that the behaviour of cylindrically curved panels is more similar to flat plates rather than shells of revolution. For that reason, the proposed methodology to compute the ultimate strength is based on the effective width method and it has a similar framework to EN1993-1-5:2006. In a broad way, the methodology comprises formulae:

- To compute the elastic critical stress of cylindrically curved panels under uniaxial compressive stresses. In this proposed methodology, a large number of numerical linear buckling analyses of curved panels with boundary conditions type 2 were used to derive new expressions. To simplify the interpretation of new expressions, these are organised in a similar way to EN1993-1-5:2006 (CEN, 2006a). Additionally, expressions suitable to compute the elastic critical stress of cylindrically curved panels with boundary conditions type 2 and 3 are also derived, but exclusively recurring to analytical methods. This expression results from an energy formulation which, using additional degrees-of-freedom, may be used to obtain the elastic critical stress of short and long curved panels (from aspect ratios equal to 0.2 up to 4.0) with boundary conditions type 2 and 3 under pure compressive stresses.;
- To compute the ultimate load of short and long cylindrically curved panels under pure compression and pure in-plane bending. As for the methodology for computing the elastic critical stress of cylindrically curved panels, this one is also based on numerical results. For long curved panels, due to an unexpected effect of geometric imperfections (that was thoroughly analysed in Chapter 6), the calibration of a correction factor applied to results for short curved panels was necessary. Furthermore, the effect of geometric imperfections was thoroughly examined. The main conclusions were that the postbuckling path and the ultimate load

are very sensitive to imperfections amplitude and pattern also depending strongly on the curvature parameter and aspect ratio (as stated before, the highest sensitivity to geometric imperfections is obtained for long cylindrically curved panels characterised by a curvature parameter, Z , around 30). Additionally, the application of proposed formulae to cross-sections in which the curved bottom flange is under combinations of pure compression and in-plane bending was also addressed.

Albeit without a new proposed methodology, the structural response of cylindrically curved panels under biaxial loading was also studied. Among other, it was concluded that the reduction on the ultimate strength of cylindrically curved panels is more pronounced when stresses in the less stiff direction (*i.e.* the circumferential direction) are dominant.

9.2. Future research

The development of new knowledge raises invariably new questions. Not surprisingly, during the research presented in this work several unexpected problems have arose. Some of them were answered, but some are still open questions waiting for new research to tackle them. The following direct questions are believed to be dealt with in the near future:

- Calibration of a safety factor for the proposed formulae in sec. 8.6;
- Comprehensive studies (both numerical and experimental) on the behaviour of cross-sections incorporating cylindrically curved panels. The experimental tests will be performed on isolated cylindrically curved panels and on structures or substructures incorporating cylindrically curved steel panels (*e.g.* box-girder bridge segments). These experimental results are necessary to fully validate new proposals and to further evaluate their safety level;
- Development of new interaction formulae for cylindrically curved steel panels under biaxial loading. This is believed to be possible by adapting the existent interaction formula proposed by Braun (2010) for plates. This will be done by calibrating an interaction factor (V in Braun's pro-

positional, see Eq. (3.33)) and by proposing a new expression able to compute the reduction factor ρ_z in z-direction (circumferential compression);

- Extension of the energy formulation to cover and predict the postbuckling behaviour of cylindrically curved panels under compressive stresses;

Besides these direct questions, others appear as promising and challenging future research work:

- Study of cylindrically curved steel panels under combined non-uniform compression and shear loading: besides introductory works of Featherston & Ruiz (1998), Featherston (2000) and Featherston (2003), there is no more references and, to the best of the author's knowledge, there is no interaction formulae dealing with isolated cylindrically curved panels under combined non-uniform compression and shear loading;
- Study of cylindrically curved panels under combined non-uniform and out-of-plane pressure: offshore construction design standards (namely DNV-RP-C202) have interaction formulae which are suitable to compute the ultimate strength of full revolution cylinders in which the buckling of curved panels is seen as a possible failure mode.

Overall, these loading conditions (combinations of compression, shear loading and pressure) are very common in submerged substructures of offshore facilities. Nevertheless, this topic will always be a stimulating one because it is still required to translate these rules to onshore construction. As highlighted in some chapters, boundary conditions for offshore structures are not necessarily the same for bridge and building construction. Additionally, safety levels and reliability indexes are not equal for both offshore and onshore construction.

9.3. Original contributions

The main original contribution of this thesis is the proposal of a methodology that allows verifying the level of safety of cross-sections built-up with cylindrically curved panels under several loading arrangements (from pure com-

pression to biaxial bending). Specifically, the following original contributions are highlighted:

- Derivation of a set of formulae capable of accurately predicting the minimum value of elastic critical buckling factor of cylindrically curved panels under compressive stresses (from pure axial compression to pure in-plane bending) and with boundary conditions type 2;
- Derivation of simple analytical expression able to compute accurately the minimum value of elastic buckling factor of cylindrically curved panels under pure axial compressive stresses and with boundary conditions type 2 and 3;
- Derivation of simple analytical expression able to compute accurately the value of elastic buckling factor of cylindrically curved panels with varying aspect ratio and curvature parameter up to 10 ($0.2 \leq \alpha \leq 1$ and $Z \leq 10$) under pure axial compressive stresses and with boundary conditions type 2 and 3;
- Modification of expressions from EN1993-1-5:2006 and EN1993-1-6:2007 to compute the maximum amplitude of initial equivalent geometric imperfections in cylindrically curved panels for numerical analysis purposes;
- Development of a set of new expressions based on the effective width method to accurately compute the ultimate strength of cylindrically curved panels and cross-sections built-up with cylindrically curved panels under combinations of pure compression and bending;

9.4. Publications

The following publications have, to this point, resulted from the research work presented in this thesis:

Journal papers:

- Martins, J. P., Simões da Silva, L., Reis, A. (2013) Eigenvalue analysis of cylindrically curved under compressive stresses – extension of rules from EN1993-1-5. *Thin-Walled Structures*, 68, 183–194;

- Martins, J. P., Simões da Silva, L., Reis, A. (2014) Ultimate load of cylindrically curved panels under in-plane compression and bending – Extension of rules from EN1993-1-5. *Thin-Walled Structures*, 77, 36–4;
- Martins, J. P., Simões da Silva, L., Marques, L. and Pircher, M. (2014), Eigenvalue analysis of curved sandwich panels loaded in uniaxial compression. *Romanian Journal of Technical Sciences* (in press).
- Martins, J. P., Beg, D., Sinur, F., Simões da Silva, L. and Reis, A. Imperfection sensitivity of cylindrically curved steel panels. (Submitted to *Thin-Walled Structures* for publication on 21st October, 2014).

Conference Proceedings:

- Martins, J. P., Simões da Silva, L. and Reis, A. (2011) Efeito da geometria na resistência de painéis curvos em aço. In: *VIII Congresso de Construção Metálica e Mista*, Guimarães, Portugal. pp. 365-362 (in portuguese);
- Martins, J. P. and Simões da Silva (2012) Eigenvalue Analysis of Sandwich Panels Loaded in Uniaxial Compression. In: *6th International Conference on Coupled Instabilities in Metal Structures*, Glasgow, Scotland. pp. 603-610;
- Martins, J. P., Luís Simões da Silva and Reis, A. (2013) Determinação da resistência última de placas curvas em aço. In: *IX Congresso de Construção Metálica e Mista, I Congresso Luso-Brasileiro de Construção Metálica Sustentável*, Porto, Portugal. pp. 507-516 (in portuguese);
- Martins, J. P., Beg, D., Sinur, F., Simões da Silva, L. (2014) Imperfection sensitivity analysis of cylindrically curved steel panels. In: *Eurosteel 2014 – 7th European Conference on Steel Structures*, Naples, Italy. Paper 08-173.

TWG 8.3 Meeting Presentations:

- Martins, J. P. and Simões da Silva, L. (2011) Effect of geometry on the resistance of curved panels, 12th Official meeting, May 6th, Paris;
- Martins, J. P. and Simões da Silva, L. (2012) Eigenvalue analysis of cylindrically curved panels under compressive stresses, 15th Official meeting, October 26th, Liège;

- Martins, J. P. and Simões da Silva, L. (2013) Ultimate load of cylindrically curved panels under compressive stresses, 16th Official meeting, March 15th, Barcelona;
- Martins, J. P., Simões da Silva, L. and Beg, D. (2013) Imperfection sensitivity study on long cylindrically curved panels, 17th Official meeting, October 4th, Berlin;
- Martins, J. P., Simões da Silva, L. and Sinur, F. (2014) Ultimate resistance of long cylindrically curved panels: Influence of geometric imperfections, 18th Official meeting, March 21st, Bratislava;

Other Publications not related to the work presented in this thesis:

- Simões da Silva, L., Marques, L. and Martins, J. P. (2011) Stability and Design of Thin-walled Steel Shells. In: *6th International Conference on Thin-Walled Structures*, Timisoara, Romania. pp. 87-98. (Keynote Lecture);
- Jordão, S., Pinho, M., Martins, J. P., Santiago, S. (2013) Modelação numérica de vigas de vidro laminado. In: *IX Congresso de Construção Metálica e Mista, I Congresso Luso-Brasileiro de Construção Metálica Sustentável*, Porto Portugal. pp. 847-856;
- Jordão, S., Pinho, M., Costa Neves, L., Martins, J. P. and Santiago, A. (2014) Behaviour of laminated glass beams reinforced with pre stressed cables. In: *Eurosteel 2014 – 7th European Conference on Steel Structures*, Naples, Italy. Paper 01-485 (Selected for publication in *Steel Construction – Design and Research*, Ernst & Sohn).
- Jordão, S., Pinho, M., Martins, J. P., Santiago, A. and Cruz, P. (2014) Numerical modelling of a laminated glass beam reinforced with pre-stressed cable, *Challenging Glass 4 & Cost Action TU0905 Final Conference*, Louter, Bos & Belis (eds.), Taylor & Francis Group, pp. 253-260;
- Manco, T., Martins, J. P., Rigueiro, M., Simões da Silva, L. (2015) Comparative analysis of standards for offshore structures in the design of circular tubular elements (ISO, NORSOK and EC3). In: *15th International Symposium on Tubular Structures*, Rio de Janeiro, Brazil. (Accepted for publication);

- Rigueiro, C., Martins, J. P., Simões da Silva, L. (2015) Análise numérica de ligações tubulares em estruturas *offshore*. In: *III Congresso Luso-Africano de Construção Metálica Sustentável*, Luanda, Angola. (Accepted for publication);
- Manco, T., Martins, J. P., Rigueiro, C., Simões da Silva, L. (2015) Análise comparativa de regulamentação *offshore*. In: *III Congresso Luso-Africano de Construção Metálica Sustentável*, Luanda, Angola. (Accepted for publication);

Bibliography

- ABS. (2004) *Guide for buckling and ultimate strength assessment for offshore structures*. American Bureau of Shipping.
- Amabili, M. (2008) *Nonlinear Vibrations and Stability of Shells and Plates*. New York, Cambridge University Press.
- Amani, M., Edlund, B. L. O., Alinia, M. M. (2011) Buckling and postbuckling behavior of unstiffened slender curved plates under uniform shear. *Thin-Walled Structures*, 49 (8), 1017–1031.
- Baker, E. H., Kovalevsky, L., Rish, F. L. (1972), *Structural analysis of shells*. Malabar, Florida, Robert E. Krieger Publishing Company.
- Batdorf, S. B. (1947a) *A simplified Method of Elastic Stability Analysis for Thin Cylindrical Shells*. National Aeronautics and Space Administration. Technical Report number: 847.
- Batdorf, S. B. (1947b) *A simplified method of elastic-stability analysis for thin cylindrical shells I – Donnell's Equation*. National Aeronautics and Space Administration. Technical Report number: 1341.
- Batdorf, S. B. (1947c) *A simplified method of elastic-stability analysis for thin cylindrical shells II – Modified Equilibrium Equation*. National Aeronautics and Space Administration. Technical Report number: 1342.
- Becker, H. & Colao, A. (1977) *Compressive strength of ship hull girders. Part III - Theory and additional experiments*. Ship Structure Committee. Technical Report: 267.

- Becker, H., Goldman, R. and Prozerycki, J. (1970) *Compressive strength of ship hull girders. Part I - Unstiffened Plates*. Ship Structure Committee. Technical Report: 217.
- Beg, D., Kuhlmann, U., Davaine, L., Braun, B. (2010) *Design of plated structures*. Mem Martins, ECCS.
- Berger, M. S. & Fife, P. C. (1966) On von Karman's equations and the buckling of a thin elastic plate. *Bulletin of the American Mathematical Society*, 72 (6), 1006-1011.
- Bijlaard, P. P. (1957) Buckling of Plates under Nonhomogeneous Stress. *Journal of the Engineering Mechanics Division American Society of Civil Engineers (ASCE)*, 83 (EM3), Proc. paper 1293.
- Bleich, F. (1952) *Buckling Strength of Metal Structures*. New York, McGraw-Hill.
- Braun, B. (2010) *Stability of steel plates under combined loading*. PhD Thesis. Institut für Konstruktion und Entwurf der Universität Stuttgart.
- Brush, D. O. & Almroth, B. O. (1975) *Buckling of Bars, plates and Shells*. New York, MacGraw-Hill.
- BSI. (2000) BS5400-3. *Steel, concrete and composite bridges: code of practice for design of steel bridges*. London, British Standards Institution.
- Budiansky, B. & Hutchinson, J. W. (1964) Dynamic Buckling of Imperfection Sensitive Structures. In: *Proceedings of the 11th IUTAM Congress*, Munich, Germany. pp. 636-651.
- Calladine, R. C. (1983) *Theory of Shell Structures*. Cambridge, Cambridge University Press.
- CEN. (2004) EN 10025-2. *Hot rolled products of structural steels - Part 2: Technical delivery conditions for non-alloy structural steels*. Brussels, European Committee for Standardization.
- CEN. (2005) EN1993-1-1. *Design of steel structures: General Rules and Rules for Buildings*. Brussels, European Committee for Standardisation.

- CEN. (2006a) EN1993-1-5. *Design of steel structures: Plated Structural Elements*. Brussels, European Committee for Standardisation.
- CEN. (2006b) EN1993-1-3. *Design of steel structures: Supplementary rules or cold-formed members and sheeting*. Brussels, European Committee for Standardisation.
- CEN. (2007) EN 1993-1-6. *Design of steel structures: Strength and Stability Shells Structures*. Brussels, European Committee for Standardisation.
- CEN. (2008), EN 1090-2. *Execution of steel and aluminium structures, Part 2: Technical requirements for steel structures*. Brussels, European Committee for Standardization.
- Chajes, A. (1974) *Principles of Structural Stability Theory*. New Jersey, Prentice-Hall.
- Chung, J. S., Hong, S. W., Prinsenber, S., Nagata, S. (eds.) (2008) *The Proceedings of The Eighteenth International Offshore and Polar Engineering Conference, 6-11 July, 2008, Vancouver, Canada, ISOPE*.
- Chung, J. S., Hong, S. W., Prinsenber, S., Nagata, S. (eds.) (2009) *The Proceedings of The Nineteenth International Offshore and Polar Engineering Conference, 21-26 June, 2009, Osaka, Japan, ISOPE*.
- Clarín, M. (2007) *Plate Buckling Resistance – Patch Loading of Longitudinally Stiffened Webs and Local Buckling*. PhD Thesis. Luleå tekniska universitet.
- Correia (2009) *Ponte pedonal Pedro e Inês, Coimbra, Portugal*. [Online] Available from <http://upload.wikimedia.org/wikipedia/commons/0/00/PontePedroInes.jpg> [Accessed: 7th June 2014].
- Cox, H. & Clenshaw, W. (1941) *Compression tests on curved plates of thin sheet duralumin*. HM Stationary Office.
- Crate, H. & Levin, L. R. (1943) *Data on buckling strength of curved sheet in compression*. National Advisory Committee for Aeronautics. Technical Report number: L-557.

- Crisfield, M. A. (1997) *Nonlinear Finite Element Analysis of Solids and Structures*. Vols. 1 & 2. London, John Wiley & Sons.
- CTICM. (2007) *EBPlate* (version 2.01). Available from: www.cticm.com.
- Cui, W., Wang, T. and Pedersen, P. T. (2002) Strength of ship plates under combined loading. *Marine Structures*, 15(1), 75–97.
- Davaine, L. & Tran, K. (2010) *Study of the resistance and the stability of cylindrical steel panels. Application to engineering structure* [Presentation]. Cottbus, ECCS – TWG 8.3: 10th official meeting, 29th April.
- Dier, A.F. & Dowling, P. S. (1980) Plates under combined loading and lateral compression. Department of Civil Engineering, Imperial College, London. Technical report: CESLIC Report SP8.
- DNV. (1977) *Rules for the Design, Construction and Inspection of Offshore Structures. Appendix C - Steel Structures*. Det Norske Veritas.
- DNV. (2010a) DNV-RP-C201. *Buckling strength of plated structures*. Det Norske Veritas.
- DNV. (2010b) DNV-RP-C202. *Buckling strength of shells*. Det Norske Veritas.
- Domb, M. M. & Leigh, B. R. (2001) Refined design curves for compressive buckling of curved panels using nonlinear finite element analysis. In: *42nd AIAA / ASME / AHS / ASC Structures, Structural Dynamics and Materials Conference*, Seattle, U.S.A. Paper 1348.
- Domb, M. M. & Leigh, B. R. (2002) Refined curves for shear buckling of curved panels using nonlinear finite element analysis. In: *43rd AIAA / ASME / AHS / ASC Structures, Structural Dynamics and Materials Conference*, Denver, U.S.A, Paper #2002-1257.
- Domb, M. M. (2002) Nonlinear buckling predictions of curved panels under combined compression and shear loading. In: *23rd Congress of International Council of the Aeronautical Sciences, ICAS2002*, Toronto, Canada, pp. 322.1 – 322.8.

- Donnell, L. H. & Wan C. C. (1945) Effect of imperfections on buckling of thin cylinders and columns under axial compression. *Journal of Applied Mechanics of the American Society of Mechanical Engineers (ASME)*, 17, 73-83.
- Donnell, L. H. (1934) A new theory for the buckling of thin cylinders under axial compression and bending. *Transactions of the American Society of Mechanical Engineers (ASME)*, 56, 795.
- Dubas, P. & Gehri, E. (eds.) (1986) *Structural Stability, Behaviour and Design of steel Plated Structures*. (Eds.). Zurich, European Convention for Constructional Steelwork (ECCS), Publication number: 44.
- Dunn, A. (2000) *British Museum Great Court roof*. [Online] Available from <http://www.andrewdunnphoto.com> [Accessed: 24th August 2014].
- Eipakchi, H. R. & Shariati, M. (2011) Buckling analysis of a cylindrical panel under axial stress using perturbation technique. *Journal of Applied Mathematics and Mechanics*, 91 (2), 138-145.
- Ertürk, A. (2014) *Chicago, Cloud Gate portrait*. [Online] Available from <http://alierturk.deviantart.com/art/Chicago-Cloud-Gate-portrait-203059089> [Accessed: 14th March 2014].
- Faulkner, D., Adamschak, J. C., Snyder, G. J. and Vetter, M. F. (1973) Synthesis of welded grillages to withstand compression and normal loads. *Computers & Structures*, 3, 221-246.
- Featherston, C. A. & Ruiz, C. (1998) Buckling of curved panels under combined shear and compression. *Proceedings of the Institution of Mechanical Engineers, Part C: Journal of Mechanical Engineering Science*, 212 (3), 183-196.
- Featherston, C. A. (2000) The use of finite element analysis in the examination of instability in flat plates and curved panels under compression and shear. *International Journal of Non-Linear Mechanics*, 35 (3), 515-529.

- Featherston, C. A. (2003) Imperfection sensitivity of curved panels under combined compression and shear. *International Journal of Non-Linear Mechanics*, 38, 225-238.
- Featherston, C. A. (2012) Geometric imperfection sensitivity of curved panels under combined compression and in-plane bending – A study using adaptive meshing and DIC. *Strain*, 48, 286-295.
- Foreign Office Architects (2009) *Birmingham New St. Station as viewed from Stephenson St.*, Birmingham New St. Station Project presentation.
- Frey, F. & Jirousek, J. (2001) *Analyse des structures et milieux continus – Méthode des éléments finis*. Trait de Génie Civil, vol. 6. Lausanne, Presses Polytechniques et Universitaires Romandes.
- Fricke, W. & Bronsart, R. (eds.) (2012) *Proceedings of the 18th International Ship and Offshore Structures Congress (ISSC)*, 10-13 September, 2012, Rostock, Germany, University of Rostock.
- Frieze, P. A. & Sheno, R. A. (eds.) (2006) *Proceedings of the 16th International Ship and Offshore Structures Congress (ISSC)*, 20-25 August, 2006, Southampton, United Kingdom, University of Southampton Press.
- Galéa, Y. & Martin, P. -O. (2010) Longitudinally stiffened plates in Eurocode 3: Calculation of the global critical buckling stress. *Journal of Constructional Steel Research*, 66, 1345–1353.
- Gardner, L. & Ministro, A. (2004) Testing and numerical modelling of structural steel oval hollow sections. Imperial College. Research report number: 04-002-ST.
- Gerard, G. & Becker, H. (1957) *Handbook of Structural Stability: Part III – Buckling of Curved Plates and Shells*. National Advisory Committee for Aeronautics. Technical Report number: 3783.

- Gerard, G. (1957) *Handbook of Structural Stability: Part IV – Failure of plates and composite elements*. National Advisory Committee for Aeronautics. Technical Report number: 3784.
- Gerard, G. (1959) *Handbook of Structural Stability: Supplement to Part III – Buckling of Curved Plates and Shells*. National Aeronautics and Space Administration. Technical Report number: D-163.
- Girish, J. & Ramachandra, L. S. (2008) Stability and vibration of composite cylindrical shell panels under axial compression and secondary loads, *Journal of Applied Mechanics (ASME)*, 75, 041007-1-11.
- Guedes Soares, C. & Gordo, J. M. (1996) Compressive strength of rectangular plates under biaxial load and lateral pressure. *Thin-Walled Structures*, 24, 231-259.
- Hilburger, M. W., Nemeth, M. P. and Starnes, J. H. (2001) Nonlinear and buckling behavior of curved panels subjected to combined loads, In: 42nd AIAA / ASME / AHS / ASC Structures, Structural Dynamics and Materials Conference, Seattle, U.S.A. Paper 1398.
- Jacques, T. H., Maquoi, R., Fonder, G (1983) Buckling of unstiffened compression curved plates, *Journal of Constructional Steel Research*, 3 (1), 28-34.
- Jang, C. D. & Hong, S. Y. (eds.) (2009) *Proceedings of the 17th International Ship and Offshore Structures Congress (ISSC)*, 16-21 August, 2009, Seoul, Republic of Korea, National University.
- Janjic, D. (2008) Experience from the Global Analysis of Stonecutter's Bridge and Sutong Bridge. In: 25th Annual International Bridge Conference, 2-4 June, Pittsburgh, Pennsylvania, USA, Curran Associates, Inc., pp. 207-277.
- Jetteur, P. and Maquoi, R. (1984) Larguer effective d'une tôle courbe comprimée, *Construction Métallique*, 2, 51-57.

- Johansson, B., Maquoi, R., Sedlacek, G., Müller, C., Beg, D. (eds.) (2007) *Commentary and worked examples to EN1993-1-5 "Plated Structural Elements"*. JRC Scientific and Technical Reports. EUR 22898 EN – 2007.
- Klöppel, E. & Möller, K. (1968) *Beulwerte ausgesteifter Rechteckplatten (Band II)*. Berlin, Ernst and Sohn.
- Klöppel, E. & Sheer, J. (1960) *Beulwerte ausgesteifter Rechteckplatten (Band I)*. Berlin, Ernst & Sohn.
- Koiter, W. T. (1945) *Over de Stabiliteit van het Elastische Evenwicht*. Ph.D. Thesis. Delft University (Trans. National Aeronautics and Space Agency Technical. Translation Number: TT F 10833).
- Koiter, W. T. (1956) Buckling and post-buckling behaviour of a cylindrical panel under axial compression. *Reports and Transactions National Aeronautical Research Institute*, 20, 71-84.
- Koiter, W. T. (1960) A consistent first approximation in general theory of thin elastic shells. In: *The Theory of Thin Elastic Shells*. Amsterdam, North-Holland. pp. 12-33.
- Koiter, W. T. (1967) General Equations of Elastic Stability for Thin Shells. In: *Proceedings of the Symposium on Theory of Shells to Honour L. Hamilton Donnell*, Houston, University of Houston. pp. 187-223.
- Leissa, A. W. (1973) *Vibration of Shells*. National Aeronautics and Space Administration. Monograph number: SP-288.
- Libai, A. & Simmonds, J. G. (1988) *The Nonlinear Shell Theory*. 2nd ed. New York, Cambridge University Press.
- Linzell, D., Hall, D., White, D. (2004), Historical Perspective on Horizontally Curved I Girder Bridge Design in the United States. *Journal of Bridge Engineering, American Society of Civil Engineers (ASCE)*, 208-229.
- Lopez, T. (2007) *Zubizuri Bridge*. [Online] Available from: <http://littleaesthete.com/top-5-bilbao> [Accessed: 25th June 2013].

- Love, A. E. H. (1892) *A Treatise on the Mathematical Theory of Elasticity*. 2nd ed. Cambridge, Cambridge University Press.
- Magnucki, K. & Mackiewicz, M. (2006) Elastic buckling of an axially compressed cylindrical panel with edges simply supported and one edge free. *Thin-Walled Structures*, 44 (4), 387-392.
- Marguerre, K. (1937) Apparent width of the plate in compression. *Luftfahrt Forschung*, 14 (3), 121–128. Trans. National Advisory Committee for Aeronautics. Technical Memorandum number: 833.
- Martins, J. P., Simões da Silva, L. e Reis, A. (2011) Efeito da geometria na resistência de painéis curvos em aço. In: *VIII Congresso de Construção Metálica e Mista*, Guimarães, Portugal. pp. 365-362.
- Martins, J. P., Simões da Silva, L., Reis, A. (2013) Eigenvalue analysis of cylindrically curved under compressive stresses – extension of rules from EN1993-1-5. *Thin-Walled Structures*, 68, 183–194.
- Martins, J. P., Simões da Silva, L., Reis, A. (2014) Ultimate load of cylindrically curved panels under in-plane compression and bending – Extension of rules from EN1993-1-5. *Thin-Walled Structures*, 77, 36–4.
- Möcker, T. & Reimerdes, H.-G. (2006) Postbuckling simulation of curved stiffened composite panels by the use of strip elements. *Composite Structures*, 73, 237-243.
- Moen, C. & Schafer, B. (2004) *Direct Strength Design for Cold-Formed Steel Members With Perforations*. The John Hopkins University, Progress Report to AISI members number: 1.
- Nakai, H. & Yoo, C. H. (1988) *Analysis and design of curved steel bridges*. New York, McGraw-Hill.
- National Aeronautics and Space Administration (n.d.) *Space Shuttle Program: Spanning 30 Years of Discovery* [Online]. Available from: http://www.nasa.gov/mission_pages/shuttle/main/index.html [Accessed on: 19th May 2014].

- Nemeth, M. P. & Starnes Jr., J. H. (1998) *The NASA Monographs on Shell Stability Design Recommendations – A Review and Suggested Improvements*. National Space Agency. Report number: TP-1998-206290.
- Nemeth, M. P. (2013) *A Leonard-Sanders-Budiansky-Koiter-Type Nonlinear Shell Theory with a Hierarchy of Transverse-Shearing Deformations*. National Space Agency. Report number: TP-2013-218025.
- Novozhilov, V. V. (1959) *Theory of Thin Elastic Shells*. Groningen, Noordhoff.
- Pardo, A. & Fernandez, J. C. (2010) The quest for lighter and stronger aircraft with realistic simulation. *JEC Magazine*. [Online] Available from: <http://www.jecomposites.com/news/composites-news/quest-lighter-and-stronger-aircraft-realistic-simulation> [Accessed: 12th March 2014].
- Park, J.S., Fujikubo, M., Iijima, K., Yao, T. (2009) Prediction of the secondary buckling strength and ultimate strength of cylindrically curved plate under axial compression. In: *Proceedings of the 19th International Offshore and Polar Engineering Conference, The International Society of Offshore and Polar Engineers (ISOPE)*, Osaka, Japan. pp. 740–747.
- Pircher, M. (2004) The influence of a weld-induced axi-symmetric imperfection on the buckling of a medium-length silo under wind loading. *International Journal of Solids and Structures*, 41, 5595–5610.
- Pircher, M., & Bridge, R. (2001) The influence of circumferential weld-induced imperfections on the buckling of silos and tanks. *Journal of Constructional Steel Research*, 57, 569–580.
- Pope G. G. (1965) *On the axial compression of long, slightly curved panel*. British Aeronautical Research Council, Ministry of Aviation, Reports and Memoranda Number: 3392.
- Reddy, J. N. (2007) *Theory and Analysis of Elastic Plates and Shells*. 2nd ed. Boca Raton, CRC Press.
- Reddy, J.N. (2002) *Energy Principles and Variational Methods in Applied Mechanics*. 2nd ed. New York, John Wiley & Sons.

- Redshaw, S. C. (1934). *The Elastic Instability of a Thin Curved Panel Subjected to an Axial Thrust, Its Axial and Circumferential Edges Being Simply Supported*. British Aeronautical Research Committee. Report and Memorandum number: 1565.
- Reis, A. & Camotim, D. (2012) *Estabilidade e Dimensionamento de Estruturas*. Amadora, Edições Orion.
- Ribeiro, F. (2008) *Ponte Pedonal Chaves*. [Online] Available from: <http://www.flickr.com/photos/fer-ribeiro/3097186412> [Accessed: 25th June 2013].
- Rotter, J. M. & Schimdt, H. (eds.) (2008) *Buckling of shells, European Design recommendations*, 5th edition. Brussels, European Convention for Constructional Steelwork (ECCS), Publication number: 128.
- Rotter, J. M. (2004) Buckling of cylindrical shells under axial compression. In: Teng, J. G. & Rotter, J. M. (eds.) *Buckling of Thin Metal Shells*. London, Spon, pp. 42-87.
- Rusch, A. & Lindner, J. (2001) Tragfähigkeit von beulgefährdeten Querschnittelementen unter Berücksichtigung von Imperfektionen. *Stahlbau*, 70 (10), 765-774.
- Samuelson, L. A. & Eggwertz, S. (eds.) (1992) *Shell Stability Handbook*. London, Elsevier.
- Schenk, C. A. & Schüeller, G. I. (2003) Buckling analysis of cylindrical shells with random geometric imperfections. *International Journal of Non-Linear Mechanics*, 38, 1119 – 1132.
- Schmidt, H. (2000) Stability of steel shell structures – General Report. *Journal of Constructional Steel Research*, 55, 159-181.
- Schuette, E. (1948) Buckling of curved sheet in compression and its relation to the secant modulus. *Journal of the Aeronautical Sciences*, 15 (1), 18-22.

- Seide, P. & Stein, M. (1949) *Compressive Buckling of Simply supported of Plates with Longitudinal Stiffeners*. National Advisory Committee for Aeronautics. Technical Note number: 1825.
- Silva Gomes, J. F. (2007) *Análise de Tensões em Placas, Casca e Reservatórios*. Porto, Edições INEGI.
- Simões da Silva, L. & Gervásio, H. (2007) *Manual de Dimensionamento de Estruturas Metálicas: Métodos Avançados*. Coimbra, CMM.
- Simões da Silva, L. (1988) *Modal Interactions in bending and buckling of sandwich structures*. PhD thesis. Imperial College London.
- Simulia (2011) *ABAQUS FEA (version 6.11)* [Software] Simulia Dassault Systèmes.
- Singer, J., Arbocz, J., Weller, T. (2002) *Buckling Experiments: Experimental Methods in Buckling of Thin-Walled Structures: Shells, Built-up Structures, Composites and Additional Topics - Volume 2*. New York, John Wiley & Sons.
- Song, C. Y., Teng, J. G., Rotter, J. M. (2004). Imperfection sensitivity of thin elastic cylindrical shells subject to partial axial compression. *International Journal of Solids and Structures*, 41, 7155–7180.
- Stonor, R.W.P., Bradfield, C.D., Moxham, K. E. and J.B. Dwight, K. E. (1983) *Tests on plates under biaxial compression*. Cambridge University Engineering Department. Technical report: CUED/D-STRUCT/TR.98.
- Stowell, E. Z. (1943) Critical compressive stress for a curved sheet supported along all edges and elastically restrained against rotation along the unloaded edges. *National Advisory Committee for Aeronautics*. War Report number: L-691.
- Tamate, O. & Sekine, H. (1969) Postbuckling behavior of thin curved panels under axial compression. *Bulletin of Japan Society of Mechanical Engineering*, 12 (51), 415-420.
- Tauchert, T. R. (1974) *Energy Principles in Structural Mechanics*. Tokyo, McGraw-Hill.

- Teng, J. G. & Hong, G. (1998) Nonlinear thin shell theories for numerical buckling predictions. *Thin-Walled Structures*, 31, 89–115.
- Teng, J. G. & Rotter, J. M. (eds.) (2004) *Buckling of thin metal shells*. London, Spon Press.
- Teng, J. G. & Song, C. Y. (2001) Numerical models for nonlinear analysis of elastic shells with eigenmode-affine imperfections. *International Journal of Solids and Structures*, 38, 3263–3280.
- Thompson, J. M. T. & Hunt, G. W. (1984) *Elastic instability phenomena*. London, Wiley.
- Timoshenko, S. P. & Gere, J. M. (1961) *Theory of Elastic Stability*. 2nd Ed. New York, Dover Publications.
- Tran, K. (2012) *Étude de la résistance et de la stabilité des tôles courbes en acier. Application aux ouvrages d'art*. PhD thesis. Université Paris-Est.
- Tran, K. L., Douthe, C., Sab, K., Dallot, J., Davaine, L. (2014) A preliminary design formula for the strength of stiffened curved panels by design of experiment method. *Thin-Walled Structures*, 79, 129–137.
- Tran, K., Davaine, L., Douthe, C., Sab, K. (2012) Stability of curved panels under uniform axial compression. *Journal of Constructional Steel Research*, 69, 30–8.
- Ugural, A. C. (1981) *Stresses in plates and Shells*. New York, McGraw-Hill.
- Unknown author (1885) *New Street Station in Victorian Times, before redevelopment in the 1960's*. [Online] Available from <http://www.historycultures.bham.ac.uk/undergrad/image/NewStreetStation.jpg> [Accessed: 4th March 2014].
- Unknown author (1897) *Diagrid Shell by Vladimir Shukhov during construction, Russia*. [Online] Available from http://upload.wikimedia.org/wikipedia/commons/a/a4/Double_curvature_steel_lattice_Shell_by_Shukhov_in_Vyksa_1897_shell.jpg [Accessed: 4th March 2014].

- Unknown Author (1905) Arch Bridge (Bellows Falls) [Online]. Available from [http:// en.wikipedia.org](http://en.wikipedia.org) [Accessed 7th March 2014].
- Unknown author (2007) *New Sheppy Bridge*. [Online] Available from: [http://www.flickr.com/photos/ its-only-lines/ 346981731](http://www.flickr.com/photos/its-only-lines/346981731) [Accessed: 25th June 2013].
- Unknown author (2010) *SPAR platform under constructrion*. [Online] Available from: <http://www.oj.com/articles/shell/perdido/2010/04/building-the-worlds-deepest-drilling-and-production-platform.html> [Accessed: 16th May 2014].
- Usami, T. (1993) Effective width of locally buckled plates in compression and bending. *Journal of Structural Engineering*, 119 (5), 1358-1373.
- Valsgard, S. (1979) *Ultimate capacity of plates in biaxial inplane compression*. Det Norske Veritas. Technical Report: 76-678.
- Valsgard, S. (1980) Numerical design prediction of the capacity of plates in in-plane compression. *Computers & Structures*, 12, 729-739.
- Vejrum, T. (2008) *Danish Engineers behind the behind World's largest Cable Stayed Bridges: Sutong and Stonecutters Bridge* [Presentation] Oslo, Norsk Ståldag 2008, 29th October.
- Veljkovic, M. & Johansson, B. (2009) Review of plate buckling rules in EN1993-1-5. *Steel Construction*, 2 (4), 228-234.
- Ventsel, E. & Krauthammer, T. (2001) *Thin Plates and Shells: Theory, Analysis and Applications*. New York, Taylor & Francis.
- Vlasov, V. Z. (1949) *General Theories of Shells and its Applications in Engineering*. Trans. National Advisory Committee for Aeronautics. Technical Translation number: 99.
- Volmir, A. S. (1963) *Stability of elastic systems*. Fizmatig, Moscow. Trans. National Aeronautics and Space Administration. Technical Memorandum number: AD628508.

- von Kármán T. H. & Tsien H. S. (1941) The buckling of thin cylindrical shells under axial compression. *Journal of the Aeronautical Sciences*, 8 (8), 303-312.
- von Kármán, T., Sechler, E. E., Donnell, L. H. (1932) Strength of Thin Plates in Compression. *Transactions of the American Society of Mechanical Engineers*, 54, 53-57.
- Welter, G. (1946) The effect of the radius of curvature and preliminary artificial eccentricities on buckling loads of curved thin aluminium-alloy sheets for monocoque constructions. *Journal of the Aeronautical Sciences*, 13 (11), 593-596.
- Wilde, R., Zawodny, K., Magnucki, K. (2007) Critical state of an axially compressed cylindrical panel with three edges simply supported and one edge free. *Thin-Walled Structures*, 45, 955-959.
- Winter, G. (1947) Strength of Thin Steel Compression Flanges. *Transactions of American Society of Civil Engineers*, 112, 527-554.
- Wolfram (2010) *Mathematica* (version 8.0) [Software] Wolfram Research, Inc.
- Yamaki, N., (1984) *Elastic stability of circular cylindrical shells*. Amsterdam, North-Holland.
- Yao, T., Brunner, E., Cho, S. R., Choo, Y. S., Czujko, J., Estefen, S. F., Gordo, J. M., Hess, P. E., Naar, H., Pu, Y., Rigo, P., Wan, Z. Q. (2006) *Ultimate Strength (Committee III.1), 16th International Ship and Offshore Structures Congress (ISSC)*, Southampton, United Kingdom.
- Young, H. D. & Freedman, R. A. (1999) *Sears and Zemansky's University Physics*. 10th ed. Reading, Addison-Wesley.
- Ziemian, R. D. (ed.) (2010) *Guide to stability design of metal structures*. 6th ed. New Jersey, John Wiley & Sons.

**A. Examples of Mathematica code
developed for the analytical study**

Analytical derivation: Elastic critical stress: boundary conditions type 3 and 3 degrees-of-freedom

Inpute variables

```

In[1]: Clear[a1, a21, a31, A, a, B, b, c, d, e, niu, m, P, R, t, Z];
      R = b^2 / (Z * t);
      d = e * t^3 / (12 * (1 - niu^2));
      c = e * t / (1 - niu^2);

```

Displacement functions

```

In[2]: u = a1 * x;
      v = a21 * Cos[Pi * y / b];
      w = a31 * Sin[m * Pi * x / a] * Sin[Pi * y / b];

```

Strain-displacement relations

```

In[3]: ex = D[u, x] - 1 / 2 * (-D[w, x])^2;
      ey = -niu * D[u, x] + D[v, y] + w / R - 1 / 2 * (-D[w, y])^2;
      gxy = D[w, x] * D[w, y];
      xx = -D[D[w, x], x];
      xy = -D[D[w, y], y];
      xxy = -D[D[w, x], y];

```

Strain Energy expressions

```

In[14]: U = c / 2 * Integrate[Integrate[ex^2 + ey^2 + 2 * niu * ex * ey + (1 - niu) / 2 * gxy^2,
      {x, 0, a}], {y, 0, b}] + d / 2 * Integrate[Integrate[
      xx^2 + xy^2 + 2 * niu * xx * xy + 2 * (1 - niu) * xxy^2, {x, 0, a}], {y, 0, b}];
      W = P * Integrate[Integrate[D[u, x], {x, 0, a}], {y, 0, b}];
      Ve = Collect[Expand[Refine[(U - W), Element[{m}, Integers]]], {a1, a21, a31}];

```

Passive coordinate a1 elimination

```

In[17]: alaux = Expand[Solve[D_a1 (Ve) == 0, a1]];
      alaux[[1]];
      Vfinal = Collect[Expand[Ve] /. alaux[[1]], {a21, a31}];

```

Quadratic coefficients of the reduced form of the Strain Energy expression

```
Vfinalist = MonomialList[Vfinal, {a21, a31}];
V2121F = Collect[Expand[Vfinalist[[1]] * 2], a21] / a21^2
V2131F = Collect[Expand[Vfinalist[[3]]], {a21, a31}] / (a21 + a31)
V3131F = Collect[Expand[Vfinalist[[6]] * 2], a31] / a31^2
```

$$\text{Out[21]} = \frac{a e \pi^2 t}{2 b (1 - \text{niu}^2)}$$

$$\text{Out[22]} = -\frac{a e t^2 Z}{2 b^2 m (1 - \text{niu}^2)} + \frac{(-1)^n a e t^2 Z}{2 b^2 m (1 - \text{niu}^2)}$$

$$\text{Out[23]} = -\frac{b m^2 P \pi^2}{4 a} + \frac{a e \pi^4 t^3}{48 b^3 (1 - \text{niu}^2)} + \frac{e m^2 \pi^4 t^3}{24 a b (1 - \text{niu}^2)} + \frac{b e m^4 \pi^4 t^3}{48 a^3 (1 - \text{niu}^2)} + \frac{a e t^3 Z^2}{4 b^3 (1 - \text{niu}^2)}$$

Critical Loads

```
determinant = Det[{{V2121F, V2131F}, {V2131F, V3131F}}];
FullSimplify[Solve[determinant == 0, P]]
```

$$\text{Out[25]} = \left\{ \left\{ P \rightarrow -\frac{e t^3 (2 a^2 b^2 m^4 \pi^6 + b^4 m^6 \pi^6 + a^4 (-24 (-1 + (-1)^n)^2 Z^2 + m^2 (\pi^6 + 12 \pi^2 Z^2)))}{(12 a^2 b^4 m^4 (-1 + \text{niu}^2) \pi^4)} \right\} \right\}$$

Analytical derivation: Elastic critical stress: Boundary conditions type 3 and 9 degrees-of-freedom

Input variables

```

In[1]= Clear[a1, a21, a31, a32, a33, a34, a35,
          a36, a37, A, a, B, b, c, d, e, niu, m, P, R, t, Z];
R = b^2 / (Z + t);
d = e * t^3 / (12 * (1 - niu^2));
c = e * t / (1 - niu^2);

```

Displacement functions

```

In[2]= u = a1 * x;
v = a21 * Cos[Pi * y / b];
w = a31 * Sin[Pi * x / a] * Sin[Pi * y / b] +
    a32 * Sin[2 * Pi * x / a] * Sin[Pi * y / b] + a33 * Sin[3 * Pi * x / a] * Sin[Pi * y / b] +
    a34 * Sin[4 * Pi * x / a] * Sin[Pi * y / b] + a35 * Sin[5 * Pi * x / a] * Sin[Pi * y / b] +
    a36 * Sin[6 * Pi * x / a] * Sin[Pi * y / b] + a37 * Sin[7 * Pi * x / a] * Sin[Pi * y / b];

```

Strain-displacement relations

```

In[3]= ex = D[u, x] - 1 / 2 * (-D[w, x])^2;
ey = -niu * D[u, x] + D[v, y] + w / R - 1 / 2 * (-D[w, y])^2;
gxy = Expand[D[w, x] * D[w, y]];
gxysquare = Expand[gxy^2];
xx = -D[D[w, x], x];
xy = -D[D[w, y], y];
xxy = -D[D[w, x], y];

```

Strain Energy expressions

```

U = c / 2 * Integrate[Integrate[ex^2 + ey^2 + 2 * niu * ex * ey + (1 - niu) / 2 * gxy^2,
    {x, 0, a}], {y, 0, b}] + d / 2 * Integrate[Integrate[
    xx^2 + xy^2 + 2 * niu * xx * xy + 2 * (1 - niu) * xxy^2, {x, 0, a}], {y, 0, b}];
W = P * Integrate[Integrate[D[u, x], {x, 0, a}], {y, 0, b}];
Ve = Expand[U - W];

```

Passive coordinate a1 elimination

```

In[20]= a1aux = Expand[Solve[D_a1 (Ve) == 0, a1]];
a1aux[[1]];
Vfinal = Expand[Ve] /. a1aux[[1]];

```

Quadratic coefficients of the reduced form of the Strain Energy expression

```

Clear[a1, a21, a31, a32, a33, a34, a35, a36, a37]
V2121 = MonomialList[Refine[Vfinal,
  {a31 == 0, a32 == 0, a33 == 0, a34 == 0, a35 == 0, a36 == 0, a37 == 0}], a21];
V2121F = Collect[Expand[V2121[[1]] * 2], a21] / a21^2
Clear[a1, a21, a31, a32, a33, a34, a35, a36, a37]
V3131 = MonomialList[Refine[Vfinal,
  {a21 == 0, a32 == 0, a33 == 0, a34 == 0, a35 == 0, a36 == 0, a37 == 0}], a31];
V3131F = Collect[Expand[V3131[[3]] * 2], a31] / a31^2
Clear[a1, a21, a31, a32, a33, a34, a35, a36, a37]
V3232 = MonomialList[Refine[Vfinal,
  {a21 == 0, a31 == 0, a33 == 0, a34 == 0, a35 == 0, a36 == 0, a37 == 0}], a32];
V3232F = Collect[Expand[V3232[[2]] * 2], a32] / a32^2
Clear[a1, a21, a31, a32, a33, a34, a35, a36, a37]
V3333 = MonomialList[Refine[Vfinal,
  {a21 == 0, a31 == 0, a32 == 0, a34 == 0, a35 == 0, a36 == 0, a37 == 0}], a33];
V3333F = Collect[Expand[V3333[[3]] * 2], a33] / a33^2
Clear[a1, a21, a31, a32, a33, a34, a35, a36, a37]
V3434 = MonomialList[Refine[Vfinal,
  {a21 == 0, a31 == 0, a32 == 0, a33 == 0, a35 == 0, a36 == 0, a37 == 0}], a34];
V3434F = Collect[Expand[V3434[[2]] * 2], a34] / a34^2
Clear[a1, a21, a31, a32, a33, a34, a35, a36, a37]
V3535 = MonomialList[Refine[Vfinal,
  {a21 == 0, a31 == 0, a32 == 0, a33 == 0, a34 == 0, a36 == 0, a37 == 0}], a35];
V3535F = Collect[Expand[V3535[[3]] * 2], a35] / a35^2
Clear[a1, a21, a31, a32, a33, a34, a35, a36, a37]
V3636 = MonomialList[Refine[Vfinal,
  {a21 == 0, a31 == 0, a32 == 0, a33 == 0, a34 == 0, a35 == 0, a37 == 0}], a36];
V3636F = Collect[Expand[V3636[[2]] * 2], a36] / a36^2
Clear[a1, a21, a31, a32, a33, a34, a35, a36, a37]
V3737 = MonomialList[Refine[Vfinal,
  {a21 == 0, a31 == 0, a32 == 0, a33 == 0, a34 == 0, a35 == 0, a36 == 0}], a37];
V3737F = Collect[Expand[V3737[[3]] * 2], a37] / a37^2
Clear[a1, a21, a31, a32, a33, a34, a35, a36, a37]
V2131 = MonomialList[Refine[Vfinal,
  {a32 == 0, a33 == 0, a34 == 0, a35 == 0, a36 == 0, a37 == 0}], {a21, a31}];
V2131F = Collect[Expand[V2131[[3]]], {a21, a31}] / (a21 * a31)
Clear[a1, a21, a31, a32, a33, a34, a35, a36, a37]
V2133 = MonomialList[Refine[Vfinal,
  {a31 == 0, a32 == 0, a34 == 0, a35 == 0, a36 == 0, a37 == 0}], {a21, a33}];
V2133F = Collect[Expand[V2133[[3]]], {a21, a33}] / (a21 * a33)
Clear[a1, a21, a31, a32, a33, a34, a35, a36, a37]
V2135 = MonomialList[Refine[Vfinal,
  {a31 == 0, a32 == 0, a33 == 0, a34 == 0, a36 == 0, a37 == 0}], {a21, a35}];
V2135F = Collect[Expand[V2135[[3]]], {a21, a35}] / (a21 * a35)
Clear[a1, a21, a31, a32, a33, a34, a35, a36, a37]
V2137 = MonomialList[Refine[Vfinal,
  {a31 == 0, a32 == 0, a33 == 0, a34 == 0, a35 == 0, a36 == 0}], {a21, a37}];
V2137F = Collect[Expand[V2137[[3]]], {a21, a37}] / (a21 * a37)

```


$$\begin{aligned}
\text{Ou(68)*} &= \frac{ae\pi^2 t}{2b(1-\nu^2)} \\
\text{Ou(71)*} &= \frac{ae\pi^4 t^3}{48b^3(1-\nu^2)} + \frac{e\pi^4 t^3}{24ab(1-\nu^2)} + \frac{be\pi^4 t^3}{48a^3(1-\nu^2)} + \frac{ab^3e^2 P\pi^2 t^2}{4(1-\nu^2)^2 \left(\frac{abet}{1-\nu^2} - \frac{abeniu^2 t}{1-\nu^2}\right)^2} \\
&\quad + \frac{ab^3e^2 \nu^2 P\pi^2 t^2}{2(1-\nu^2)^2 \left(\frac{abet}{1-\nu^2} - \frac{abeniu^2 t}{1-\nu^2}\right)^2} + \frac{ab^3e^2 \nu^4 P\pi^2 t^2}{4(1-\nu^2)^2 \left(\frac{abet}{1-\nu^2} - \frac{abeniu^2 t}{1-\nu^2}\right)^2} \\
&\quad + \frac{b^3 e P\pi^2 t}{2(1-\nu^2) \left(\frac{abet}{1-\nu^2} - \frac{abeniu^2 t}{1-\nu^2}\right)} + \frac{b^2 e \nu^2 P\pi^2 t}{2(1-\nu^2) \left(\frac{abet}{1-\nu^2} - \frac{abeniu^2 t}{1-\nu^2}\right)} + \frac{aet^3 Z^2}{4b^3(1-\nu^2)} \\
\text{Ou(74)*} &= \frac{ae\pi^4 t^3}{48b^3(1-\nu^2)} + \frac{e\pi^4 t^3}{6ab(1-\nu^2)} + \frac{be\pi^4 t^3}{3a^3(1-\nu^2)} + \frac{ab^3e^2 P\pi^2 t^2}{(1-\nu^2)^2 \left(\frac{abet}{1-\nu^2} - \frac{abeniu^2 t}{1-\nu^2}\right)^2} \\
&\quad + \frac{2ab^3e^2 \nu^2 P\pi^2 t^2}{(1-\nu^2)^2 \left(\frac{abet}{1-\nu^2} - \frac{abeniu^2 t}{1-\nu^2}\right)^2} + \frac{ab^3e^2 \nu^4 P\pi^2 t^2}{(1-\nu^2)^2 \left(\frac{abet}{1-\nu^2} - \frac{abeniu^2 t}{1-\nu^2}\right)^2} \\
&\quad + \frac{2b^3 e P\pi^2 t}{(1-\nu^2) \left(\frac{abet}{1-\nu^2} - \frac{abeniu^2 t}{1-\nu^2}\right)} + \frac{2b^2 e \nu^2 P\pi^2 t}{(1-\nu^2) \left(\frac{abet}{1-\nu^2} - \frac{abeniu^2 t}{1-\nu^2}\right)} + \frac{aet^3 Z^2}{4b^3(1-\nu^2)} \\
\text{Ou(77)*} &= \frac{ae\pi^4 t^3}{48b^3(1-\nu^2)} + \frac{3e\pi^4 t^3}{8ab(1-\nu^2)} + \frac{27be\pi^4 t^3}{16a^3(1-\nu^2)} + \frac{9ab^3e^2 P\pi^2 t^2}{4(1-\nu^2)^2 \left(\frac{abet}{1-\nu^2} - \frac{abeniu^2 t}{1-\nu^2}\right)^2} \\
&\quad + \frac{9ab^3e^2 \nu^2 P\pi^2 t^2}{2(1-\nu^2)^2 \left(\frac{abet}{1-\nu^2} - \frac{abeniu^2 t}{1-\nu^2}\right)^2} + \frac{9ab^3e^2 \nu^4 P\pi^2 t^2}{4(1-\nu^2)^2 \left(\frac{abet}{1-\nu^2} - \frac{abeniu^2 t}{1-\nu^2}\right)^2} \\
&\quad + \frac{9b^3 e P\pi^2 t}{2(1-\nu^2) \left(\frac{abet}{1-\nu^2} - \frac{abeniu^2 t}{1-\nu^2}\right)} + \frac{9b^2 e \nu^2 P\pi^2 t}{2(1-\nu^2) \left(\frac{abet}{1-\nu^2} - \frac{abeniu^2 t}{1-\nu^2}\right)} + \frac{aet^3 Z^2}{4b^3(1-\nu^2)} \\
\text{Ou(80)*} &= \frac{ae\pi^4 t^3}{48b^3(1-\nu^2)} + \frac{2e\pi^4 t^3}{3ab(1-\nu^2)} + \frac{16be\pi^4 t^3}{3a^3(1-\nu^2)} + \frac{4ab^3e^2 P\pi^2 t^2}{(1-\nu^2)^2 \left(\frac{abet}{1-\nu^2} - \frac{abeniu^2 t}{1-\nu^2}\right)^2} \\
&\quad + \frac{8ab^3e^2 \nu^2 P\pi^2 t^2}{(1-\nu^2)^2 \left(\frac{abet}{1-\nu^2} - \frac{abeniu^2 t}{1-\nu^2}\right)^2} + \frac{4ab^3e^2 \nu^4 P\pi^2 t^2}{(1-\nu^2)^2 \left(\frac{abet}{1-\nu^2} - \frac{abeniu^2 t}{1-\nu^2}\right)^2} \\
&\quad + \frac{8b^3 e P\pi^2 t}{(1-\nu^2) \left(\frac{abet}{1-\nu^2} - \frac{abeniu^2 t}{1-\nu^2}\right)} + \frac{8b^2 e \nu^2 P\pi^2 t}{(1-\nu^2) \left(\frac{abet}{1-\nu^2} - \frac{abeniu^2 t}{1-\nu^2}\right)} + \frac{aet^3 Z^2}{4b^3(1-\nu^2)} \\
\text{Ou(83)*} &= \frac{ae\pi^4 t^3}{48b^3(1-\nu^2)} + \frac{25e\pi^4 t^3}{24ab(1-\nu^2)} + \frac{625be\pi^4 t^3}{48a^3(1-\nu^2)} + \frac{25ab^3e^2 P\pi^2 t^2}{4(1-\nu^2)^2 \left(\frac{abet}{1-\nu^2} - \frac{abeniu^2 t}{1-\nu^2}\right)^2} \\
&\quad + \frac{25ab^3e^2 \nu^2 P\pi^2 t^2}{2(1-\nu^2)^2 \left(\frac{abet}{1-\nu^2} - \frac{abeniu^2 t}{1-\nu^2}\right)^2} + \frac{25ab^3e^2 \nu^4 P\pi^2 t^2}{4(1-\nu^2)^2 \left(\frac{abet}{1-\nu^2} - \frac{abeniu^2 t}{1-\nu^2}\right)^2} \\
&\quad + \frac{25b^3 e P\pi^2 t}{2(1-\nu^2) \left(\frac{abet}{1-\nu^2} - \frac{abeniu^2 t}{1-\nu^2}\right)} + \frac{25b^2 e \nu^2 P\pi^2 t}{2(1-\nu^2) \left(\frac{abet}{1-\nu^2} - \frac{abeniu^2 t}{1-\nu^2}\right)} + \frac{aet^3 Z^2}{4b^3(1-\nu^2)}
\end{aligned}$$

$$\begin{aligned} \text{Out[98]} &= \frac{ae\pi^4 t^3}{48b^3(1-\text{niu}^2)} + \frac{3e\pi^4 t^3}{2ab(1-\text{niu}^2)} + \frac{27be\pi^4 t^3}{a^3(1-\text{niu}^2)} + \frac{9ab^3e^2 P\pi^2 t^2}{(1-\text{niu}^2)^2 \left(\frac{abet}{1-\text{niu}^2} - \frac{abeniu^2 t}{1-\text{niu}^2}\right)^2} - \\ & \frac{18ab^3e^2 \text{niu}^2 P\pi^2 t^2}{(1-\text{niu}^2)^2 \left(\frac{abet}{1-\text{niu}^2} - \frac{abeniu^2 t}{1-\text{niu}^2}\right)^2} + \frac{9ab^3e^2 \text{niu}^4 P\pi^2 t^2}{(1-\text{niu}^2)^2 \left(\frac{abet}{1-\text{niu}^2} - \frac{abeniu^2 t}{1-\text{niu}^2}\right)^2} - \\ & \frac{18b^2 e P\pi^2 t}{(1-\text{niu}^2) \left(\frac{abet}{1-\text{niu}^2} - \frac{abeniu^2 t}{1-\text{niu}^2}\right)} + \frac{18b^2 e \text{niu}^2 P\pi^2 t}{(1-\text{niu}^2) \left(\frac{abet}{1-\text{niu}^2} - \frac{abeniu^2 t}{1-\text{niu}^2}\right)} + \frac{aet^3 Z^2}{4b^3(1-\text{niu}^2)} \\ \text{Out[99]} &= \frac{ae\pi^4 t^3}{48b^3(1-\text{niu}^2)} + \frac{49e\pi^4 t^3}{24ab(1-\text{niu}^2)} + \frac{2401be\pi^4 t^3}{48a^3(1-\text{niu}^2)} + \frac{49ab^3e^2 P\pi^2 t^2}{4(1-\text{niu}^2)^2 \left(\frac{abet}{1-\text{niu}^2} - \frac{abeniu^2 t}{1-\text{niu}^2}\right)^2} - \\ & \frac{49ab^3e^2 \text{niu}^2 P\pi^2 t^2}{2(1-\text{niu}^2)^2 \left(\frac{abet}{1-\text{niu}^2} - \frac{abeniu^2 t}{1-\text{niu}^2}\right)^2} + \frac{49ab^3e^2 \text{niu}^4 P\pi^2 t^2}{4(1-\text{niu}^2)^2 \left(\frac{abet}{1-\text{niu}^2} - \frac{abeniu^2 t}{1-\text{niu}^2}\right)^2} - \\ & \frac{49b^2 e P\pi^2 t}{2(1-\text{niu}^2) \left(\frac{abet}{1-\text{niu}^2} - \frac{abeniu^2 t}{1-\text{niu}^2}\right)} + \frac{49b^2 e \text{niu}^2 P\pi^2 t}{2(1-\text{niu}^2) \left(\frac{abet}{1-\text{niu}^2} - \frac{abeniu^2 t}{1-\text{niu}^2}\right)} + \frac{aet^3 Z^2}{4b^3(1-\text{niu}^2)} \\ \text{Out[100]} &= \frac{aet^2 Z}{b^2(1-\text{niu}^2)} \\ \text{Out[101]} &= \frac{aet^2 Z}{3b^2(1-\text{niu}^2)} \\ \text{Out[102]} &= \frac{aet^2 Z}{5b^2(1-\text{niu}^2)} \\ \text{Out[103]} &= \frac{aet^2 Z}{7b^2(1-\text{niu}^2)} \end{aligned}$$

Critical Loads

```

In[104]:= deter = Expand[
  Det[{{(V2121A, V2131A, 0, V2133A, 0, V2135A, 0, V2137A), {V2131A, V3131A, 0, 0,
    0, 0, 0}, {0, 0, V3232A, 0, 0, 0, 0, 0}, {V2133A, 0, 0, V3333A, 0, 0, 0, 0},
    {0, 0, 0, 0, V3434A, 0, 0, 0}, {V2135A, 0, 0, 0, 0, V3535A, 0, 0},
    {0, 0, 0, 0, 0, 0, V3636A, 0}, {V2137A, 0, 0, 0, 0, 0, 0, V3737A}}]]]
Out[104]= -V2137A^2 V3131A V3232A V3333A V3434A V3535A V3636A -
  V2135A^2 V3131A V3232A V3333A V3434A V3636A V3737A -
  V2133A^2 V3131A V3232A V3434A V3535A V3636A V3737A -
  V2131A^2 V3232A V3333A V3434A V3535A V3636A V3737A +
  V2121A V3131A V3232A V3333A V3434A V3535A V3636A V3737A

```

Values

```

In[120]:= Clear[a1, a21, a31, a32, a33, a34, a35, a36, a37, A, a, B, b,
  c, d, e, niu, m, P, Pcr, R, t, Z, V2121A, V3131A, V3232A, V3333A,
  V3434A, V3535A, V3636A, V3737A, V2131A, V2133A, V2135A, V2137A];
m = 1;
b = 1;
t = 0.01;
Z = 100;
niu = 0.3;
e = 210000;
V2121A = V2121F;
V3131A = V3131F;
V3232A = V3232F;
V3333A = V3333F;
V3434A = V3434F;
V3535A = V3535F;
V3636A = V3636F;
V3737A = V3737F;
V2131A = V2131F;
V2133A = V2133F;
V2135A = V2135F;
V2137A = V2137F;
For[a = 0.1, a <= 6, a = a + 0.025,
  Pc = Solve[-V2137A^2 V3131A V3232A V3333A V3434A V3535A V3636A -
    V2135A^2 V3131A V3232A V3333A V3434A V3636A V3737A -
    V2133A^2 V3131A V3232A V3434A V3535A V3636A V3737A -
    V2131A^2 V3232A V3333A V3434A V3535A V3636A V3737A + V2121A V3131A
    V3232A V3333A V3434A V3535A V3636A V3737A == 0, P]; Print[Pc[[1]]]]

{P -> 19.8041}
{P -> 13.2207}
{P -> 9.81249}
{P -> 7.93051}
{P -> 6.88386}
{P -> 6.33953}
{P -> 6.11782}
{P -> 6.11075}
{P -> 6.24494}
{P -> 6.46306}
{P -> 6.71423}
{P -> 6.95129}
{P -> 7.13529}
{P -> 7.24503}
{P -> 7.28274}

```

{P → 7.2681}	{P → 8.54095}	{P → 16.6927}	{P → 30.9229}
{P → 7.22557}	{P → 8.65627}	{P → 16.9882}	{P → 31.3579}
{P → 7.17516}	{P → 8.77707}	{P → 17.2876}	{P → 31.7964}
{P → 7.12963}	{P → 8.90335}	{P → 17.5908}	{P → 32.2383}
{P → 7.0954}	{P → 9.03508}	{P → 17.8977}	{P → 32.6836}
{P → 7.07447}	{P → 9.17224}	{P → 18.2085}	{P → 33.1323}
{P → 7.06608}	{P → 9.31479}	{P → 18.523}	{P → 33.5844}
{P → 7.06802}	{P → 9.46268}	{P → 18.8413}	{P → 34.0399}
{P → 7.07745}	{P → 9.61587}	{P → 19.1633}	{P → 34.4988}
{P → 7.09155}	{P → 9.77429}	{P → 19.4889}	{P → 34.961}
{P → 7.10794}	{P → 9.93789}	{P → 19.8183}	{P → 35.4266}
{P → 7.1249}	{P → 10.1066}	{P → 20.1514}	{P → 35.8956}
{P → 7.14146}	{P → 10.2804}	{P → 20.4881}	{P → 36.368}
{P → 7.15734}	{P → 10.4592}	{P → 20.8285}	{P → 36.8437}
{P → 7.17275}	{P → 10.6429}	{P → 21.1725}	{P → 37.3228}
{P → 7.18827}	{P → 10.8316}	{P → 21.5201}	{P → 37.8053}
{P → 7.20458}	{P → 11.025}	{P → 21.8714}	{P → 38.2911}
{P → 7.22239}	{P → 11.2232}	{P → 22.2262}	{P → 38.7803}
{P → 7.2423}	{P → 11.4261}	{P → 22.5846}	{P → 39.2728}
{P → 7.26482}	{P → 11.6337}	{P → 22.9466}	{P → 39.7687}
{P → 7.29029}	{P → 11.8459}	{P → 23.3121}	{P → 40.2679}
{P → 7.31897}	{P → 12.0626}	{P → 23.6813}	{P → 40.7705}
{P → 7.35104}	{P → 12.2839}	{P → 24.0539}	{P → 41.2764}
{P → 7.38662}	{P → 12.5095}	{P → 24.4301}	{P → 41.7857}
{P → 7.42581}	{P → 12.7396}	{P → 24.8098}	{P → 42.2983}
{P → 7.46872}	{P → 12.9741}	{P → 25.193}	{P → 42.8142}
{P → 7.51547}	{P → 13.2128}	{P → 25.5797}	{P → 43.3334}
{P → 7.56619}	{P → 13.4559}	{P → 25.9699}	{P → 43.856}
{P → 7.62103}	{P → 13.7032}	{P → 26.3636}	{P → 44.3819}
{P → 7.68016}	{P → 13.9546}	{P → 26.7608}	{P → 44.9112}
{P → 7.74375}	{P → 14.2103}	{P → 27.1615}	{P → 45.4437}
{P → 7.81197}	{P → 14.47}	{P → 27.5657}	{P → 45.9796}
{P → 7.88499}	{P → 14.7338}	{P → 27.9733}	{P → 46.5188}
{P → 7.96296}	{P → 15.0017}	{P → 28.3843}	{P → 47.0614}
{P → 8.04601}	{P → 15.2737}	{P → 28.7988}	{P → 47.6072}
{P → 8.13427}	{P → 15.5496}	{P → 29.2168}	{P → 48.1564}
{P → 8.22783}	{P → 15.8295}	{P → 29.6381}	{P → 48.7089}
{P → 8.32676}	{P → 16.1133}	{P → 30.063}	{P → 49.2646}
{P → 8.43113}	{P → 16.4011}	{P → 30.4912}	{P → 49.8237}